HEAT TRANSFER STUDIES OF LIQUID/PARTICLE MIXTURES IN CANS SUBJECTED TO END-OVER-END PROCESSING

by

Shyam Swaroop Sablani

Department of Food Science and Agricultural Chemistry
Macdonald Campus of McGill University
Montreal, Canada

October, 1996

A thesis submitted to the Faculty of Graduate Studies and Research in partial fulfilment of the requirements for the degree of Doctoral of Philosophy

ISBN 0-612-19770-0

Canada

Suggested short Title:

HEAT TRANSFER IN ROTARY PROCESSING OF CANNED LIQUID/PARTICLE MIXTURES

ABSTRACT

Overall heat transfer coefficient (U) and fluid to particle heat transfer coefficient (h_{fp}) in canned liquid/particle mixtures, subjected to end-over-end processing, were experimentally evaluated. A methodology was developed to measure heat transfer coefficients, while allowing the movement of the particle inside the can, by attaching it to a flexible fine wire thermocouple. The overall heat transfer coefficient was calculated from the thermal energy balance on the can. The fluid to particle heat transfer coefficient was evaluated using a finite difference computer program, by matching the particle time-temperature data with those obtained by solving the governing partial differential equations of conduction heat transfer in spherical geometry, with appropriate initial and boundary conditions. Heat transfer coefficients were evaluated under two conditions: 1) with a single particle in the can, 2) with multiple particles in the can.

In the single particle experiments, a spherical particle was used to evaluate the influence of system parameters such as: retort temperature (110 to 130 °C), rotational speed (0 to 20 rpm), radius of rotation (0 to 27 cm) and can headspace (6.4 and 10 mm); and product parameters such as: particle density (830 to 2210 kg/m^3) and liquid viscosity (kinematic viscosity 1.0 x 10^{-6} and 1.0 x 10^{-4} m^2/s) on associated U and h_{fp}. Increasing values of all four system variables improved the heat transfer coefficients; and the effects of rotational speed and headspace were more significant than those of retort temperature and radius of rotation. The particle density had no significant effect ($p > 0.05$), but the other product variables, of liquid viscosity and rotational speed, had significant effects ($p \leq 0.0001$) on U. The h_{fp} values were influenced by rotational speed, liquid viscosity and particle density. The effect of particle density on h_{fp} was more significant than those of liquid viscosity and rotational speed. The U values varied from 118 to 800 W/m^2 K and h_{fp} values varied from 23 to 825 W/m^2 K, depending on the operating conditions.

With multiple particles (Nylon) in cans, the associated convective heat transfer coefficients (U and h_{fp}) were evaluated during end-over-end rotation using the same two liquids (kinematic viscosities, 1.0 x 10^{-6} and 1.0 x 10^{-4} m^2/s), different can rotation speeds (10 to 20 rpm), particle diameters (19 to 25 mm), particle concentrations (single particle

to 40% v/v) and particle shapes (sphere, cylinder and cube). The U values ranged from 110 to 800 W/m^2 K, and the h_{fp} values varied 170 to 1550 W/m^2 K depending upon process conditions. Heat transfer coefficients increased with decreasing particle diameter, increasing particle concentration (up to 20% for U and 30% for h_{fp}) and increasing sphericity. A further increase in particle concentrations upto 40% decreased the heat transfer coefficients.

Flow visualization studies were carried out to characterize the particle motion/mixing behavior of liquid/particle mixtures. Particle motion/mixing in transparent containers was video taped under end-over-end rotational conditions used in the heat transfer study. With a single particle in the can, liquid viscosity, particle density and rotational speed influenced the particle motion. With multiple particles in cans, particle motion/mixing was influenced by particle concentration, particle size, particle shape, liquid viscosity and rotational speed.

Dimensionless correlations were developed for the predictive modeling of convective heat transfer coefficients under rotational processing conditions. For U with a single particle in the can (or liquid only situation), Nusselt number (Nu) was correlated to Reynolds number (Re), Prandtl number (Pr) and relative can headspace while with multiple particles, Re, Pr, ratio of particle to liquid concentration, relative particle diameter and particle sphericity were found to be significant parameters. For h_{fp} with a single particle in the can, three different correlations, one each for a sphere, a cylinder and a cube were developed and the Nu was correlated to Re [or Froude number (Fr)], Pr, density simplex (a), relative can headspace and the ratio of the sum of the diameter of rotation and diameter of the can to the can diameter. With multiple particles Nu was correlated to Re or Peclet number, ratio of particle to liquid thermal conductivity, particle to liquid concentration and particle sphericity.

A multi-layer artificial neural network (ANN) was also used to model heat transfer parameters under conduction and convection heating conditions. In order to test the applicability of ANN, initially, computer simulated data were used for optimal process parameters of conduction heated canned foods under typical thermal process conditions. The trained multi-layer neural network was found to predict optimal sterilization

temperatures with an accuracy of $\pm$ 0.5°C, and other responses such as process time and integrated heating time for quality attribute with less than 5% associated errors. Subsequently, multi-layer neural network models were trained based on the experimental values of U and h_{fp}, the two important parameters needed in theoretical modeling, of liquid/particle mixtures in cans subjected to end-over-end processing. Optimal configuration of the neural network, with 7 input and 2 output neurons (for a single particle in the can), and 6 input and 2 output neurons (for multiple particles in the can), was obtained by varying the number of hidden layers, the number of neurons in each hidden layer and number of learning runs. The trained network was found to predict U and h_{fp} with less than 3% and 5% errors, respectively. The neural network models were more accurate, than the dimensionless number models, for predicting U and h_{fp}.

RÉSUMÉ

Le coefficient de transfert global (U) et le coefficient de transfert à l'interface d'un fluide et d'une particule (h_{fp}) ont été évalués expérimentalement pour des conserves soumises à un procédé de stérilisation en rotation complète. Une méthode a été développée pour mesurer les coefficients de transfert de chaleur de particules en mouvement dans une conserve en attachant un fil de thermocouple flexible très fin au centre de la particule. Le coefficient de transfert de chaleur global a été calculé à partir du bilan d'énergie thermique effectué sur la conserve. Le coefficient de transfert de chaleur entre le fluide et la particule a été calculé en égalisant les données de temps-température de la particule à celles obtenues par la résolution des équations différentielles partielles de transfert de chaleur par conduction pour une géométrie sphérique en utilisant des conditions initiales et limites appropriées et la méthode numérique des différences finies. Les coefficients de transfert de chaleur ont été évalués sous deux conditions: 1) avec un particule dans une conserve, 2) avec plusieurs particules dans une conserve.

Pour l'expérimentation d'une particule unique, on a utilisé une particule sphérique pour évaluer l'influence des paramètres du système comme la température de l'autoclave (110 à 130 °C), la vitesse de rotation (0 à 20 rpm), le rayon de la rotation (0 à 27 cm), l'espace de tête (6.4 et 10 mm) et les paramètres du produit comme la densité de la particule (830 à 2210 kg/m^3) et la viscosité du fluide (viscosité cinématique 1.0×10^{-6} et 1.0×10^{-4} m^2/s) sur U et h_{fp}. On a trouvé que l'augmentation des valeurs des 4 variables du système améliorait les coefficients de transfert de chaleur. Les effets de la vitesse de rotation et de l'espace de tête étaient plus significatifs que ceux de la température de l'autoclave et du rayon de rotation. L'effet de la densité de la particule était négligeable ($p>0.05$) alors que les autres variables de produit, viscosité du liquide et vitesse de rotation, ont eu des effets significatifs ($p\leq0.0001$) sur U. Les valeurs de h_{fp} étaient influencées par la vitesse de rotation, la viscosité du liquide et la densité de la particule. L'effet de la densité de la particule sur h_{fp} était plus significatif que ceux de la viscosité du fluide et de la vitesse de rotation. Les valeurs de U ont varié de 118 à 800 W/m^{2}K et celles de h_{fp} de 23 à 825 W/m^{2}K dépendamment des conditions de fonctionnement du

système.

Pour les expériences avec plusieurs particules en conserve, les coefficient de transfert de chaleur associés (U et h_{fp}) ont été évalués durant la rotation complète en autoclave en utilisant deux types de liquide (viscosité cinématique de 1.0×10^{-6} et de 1.0×10^{-4} m^2/s), des vitesses de rotation de 10 à 20 rpm, des diamètres de particules de 19 à 25 mm, des concentrations de particules variant d'une simple particule à 40% v/v et des formes variées (sphère, cylindre et cube). Les valeurs de U obtenues ont variées de 110 à 800 W/m^2 K et celles de h_{fp} de 170 à 1550 W/m^2 K dépendamment des conditions du procédé. On a trouvé que les coefficients de transfert de chaleur augmentaient lorsque le diamètre diminuait, la concentration de particules augmentait jusqu'à 20% pour U et 30% for h_{fp} et la sphéricité augmentait.

Des études de visualisation des débits ont été conduites pour caractériser le comportement des liquides contenant des particules. Le mouvement/mélange des particules dans des conserves transparentes a été pris en image sur vidéo durant des conditions de rotation complète lors d'un procédé de chauffage en autoclave. Pour les expériences d'une particule unique dans une conserve, on a trouvé que la viscosité du fluide, la densité de la particule et la vitesse de rotation influençaient le mouvement de la particule. Pour l'expérimentation à plusieurs particules, le mouvement/mélange des particules était influencé par la concentration de particules, la grosseur et la forme des particules, la viscosité du liquide et la vitesse de rotation.

Des corrélations sans dimensions ont été développées pour la prédiction des coefficients de transfert de chaleur au cours d'un procédé de chauffage en rotation. Pour U, en situation d'une simple particule en conserve ou liquide seulement, le nombre de Nusselt (Nu) a été correlé au nombre de Reynolds (Re), nombre de Prandtl (Pr) et à l'espace de tête relatif. Dans des conditions d'expérience contenant plusieurs particules, on a observé que Re, Pr, le ratio de particule à la concentration de fluide, la diamètre relatif des particules et la sphéricité étaient significatifs. Trois corrélations ont été développées pour h_{fp} dans le cas d'une particule en conserve : une pour la sphère, une pour le cylindre et une pour le cube. On a trouvé que le nombre de Nusselt (Nu) était correlé à Re ou Fr(Froude number), Pr, le simplexe de densité (a), l'espace de tête relatif

et le ratio de la somme du diamètre de rotation et du diamètre de la conserve sur le diamètre de la conserve. Quant à la situation de conserves contenant plusieurs particules, Nu était correlé à Re, au nombre de Peclet, au ratio de la conductivité thermique de la particule par rapport au liquide, à la concentration de particules par rapport au liquide et à la sphéricité des particules.

Un réseau artificiel de neurones (RAN) à plusieurs couches a été utilisé pour modéliser les paramètres de transfert de chaleur sous des conditions de chauffage en conduction et en convection. Pour tester l'applicabilité du RAN, des données simulées sur ordinateur pour des paramètres optimaux de procédé de chauffage de conserve par conduction ont été utilisées pour l'entraînement. On a trouvé que le RAN entraîné a permis la prédiction des températures de stérilisation optimales avec une précision de $\pm$ 0.5°C et d'autres réponses comme le temps du procédé et le temps de chauffage intégré pour les attributs de qualité avec moins de 5% d'erreur. Par la suite, les modèles de RAN à plusieurs couches ont été entraînés en se basant sur les valeurs expérimentales de U et h_{fp}, les deux paramètres les plus importants dans la modélisation théorique de conserves de liquide contenant des particules soumises à la rotation complète en autoclave. Les configurations optimales du RNA soit 7 neurones d'entrée et 2 neurones de sortie (pour une particule dans une conserve) et de 6 neurones d'entrée et 2 neurones de sortie (pour plusieurs particules dans une conserve) ont été obtenues en variant le nombre de couches cachées, le nombre de neurones dans chaque couche cachée et le nombre d'essais d'apprentissage. On a trouvé que le RAN entraîné pouvait prédire U et h_{fp} avec moins de 3% et 5% d'erreur respectivement et que ceux-ci étaient plus précis que les corrélations sans dimensions pour la prédiction de U et h_{fp}.

ACKNOWLEDGEMENTS

I extend my sincere thanks and appreciation to Dr. H. S. Ramaswamy, my thesis supervisor, for his friendly guidance, advice, understanding, invaluable criticism, and encouragement throughout the course of this study.

Sincere thanks are also extended to Dr. A. S. Mujumdar for helpful suggestions and advice on various aspects of the study, especially on the flow visualization study and dimensional analysis. I am grateful to Dr. S. O. Prasher for his time and recommendations regarding the neural network analysis and NMOL programming and Dr. G. S. V. Raghavan (Chair, Department of Agricultural and Biosystems Engineering) for his help.

Thanks are also extended to all the friendly staff members of the Department of Food Science and Agricultural Chemistry who have helped me to get adapted to the food science program, especially Dr. F. R. van de Voort, Past-Chair and Dr. I. Alli, Chair, Department of Food Science and Agricultural Chemistry.

I want to thank a special friend, Dr. Stefan Grabowski, who encouraged my ideas and with whom I had many interesting and lively discussions, to Ms. Carla Abbatemarco for "teaching" me heat penetration data gathering, to Ms. Sasithorn Tajchakavit for helpful suggestions and assistance during long experimental runs, to Mme. Michele Marcotte for the French translation of the abstract. My sincere thanks go to my colleagues and most importantly, Mr. A. R. Taherian, Mr. M. R. Zareifard, Mrs. S. Basak, Mrs. D. Moussa, Dr. G. S. Bhat, Ms. F. Nsoonzi, Mr. P. K. Pandey and to my friends R. K. Singh, Dr. T. N. Tulasidas and Dr. B. Ranganna. My heartfelt appreciation goes particularly to the families of Dr. Ramaswamy, Dr. Prasher, and Dr. Raghavan for their concern, love, help and moral support during the difficult times. A special thanks to Dr. Sreekanth for his friendship, love and help in finding me a place in McGill University!

The financial assistance of a McGill Major (Hydro Quebec) Fellowship and research funding from the Partnership Grant Program (Agricultural Canada, NSERC and Cordon Bleu Ltd.) are gratefully acknowledged.

I would like to dedicate this effort to my parents for the love and support they gave me all my life, and to my dear wife Sunita and son Nikhil for their patience, sacrifice, understanding, constant support and encouragement.

NOMENCLATURE

a	Radius of a sphere or cylinder or half length of the side of cube; or radius of a can, m
A_c	Total external surface area of can, m^2
A_p	Surface area of the particle, m^2
A_{sph}	Surface area of an equivalent sphere (diameter d_e), m^2
C	Concentration of any component of interest
C_D	Drag coefficient
C_p	Heat capacity, J/kg K
d	Desired response of neuron; or diameter, m
d_{ch}	Characteristic dimension, m
d_{cyl}	Diameter of cylindrical particle, m
d_e	Particle equivalent diameter [= $(6V_p/\pi)^{0.33}$], m
d_p	Particle shortest dimension, m
d_s	Diameter of sphere, m
D	Decimal reduction time, min
D_c	Diameter of can, m
D_{ci}	Internal can diameter, m
D_r	Diameter of rotation, m
E_a	Activation energy, kJ/mole
f_h	Heating rate index, min
F_o	Process lethality, min
F_{oq}	Integrated heating time with respect to quality attribute, min
g	Acceleration due to gravity, 9.81 m/s^2
h_{fp}	Fluid-to-particle heat transfer coefficient, W/m^2 K
h_s	Can headspace, m
H	Height of the can, m
H1#	Height from the bottom of can, mm
H_{ce}	Effective can length (can length - can headspace), m
j_{ch}	Heating lag factor
k	Thermal conductivity, W/m K
k_l, k_p	Thermal conductivity of fluid and solid particles respectively, W/m K
L	Half length of cylinder, m
L1#	Length of thermocouple, mm
l_{cu}	Cube edge length , m
l_{cyl}	Length of the cylindrical particle, m
m	Mass, kg, or Layer number
M	Number of subdivision in axial direction (in cylindrical coordinate system)
N	Quality factor, or Rotational speed, rpm; Number of subdivision in radial direction (in spherical or cylindrical coordinates)
PT	Process time, min
r	Radial coordinate (in spherical or cylindrical coordinates)

R	Universal gas constant, kJ/mole K
S	Output of neuron; or radius of the reel in the agitated retort, rpm
t	Time, s
t_l	Time in the curvilinear portion of the heating curve, s
T	Temperature, °C
T_R	Retort temperature, °C
U	Overall heat transfer coefficient, W/m^2 K
V	Volume, m^3
V_c	Volume of can, m^3
V_h	Volume of can headspace, m^3
w	weight coefficient, angular velocity, 1/s
W	Set of weight coefficients
x	Input value to neuron or coordinate (in rectangular system)
x,y,z	Cartesian coordinates
X	Set of inputs
y	Coordinate (in rectangular system)
z	Axial coordinates (in cylindrical or rectangular systems), Temperature sensitivity indicator, C°
< >	Volumetric average
Δ	Step size (used with space or time)

Greek Symbols

α	Thermal diffusivity, m^2/s
β	Root of the equation : $\beta \cot \beta + Bi - 1 = 0$
ε	Particle concentration, % (Volume of particle(s)/Total volume of can)
ρ_l, ρ_p	Density of liquid and solid particles respectively, kg/m^3
μ	Dynamic viscosity, kg/m s
υ	Kinematic viscosity, m^2/s
σ	Surface tension, kg/s^2
τ_l	Time constant for liquid, $UA_c/m_l C_{pl}$
τ_p	Time constant for particle, $\alpha \beta^2/a_p^2$
Ψ	Sphericity of the particle, - (A_{sph}/A_p)
ω	Can angular velocity, $(2\pi N/60)$, 1/s
ε	Error

Subscripts

0, 1.	Integer numbers
cal	Calculated
fi	Final condition
i	Initial condition, space index
j	Space index
l	Liquid

m	Micro-organism
opt	Optimal
p	Particle
q	Quality
R	Retort
ref	Reference
s	Surface
∞	Heating medium

Dimensionless number

a	Density simplex $[I(\rho_p-\rho_l)I/\rho_f]$
Ar	Archimedes number, $[g\ d_{ch}^3\ a\ /\nu^2]$
Bi	Biot number $(h_{fp}\ a/k_p)$
Fr	Froude number, $[(\pi d_{ch}N/60)^2/(g\ d_{ch})]$
Nu	Nusselt number, $[U$ (or $h_{fp})\ d_{ch}/k_f]$
Pe	Peclet number, (Re.Pr) $[(\pi d_{ch}N/60)\ d_{ch}/\alpha]$
Pr	Prandtl number, $[\nu/\alpha]$
Re	Reynolds number, $[(\pi d_{ch}N/60)\ d_{ch}/\nu]$
We	Weber number, $[(\omega^2H^2\pi D_c)/\sigma]$

Abbreviations

ANN	Artificial neural network
DC	Dimensionless correlation
HTST	High temperature short time
LALD	Least Absolute Lethality Difference
LMS	Least mean square
LSTD	Least sum of Squared Temperature Differences
MAE	Mean absolute error
MRE	Mean relative error
SDE	Standard deviation of error
SRE	Standard deviation of relative error
TTI	Time temperature integrator

TABLE OF CONTENTS

LIST OF TABLES

LIST OF FIGURES

CHAPTER 1

INTRODUCTION

Thermal processing, or canning, is one of the most effective methods of food preservation and assurance of bacteriological safety. In the United States, the canning industry annually processes approximately 33 billion pounds of food that are packed in about 36 billion containers (Lopez, 1987). Ever since 1809, when Nicholas Appert developed this new means of preserving food, the canning industry has gone through tremendous changes in processing methodology, equipment, energy efficiency, product quality and product safety.

In 1920, Bigelow and Ball presented the first scientifically based graphical method for calculating the minimum process conditions for safe sterilization. In 1923, Ball developed a mathematical method to determine sterilization processes. In 1939, Olson developed a nomographic method for process determination. In 1957, Ball and Olson combined the research of others with their own and published a book on heat processing. Since then scientists and engineers have refined the mathematics of heat process determination concepts and applications.

It has been recognized that thermal processing, in addition to ensuring a safe food supply, also affects food quality attributes, such as: color, texture, flavor and nutrients. For convection heating products, high temperature short time (HTST) processes are beneficial since microorganisms are destroyed before the food quality factors are seriously affected. Conduction-heating foods do not benefit from this concept because of their slower heating rates. Recent commercial developments have focused primarily on increasing the rate of heat transfer into the food product, in order to maximize the retention of quality factors. Three major developments have been : (i) thin profile packaging, (ii) aseptic processing, and (iii) agitation processing. The thin processing utilizes high process temperatures with foods packaged in retort pouches or thin profile semi-rigid containers, with their thinner profile and larger surface area permitting faster heating and cooling of the cold spot. In aseptic processing, the food is first heated in

scraped surface heat exchangers (SSHE) and held for a pre-determined time in a hold tube, cooled quickly through a second set of SSHEs and then filled and sealed aseptically into sterile containers. However, problems of uncertain residence time distribution (RTD) of particles and uncertain fluid to particle heat transfer coefficient (h_{fp}), have limited its use to liquid-type products and liquid containing very small particles such as soups. In the last 15 years, extensive research has been carried out on the calculation of RTD and h_{fp}; however, aseptic processing of liquid foods containing particles is yet to be commercialized. Since the early 1950s (Clifcorn et al., 1950), agitation sterilization with HTST processing has been recognized as an effective method for achieving high quality foods. It has been observed that heat penetration to the cold spot in a container, with a viscous or semi-solid product, could be achieved much faster with agitation processing. Mechanically induced forced convection, in a rotary retort, decreases the temperature difference between the surface and the center of the product and favors quality retention because the product receives a more uniform and shorter heat treatment.

The potential of mathematical modeling has been demonstrated in the design, optimization and validation of thermal processing of foods. Appropriate models are important in reducing the number and cost of experiments required to achieve desired product safety and quality. In the last three decades, extensive mathematical analyses of conduction heating foods have been carried out by many researchers (Hayakawa, 1970, 1978; Manson et al., 1970; Pflug et al., 1965; Stumbo, 1973; Teixeira et al., 1969a, b; Teixeira, 1978). The studies on convection heating foods are more difficult. A few studies have been carried out on the convection heating of liquid foods without particles, thereby evaluating overall heat transfer coefficient, U, and these have been presented in a review article by Rao and Anantheswaran (1988). Recently, Datta (1992) presented a comprehensive paper on the modeling of the physical process involved in the thermal sterilization of liquid food.

During agitation processing, heat transfer to canned liquid/particle mixtures is considerably more complex. Earlier studies on convective heat transfer, in the presence of particles, have focused only on the liquid portion of the canned foods, thus determining the effects of various heat transfer rates to the liquid (Berry et al. 1979; Berry and

Bradshaw, 1980, 1982; Berry and Dickerson, 1981). During agitation processing, heat transfer modeling of canned liquid/particle mixtures will require data on the thermo-physical properties of food materials and the associated convective heat transfer coefficients. In such systems, both the overall heat transfer coefficient from the retort heating medium to the can liquid, U, and the fluid to particle heat transfer coefficient, h_{fp}, are needed to predict heat transfer rates to the particle at the coldest point in can. Because of the practical difficulty in monitoring the transient temperature history of a particle moving in an agitating liquid, the associated h_{fp} is one of the important gaps in our knowledge on heat transfer (Maesmans et al., 1992).

Most earlier studies reported h_{fp} values between a stationary particle fixed on to a rigid thermocouple and a liquid moving around it (Lenz and Lund, 1978; Lekwauwa and Hayakawa, 1986; Deniston et al., 1987 and Fernandez et al., 1988). McKenna et al. (1990) suggested that further work should be carried out to develop a reliable method to determine h_{fp}. Recently, efforts have been made to measure h_{fp} while allowing particle movement inside the can during agitation processing (Stoforos and Merson, 1990 and 1991; Weng et al., 1992).

During rotational sterilization, there are several factors that influence the heat penetration rate into the food particles in a container . The most relevant factors include: retort temperature, rotational speed, radius of rotation, can headspace, product viscosity, liquid to particle ratio, particle size and particle shape (Eisner, 1988). The several factors involved obviously suggest the difficulty in determining optimal process conditions for maximizing quality retention. Moreover, due to the short process times involved, a thorough understanding of these critical factors is necessary in order to employ rotational processing efficiently, while producing high quality products and ensuring the minimum required sterility.

The following were the objectives of this research :

1. Development of a methodology to measure convective heat transfer coefficients in canned liquid/particle mixtures subjected to end-over-end processing.

2. Evaluation of the convective heat transfer coefficients, as influenced by system and product parameters: a) studies with a single particle in the can.
3. Evaluation of the convective heat transfer coefficients, as influenced by system and product parameters: b) studies with multiple particles in the can.
4. Study of the motion of single and multiple particles in containers subjected to end-over-end rotation, as influenced by system and product parameters.
5. Development of dimensionless correlations, for the prediction of convective heat transfer coefficients, in canned liquid/particle mixtures subjected to end-over-end processing.
6. Evaluation of neural network models for the prediction of heat transfer parameters, with conduction and convection heating conditions.

CHAPTER 2

LITERATURE REVIEW

Thermal processing involves the destruction of microorganisms contained in food, so that it can be stored for a longer period and prove safe for consumption. Foods packaged in hermetically sealed containers are rendered "commercial sterile" by the application of heat, generally in combination with pH, vacuum, water activity or chemical treatment. Commercial sterility means that the application of the heat achieves conditions in a product which render it free of microorganisms, capable of reproducing in non-refrigerated conditions of storage and distribution. The primary objective of thermal processing has been the destruction of microorganisms of public health concern, as well as microorganisms, and enzymes which cause spoilage of food. The main public health concern, with low-acid canned foods, is the toxin producing, heat resistant bacterium *Clostridium botulinum*. Prevention of the formation of botulinum toxin is the major purpose for canning low acid food products.

Principles of thermal processing

The successful establishment of thermal processes for canned foods is based on a sound knowledge of thermobacteriology and understanding of the mechanism of heat transfer. In thermal processing, most pathogenic and spoilage type microorganisms are destroyed in a hermetically sealed container; and an environment is created inside the package that does not support the growth of remaining microorganisms and/or their spores (Figure 2.1, adapted from Ramaswamy and Abbatemarco, 1996). It is a complex procedure to determine the proper process temperature and length of time of sterilization for a container of food. It depends on several factors, including the type and heat resistance of the target microorganism, the pH of the food, storage conditions following the process, the heating conditions and thermophysical properties of the food, the container shape and size. The temperature and pH requirements of some common spoilage microorganisms are summarized in Table 2.1 (Adapted from Lund, 1975). The thermal destruction rate of the

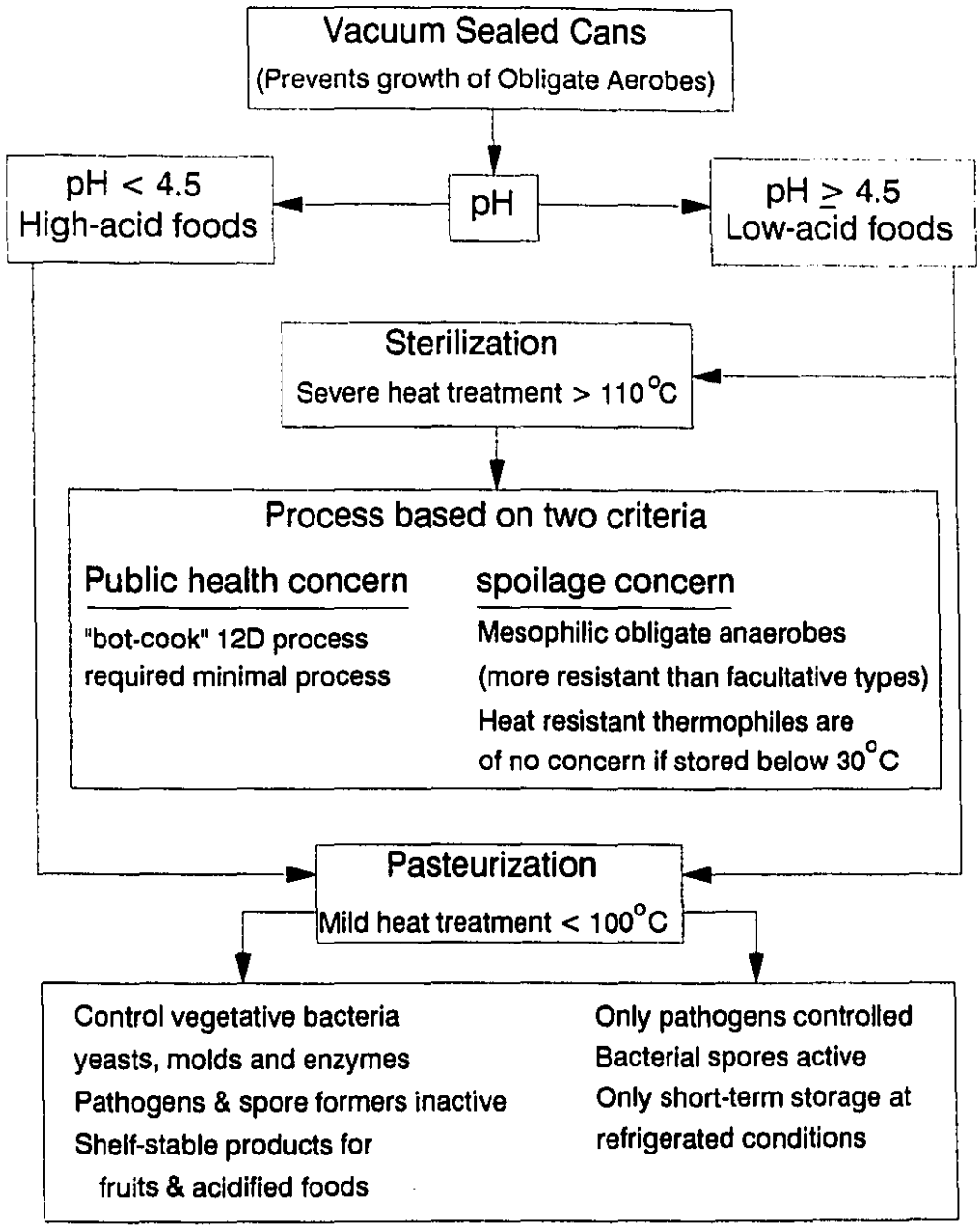

Figure 2.1 A schematic illustrating the principles involved in thermal process applications (Source: Ramaswamy and Abbatemarco, 1996)

target microorganism must be determined under conditions that normally prevail in the container, so that an appropriate heating time can be determined at a given temperature. Furthermore, because canned foods cannot be heated to process temperatures instantaneously, data on temperature dependence of the microbial destruction rate are also needed in order to integrate the destruction effect through the temperature profile under processing conditions.

Table 2.1 Spore-forming bacteria of importance in spoilage of food

Approximate temperature (°C) range for vigorous growth	Acidity of food	
	Acid $3.7 < pH < 4.5$	Low acid $pH \geq 4.5$
Thermophilic (55-35°)	*B. coagulans*	*C.thermosaccharolyticum* *C. nigrificans* *B. stearothermophilus*
Mesophilic (40-10°)	*C. butyricum* *C. pasteurianum* *B. mascerans* *B. polymyxa*	*C. botulinum*, A and B *C. sporagenes* *B. licheniformis* *B. subtilis*
Psychrophilic (35-<5°)		*C. botulinum*, E

Regulatory agencies require the establishment of a process schedule to produce a commercially sterile product by a processing authority. The scheduled process includes thermal process parameters such as: product initial temperature, process temperature, process time, and critical factors that may affect the attainment of commercial sterility.

Measure of sterilization

Arrhenius model: The destruction of microorganisms (or quality factors) in foods is generally described using first order reaction kinetics:

$$-\left(\frac{dC}{dt}\right) = k_T\, C \qquad (2.1)$$

where C = concentration of the component of interest, t = time, k_T = reaction rate constant at temperature T. The temperature dependency of the rate constant is given by the Arrhenius equation:

$$k_T = k_0\, e^{-E_a / RT} \qquad (2.2)$$

where k_0 = frequency factor, E_a = activation energy, R = gas constant. The temperature T normally varies in a heating process. The final concentration can be obtained by integrating Eq. (2.1) between initial concentration C_i and final concentration C at time t:

$$\ln\frac{C_i}{C} = k_0 \int_0^t e^{-E_a / RT}\, dt \qquad (2.3)$$

The process of sterilization or heat treatment is measured using lethality, F-value. A unit of lethality is taken as an equivalent heating of 1 min at a reference temperature (usually 121.1 °C or 250 °F for thermal sterilization). At a reference temperature of T_0 the integrated process lethality can be obtained using Eq. (2.4) (Datta, 1992):

$$F_0 = \int_0^t \exp\left[\frac{E_a}{R}\left(\frac{1}{T_R} - \frac{1}{T}\right)\right] dt \qquad (2.4)$$

TDT approach : The heat resistance of microorganisms varies considerably. At any given temperature, the microbial destruction rate can be defined as a decimal reduction time (D), which is the heating time required to reduce the number of microorganism by 90%:

$$D = \frac{(t_2 - t_1)}{[\log(a) - \log(b)]} \qquad (2.5)$$

where a and b represent the survivors following heating treatment for time t_1 and t_2 min, respectively. D value can also be obtained from the rate constant, k_T:

$$D_T = \frac{2.303}{k_T} \tag{2.6}$$

The temperature sensitivity of these D-values is expressed in terms of a z-value, which represents the temperature range that results in a 10-fold change in the D-values:

$$z = \frac{(T_2 - T_1)}{[\log(D_1) - \log(D_2)]} \tag{2.7}$$

where D_1 and D_2 are D-values at T_1 and T_2, respectively. In a real process the food passes through a time-temperature profile, and the lethal effect of temperatures are integrated over the heating time to give process lethality F_0 [similar to Eq. (2.4)]:

$$F_0 = \int_0^t 10^{\frac{(T - T_0)}{z}} dt \tag{2.8}$$

Because the decimal reduction time is based on a logarithmic destruction, complete destruction of microbial population is not feasible. Generally, a probability approach is employed. From the public health viewpoint, a 12D process with reference to *C. botulinum* (bot cook) is taken for low acid foods. A *bot cook*, although adequate for public health, may be inadequate when the contaminant is one of the other more heat-resistant microorganisms. Some typical D- and z- values of selected microorganisms are given in Table 2.2 (Adapted from Lund, 1975).

Thermal process calculations

The thermal process is established using thermal destruction kinetics of target microorganisms and the heat penetration data of a specific product (Figure 2.2). The purpose of the thermal process calculations is to determine the required process time under a given set of heating conditions, which result in a required process lethality, or alternatively to estimate the achieved lethality of a process. In a processing situation, the product goes through a temperature ramp and the process calculation methods integrate the lethal effects of the transient temperature profile. The desired degree of lethality F_0

Table 2.2 Thermal resistance of spore forming microorganisms used as a basis for thermal processing

Microorganism	D_{250}-value min	z-value C°
B. stearothermophilus	4.0	7.0
B. subtilis	0.48-0.76	7.4-13.0
B. cereus	0.0065	9.7
B. megaterium	0.04	8.8
C. perfringens		10.0
C. sporogenes	0.15	13.0
C. sporogenes (PA 3679)	0.48-1.4	10.6
C. botulinum	0.21	9.9
C. thermosaccharolyticum	3.0-4.0	8.9-12.2

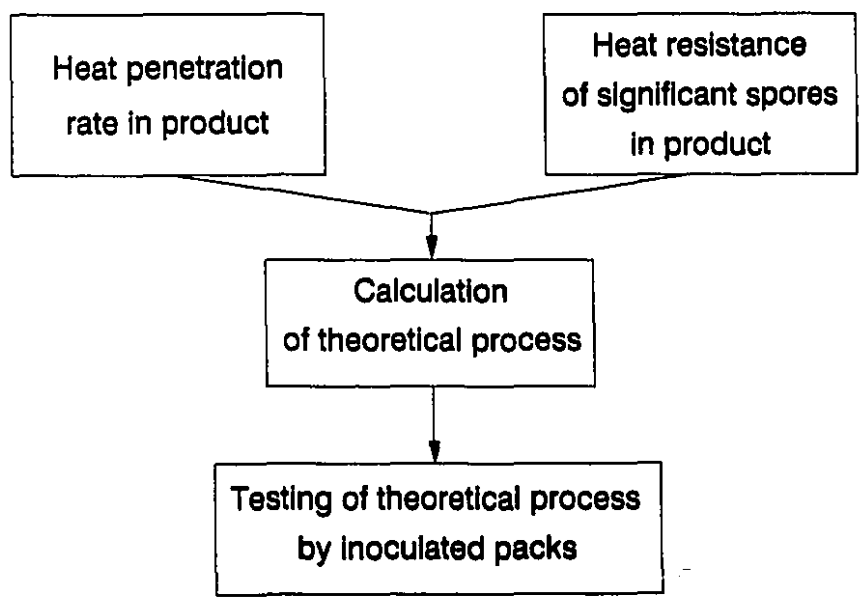

Figure 2.2 Establishment of the thermal process

is generally pre-established and the processes are designed to deliver the minimum of this preset value to thermal center. The process calculation methods are broadly divided into two classes: (i) General methods and (ii) Formula methods. The General methods integrate the lethal effects by a graphical or numerical integration procedure, based on the time-temperature data obtained from test containers processed under actual commercial processing conditions. The Formula methods make use of parameters obtained from this heat penetration data, together with several mathematical procedures to integrate the lethal effects (Ramaswamy et al., 1992).

Food quality

The primary objective of thermal processing has been the destruction of microorganisms of public health concern and those causing spoilage of food packaged in hermetically sealed containers. There has been increasing public concern with the lower quality of thermally processed foods, which has prompted several studies to minimize quality degradation in thermally processed foods. The high temperature short time (HTST) and ultra-high temperature (UHT) processes promote better nutrient retention in the processed foods, taking advantage of the increased sensitivity of microorganisms than of quality factors to thermal destruction at elevated temperatures. Representative kinetic data for some quality factors and enzymes are given in Table 2.3 (Adapted from Lund, 1975 and Ramaswamy et al., 1989). The HTST and UHT concepts have been successfully applied to liquid foods. However, these approaches are generally not beneficial for conduction heating food products, because of the relatively slow rate of heat transfer and existence of large temperature gradients between the surface and center of the container. Optimized conditions for these might occur at intermediate temperatures (Teixeira et al., 1969a, b). Variable retort temperatures and thin profile packages (retort pouches) have been considered in order to promote better quality in conduction heated products (Teixeira et al., 1975; Ramaswamy and Tung, 1986; Teixeira and Shoemaker, 1989).

Table 2.3 Kinetic parameters for thermal destruction of various food components[1]

Component	Medium	pH[2]	Temperature range (°C)	z (C°)	Ea (kcal /mole)	D_{250} (min)
Vitamins						
Thiamine	Whole peas	Nat.	104-132	26.1	21.2	164
	Carrot puree	5.9	109-149	25.0	27.0	158
	Green bean puree	5.8	109-149	25.0	27.0	145
	Green pea puree	6.6	109-149	25.0	27.0	163
	Spinach puree	6.5	109-149	25.0	27.0	134
	Beef liver puree	6.1	109-149	25.0	27.0	124
	Beef heart puree	6.1	109-149	25.0	27.0	115
	Lamb puree	6.2	109-149	25.0	27.0	120
	Pork puree	6.2	109-149	25.0	27.0	157
C	Liquid multi-vitamin prep.	3.2	4-70	27.8	23.1	1612
B_{12}	Liquid multi-vitamin prep.	3.2	4-70	27.8	23.1	2793
Folic acid	Vitamin prep.	3.2	4-70	36.7	16.8	2808
A	Vitamin prep.	3.2	4-70	40.0	14.6	18432
Color						
Chlorophylla	Spinach	6.5	127-149	51.1	15.5	13
Chlorophyllb	Spinach	5.5	127-149	79.4	7.5	14.7
Chlorophyll (Blanched)	Pea puree	Nat.	116-138	36.7	16.1	14
Chlorophyll (Unblanched)	Pea puree	Nat.	116-138	45.0	12.6	13.9
Texture and Overall quality						
	Peas	Nat.	99-116	32.2	19.5	2.5
	Beats	Nat.	82-99	18.9	34.0	2.0
	Whole corn	Nat.	100-121	36.7	16.0	2.4
	Carrot	Nat.	80-116	16.7	38.0	1.4
	Potato	Nat.	72-116	23.3	27.5	1.2

[1]Lund (1975) and Ramaswamy et al. (1989); [2] Nat. = Natural pH

Types of retorts

Still retorts : A still retort is a batch-type, vertical or horizontal, non-agitating pressure vessel, used for processing foods packaged in hermetically sealed containers. Generally containers are stacked into racks, baskets or trays for loading and unloading the retort. The high temperatures required for commercial sterilization are obtained from steam or superheated water under pressure.

Agitating retorts: Mechanical agitation is frequently used to enhance heat transfer, by increasing the rate of heat transfer into the product being processed. Some common types of agitation used are shown in Figure 2.3 (Adapted from Parchomchuk, 1977). Agitating or rotary retorts provide product agitation during processing, especially with liquid or liquid/particle mixtures. The continuous container handling type of retorts are constructed of two cylindrical shells in which processing and cooling take place, and cans are subjected to axial rotation. The shell can be used for pressure processing in steam or cooling with or without pressure. Other retorts are batch type pressure vessels which offer both axial and end-over-end rotation. The heating medium can be steam, water spray or full-water immersion with air-overpressure. In another rotating method of agitation (Parchomchuk, 1977) the cans are rotated in a circular path (Figure 2.3) in such a way that the can orientation remains fixed. Agitation forces similar to those end-over-end agitation are produced in this system.

Thermally processed foods in thin-profile packages, such as retort pouches and semi-rigid plastic containers are becoming popular. During thermal processing, internal pressures of such containers may exceed the saturation pressure of the steam because of the presence of residual air (internal pressure = air pressure + water-vapor pressure at the retort temperature). Also during the cooling cycle, the internal pressure may be considerably higher than the external pressure, especially when cooling water collapses the steam, resulting in a sudden pressure drop in the retort. This may cause serious deformation of containers, loss of seal integrity or even explosion of containers, if the internal pressure is not properly counterbalanced with an external pressure. Compressed air is generally used to provide the counterbalancing overpressure.

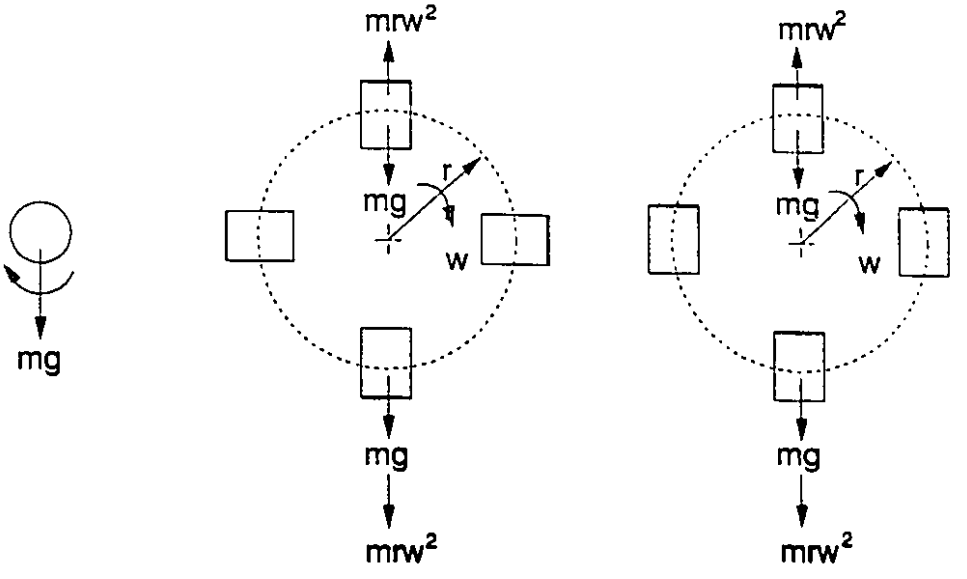

Figure 2.3 Schematics of different types of can rotation (Source: Parchomchuk, 1977)

Heating of foods in cans

Heat energy is transferred by conduction, convection and radiation. In the retort used in canning, conduction and convection are important. From the heat transfer point of view, foods can be divided into three categories, (i) solid foods heated by conduction e.g. tightly packed fruits, vegetables or meats; (ii) liquid foods heated by convection, e.g. milk, soups; and (iii) liquid foods with suspended solid food particles, where heat is brought to the particle surface by convection and then further transmitted to the particle center by conduction, e.g. vegetables in brine, fruits in syrup, meat or vegetables thin broth and soups. In liquid or liquid/particulate foods the rate of heat penetration, into the material in the can, is increased by agitation of the can. This has facilitated the use of the high temperature short time (HTST) approach. The benefits include a better quality of final product and a potential increase in the capacity of processing plant.

The kinetics of thermal destruction of microorganisms and time-temperature data, at the slowest heating location of the product in the can, are required to establish the thermal process schedule. The time-temperature data can be obtained experimentally using devices that monitor the change in temperature of the heating food. Such determinations are achieved with a temperature sensor located in the product at the slowest heating region of the container. Numerous experimental studies have been carried out to understand the time-temperature relationships for different types of pure conduction or convection heating foods. In comparison, there have been fewer experimental studies on liquid/particle systems. Thus, the data obtained are specific in nature valid for the type of food, its formulation, the container size in which it is processed and the kind of retort system used. Such data cannot be easily generalized and may sometimes be difficult to carry out experimentally under certain processing conditions.

The product time-temperature data at the slowest heating point of the container can also be obtained using mathematical models. The models can be valuable in the design, optimization and validation of thermal processing of foods (Clark, 1978). Appropriate models are important for reducing the number and cost of experiments required to achieve product safety and quality. Several studies have been presented on the use of mathematical modelling and computer simulations for conduction heated foods. Teixeira

et al. (1969a, b) were probably the first to use computer simulation for quality optimization. They used a finite difference solution for conduction heat transfer equations of cylindrical cans, coupled with kinetic data on nutrient degradation. Since then, several researchers have used such models for predicting optimal conditions for thermal processing of foods (Saguy and Karel, 1979; Ohlsson, 1980; Thijssen and Kochen, 1980; Hendrickx et al., 1989, 1993, Ramaswamy and Ghazala, 1990; Ghazala et al, 1991; Silva et al., 1992).

The convective (natural or forced) heat transfer to pure liquids has been modelled using the equations of continuity, motion and energy. These three equations have been solved for selected boundary conditions, for several heat transfer problems. However, a mathematical solution of these equations, for temperatures within the can as a function of time and position, is more complex. This is due to the lack of appropriate mathematical models for the temperature and velocity distribution of the randomly moving liquid within the agitating can (Rao and Anatheswaran, 1988). Detailed spatial variations of temperature and velocity are often neglected due to the complexities of a theoretical or experimental study, and the presence of fairly uniform temperatures inside the agitated container,. Instead, a bulk mean temperature is often measured and the overall heat transfer coefficient (U) between the heating medium and can liquid is calculated, using the equation of energy balance on the can:

$$U A_c (T_R - T_l) = m_l C_p \left(\frac{dT_l}{dt}\right) \qquad (2.9)$$

where T_f is the bulk mean temperature of the liquid in the container, T_R is the temperature of the heating medium, A_c is the container surface area, m_f is the mass of the can liquid, and C_p is its specific heat. The initial condition is usually the uniform temperature of the liquid:

$$T = T_i \qquad \text{at} \quad t = 0 \qquad (2.10)$$

The solution of Eq. (2.9) with the initial condition gives:

$$\left[\frac{T_R - T}{T_R - T_i}\right] = e^{-\left(\frac{UA}{mC_p}\right)t} \tag{2.11}$$

which can also be written in the form:

$$\log\left[\frac{T_R - T}{j(T_R - T_i)}\right] = -\frac{t}{f} \tag{2.12}$$

where j is defined as the lag factor (j=1 for liquids) and f is the heating rate index ($f = mC_p/2.303UA$). Thus, a plot of $\log[(T_R-T)/(T_R-T_i)]$ vs t would be a straight line characterized by the slope of (-1/f) and intercept j.

The presence of solid particles in the liquid results in a complex heat transfer system. The liquid and particles in the container need to be sterilized. Typical temperature profiles are shown in Figure 2.4. In the presence of particles, an additional critical parameter is the convective surface heat transfer coefficient between the fluid and the particles (h_{fp}). The temperatures of the particles are given by:

$$\frac{\partial T}{\partial t} = \alpha_p \nabla^2 T \tag{2.13}$$

with the boundary condition:

$$-k_p \frac{\partial T}{\partial n} = h_{fp} (T - T_i) \tag{2.14}$$

where α_p and k_p are the thermal diffusivity and conductivity of the particle, respectively. The temperature gradient $\partial T/\partial n$ is along the normal direction to the surface. The h_{fp} can be back-calculated if the particle and liquid transient temperatures are available. The analytical solution of Eq. (2.13), with a convective boundary condition, is complex due to time-varying liquid temperatures. Studies on the measurement of h_{fp} are limited due to difficulties in measuring of the randomly moving particles without affecting their motion.

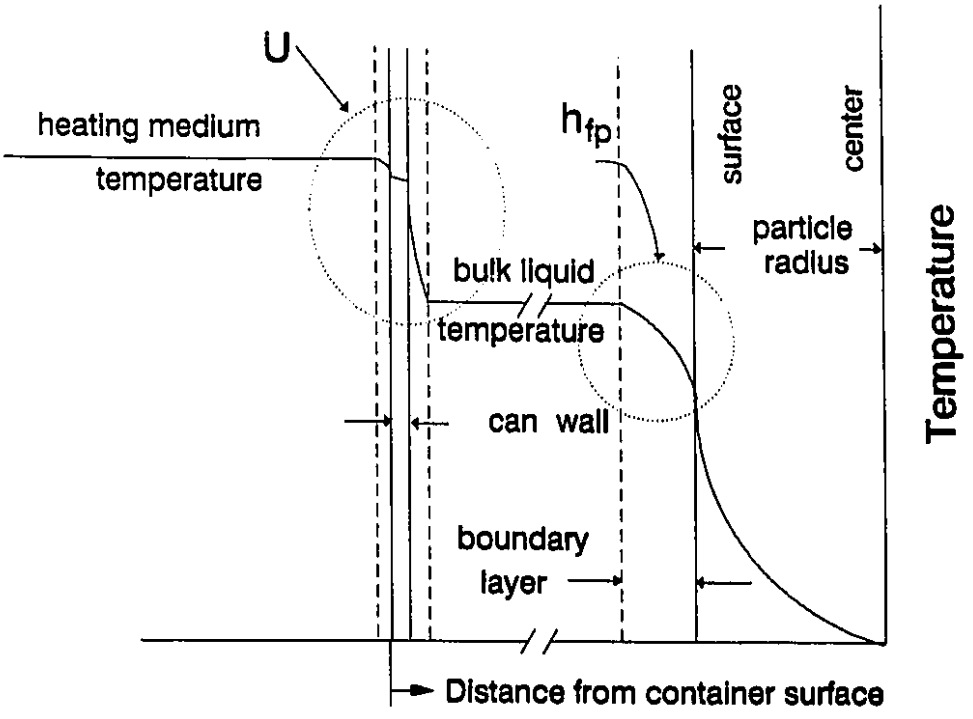

Figure 2.4 Typical temperature profile from heating medium to particle center in a canned liquid/particle system showing heat resistance at particle surface, at the internal and external can surfaces and in the can wall

Determination of U and h_{fp}

Accurate prediction of particle center temperature (coldest point, Figure 2.4) through mathematical models depends on how well U and h_{fp} data are estimated under simulated process conditions; where both system and product parameters are expected to be influencing factors. Traditionally, U and h_{fp} are determined from measurement of the temperature responses of the particle and liquid under well characterized initial and boundary conditions (Maesmans et al, 1992). Particle and liquid temperatures are generally measured using thermocouples. In real processing situations involving rotational retorts, the particle motions are expected to be influenced by centrifugal, gravitational, drag and buoyancy forces and hence, the associated U and h_{fp}. The particle, attached to a rigid thermocouple, will not simulate the particle motion during agitation processing, which in turn causes some deviations in the measured heat transfer coefficients. Recently, attempts have been made to monitor the temperature of the particle without inhibiting particle motion during agitation processing. Apart from difficulties in measuring the temperature of the moving particle, the mathematical solution, of the governing equation of the energy balance on the can (containing liquid and particles), is also complex due to the time variant temperature of the can liquid. Table 2.4 summarizes published methods to determine U and h_{fp} in liquid containing particles, in cans subjected to agitation processing, together with a description of experimental procedure and the mathematical solution. The procedures used for the determination of U and h_{fp} are classified into two groups, based on the motion of the experimental particle whose temperatures are monitored: (i) fixed particle and (ii) moving particle during agitation processing.

Mathematical procedures to determine U and h_{fp}

The fluid to particle heat transfer coefficient, h_{fp}, is determined using an inverse heat transfer approach, in which the boundary condition is determined using measured transient temperatures. The governing partial differential equations have to be solved; these describe the conduction heat flow inside the particle with appropriate initial and boundary conditions. Experimental data needed for this analysis are: the transient temperatures of both liquid and particle and thermo-physical properties of the particle. The

liquid bulk temperatures are measured using a needle-type copper-constantan thermocouple with its tip located at an appropriate location of the can, and a thermocouple, embedded into a pre-defined location in the particle, is used to monitor particle transient temperatures.

Table 2.4 Methods employed for determining U and h_{fp}, with canned liquid/particle mixtures, subjected to agitation processing

Reference	Motion of test particle	Particle temperature measurement	Mathematical procedure
Lenz and Lund (1978)	restricted	particle center	Lumped capacity Duhamel's theorem
Hassan (1984)	restricted	particle surface	Integration of overall energy balance equation
Lekwauwa and Hayakawa (1986)	restricted	particle center	Empirical formulae containing f and j, Duhamel's theorem
Deniston et al., (1987)	restricted	particle surface	Integration of overall energy balance equation
Fernendez et al., (1988)	restricted	particle center	Lumped capacity Duhamel's theorem
Stoforos and Merson (1990)	free	only liquid temperature needed	Analytical solution in the Laplace transform plane
Stoforos and Merson (1991)	free	particle surface liquid crystal	Using Integration of overall energy balance equation
Weng et al. (1992)	free	indirect, accumulated process lethality at center	Numerical solution of heat conduction equation with convective boundary condition

The overall thermal energy balance on a particulate-liquid food system is used to calculate associated convective heat transfer coefficients. The governing equation for heat transfer in such systems can be written as (all symbols are detailed in nomenclature):

$$U A_C (T_R - T_l) = m_l c_{pl} \frac{dT_l}{dt} + m_p c_{pp} \frac{d<T_p>}{dt} \qquad (2.15)$$

The following are assumed in the solution of the Eq. (2.15): uniform initial and transient temperatures for the liquid, constant heat transfer coefficients, constant physical and thermal properties for both liquid and particles, and no energy accumulation in the can wall.

The second term on the right side of the Eq. (2.15) is equal to the heat transferred to particles from liquid through the particle surface:

$$m_p C_{pp} \frac{d<T_p>}{dt} = h_{fp} A_p (T_l - T_{ps}) \qquad (2.16)$$

It is also assumed that the particle receives heat only from the liquid and not from the can wall when it impacts, i.e. heat is transferred first from the can wall to liquid and then to particle. For example, the heat flow in a spherical particle immersed in liquid can be described by the following partial differential equation:

$$\frac{\partial T}{\partial t} = \alpha_p \left(\frac{\partial^2 T}{\partial r^2} + \frac{2}{r} \frac{\partial T}{\partial r} \right) \qquad (2.17)$$

The initial and boundary conditions are :

$$T(r,0) = T_i \qquad \text{at} \quad t = 0 \qquad (2.18)$$

$$\frac{\partial T(0,t)}{\partial r} = 0 \qquad \text{at} \quad t > 0 \qquad (2.19)$$

$$k_p \frac{\partial T}{\partial r} = h_{fp} (T_l - T_{ps}) \qquad \text{at} \quad r = a \qquad (2.20)$$

The solution of Eqs. (2.15) to (2.20) is complex because of time dependent liquid temperatures.

Experimental procedures with restricted particle motion

Lenz and Lund (1978) developed a numerical solution using the 4th-order Runge-Kutta method and Duhamel's theorem to determine U and h_{fp} for the low Biot number (<0.1) situation. They measured the transient temperatures of a lead particle fixed at the geometric center of the can with liquid moving around it, and verified that the lead particle quickly approached one temperature at all the points. Assuming that the retort temperature instantly reached its operating condition, they proposed the following solution of Eq. (2.17) for the temperature at any position in the particle:

$$\left[\frac{T_R - T}{T_R - T_i}\right] = \frac{2\,Bi}{(r/a)} \sum_{n=1}^{\infty} \left(\frac{\beta_n^2 + (Bi-1)^2}{\beta_n^2 + Bi(Bi-1)} \right) \frac{\sin\beta_n}{\beta_n^2} \sin\beta_n\,(r/a)$$

$$X \quad \left[\exp(-\tau_p t) + \left(\frac{\tau_p}{\tau_p - \tau_l} \right) [\exp(-\tau_l t) - \exp(-\tau_p t)] \right] \qquad (2.21)$$

They estimated the h_{fp} by minimizing the sum of the squared deviations between measured and predicted particle temperature profile. They also obtained the equation for the particle average temperature from the above Eq. (2.21), and used it in Eq. (2.15) to calculate the overall heat transfer coefficient.

Hassan (1984) derived the following equations for U and h_{fp} by integrating Eqs. (2.15) and (2.16), respectively allowing heating time to approach infinity ($<T_p(\infty)> = T_l(\infty) = T_R$):

$$U = \frac{m_l C_{pl}}{A_c} \frac{T_R - T_{li}}{\int_0^\infty (T_R - T_l)\, dt} + \frac{m_p C_{pp}}{A_c} \frac{(T_R - T_{pi})}{\int_0^\infty (T_R - T_l)\, dt} \qquad (2.22)$$

$$h_{fp} = \frac{m_p C_{pp} (\langle T_p \rangle_{final} - \langle T_p \rangle_{initial})}{A_p \int_0^\infty (T_l - T_{ps})} \qquad (2.23)$$

For cans subjected to end-over-end rotation, Lekwauwa and Hayakawa (1986) developed a model using an overall heat balance equation in combination with an equation for transient heat conduction in a particle. They considered the probability function representing the statistical particle volume distribution. The temperature distribution for individual particles was obtained using Duhamel's theorem and empirical formulae describing the heat transfer to spherical, cylindrical or oblate spheroidal-shaped particles in a constant temperature liquid. In their numerical solution, they assumed that within each time step the liquid temperature was a linear function of time, the coefficients of these functions being determined iteratively such that the resulting particle and liquid temperatures satisfied the overall heat balance equation.

Deniston et al. (1987) used Eqs. (2.22) and (2.23) to determine U and h_{fp} in axially rotating cans. In their experiments, heating time was sufficiently long to allow liquid and particle average temperatures to reach the heating medium temperature to satisfy infinite time limits in the above equations. They measured the transient temperature at the particle surface using rigid-type thermocouples. They recognized the difficulties and errors associated with the measurement of the surface temperatures.

Fernendez et al. (1988) determined the convective heat transfer coefficients for bean-shaped particles, in cans processed in an agitated retort. They preferred a high conductivity material aluminium, to give a low Biot number (Bi < 0.01) condition and used the lumped capacity method for U and h_{fp} evaluation. They measured time-temperature data for both the liquid and particle using rigid-type thermocouples and used the scheme developed by Lenz and Lund (1978) to solve heat balance equations.

Recently, Stoforos and Merson (1995) proposed a solution to the differential equations governing heat transfer to axially rotating cans containing liquid/particle mixtures. They used an analytical solution, Duhamel's theorem for particle temperature and a numerical solution based on the 4th order Runge-Kutta scheme for the liquid temperature. The solution avoided the need for empirical formulae or a constant heating medium within short time intervals. Their comparison between predicted values and experimental data from Hassan (1984) showed good agreement for liquid temperature; however, it deviated for particle surface temperatures.

Experimental procedures allowing particle motion

From liquid temperature only: Stoforos and Merson (1990) used a mathematical procedure requiring only the measurement of liquid temperature to estimate U and h_{fp} in axially rotating cans. They solved an overall energy balance equation (Eq. 2.15) for a can and the differential equation for a spherical particle with appropriate initial and boundary conditions (Eqs. 2.17-2.20). Since can liquid temperature depends on both U and h_{fp}, by systematically varying these coefficients and minimizing the error between experimental and predicted liquid temperatures (in Laplace plane), they estimated the U and h_{fp}. This method allows for free movement of particles. The authors reported that calculated h_{fp} values did not always coincide with those determined from particle surface temperature measurements.

Liquid crystal: Stoforos and Merson (1991) extended the solution procedure for the overall energy balance of the can for finite heating time, previously used by Hassan (1984) to determine U and h_{fp}. They used a liquid crystal, which changes color with temperature, as a sensor to monitor the particle surface temperature. The method involved coating the particle surface with an aqueous solution of liquid crystals, videotaping of the color changes on the particle surface as a function of temperature, and comparing it with standard color charts after calibration. This method does not impose any restriction on particle motion, while monitoring the particle temperature during can rotation. They measured the liquid temperatures using rigid thermocouples for finite heating time, and exponentially extrapolated it to obtain liquid temperature data for "long time"

approximation of heating time in the solution equation (Eq. 2.21). They used an iterative procedure to calculate the average particle temperature, required in the solution equation for h_{fp} calculation. By using the first term approximation to the series solution, for average particle temperature ($<T_p>$) as a function of particle surface temperature and Biot number, (Stoforos, 1988) they obtained an analytical expression. Initially, as a first approximation h_{fp} was estimated by assuming $<T_p(t)> = T_{ps}(t)$ in Eq. (2.22), the particle average temperature was obtained from analytical expression. This value for average particle temperature was substituted into Eq. (2.22) to find an improved value for h_{fp}. The authors reported that one or two iterations were usually enough for convergence. However, they cautioned that the first term approximation in the expression of particle average temperature was limited to low particle thermal diffusivity materials, and suggested that for a high thermal diffusivity particle $<T_p(t)> = T_{ps}(t)$ may be a good assumption. The experiments were carried out between the temperature range of 20 to 50 °C.

Time Temperature Integrator (TTI): The combined use of time temperature indicator (TTI) has been proposed in the form of microorganisms, chemicals or enzymes and a mathematical model to determine convective heat transfer coefficient. In this approach, a particle loaded with indicator at the center can be processed without affecting its motion in real processing conditions. The process lethality received by a particle during processing can be calculated from TTI's initial (N_o) and final (N) status:

$$F_{TTI} = D_{ref} \log\left(\frac{N_o}{N}\right) \qquad (2.24)$$

By using heating liquid temperature and assuming a constant h_{fp}, a time-temperature profile at the particle center can be generated using a mathematical model and F_{model} could calculated:

$$F_{model} = \int_0^t 10^{\frac{(T - T_{ref})}{z}} dt \qquad (2.25)$$

The h_{fp} is estimated by minimizing the difference between F_{TTI} and F_{model}. Hunter (1972) and Heppel (1985) were the first to use this approach and used microorganisms suspended

in beads to back calculate the convective heat transfer coefficients, during continuous sterilization. Weng et al. (1992) used a time-temperature integrator, in the form of immobilized peroxidase, and determined the heat transfer coefficients in cans at pasteurization temperatures. A polyacetal sphere loaded with the indicator at the center, was hooked onto a thermocouple and placed at the geometric center of a can. They calculated the time-temperature history and associated lethality from the equation of the heat conduction, with assumed h_{fp} and known thermo-physical properties, using an explicit finite difference method. The h_{fp} was modified and lethality re-calculated until the difference between the predicted and actual lethalities fell within a tolerance limit. The authors named this approach as Least Absolute Lethality Difference (LALD) method. They also gathered the transient temperature data for liquid and particle, during heating and cooling in the same experiments, and estimated the h_{fp} by minimizing the sum of the squared of the temperature difference (LSTD) between measured particle center temperature and predicted center temperature, using the mathematical model. Maesmans et al. (1994) studied the feasibility of this method and the factors which can affect the choice of this methodology. Since these factors can influence the measurement of h_{fp}, care is necessary in the design of experiments to obtain accurate results with this method (Maesmans et al., 1994).

Factors affecting heat transfer coefficients

Mechanical agitation of cans in a rotary retort enhances heat transfer rates to both liquid and particle, and has the potential to improve the quality retention, compared with those foods processed in a still retort. Few studies have dealt with the determination of U and h_{fp} in thermal processing of liquid canned foods containing particles. Several studies have been published on liquid foods thereby evaluating the effect of system and product parameters on U (Quast and Siozawa, 1974; Duquenoy, 1980; Naveh and Kopelman, 1980; Soule and Merson, 1985; Anantheswaran and Rao, 1985a, b; Rao et al., 1985), and this has been presented in a review article by Rao and Anantheswaran (1988). Hence, the discussion related to parameter effects on U are not replicated. Some studies on convective heat transfer in the presence of particles have also been carried out, but

they only focused on the liquid portion of the canned food, thus determining the effects of system and product parameters on U, again in the presence of solid particles (Berry et al., 1979; Berry and Bradshaw, 1980, 1982; Berry and Dickerson, 1981). Table 2.5 shows a summary of published data on U and h_{fp} in canned liquid/particle mixtures, as influenced by system conditions and liquid/particles properties.

Rotational speed: The influence of rotational speed on heat transfer rates of liquids (either only liquids or in the presence of the particles) and the resulting decrease in sterilization times has been very well documented in early literature. Since h_{fp} is needed to predict the time-temperature profiles of particles processed in a rotary retort, it is important to quantify the effect of rotation speed. Lenz and Lund (1978) determined the effect of rotational speed on U and h_{fp} with axially rotating cans at 121 °C. Both U and h_{fp} increased with an increase in reel speed in all processing conditions. On average, U increased by 33% and h_{fp} increased by 44% with real speed increasing from 3.5 to 8 rpm. The rotational speed effects were more pronounced at lower particle concentration than at higher particle concentration. Hassan (1984) measured the convective heat transfer coefficients with Teflon, aluminum and potato spheres in a single can, axially rotating in a simulator. Varying the can speed from 9.3 to 101 rpm had more effect on U than on h_{fp}. In the case of 34.9 mm diameter potato spheres with 30% particle concentration and 25.4 mm diameter Teflon spheres with 20% particle concentration, both immersed in water, h_{fp} was reported to be highest at the lowest rotational speed (9.3 rpm), intermediate at the highest rotational speed (101 rpm) and lowest at the intermediate rotational speed (55.5 rpm) (Maesmans et al., 1992).

Deniston et al. (1987) found that U increased about 1.2 to 2.0 times with increasing rotational speed from 9.3 to 101 rpm. The rotational speed effects were more pronounced with the larger size particle. However, the h_{fp}s determined were rather insensitive to these rotational speeds. The authors attributed this to small relative particle to liquid velocity because of: (i) restricted movement of the particle attached to a rigid thermocouple, (ii) particle settling due to gravity was minimal since liquid and particle densities were close, and (iii) since the particle was located at the center, centrifugal force acting on it was small. Stoforos and Merson (1992) indicated that increasing rotational

Table 2.5 Published data on overall heat transfer coefficient (U) and liquid to particle heat transfer coefficient (h_{fp}), with canned liquid/particle mixtures, subjected to agitation processing

Particle diameter (mm)	particle concentration (% v/v)	Liquid	Rotational Speed (rpm)	U (W/m^2 K)	h_{fp} (W/m^2 K)
Lenz and Lund (1978)					
Lead (spheres)					
9.5	single	water	3.5-8.0	732-970	522-534
20.7	single	water	3.5-8.0	732-970	1527-1175
30.2	single	water	3.5-8.0	732-970	2084-1811
9.5	single	60% sucrose	3.5-8.0	562-709	948-1175
20.7	single	60% sucrose	8.0	562-709	539
30.2	single	60% sucrose	3.5-8.0	562-709	698-761
9.5	68%	water	3.5-8.0	210-330	341-659
20.7	59%	water	3.5-8.0	-	1260-1453
30.2	55%	water	3.5	-	1550
9.5	68%	60% sucrose	3.5-8.0	170-244	534-818
20.7	59%	60% sucrose	3.5-8.0	-	431-488
30.2	55%	60% sucrose	3.5-5.5	-	1198-1096
Hassan (1984)					
Potato (spheres)					
22.2	-	water	9.3-101	-	142-165
28.6	-	water	9.3-101	-	126-98
34.9	-	water	9.3-101	-	120-105
Teflon					
25.4		water	9.3-101	-	84-75
12.7		50 cst	9.3-101	-	56-108
12.7		350 cst	9.3-101	-	54-105
38.1		50 cst	9.3-101	-	37-39
38.1		350 cst	9.3-101	-	32-34
Aluminium					
19.1		1.5 cst	9.3-101	-	307-735
19.1		50 cst	9.3-101	-	139-362
19.1		350 cst	9.3-101	-	103-275
25.4		1.5 cst	9.3-101	-	204-468
25.4		50 cst	55.5-101	-	227-280
25.4		350 cst	9.3-101	-	100-242

Table 2.5 ...Continued

Particle diameter (mm)	particle concentration (% v/v)	Liquid	Rotational Speed (rpm)	U (W/m^2 K)	h_{fp} (W/m^2 K)
31.7		1.5 cst	9.3-55.5	-	277-464
31.7		50 cst	9.3-55.5	-	263-387
31.7		350 cst	9.3-55.5	-	308-480
Lekwauwa and Hayakawa (1986)					
Potato (spheroidal)		water	13	113-1704	60-2613
Deniston et al. (1987)					
Potato (spheres)					
22.2	29.3	water	9.3-101	1040-2300	177-200
28.6	29.3	water	9.3-101	1170-3000	135-163
35.0	29.3	water	9.3-101	950-2870	133-140
28.6	10.7	water	29.1	1300	175
28.6	18.7	water	29.1	1450	176
28.6	40.0	water	29.1	1640	190
28.6	45.3	water	29.1	1610	146
28.6	50.6	water	29.1	1360	127
Stoforos and Merson (1992)					
Aluminium (spheres)					
25.4		water	52.6	201	1155
25.4		1.5 cst	9.3	-	128.7
25.4		1.5 cst	52.9	142	1191-1296
Teflon (spheres)					
25.4		water	9.3	-	712
25.4		water	53.1	192	1406
25.4		1.5 cst	54.1	134	1826-1933
25.4		350 cst	54.5	83	2071
25.4		350 cst	100	90	410
Potato (spheres)					
25.4		water	9.3	-	233

- not available

speed from 15.5 to 100 rpm increased U from 55.2 to 83.0 W/m^2 K. With Teflon spheres, heated in silicone oil at 50 °C, they found a tremendous drop in the h_{fp} from 2071 to 410 W/m^2 K with increasing rotational speed from 54.5 to 100 rpm. This was attributed to lower relative particle to liquid velocity at higher rotational speeds. Their particle motion study revealed that at increased rotational speeds, the high density Teflon particles moved as a solid body due to larger centrifugal forces. Fernendez et al. (1988) studied the effects of various parameters on convective heat transfer in axially rotating cans containing liquid and particles and presented the results in the form of dimensionless correlations. The Nusselt number (based on h_{fp}) improved with increasing Reynolds number (based on rotational speed).

Liquid viscosity: Higher liquid viscosity retards heat transfer because the decreased turbulence lowers the effective particle to liquid velocity. Lenz and Lund (1978) found that increasing liquid viscosity significantly lowered the U and h_{fp} values under the same processing conditions. On average, the convective heat transfer coefficients were lower by about 30% for particles processed in a 60% aqueous sucrose solution, than for particles processed in water. Hassan (1984) reported that convective heat transfer coefficients with Teflon particles were lowered with increasing liquid viscosity [water, silicone oil 1.5, 50 and 350 centistokes (cst)]. Similar trends were observed with aluminium particles, except that for 31.7 mm diameter particles higher h_{fp} values were found with 350 cst oil than 1.5 and 50 cst silicone oil. Stoforos and Merson (1992) observed that U decreased at increased liquid viscosity; however, opposite trends were found with h_{fp}. Their particle motion study showed that particle to liquid relative velocity increased at higher liquid viscosity (from water to silicone oil of 1.5, 50 and 350 cst) and that h_{fp} increased with the more viscous liquids.

Particle concentration: The presence of particles in canned liquid may influence the flow pattern and level of mixing and, thus, the heat transfer coefficients. The particles are expected to cause secondary agitation, thus contributing to a mixing of can contents due to their motion. However, higher particle concentrations may influence the velocity gradient surrounding each particle. Stoforos and Merson (1992) observed that particle motion contributed to homogeneous temperature distribution in the can. Lenz and Lund

(1978) observed that adding multiple particles to pure liquid decreased the U values in both water and 60% aqueous sucrose solution. Their data indicated that higher particle concentrations also decreased the h_{fp}. Hassan (1984) observed that for 25.4 mm diameter Teflon spheres, h_{fp} improved with an increase in particle concentration from 20 to 31%. Deniston el al. (1987) reported that U increased with increasing particle concentration up to a certain level, but then decreased. Similar trends were observed with h_{fp} at a lower magnitude.

Particle size: The particle size has significant effects on U and h_{fp}; however, no clear relationship has been established. Lenz and Lund (1978) showed that U in water and 60% aqueous sucrose solution increased with increasing particle size. Similar trends were observed with h_{fp} between lead particles and water; however, with a 60% aqueous sucrose solution U values were lowest with the medium size particle. Experimental data of Deniston et al. (1987), on U with water and potato spheres, showed no straightforward relationship with particle size. A small decrease in h_{fp} was observed with increasing particle size. Hassan (1984) showed that h_{fp} increased with decreasing particle size.

Any factor that affects the liquid mixing and particle motion affects the associated U and h_{fp}. The influence of can headspace and radius of rotation on U has been reported in the literature (Naveh and Kopelman, 1980). Temperature has a significant effect on liquid viscosity; thus, processing (retort) temperature may influence U and h_{fp}. The influence of these system parameters on U and h_{fp} in canned liquid/particulate system has not been studied. The particle shape may influence the flow field around the particle and liquid mixing and, thus, U and h_{fp}. The particle settling velocity in liquid may also be affected by liquid to particle relative density and, hence, the resulting heat transfer coefficients. The effect of such product related parameters on U and h_{fp} have also not been quantified.

Flow visualization

In a flow visualization study the flow patterns of a liquid are evaluated to characterize the development of flow. Such techniques can be used to improve the understanding of physical processes related to fluid mechanics. Flow visualization

methods are often used to derive the qualitative information of the flow process; however, with the availability of advanced measuring probes and improved optical methods, one can also obtain some quantitative data (Macagno, 1969; Merzkirch, 1987). The study of velocity profiles and flow patterns assists the understanding of associated heat transfer mechanisms within cans (Rao and Anatheswaran, 1988). Hiddink (1975) studied the flow pattern of liquids (75% glycerol, water and silicone oils) in cans during natural convection heating. In this study a particle-streak method was used to observe the flow patterns. Merson and Stoforos (1990) studied the motion of spherical particles in a liquid in axially rotating cans. They calculated the relative liquid to particle velocity from the idealized particle motion and liquid velocities. These velocities were used to predict heat transfer coefficients using dimensionless correlations. Subsequently, Stoforos and Merson (1992) attempted to relate particle motion to heat transfer in order to explain the decrease in fluid to particle heat transfer coefficient with increasing rotational speed and decreasing liquid viscosity. In general, particle properties such as particle concentration, size, shape and density may affect the liquid and particle motion/mixing within the cans subjected to agitation processing. The flow visualization study of canned liquid/particle mixtures, during agitation processing, help to reveal the particle motion/mixing behavior and to explain the differences in heat transfer coefficients under various processing conditions. Such flow visualization techniques have not been applied to canned liquid/particle mixtures, subjected to end-over-end processing.

Prediction models for U and h_{fp}

Dimensionless correlations: For the optimization of process design it is important to quantify the effects of various parameters on heat transfer coefficients. It is also meaningful to generalize these effects in order to broaden their scope for scale-up considerations. Dimensional analysis is a useful method to generalize experimental data in the form of dimensionless numbers, grouped from physical variables. This analysis gives more insight to the physical phenomena and can also be used for scale-up purpose. Thus, the convective heat transfer coefficient, in the form of a Nusselt number, is correlated with other dimensionless numbers e.g. Reynolds number, Prandtl number.

Earlier studies, focusing on only liquid foods, have reported correlations for U and this has been presented in a review article by Rao and Anantheswaran (1988). Little information is available on the use of dimensional analysis for canned a liquid/particle system. The Nusselt number (based on U) correlations with axially rotating cans have been developed by Lenz and Lund (1978) and Deniston et al. (1987). The only correlation for h_{fp} in cans with axial rotation was presented by Fernendez (1988). These correlations accounted only a small number of variables within their limited ranges. No correlations have been reported for U and h_{fp} in cans with end-over-end in the presence of multiple particles.

Artificial neural network : An artificial neural network (ANN) is a computer based information processing technique which attempts to simulate the function of living nervous systems. ANN models are based on neurons similar to those in the brain and the synapses that connect them, thereby enabling the computer to simulate many of the brain's abilities. ANN models have the capability of correlating large and complex data sets without any prior knowledge of the relationship between them. In the past few years, neural networks have been shown to be more powerful than many other statistical methods, when solving nonlinear prediction problems (Bochereau et al., 1992). A major theoretical advantage of a neural network over statistical methods, such as multiple linear regression or principle component regression, is that neural network does not impose a linear relationship between factors and yield (Horimoto et al., 1995). In recent years, ANN has been the focus of interest in modelling problems in many areas including food and agricultural applications. ANN applications have been numerous: in sensory science (Galvin and Waldrop, 1990; Thai and Shelwfelt, 1991; Park et al., 1994; Tomlins and Gay, 1994); baking (Horimoto et al., 1995), rheology (Ruan et al., 1995); fuzzy control of twin-screw extrusion (Linko et al., 1992); image recognition analysis (Liao, 1993; Sayeed et al., 1995). No information is available on the use of a neural network model in thermal processing.

CHAPTER 3

DEVELOPMENT OF A METHODOLOGY TO MEASURE CONVECTIVE HEAT TRANSFER COEFFICIENTS IN CANNED LIQUID/PARTICLE MIXTURES, SUBJECTED TO END-OVER-END PROCESSING

ABSTRACT

A methodology was developed and standardized for the evaluation of convective heat transfer coefficients in canned liquid/particle mixtures subjected to end-over-end processing. The overall heat transfer coefficient, U, was determined using a lumped capacity heat balance approach and the fluid to particle heat transfer coefficient, h_{fp}, was determined from transient temperature data at the center of the particle, using a finite difference computer simulation. A polypropylene spherical particle (diameter = 19 mm) was suspended in a can filled with a high temperature bath oil using a flexible fine-wire (0.0762 mm) thermocouple attached to the can wall. The technique permitted the particle to move to any location within the can and also provided a fairly uninhibited heat transfer condition, due to the presence of one single particle in the entire can. To test the feasibility of the technique, four rotational speeds (0 to 20 rpm) were employed as variables in a water immersion rotary retort (Stock PR-900). U values varied from 118 to 195 W/m^2 K and h_{fp} values varied from 34 to 130 W/m^2 K depending on processing conditions. The measured h_{fp} values were higher with moving particles compared to those for a fixed particle. The method differentiated U and h_{fp} values at different rotational speeds.

INTRODUCTION

In recent years there has been a growing interest in mathematical modelling of heat transfer to particulate food systems. Appropriate models are important for reducing the number of experiments and costs required to achieve desired product safety and

quality (Maesmans et al., 1992). Agitation of the container in a rotary retort during processing offers several advantages over still-retort processing. Such advantages include: improved quality and shorter sterilization times, as a result of increased heat transfer rates. However, prediction of heat transfer rates of canned liquid food with suspended particles requires data on the fluid-to-particle heat transfer coefficient (h_{fp}) and the overall heat transfer coefficient (U) from heating medium to liquid. The majority of studies involve canned liquid foods without particles, thereby evaluating only U. Rao and Anantheswaran (1988) have presented an excellent review on convective heat transfer coefficient with liquid food processing.

Earlier studies on heat transfer in particulate food systems were mainly focused on the effect of various processing conditions, on the heating behaviour of food systems. Some researchers (Lenz and Lund, 1978 and Fernendez et al., 1988) measured the fluid to particle heat transfer coefficient using a metal particle, to give a low Biot number ($Bi<0.01$) condition and also used a lumped capacity method (Kreith, 1965) for h_{fp} evaluation. The errors, associated with the temperature measurement of the experimental particle in such situations, were negligible due to the prevailing small temperature gradients in the particle during processing. However, in the above studies the particle movement was completely restricted because it was secured in one location. The h_{fp}, however, depends on the relative velocity between particle and liquid which will be different when the particle is free to move. In such situations metal particles cannot be used, due to large density differences between metal and real food particles. Hassan (1984) and Deniston et al. (1987) used an overall energy balance approach to measure the h_{fp} in axially rotating cans. They recognized the difficulties and errors associated with the measurement of surface temperatures. Lekwauwa and Hayakawa (1986) presented a semi-theoretical method, which utilized Duhamel's theorem and empirical formulae, to analyze heat transfer in canned potatoes-in-brine during agitation processing. In these studies, motion of the experimental particle was completely restricted by a rigid thermocouple, used for temperature measurement. These studies suggest that an experimental procedure should be developed to allow some particle movement in the can during processing in order to obtain more realistic estimates of the h_{fp} value.

Recently, efforts have been made to measure h_{fp}, while allowing particle movement inside the can during agitation sterilization. Stoforos and Merson (1990) used a mathematical procedure, requiring only the measurement of liquid temperature to estimate h_{fp} and U. This method allows for free movement of particles. The authors reported that calculated h_{fp} values did not coincide with the those determined from direct particle surface temperature measurements. Maesmans et al. (1992) feared the uncertainty of the procedure because two parameters were estimated from one input parameter. Stoforos and Merson (1991) used liquid crystals to measure surface temperatures, as the particle moved freely in cans during axial rotation. However, the liquid crystals used in the study covered only a narrow temperature range (26 to 50 °C). Chandarana et al. (1990) suggested that heat transfer coefficients must be experimentally determined under conditions that approximate the actual situation. Recently, Weng et al. (1992) proposed the use of combined time temperature integrators (TTI) and a mathematical model to determine h_{fp} in liquid canned foods containing particles. Maesmans et al. (1994) studied the feasibility of this method and the various factors which can affect the choice of this methodology. Since various factors can influence the measurement of h_{fp}, care is necessary in the design of experiments to obtain accurate result with this method (Maesmans et al., 1994).

The objective of this study was to develop a methodology to measure the convective heat transfer coefficients (U and h_{fp}) associated with canned liquid/particle mixtures, subjected to end-over-end processing, by allowing the particle to move within the can during the process.

THEORETICAL BACKGROUND

In thermal processing of canned liquid/particle systems, the heat is transferred from the heating medium to liquid inside the cans and then to particles. An overall heat energy balance on such system can be used to calculate associated convective heat transfer coefficients. The governing equations for heat transfer in such systems have been detailed in the preceding section [Chapter 2; Eqs. 2.15 to 2.20, p 21-22]. They are reproduced for the sake of continuity (all symbols are detailed in nomenclature):

$$U\ A\ (T_R - T_l) = m_l\ C_{pl}\ \frac{dT_l}{dt} + m_p\ C_{pp}\ \frac{d<T_p>}{dt} \qquad (3.1)$$

The following are assumed for deriving the Eq. (3.1): uniform initial and transient temperatures for the liquid, constant heat transfer coefficients, constant physical and thermal properties for both liquid and particles, and no heat resistance at the outside can surface and can walls.

The second term on the right side the Eq. (3.1) is equal to the heat transferred from liquid through the particle surface:

$$m_p\ C_{pp}\ \frac{d<T_p>}{dt} = h_{fp}\ A_p\ (T_l - T_{ps}) \qquad (3.2)$$

It is also assumed that the particle receives heat only from the liquid and not from the can wall when it impacts, i.e. heat is transferred first from the can wall to the liquid and then to the particle. The transient heat flow in a spherical particle immersed in liquid can be described by the following partial differential equation (Ozisik, 1989);

$$\frac{\partial T}{\partial t} = \alpha_p \left(\frac{\partial^2 T}{\partial r^2} + \frac{2}{r}\ \frac{\partial T}{\partial r} \right) \qquad (3.3)$$

The initial and boundary conditions are:

$$T(r,0) = T_i \qquad \text{at}\ \ t = 0 \qquad (3.4)$$

$$\frac{\partial T(0,t)}{\partial r} = 0 \qquad \text{at}\ t > 0 \qquad (3.5)$$

$$k_p\ \frac{\partial T}{\partial r} = h_{fp}\ (T_l - T_{ps}) \qquad (3.6)$$

MATERIALS AND METHODS

Most food products undergo chemical changes during heating, resulting in some changes of their thermo-physical properties. In order to have constant property data for the purpose of evaluating heat transfer coefficients, a model liquid and particle were used in the present study. A high temperature bath oil (100 cst at 38 °C, Fisher Scientific Ltd., Montreal) and polypropylene spheres (Small Parts Inc., Miami, FL) of diameter 19 mm were used as the model liquid and particle, respectively. Thermo-physical properties for the liquid and particle were experimentally determined and are summarized in Table 3.1. The density of the polypropylene sphere was obtained from the volume of water displaced by the spheres and their weight; specific heat was measured using a calorimetric method. The thermal diffusivity of the polypropylene sphere was evaluated, using the heating rate index method, by heating it in a steam cabinet (Singh, 1982). The thermal conductivity of the particle was back-calculated from measured values of thermal diffusivity, density and specific heat. The oil density was obtained by measuring the volume using a pycnometer and the mass of the oil. The heat capacity of the oil was measured by comparing the heating rates of equal masses of oil and water for the same power input. The thermal conductivity of oil was measured using a conductivity probe (Ramaswamy and Tung, 1981).

Table 3.1 Physical properties of test materials used in this study

Marerial	Density (kg/m^3)	Heat capacity (J/kg K)	Thermal-conductivity (W/m K)	Thermal-diffusivity (m^2/s)
Polypropylene	830	1840	0.359	2.35×10^{-7}
Oil[a] (100 cst)	880	2210	0.165	-

[a] Kinematic viscosity = 1.0×10^{-4} m^2/s

A pilot-scale rotary, single cage, full-water immersion retort (Stock Rotomat-PR 900; Hermann Stock Maschinenfabrick, Germany) was employed for the experiments. A

common air-overpressure of 70 kPa was used for all test runs with the Rotomat. The cans were arranged in a vertical orientation (can axis perpendicular to axis of rotation) to give end-over-end rotation.

The can liquid temperature was measured at the geometric center of the cans, using CNS copper-constantan needle type thermocouples (Locking connector, C-10, Ecklund Harrison Technologies, Inc., Cape Coral, FL). For the purpose of measuring particle transient temperatures, a fine hole was drilled to the center of the spherical particle, which was filled with a 50%:50% mixture of epoxy resin and hardener, and a fine-wire (0.0762 mm diameter) copper-constantan thermocouple was inserted to the center. In this way, the trapping of air along the channel was minimized. The thermocouple equipped particle was mounted inside the can using a brass connector (stuffing box for plastic pouches C-5.2, Ecklund Harrison Technologies, Inc., Cape Coral, FL) at the half height of the can (Fig. 3.1). The length of the thermocouple wire inside the can was kept approximately equal to half the height of the can in order to allow particle movement inside the can. The thermocouples for test cans were passed through a 32- circuit slip-ring attached to the retort and connected to a data acquisition system [μ-MEGA 1050 remote intelligent measurement and control system (OM-1050), two 16-channel thermocouple/low level voltage expander boards (OMX-STB-TC) and a 5-V battery pack; all from Omega Engineering Corp., Stamford, CT]. Thermocouple signals were recorded at 15 s time intervals using *Labtech Notebook* software (Laboratory Technologies Corporation, Wilmington, MA).

Heat penetration tests, for the cans containing the test liquid and suspended particle, were conducted in the Rotomat. Cans of size 307 x 409 were closed with a 10 mm headspace. Only one particle per can was used. In each test, experimental cans (four replicates) were placed in the cage at the same diameter of rotation (38 cm) and the remaining space was filled with dummy cans. Experiments were conducted at four rotation speeds (0, 10, 15 and 20 rpm) at 120 °C, and each test was repeated two times.

In order to verify the temperature uniformity in cans during the processing (a fundamental assumption used in deriving the thermal energy balance on the can), needle type thermocouples of different lengths (#L1 = 42 mm, #L2 = 33 mm and #L3 = 21 mm)

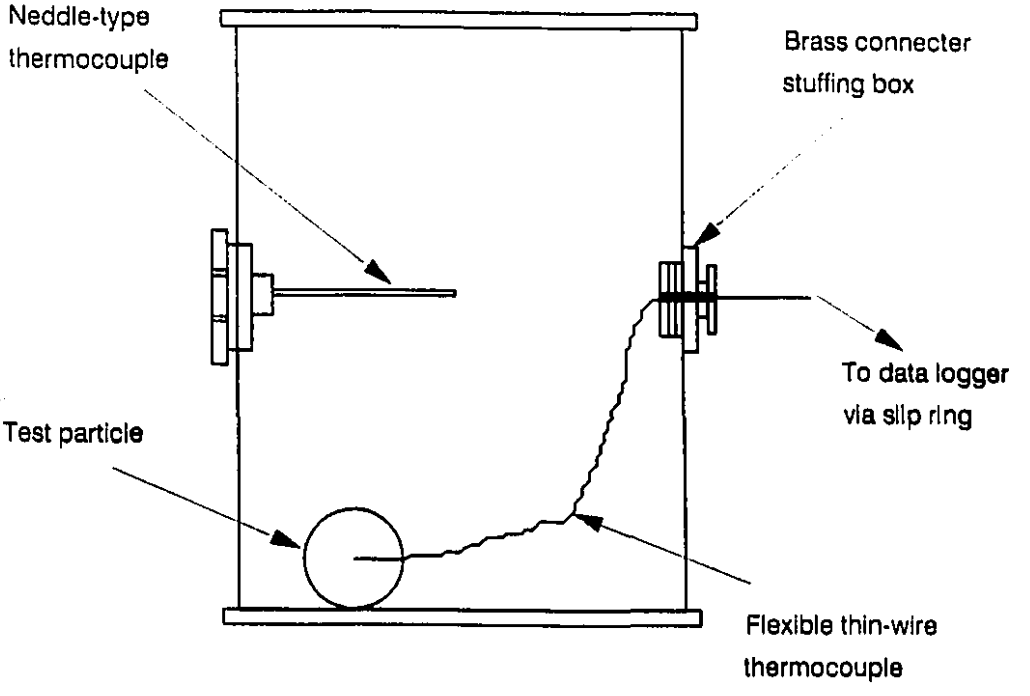

Figure 3.1 A schematic showing thermocouple equipped particle mounted inside the can using a brass connector

were mounted on each of two cans of size 307 x 409, at different heights (#H1 = 20 mm, #H2 = 56 mm and #H3 = 85 mm, from bottom of the can). These cans were processed at rotational speeds of 0, 10, 15 and 20 rpm at 120 °C.

In order to evaluate whether the flexible thermocouple technique gives h_{fp} data different from the fixed thermocouple technique, experiments were also carried out by fixing a particle to the tip of a rigid thermocouple at the geometric center of the can. In the case of restricted particle, experiments were carried out at four rotational speeds. All experiments were repeated twice.

Mathematical solution

In each experiment, the heating time was kept sufficiently long such that the liquid and particle temperatures equilibrated to the heating medium temperature. The equilibrated liquid and particle temperatures were corrected to match the heating medium temperature. Temperature data were discarded if thermocouple breakage occurred during runs (about 15% of test cans suffered thermocouple breakages due to the use of fine wire thermocouples). Since small differences in initial and retort temperatures were unavoidable, the data were, therefore, normalized to an initial temperature of 20 °C and the respective set point retort temperature (120 °C), according to a procedure detailed in Stumbo (1973).

A single particle, attached to a flexible and fine thermocouple wire, was used in these experiments. The amount of heat absorbed (second term in Eq. 3.1) by the particle, therefore, can be neglected when compared to the heat absorbed by the liquid. The heat transfer across the can wall will thus be equal to the heat absorbed by the liquid, resulting in an increase in its bulk temperature. The overall heat transfer coefficient can then be obtained using Eq. (3.7) (Ramaswamy et al., 1993):

$$U = \frac{2.303\ m_l\ C_{pl}}{f_h\ A_c} \qquad (3.7)$$

In order to determine h_{fp}, the partial differential equation with associated initial and boundary conditions was solved using a finite difference method. The Crank-Nicholson

scheme for space derivatives and a fully implicit scheme for time derivative were employed (Ozisik, 1989). The numerical procedure involved with the finite difference method is detailed in the appendix. Three different grid sizes (10, 20, 50) in the spatial direction were tried and finally a grid with 20 divisions was used in the analysis. Since the implicit finite difference method used here is free from stability constraints, the desired accuracy guided the choice of time increment and a 5 s-time step was used. The computer program was written in FORTRAN 77 to compute the transient temperature distribution in a particle for a given condition.

The inverse heat conduction approach, where surface heat flux is estimated using one or more measured temperatures histories inside a heat-conducting body, was used to estimate h_{fp} values. Two different approaches were used to determine the fluid to particle heat transfer coefficient (h_{fp}). In the first approach (Lenz and Lund, 1978), the h_{fp} value was obtained as the limiting value of heat transfer coefficient that minimizes the sum of the square of the difference between the experimental and predicted ***temperatures*** (LSTD); and in the second approach (Weng et al., 1992), it is taken as the limiting value of heat transfer coefficient that minimizes the difference between the measured and predicted ***lethality*** (LALD). A computer program developed to solve a set of finite difference equations could incorporate either of the approaches. The difference between measured and calculated lethality at the particle center (slowest heating point in liquid/particulate system), F_o, was finally used as an objective function (LALD approach), due to its relevance to thermal processing. The procedure involved initially comparing the calculated and measured lethality (or temperatures) at the center of the particle, based on an assumed h_{fp} value, and then subsequently changing h_{fp}, in a sequential pattern, until the calculated and measured lethality values (Eq. 3.8) matched a set value of 10 min.

$$F_o = \int_0^t 10^{\frac{(T - 121.1)}{10}} dt \qquad (3.8)$$

RESULTS AND DISCUSSION

Temperature profiles and temperature uniformity

Typical time-temperature profiles of the retort heating medium, can liquid, particle center (experimental and predicted) are shown in Fig. 3.2a and c. For the lethality values of 10 min at the particle center, temperatures predicted at the particle center (LALD) were lower than the experimental temperatures in the early part of the heating curve (below 90°C); however, during the later part, the predicted temperature showed a better match with experimental temperatures. This is due to the nature of the objective function F_o, used in the present case. The use of F_o as the objective function gives more weightage to higher temperatures, due to their higher contribution to lethality. This is more evident from the accumulated lethality plot. Experimental lethality, measured at the particle center, almost showed a perfect match with predicted lethality (Fig 3.2b). When the measured and predicted temperature at the particle center was used an objective function (LSTD), the predicted fluid to particle heat transfer coefficients (h_{fp}) were found be considerably higher. This approach tends to over-predict the lethality as shown in Fig. 3.2d. Since this situation can potentially lead to under-processing when employed for process design, the lethality approach was considered more appropriate and used for subsequent analyses.

Temperature uniformity in cans was measured in terms of heat penetration parameters, i.e. heating rate index, f_h and heating lag factor, j_{ch}. When the cans are processed in a still retort processing condition (0 rpm), the prevailing mode of heat transfer will be mostly natural convection. Hence, large temperature variations can be expected in cans. This was evident from the studies, as shown in Table 3.2, with large location dependent differences in f_h, j_{ch} and t_l (time for the curvilinear portion of the heating curve) values. The f_h value for location No. 1 (bottom center) was nearly double, when compared to location No. 3 which was at the top corner (85 mm height from bottom) of the can. The temperature gradients for liquid inside the cans were virtually nonexistent during agitation processing. This was supported by the small differences in heat penetration parameters between different locations under 10-20 rpm. The gradual

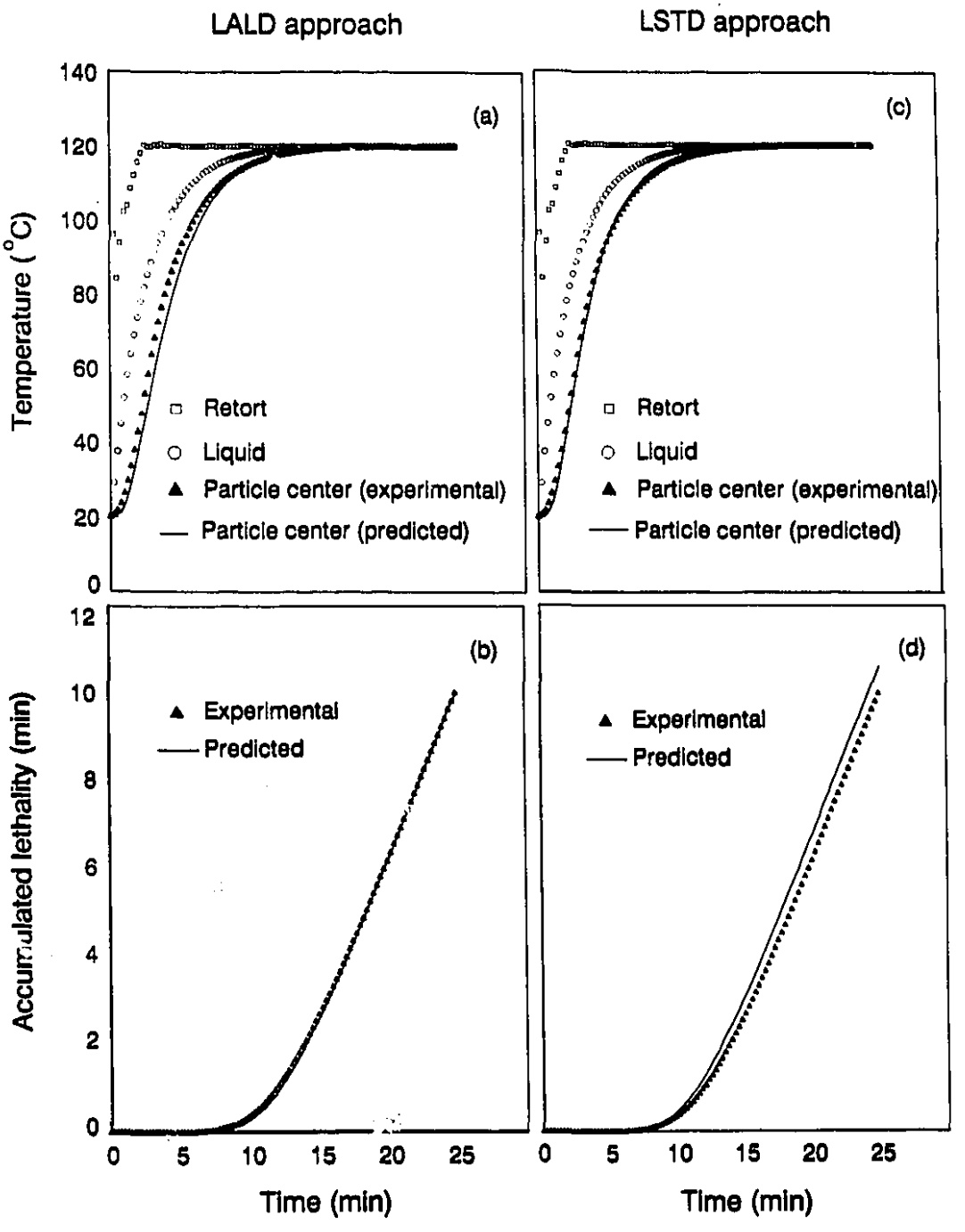

Figure 3.2 Typical experimental, predicted time-temperature profiles and lethality plots for the can processed at 120 °C retort temperature and 15 rpm rotational speed [prediction was based on two approaches: Least absolute lethality difference (LALD) and least squared temperature difference (LSTD)]

tightening of the temperature distribution, under different test runs, is shown as standard deviations in temperature with respect to time, in Fig. 3.3. Stabilizing to within 0.5 °C standard deviation occurred within 5 min under agitation processing, while it required about 20 min under still processing condition. An increase in rotational speed resulted in early stabilization, resulting in uniform temperature within the can (Fig. 3.3).

Table 3.2 Temperature uniformity of liquid within the can, processed at the retort temperature of 120 °C, at four rotational speeds

Rotational	Location 1			Location 2			Location 3			CoV	
speed (rpm)	f_h (min)	j_{ch}	t_l (min)	f_h (min)	j_{ch}	t_l (min)	f_h (min)	j_{ch}	t_l (min)	f_h (%)	j_{ch} (%)
0	8.00	1.55	3.0	6.69	1.29	1.50	4.20	1.04	0.5	-	-
	8.03	1.63	3.0	6.71	1.41	1.50	4.17	1.01	0.5	-	-
10	7.91	1.01	0.5	7.94	1.03	0.5	7.91	1.06	0.5	0.18	1.99
	7.89	1.02	0.5	7.98	1.06	0.5	7.81	1.09	0.5	0.88	2.71
15	6.22	1.16	0.5	6.19	1.12	0.5	6.19	1.16	0.5	0.23	1.64
	6.22	1.10	0.5	6.29	1.14	0.5	6.13	1.20	0.5	1.05	3.58
20	4.83	1.21	0.5	4.92	1.14	0.5	4.88	1.16	0.5	0.76	2.5
	4.95	1.12	0.5	4.96	1.16	0.5	4.84	1.20	0.5	1.16	2.82

CoV = Coefficient of variation (100 x standard deviation/mean)

Heat transfer coefficients with fixed vs moving particle

Since only one particle in each can was used, the overall heat transfer coefficient was not influenced by fixed and moving particle. With multiple particles in a can, restricting the motion of one particle probably may not influence the overall heat transfer coefficient. During agitated processing of cans, fluid to particle heat transfer coefficient values are expected to be more realistic and higher with moving particles as compared to those measured with restricted particle motion (Stoforos and Merson, 1992). In the present study, h_{fp} values were measured both with stationary and moving particles and they are summarized in Table 3.3. At all rotational speeds, h_{fp} values measured with the moving particle were higher compared to those measured with fixed particle.

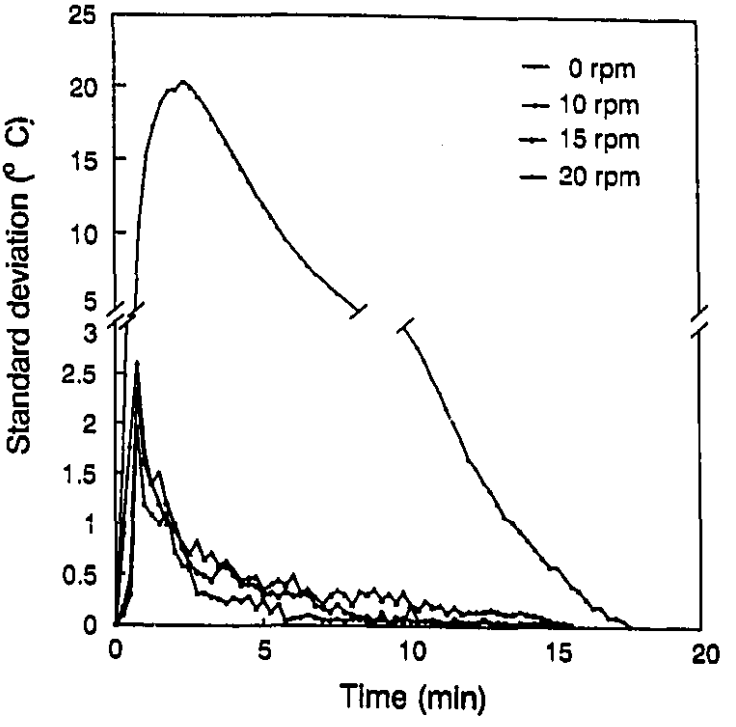

Figure 3.3 Standard deviations in temperature, as a function of heating time with respect to three thermocouple locations (42 & 20 mm; 33 & 56 mm; and 21 & 85 mm, from the can surface and bottom, respectively) in cans subjected to end-over-end processing at various rotational speeds (0 to 20 rpm)

Table 3.3 Mean heat transfer coefficients (U and h_{fp}), as influenced by rotational speed ($n \geq 3$)

Rotational speed (rpm)	Overall heat transfer coefficient (W/m^2 K)	Fluid to particle heat transfer coefficient	
		Fixed particle (W/m^2 K)	Moving particle (W/m^2 K)
0	126.3 (2.9)[1]	36.5 (3.2)	38.5 (1.1)
10	141.4 (2.9)	74.8 (6.0)	99.5 (1.5)
15	162.1 (2.9)	101.7 (3.8)	112.0 (8.8)
20	186.2 (2.6)	114.0 (3.3)	124.0 (4.8)

[1]The values in parentheses are the coefficients of variation (%)

Overall heat transfer coefficient (U)

The overall heat transfer coefficient between heating medium and can liquid (oil) was calculated using Eq. (3.7). The effect of rotational speed was determined on can liquid (Table 3.3). An increase rotational speed resulted in an increase in U values. The increasing effect of rotational speed on U could be attributed to the increased turbulence at higher rotational speeds. The average value of U for oil ranged between 118 to 195 W/m^2 K, depending upon experimental conditions.

Fluid to particle heat transfer coefficient (h_{fp})

The effect of rotational speed was determined on the fluid to particle heat transfer coefficient between oil and the polypropylene sphere (Table 3.3). The effect of rotational speed was similar to those observed with U. The overall range of h_{fp} values was 34 to 130 W/m^2 K. Hassan (1984) reported that h_{fp} between silicone oil (50 and 350 cst) and Teflon particles (12.7 to 38.1 mm diameter) were 31 to 108 W/m^2 K. On average, h_{fp} increased 4 times as the rotational speed increased from 0 to 20 rpm.

CONCLUSIONS

A methodology was developed for the measurement of convective heat transfer coefficients, in canned liquid/particle mixtures subjected to end-over-end processing. Temperature uniformity of liquid in cans was verified using heat penetration parameters and the standard deviation of temperature at different location at various rotational speeds. The lethality approach (LSTD) was found to be more appropriate for the estimation of the fluid to particle heat transfer coefficient. Higher h_{fp} values were obtained for the moving particle compared to that for the particle fixed at the can center, at all rotational speeds. The overall heat transfer coefficient for test liquid (oil) and fluid to particle heat transfer coefficient were influenced by rotational speed. End-over-end rotational processing (10-20 rpm) significantly improved both U and h_{fp} compared to still retort processing (0 rpm).

CHAPTER 4

CONVECTIVE HEAT TRANSFER COEFFICIENTS AS INFLUENCED BY SYSTEM AND PRODUCT PARAMETERS : A. STUDIES WITH A SINGLE PARTICLE IN THE CAN

ABSTRACT

The effects of various system and product parameters on forced convection heat transfer in cans were studied experimentally during end-over-end rotation. Cans filled with water or oil, and fitted with a single spherical particle (diameter = 19 mm) suspended using a flexible fine-wire thermocouple, were processed in a water immersion rotary retort (Stock PR-900). The effect of system parameters on the associated heat transfer coefficients were examined using the methodology detailed in Chapter 3. Such parameters included: retort temperature (110 to 130 °C), rotational speed (0 to 20 rpm), radius of rotation (0 to 27 cm) and can headspace (6.4 and 10 mm). The effects of product parameters such as density of particle and liquid viscosity on associated heat transfer coefficients were subsequently investigated at different rotational speeds (0 to 20 rpm), during end-over-end rotation of cans.

Higher heat transfer coefficients were obtained with increasing values of all four system variables, and the effects of rotational speed and headspace were more significant than those of retort temperature and radius of rotation. U values also improved with decreasing liquid viscosity and increasing rotational speed and the results were comparable to those reported in the literature. The h_{fp} values were affected in a similar fashion, increasing with rotational speed and density of particle and decreasing with liquid viscosity. The effect of particle density on h_{fp} was more significant than those of liquid viscosity and rotational speed. U values varied from 118 to 800 W/m^2 K and h_{fp} values varied from 23 to 825 W/m^2 K, depending on the operating conditions.

INTRODUCTION

Mathematical modelling of heat sterilization of canned liquids with suspended food particles in rotary autoclaves requires data on: (i) thermo-physical properties of both liquids and solid food particles and (ii) associated heat transfer coefficients. In such systems, both the overall heat transfer coefficient, U, and the fluid-to-particle heat transfer coefficient, h_{fp}, are needed to predict heat transferred to solid food particles. Little information is available on h_{fp} in cans during agitation processing, due to difficulties in monitoring the transient temperature of freely moving particles. Earlier studies reported h_{fp} values between a stationary particle, fixed on to a rigid thermocouple, and liquid moving around it. Recently, efforts have been made to measure h_{fp} while allowing some particle movement inside the can during agitation sterilization. Mechanical agitation of cans in rotary autoclaves enhances heat transfer rates to both liquid and particle, and has the potential of improving the quality retention, compared with those foods processed in still autoclaves. However, there is a need to quantify the effect of agitation and other parameters influencing U and h_{fp}.

The effect of various parameters on h_{fp} e.g. process temperature, rotational speed, liquid viscosity, particle properties and volume fraction occupied by the particles, etc. have been experimentally investigated by Lenz and Lund (1978), Sastry (1984), Deniston et al. (1987) and Fernandez et al. (1988). In these studies, motion of the experimental particle was completely restricted by a rigid thermocouple, used for temperature measurement at the particle center. Since the relative velocity between particle and liquid influences h_{fp}, its magnitude is expected to be different when the particle is free to move. Particle density effect has not been studied, since in most of the studies the experimental particle was fixed during rotation. Stoforos and Merson (1992) investigated the effect of liquid viscosity, particle properties and rotational speed on h_{fp} and U in axially rotating cans. They measured the surface temperature using liquid crystals, as the particles moved freely in the cans during agitation. However, the liquid crystals used in the study covered only a narrow temperature range (26 to 50 °C). Naveh and Kopelman (1980) studied the effect of the mode of agitation on U with liquid foods and found that U was

improved by two to three times in end-over-end agitation, compared to the axial mode of rotation.

In Chapter 3, a method was developed to measure the convective heat transfer coefficients in cans, during agitation processing using a flexible thermocouple technique. The objective of this study was to use this flexible thermocouple approach to quantify the effect of i) system parameters, such as retort temperature, rotational speed, radius of rotation and can headspace; and ii) product parameters such as particle density and liquid viscosity, on U and h_{ip}, during end-over-end sterilization.

MATERIALS AND METHODS

Given the temperature history at a known location inside a heat conducting body and can liquid, U and h_{ip} can be estimated by using an overall thermal energy balance on the can and the partial differential equation of transient heat flow in a body immersed in liquid, with appropriate initial and boundary conditions. The theoretical background and methodology involved with calculating the associated heat transfer coefficients are detailed in Chapter 3.

Test materials

Water and high temperature bath oil (100 cst at 38 °C, Fisher Scientific Ltd., Montreal) giving different viscosity levels, were used as test liquids. Spherical particles (diameter 19 mm) made of polypropylene, Nylon, Acrylic, Delrin and Teflon (Small Parts Inc., Miami, FL), covering a wide range of density (830 kg/m^3 to 2210 kg/m^3), were used as test particles. The thermo-physical properties of the liquids and particles were measured experimentally, as detailed in Chapter 3 and are summarized in Table 4.1.

Can liquid temperatures were measured at the geometric center of the cans, using needle type thermocouples. For the purpose of measuring particle transient temperatures, a thermocouple equipped particle was mounted inside the can. The particle assembly, can preparation and data gathering are described in Chapter 3.

Table 4.1 Physical properties of test materials used in this study

Material	Density (kg/m^3)	Heat capacity (J/kg K)	Thermal conductivity (W/m K)	Thermal diffusivity (W/m^2 K)
Polypropylene	830	1842	0.359	$2.35x10^{-7}$
Nylon	1128	2073	0.369	$1.52x10^{-7}$
Acrylic	1168	1355	0.139	$0.88x10^{-7}$
Delrin	1376	1425	0.374	$1.91x10^{-7}$
Teflon	2210	984	0.290	$1.35x10^{-7}$
Oil[a] (100 cst)	880	2210	0.165	-
Water[b]	1000	4180	0.597	-

[a]Kinematic viscosity = 1.0×10^{-4} m^2/s; [b]kinematic viscosity = 1.0×10^{-6} m^2/s

Cans of size 307 x 409 containing the high temperature bath oil and thermocouple equipped particle, were processed in a batch type, rotary, full-immersion, hot-water sterilizer (Stock Rotomat-PR 900; Hermann Stock Maschinenfabrick, Germany). Only one particle per can was used. In each test run, four test cans were placed equidistant from the horizontal central axis of the rotating cage, in a vertical orientation, to give end-over-end rotation. The remaining space in the cage was filled with dummy cans containing water. Three retort temperatures (110, 120 and 130 °C), four rotational speeds (0, 10, 15 and 20 rpm), four radii of rotation (0, 9, 19 and 27 cm) and two can headspaces (6.4 and 10 mm) were employed as system (operating) variables. In the first set of experiments, a 3 x 3 x 4 full-factorial design was employed with the three retort temperatures, three rotational speeds (10, 15 and 20 rpm) and the four radii of rotations with a can headspace of 10 mm. In order to study the effect of can headspace, a 3 x 3 x 2 full-factorial design was used with the three retort temperatures, the three rotational speeds (10, 15 and 20) and the two can headspaces at a constant radius of rotation of 19 cm. Experiments were also carried out at 0 rpm (still retort processing condition) at the three retort temperatures. All test runs were repeated twice.

In order to study the effect of product parameters, five particle densities, two liquid viscosities and four rotational speeds were considered as experimental variables.

A 5 x 2 x 4 full-factorial design was employed with the five particle densities (830, 1128, 1168, 1376 and 2210 kg/m^3), two liquid viscosities (kinematic viscosity 1.0 x 10^{-4} and 1.0 x 10^{-6} m^2/s) and four rotational speeds (0, 10, 15 and 20 rpm) with a can headspace of 10 mm, a radius of rotation of 19 cm and 120 °C retort temperature. All experiments were repeated twice.

Data Analysis

Details are given in Chapter 3 regarding time-temperature data gathering, corrections, normalization and the subsequent evaluation of overall and fluid to particle heat transfer coefficients. All test results were analyzed using Analysis of Variance (ANOVA) to evaluate the level of significance of all the variables and interactions.

Variations in thermo-physical properties and temperature measurement, particle dimensions and retort operating conditions can cause uncertainty in the evaluated h_{fp} values. An error analysis was performed with respect to thermocouple location and particle thermal diffusivity. Thermocouple misplacements, of 0.9525 and 1.905 mm (10 and 20% of particle radius) from the particle center, were taken as the high-side errors with respect to thermocouple placement. The relative uncertainty in the measured particle thermal diffusivity was taken as ± 5%. A simultaneous error of ±5% in thermal conductivity was also considered, since particle thermal conductivity was back- calculated from particle density, specific heat and thermal diffusivity. The error analysis was carried out only with extreme conditions (lower and higher range values) of calculated h_{fp} values. The percentage deviation, of calculated heat transfer coefficient $h_{fp(cal)}$ from the reference $h_{fp(ref)}$, was computed as the predicted error due to error with respect to the characteristic parameter:

$$\text{Predicted error } (\%) = \left(\frac{h_{fp(cal)} - h_{fp(ref)}}{h_{fp(ref)}} \right) \times 100 \qquad (4.1)$$

Hence, a positive value in predicted error represents an overestimation of the convective heat transfer coefficient while a negative value represents the opposite.

RESULTS AND DISCUSSION

Influence of system parameters

Overall heat transfer coefficient (U)

Tables 4.2 and 4.3 summarize the overall heat transfer coefficients obtained under the different experimental conditions. U values varied from 120 to 187 W/m^2 K. Increasing the retort temperature improved the mean U value (6% increase from 110 to 130 °C). This was probably due to the lowering of liquid viscosity at a higher retort temperature. The overall heat transfer coefficient also increased with the increasing rotational speed (38% increase in mean U value between 10 and 20 rpm). Again, this was possibly due to enhanced mixing, resulting in a higher degree of turbulence. The influence of rotational speed on U was more pronounced than any other parameter studied. At 0 rpm (still report processing condition), the overall heat transfer coefficient was calculated just as with the agitated processing condition in which temperature uniformity of the liquid within the can was achieved in a short time. Since the temperature gradients, which existed in the 0 rpm test runs were large and natural convection was the predominant mode of heat transfer, the calculated U may not be a true representation of convection heat transfer. However, since the objective was to evaluate whether agitated processing improves the heat transfer rate when compared to still retort processing, a limited number of experiments were carried out with 0 rpm and the data were treated in a similar fashion. These data were only used for the purpose of comparison and not included in the statistical analysis of variance.

Moving the can away from the central axis of rotation resulted in some improvement in U values, because of the larger centripetal acceleration encountered by the liquid at larger radii of rotation. Increasing the radius of rotation from 0 to 9 cm improved the mean U value by 2%, and from 9 to 19 cm, it improved by 3%; however, a further increase in radius of rotation to 27 cm did not change the U value. Compared to other parameters overall, the effect of radius of rotation on U was small. For thermal process design, the lower the effect of radius of rotation, the higher the uniformity in terms of lethality achieved in cans placed at different locations in the retort for processing. This represents a desirable situation.

Table 4.2 Mean heat transfer coefficients (U and h_{fp}), as influenced by retort temperature, rotational speed and ***radius of rotation***

Retort temperature (°C)	Rotational speed (rpm)	Radius of rotation (cm)	Overall heat transfer coefficient (W/m^2 K)	Fluid to particle heat transfer coefficient (W/m^2 K)
110	10	0	122 (0.7)	69.6 (0.6)
		9	120 (0.1)	68.2 (4.7)
		19	123 (0.1)	95.0 (1.7)
		27	126 (2.0)	96.6 (4.0)
	15	0	148 (0.3)	86.3 (0.9)
		9	146 (2.2)	82.8 (5.7)
		19	156 (1.5)	110 (5.6)
		27	153 (0.4)	124 (5.5)
	20	0	169 (0.3)	103 (0.8)
		9	181 (0.9)	108 (7.3)
		19	182 (0.9)	123 (3.8)
		27	186 (1.3)	126 (9.8)
120	10	0	133 (0.6)	73.0 (8.2)
		9	135 (1.8)	77.7 (6.7)
		19	138 (2.4)	99.5 (1.5)
		27	135 (0.8)	94.8 (4.2)
	15	0	154 (0.3)	91.5 (1.1)
		9	154 (0.1)	95.3 (7.3)
		19	161 (0.9)	115 (12)
		27	162 (2.5)	134 (8.9)
	20	0	179 (0.7)	111 (5.0)
		9	181 (1.6)	122 (6.8)
		19	185 (0.6)	124 (4.8)
		27	188 (3.2)	137 (13)
130	10	0	135 (0.3)	88.8 (13)
		9	136 (1.0)	96.0 (2.3)
		19	140 (0.4)	109 (3.7)
		27	143 (3.2)	122 (6.2)
	15	0	154 (0.9)	110 (5.9)
		9	156 (0.7)	118 (13)
		19	165 (0.5)	138 (2.5)
		27	176 (0.8)	137 (12)
	20	0	179 (2.2)	118 (5.7)
		9	184 (1.4)	126 (3.9)
		19	181 (0.6)	143 (1.8)
		27	192 (1.9)	136 (2.1)

Table 4.3 Mean heat transfer coefficients (U and h_{fp}), as influenced by retort temperature, rotational speed and ***headspace***

Retort temperature (°C)	Rotational speed (rpm)	Headspace (mm)	Overall heat transfer coefficient (W/m^2 K)	Fluid to particle heat transfer coefficient (W/m^2 K)
110	0	6.4	121 (1.2)[1]	25.2 (6.3)
	10	6.4	122 (1.8)	49.3 (5.9)
		10	123 (0.1)	95.0 (1.1)
	15	6.4	135 (1.5)	61.3 (2.1)
		10	156 (1.5)	110 (5.6)
	20	6.4	147 (3.4)	73.3 (1.8)
		10	182 (0.9)	123 (3.8)
120	0	6.4	126 (1.0)	27.4 (4.0)
	10	6.4	131 (1.1)	53.5 (3.9)
		10	138 (2.5)	99.5 (1.5)
	15	6.4	144 (2.4)	66.5 (3.6)
		10	161 (0.9)	115 (12)
	20	6.4	165 (4.8)	94 (14)
		10	185 (0.6)	124 (4.8)
130	0	6.4	131 (2.0)	32.1 (6.2)
	10	6.4	134 (0.7)	61.2 (7.5)
		10	140 (0.4)	109 (3.7)
	15	6.4	146 (3.7)	83 (1.2)
		10	165 (0.5)	138 (1.8)
	20	6.4	159 (4.6)	101(1.5)
		10	181 (0.6)	143 (1.8)

[1]The values in parentheses are the coefficients of variation (%)

It was found that a small change in headspace also improved the mean U values. This is probably due to an increase in bubble size, resulting in more efficient mixing. However, bubble size beyond a critical level may have a dampening effect on the efficiency of mixing, due to increased drag on the can wall; thus resulting in disturbance in bubble-liquid phenomena (Naveh and Kopelman, 1980). After rotational speed, the headspace effect on U was the second most significant and an increase in headspace from 6.4 to 10 mm increased the mean U value by 16%. Analysis of variance of data revealed that all four factors were highly significant ($p \leq 0.0001$), with the influence of rotational speed on overall heat transfer coefficient being the most significant (Table 4.4 for retort temperature, rotation speed and *radius of rotation* and Table 4.5 for retort temperature, rotation speed and *headspace*). Two- way interaction effects were also significant with all factors; however, their contribution compared to the main effect were small. The main effect-plots are presented in Fig. 4.1, and demonstrate the influence of principle factors described earlier.

Fluid-to-particle heat transfer coefficient (h_{fp})

Depending on experimental conditions, the fluid-to-particle heat transfer coefficient, h_{fp}, ranged from 23 to 145 W/m^2 K. Tables 4.2 and 4.3 summarize average h_{fp} values for all the processing conditions. Analysis of variance showed that all factors studied affected h_{fp} values significantly (Tables 4.4 and 4.5). Interaction effects were not significant in this case and the main effects are shown in Fig. 4.2. Higher h_{fp} values were obtained at higher levels of all four parameters. The mean h_{fp} value increased by about 27% with an increase in the retort temperature from 110 to 130 °C. Increasing rotational speed from 10 to 20 rpm improved the mean h_{fp} value by 37%, probably due to increased particle-to-liquid relative velocity at the higher rotational speed. However, the influence of rotational speed on h_{fp} was less than that on headspace and unlike the case of U, which was probably due to associated small changes in particle to liquid velocity. The particle settling due to gravity was minimal since the density of polypropylene particles was relatively closer to that of the bath oil. The effect of radius of rotation on h_{fp}, on the other hand, was more pronounced than with U. Increasing the radius of rotation improved h_{fp}

Table 4.4 Analysis of variance showing the influence of retort temperature, rotational speed and ***radius of rotation*** on U and h_{fp}

Source	dF	Sum of square (%) U	h_{fp}
Model	35	88.8**	72.4**
Retort temperature (RT)	2	03.9**	15.8**
Rotational speed (RS)	2	78.3**	26.7**
Radius of rotation (RR)	3	03.3**	22.8**
Interactions			
RT x RS	4	0.8**	1.1
RT x RR	6	1.0**	1.3
RS x RR	6	0.8*	2.1
RT x RS x RR	12	0.7	2.6
Residual (error)	55	11.2	27.6
	77 (h_{fp})		
Total	90		
	112 (h_{fp})		

** $p \leq 0.0001$, * $p \leq 0.005$

Table 4.5 Analysis of variance showing the influence of retort temperature, rotational speed and ***headspace*** on U and h_{fp}

Source	dF	Sum of square (%) U	Sum of square (%) h_{fp}
Model	17	90.1**	80.4**
Retort temperature (RT)	2	05.5**	06.8**
Rotational speed (RS)	2	61.4**	17.6**
Headspace (HS)	1	16.7**	54.2**
Interactions			
RT x RS	4	1.0	0.6
RT x HS	2	0.2	0.3
RS x HS	2	4.2**	0.4
RT x RS x HS	4	0.7	0.5
Residual (error)	52 40 (h_{fp})	09.9	19.6
Total	65 57 (h_{fp})		

** $p \leq 0.0001$

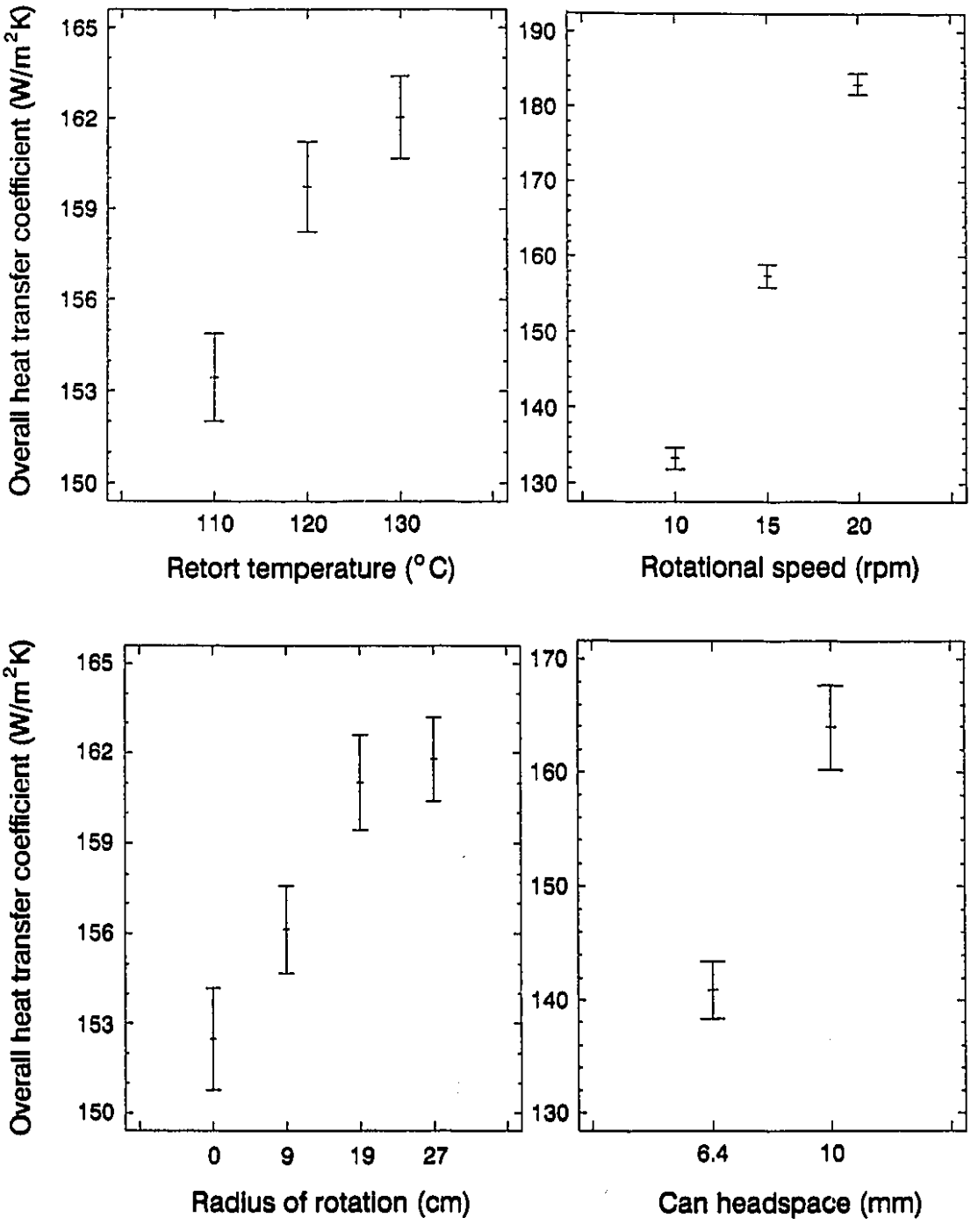

Figure 4.1 ***Overall heat transfer coefficient (U)***, as influenced by retort temperature, rotational speed, radius of rotation and can headspace

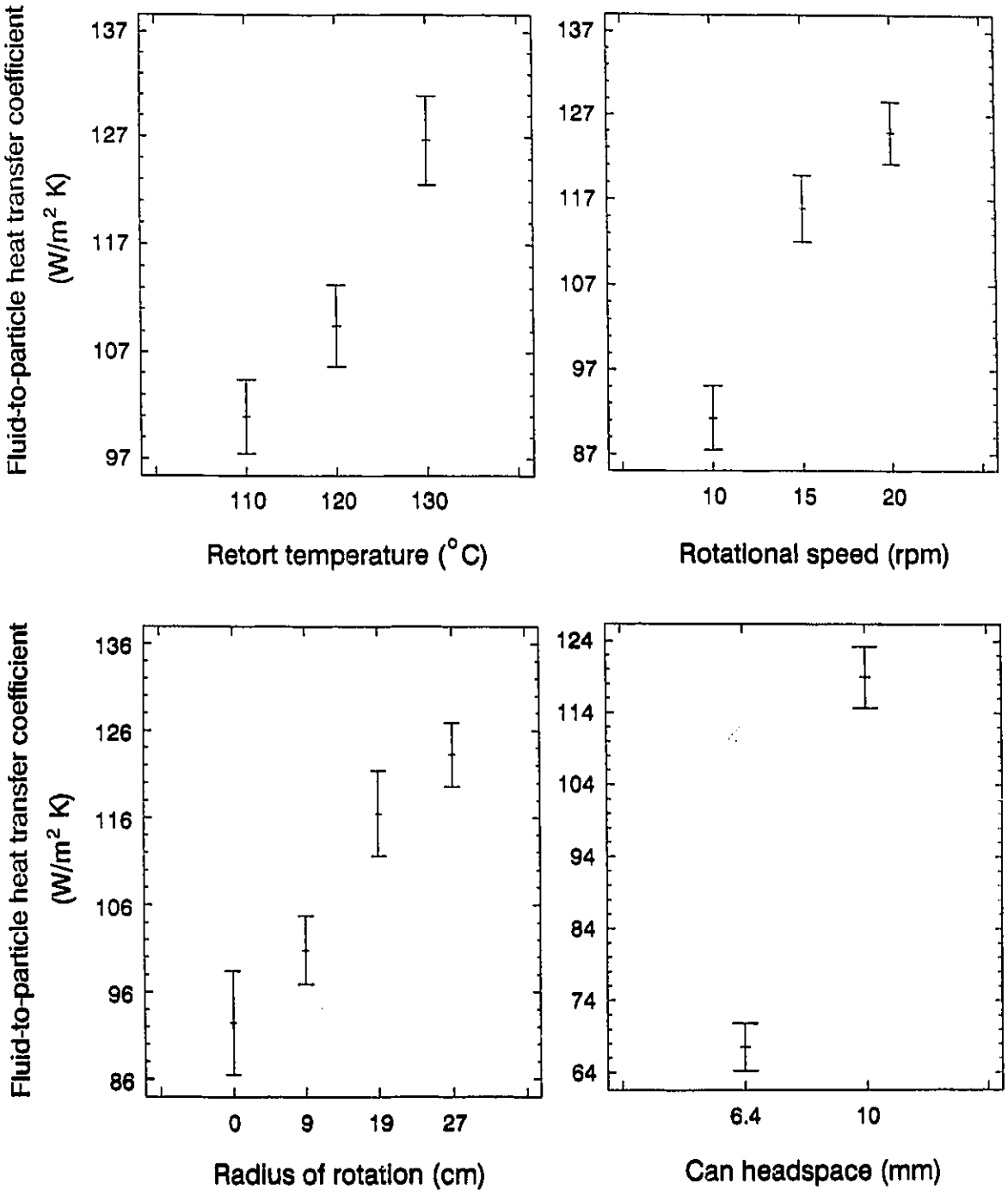

Figure 4.2 ***Fluid to particle heat transfer coefficient*** (h_{fp}), as influenced by retort temperature, rotational speed, radius of rotation and can headspace

in a sigmoidal fashion, as shown in Fig. 4.2. At the lower end, an increase in radius of rotation from 0 to 9 cm improved the mean h_{fp} by 8% and a further increase from 9 to 19 cm improved the mean h_{fp} by 16%, and again at the higher end, an increase in the radius of rotation from 19 to 27 cm changed the mean h_{fp} by only 6%. The radius of rotation effect on h_{fp}, compared to the those of can headspace and rotational speed was also less, which is again preferable from a process design point of view. Compared to the other three parameters studied, the headspace effect on h_{fp} was the most significant. A higher bubble velocity, due to larger size, resulted in better mixing and affected the particle to liquid velocity; also, this probably caused local turbulence around the particle area. A change in headspace from 6.4 to 10 mm increased the mean h_{fp} by 75%.

Influence of product parameters

Overall heat transfer coefficient (U)

Table 4.6 summarizes the mean overall heat transfer coefficients for oil and water, obtained at different rotation speeds. U values varied from 118 to 195 W/m^2 K for oil and 420 to 800 W/m^2 K for water. The U values improved significantly, even at the lower rotational speed of 10 rpm for both test liquids studied when compared to the values associated with still-processing (0 rpm). The increase in overall heat transfer coefficient, with increasing rotational speeds, can be explained by the enhanced mixing (caused by the movement of the headspace bubble and particle in the can) which resulted in a higher degree of turbulence. When the rotational speed increased from 10 to 20 rpm, the U value increased by 32% for oil and 24% for water in cans. This suggested that higher rotational speeds are more beneficial to viscous liquids. The higher U values associated with the lower viscosity liquid (water) was possibly due to the presence of a smaller thickness of boundary layer with water. The particle motion may have an important effect on the overall heat transfer coefficient, and particles with different density and volume fractions may alter the flow pattern of the can liquid. However, in the present case particle density did not influence U; this was possibly due to the presence of a single particle.

Analysis of variance of data revealed that both liquid viscosity and rotational speed effects were highly significant ($p \leq 0.0001$) with the viscosity term explaining over 90%

of total variability. Particle density effects and interactions involving particle density were not significant ($p>0.05$). The viscosity-rotational speed interaction effect was significant (Table 4.7) and their relative effects are shown in Figure 4.3.

Table 4.6 Mean overall heat transfer coefficient (U), as influenced by rotational speed and liquid viscosity ($n \geq 18$)

Rotational speed (rpm)	Overall heat transfer coefficient Oil (W/m^2 K)	Water (W/m^2 K)
0	126 (2.9)[1]	455 (5.6)
10	141 (2.9)	658 (4.9)
15	162 (2.9)	734 (3.8)
20	186 (2.6)	781 (1.4)

[1]The values in parentheses are the coefficients of variation (%)

Fluid-to-particle heat transfer coefficient (h_{fp})

Depending on experimental conditions, the fluid-to-particle heat transfer coefficient, h_{fp}, ranged from 34 to 825 W/m^2 K. Table 4.8 summarizes average h_{fp} values under different processing conditions. Analysis of variance showed that all factors under study affected the h_{fp} values significantly (Table 4.7). Two-way interaction effects of viscosity and density, and density and speed were also significant ($p\leq 0.0001$) in this case, as shown in Figure 4.4 a & b.

The effect of viscosity on h_{fp} values was similar to that observed with U. Table 4.8 demonstrates that, under all processing conditions, h_{fp} values were higher with the lower viscosity liquid; again this is possibly due to the associated lower thickness of the boundary layer. The increase in the h_{fp} values, as liquid viscosity, decreased can also be associated with a higher particle-to-liquid relative velocity. In the flow visualization study detailed in a later section (Chapter 6), a higher settling velocity of particle was observed in the lower viscosity liquid.

Maesmans et al. (1992) indicated that particle properties do not affect h_{fp} as long as the particle-liquid motion is not altered (either by density or surface roughness). In

Table 4.7 Analysis of variance showing the influence of liquid viscosity, rotational speed and particle density (only with h_{fp}) on U and h_{fp}

Source	U dF	U Sum of square (%)	h_{fp} dF	h_{fp} Sum of square (%)
Model	7	95.5*	21	94.2*
Liquid viscosity (FV)	1	88.2*	1	14.3*
Rotational speed (RS)	3	04.6*	2	03.9*
Particle density (PD)	-	-	4	51.5*
Interactions				
FV x RS	3	02.7*	2	00.0
FV x PD	-	-	4	12.4*
RS x PD	-	-	8	12.1*
Residual (error)	117	04.5	105	05.8
Total	124		126	

- not applicable
* $p \leq 0.0001$

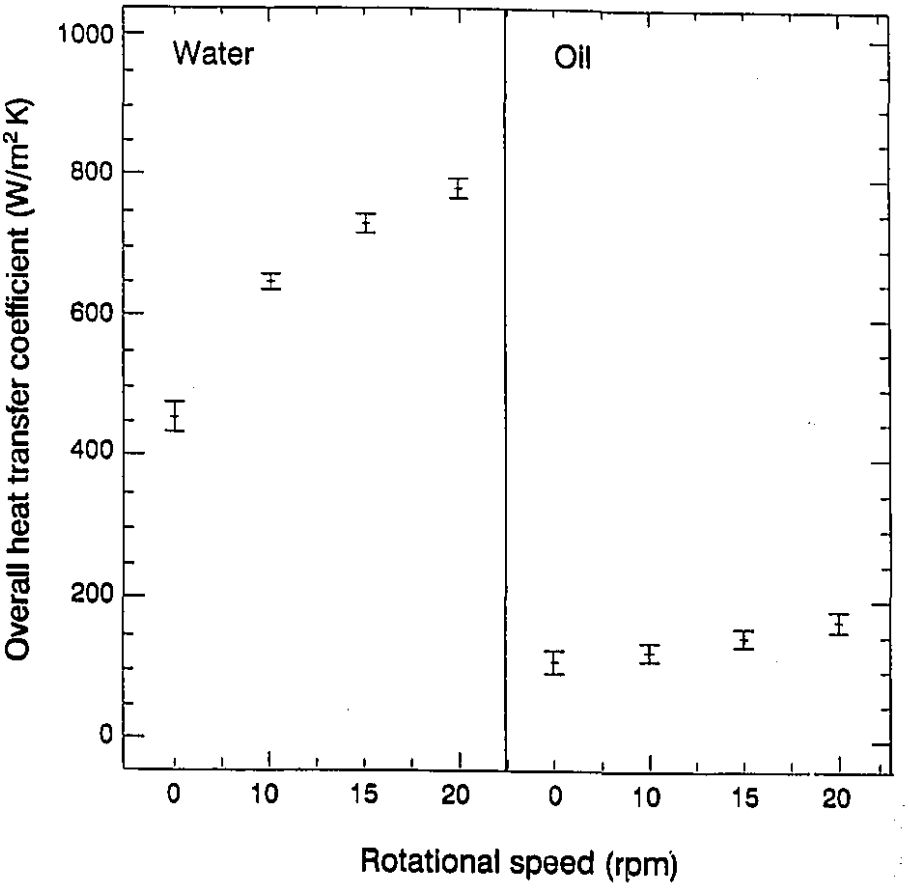

Figure 4.3 ***Overall heat transfer coefficient (U)***, as influenced by liquid viscosity and rotational speed

Table 4.8 Mean fluid to particle heat transfer coefficient (h_{fp}), as influenced by particle density, rotational speed and liquid viscosity ($n \geq 3$)

Material	Density	Rotational speed	Fluid to particle heat transfer coefficient (h_{fp})	
			Oil	Water
	(kg/m^3)	(rpm)	(W/m^2 K)	(W/m^2 K)
Polypropylene	830	0	38.5 (1.1)[1]	-
		10	100 (1.5)	115 (5.5)
		15	112 (8.8)	127 (5.9)
		20	124 (4.8)	143 (7.8)
Nylon	1128	0	37.4 (6.3)	138 (3.0)
		10	175 (6.4)	189 (7.9)
		15	229 (9.1)	279 (9.5)
		20	278 (8.1)	364 (8.5)
Acrylic	1168	0	36.3 (4.3)	140 (1.9)
		10	184 (9.9)	198 (10.8)
		15	228 (5.7)	286 (5.6)
		20	277 (7.6)	384 (8.5)
Delrin	1376	0	40.3 (2.5)	143 (1.4)
		10	205 (4.9)	338 (1.6)
		15	223 (5.6)	386 (4.7)
		20	236 (4.3)	367 (3.4)
Teflon	2210	0	40.0 (0.2)	141 (0.4)
		10	292 (7.7)	773 (5.5)
		15	312 (6.2)	520 (0.8)
		20	254 (4.1)	440 (2.3)

[1]The values in parentheses are the coefficients of variation (%)

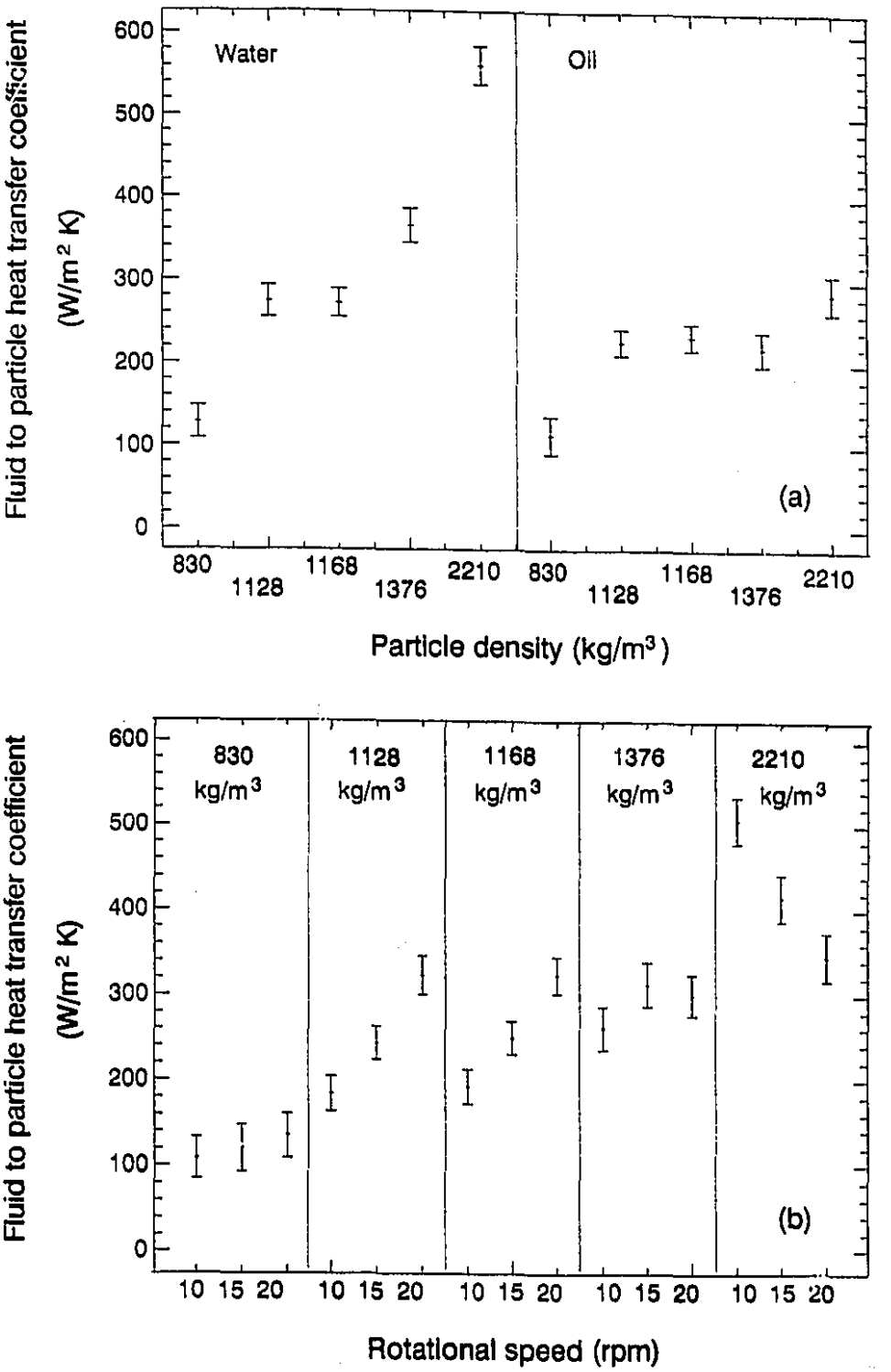

Figure 4.4 ***Fluid to particle heat transfer coefficient*** (h_{fp}), as influenced by liquid viscosity, particle density and rotational speed

earlier studies, measurement of h_{fp} was mostly done with restricted particle motion. When a particle in a can is immobilized, the particle density will not influence h_{fp}. In the present case, this can be verified by comparing h_{fp} values for different particle densities, in the still retort processing condition (0 rpm). Measured h_{fp} values were nearly same ($p>0.05$) for the different density particles at 0 rpm. However, when particle motion was included in the study, the effect of density on h_{fp} was found to be highly significant ($p\leq0.0001$). The higher density particle can have a higher settling velocity in the given liquid, resulting in a higher particle-to-liquid relative velocity and thus a higher h_{fp} value. The h_{fp} values increased with increasing particle density in both liquids. Particles with density close to each other (Nylon and Acrylic) had similar ($p>0.05$) h_{fp} values in both liquids (oil and water). It can therefore be inferred, by comparing h_{fp} values for Nylon and Acrylic in both the liquids (oil and water), that the particle thermal properties did not influence h_{fp}. Stoforos and Merson (1992) reported higher h_{fp} values for a Teflon particle when compared to an aluminum particle of the same size; both were processed in axially rotating cans. However, in addition to the altered particle motion due to differences in particle density, they attributed the difference in h_{fp} to the different thermal diffusivity of Teflon and aluminium.

On average, h_{fp} improved by 25% with an increase in rotational speed from 10 to 20 rpm; this was probably due to increased agitation at higher rotational speed. The rotational speed influence was less pronounced when the densities of particle (polypropylene) and liquid (oil) are nearly same, since the particle settling velocity (gravity) and buoyant effects were minimal. The effect of rotational speed was more pronounced with the medium density particles (Nylon and Acrylic). With particles of large densities (Delrin and Teflon), the increasing rotational speed had opposite effects. For Delrin in water and Teflon in oil, h_{fp} increased when rotational speed increased from 10 to 15 rpm; but a further increase in rotational speed from 15 to 20 rpm, decreased h_{fp}. In the case of Teflon in water, the h_{fp} decreased by 40% when the rotational speed increased from 10 to 20 rpm. Due to the larger centrifugal force at higher rotational speeds, the motion of these high density particles was completely different. Stoforos and Merson (1992) also found decreasing h_{fp} with increasing rotational speed, for Teflon particles in

silicone oil during axial rotation of cans. The particle motion detailed in a later section (Chapter 6) could explain to some extent the differences in h_{fp} values observed under different processing conditions.

Error analysis

Table 4.9 shows the error associated with calculated heat transfer coefficients, as affected by error in characteristic parameters. The thermocouple misplacement error of 0.9525 mm (10% of the particle radius) from the center of the particle resulted in an overestimation of 0.2 to 2.1% in calculated h_{fp} values at the lower end; and at the higher end, the overestimation was 0.6 to 3.6% depending upon the particle material. A further increase in error, with thermocouple misplacement up to 20% (1.9 mm from the particle center), resulted in an error of 2.6% to 17% depending upon particle properties. This suggested that when particle temperatures are measured with thermocouples, the associated error due to thermocouple misplacement will be lower if temperatures are measured at the particle center, opposed to those measured at the particle surface. This is due to associated larger temperature gradients close to the surface, when compared to the gradient at the particle center. The errors in calculated h_{fp} are small with high thermal diffusivity particles, due to the presence of lower temperature gradients in the particle. A change in thermal diffusivity of a particle by +5% overestimated h_{fp} in its lower range by 4.6 to 17%, and in the higher range by 6.9 to 36%, depending upon the particle material used. A -5% change in thermal diffusivity resulted in 6.5 to 52% and 9.0 to -171% underestimation in h_{fp}, respectively. The associated errors in calculated h_{fp} were very high with low thermal conductivity particles or under conditions with a high Biot number. This is due to the larger internal resistance to heat transfer. In this situation, heat flow was mainly governed by particle thermal diffusivity rather than the convective heat transfer at liquid-particle interface. Awuah et al. (1995) also reported that small errors in parametric values could result in very large errors in the estimated fluid to particle heat transfer coefficient, when higher Biot numbers in excess of 22 have to be predicted. In such situations, metal particles with higher thermal conductivity should be chosen (Ramaswamy et al., 1983) over the low thermal conductivity particles, in order to reduce

Table 4.9 Percentage error associated with calculated fluid to particle heat transfer coefficient, h_{fp} value, as influenced by error in characteristic parametric values

Particle material	Limiting value of h_{fp} with Bi = 10	Observed range of Bi	Thermocouple displacement error 10 to 20% of particle radius		Thermal diffusivity + 5 to - 5 %	
			Lower end of h_{fp}	Higher end of h_{fp}	Lower end of h_{fp}	Higher end of h_{fp}
Polypropylene	377	2.5 - 4.0	+0.20 to +2.6	+0.60 to +2.9	+4.60 to -6.5	+6.9 to -9.0
Nylon	387	4.5 - 9.5	+0.90 to +4.4	+1.5 to +7.3	+8.0 to -11	+17 to -32
Acrylic	146	12.5 - 27.0	+2.5 to +11	+2.5 to +14	+23 to -52	+34 to -157
Delrin	393	5.0 - 10.0	+1.1 to +5.8	+1.4 to 6.8	+9.9 to -13	+15 to -31
Teflon	305	8.0 - 26.0	+2.1 to +10	+3.6 to +17	+17 to -31	+36 to -171

the error in h_{fp} estimation due to error in parametric values. Such high thermal conductivity metal particles, however, will have a higher density which may not simulate the particle motion and heating behaviour exhibited by real food particles under thermal processing conditions. The limiting values of h_{fp} such that the associated Biot number is kept below 10 are presented in Table 4.9. Nylon and polypropylene particles should be selected over other particles, due to their more realistic particle motion and heating behaviour which close to that exhibited by real food particles and also because of their association with relatively lower errors in the estimation of h_{fp}.

CONCLUSIONS

Forced convection heat transfer coefficients (U and h_{fp}) were influenced ($p \leq 0.0001$) by all the system parameters studied. Rotational speed effect was more predominant in the case of U but headspace effect was the most significant on h_{fp}. The effect of the radius of rotation on U, and retort temperature effect on h_{fp} were the least among all the four system parameters.

Overall heat transfer coefficients were also influenced ($p \leq 0.0001$) by liquid viscosity and rotational speed. Fluid-to-particle heat transfer coefficients were influenced by liquid viscosity and rotational speed, as well as particle density. The relative magnitude of h_{fp} value, under the different processing conditions, varied depending on the combined effect of particle motion, particle-to-liquid relative velocity, level of liquid mixing during the rotation. In general, higher h_{fp} values were obtained at lower liquid viscosity, higher particle density and higher rotational speed. Particle density effect was more predominant than the effects of rotational speed and liquid viscosity on h_{fp}.

The errors associated with evaluated h_{fp} were relatively less when due to error in the thermocouple misplacement, as compared to those errors associated with particle thermal diffusivity and thermal conductivity. Particles of smaller size, with higher thermal conductivity (giving lower Bi), are preferred over others.

CHAPTER 5

CONVECTIVE HEAT TRANSFER COEFFICIENTS AS INFLUENCED BY SYSTEM AND PRODUCT PARAMETERS : B. STUDIES WITH MULTIPLE PARTICLES IN THE CAN

ABSTRACT

The heat transfer coefficients (U and h_{fp}), associated with canned liquid/particle mixtures, were evaluated with suspended Nylon particles, during end-over-end rotation. Can rotation speed (10 to 20 rpm), particle diameter (19 to 25 mm), particle concentration (single particle to 40% v/v) and particle shape (sphere, cylinder and cube) were studied as variables, using liquids of two different viscosities (1.0×10^{-6} and 1.0×10^{-4} m^2/s). The methodology for the evaluating heat transfer coefficients, detailed in Chapter 3, was slightly modified to accommodate the heat sink due to multiple particles in the can. The h_{fp} values varied from 170 to 1550 W/m^2 K and U values varied from 110 to 800 W/m^2 K, depending upon process conditions. The h_{fp} increased by 10 to 60% with particle diameter decreasing from 25 to 19 mm, while h_{fp} increased about three fold as the particle concentration changed from a single particle to 30%. Further increase in particle concentration to 40% decreased h_{fp} by 5 to 20%, depending upon processing conditions. Analysis of variance showed that particle shape effects on h_{fp} were significant ($p \leq 0.0001$) with both single and multiple particles. With a single particle in the can, the spherical particle (0.95 cm diameter) showed lowest h_{fp}, foliowed in increasing order by cylindrical particle (0.95 cm diameter and 0.95 cm length) and cube shaped particle (0.95 cm length). With multiple particles in the can, an opposite trend was observed, giving the lowest values of h_{fp} with cubes and the highest values with spherical particles. With multiple particles in the can, effects of particle shape, particle size and particle concentration on U were similar to those obtained with h_{fp}, but the magnitudes were lower.

INTRODUCTION

Heat transfer rates to canned food products, such as a liquid containing discrete particles, can be increased by mechanical agitation. This has permitted the use of high temperature short time (HTST) concept with agitation processing. The thermal processing schedule for canned foods has been traditionally established using experimental heat penetration data. In recent years, growing interest in mathematical modelling has prompted further attention to the mechanism of heat transfer in particulate food systems. Theoretical models can be used for the design, optimization and validation of such food systems. However, the usefulness of theoretical models depends upon the accuracy of the input physical parameters. The overall heat transfer coefficient from the heating medium to the can liquid (U) and the fluid-to-particle heat transfer coefficient (h_{fp}) are important parameters, beside thermo-physical properties of food materials.

The overall heat transfer coefficient and the fluid-to-particle heat transfer coefficient in cans are influenced by various environmental conditions and physical properties of the liquid and particles. Since the flow around the particle may differ for different geometrical shapes, the heat transfer coefficients may reflect such variations; in turn these variations will affect the heating rates. Particle shape effect has not been studied on U and h_{fp} in cans with end-over-end rotation. In earlier studies, spherical particles have been used to quantify the effect of various parameters influencing U and h_{fp}. Lekwauwa and Hayakawa (1986) presented a semi-theoretical method, which utilized Duhamel's theorem and empirical formulae, to analyze the heat transfer for different particle shapes. However, they did not quantify the effect of particle shape on the associated heat transfer coefficients.

The effect of system and product parameters on associated convective heat transfer coefficient, in cans with a single particle in the can, were reported in Chapter 4. This Chapter highlights the use of the flexible thermocouple approach, reported earlier (Chapter 3). This approach quantifies the effects of system and product parameters on U and h_{fp}, in cans containing multiple particles subjected to end-over-end processing.

Determination of heat transfer coefficients

Using a finite difference method, the fluid-to-particle heat transfer coefficient (h_{fp}) was determined by solving the governing partial differential equation of conduction heat transfer in each geometrical shape with associated initial and boundary conditions. Appropriate equations and numerical procedures involved with the finite difference method are detailed in the appendix. Chapter 3 details theoretical background involved with calculating the associated fluid to particle heat transfer coefficient.

In order to calculate the overall heat transfer coefficient (U), an expression was obtained by integrating Eq. (3.1) (Chapter 3). The time of integration was considered to be the time, t_{pt} (time required to achieve a lethality of 10 min at the particle center), obtained previously from the determination of h_{fp}. By integrating Eq. (3.1) with respect to time the following Eq. (5.1) is obtained:

$$U A_c \int_0^{t_{pt}} (T_R - T_l)\, dt = m_l C_{pl} \int_0^{t_{pt}} dT_l + h_{fp} A_p \int_0^{t_{pt}} (T_l - T_{ps}) \qquad (5.1)$$

To calculate the overall heat transfer coefficient from the above Eq. (5.1), it is necessary to have transient temperatures of liquid and particle surface. For the transient temperatures of liquid, experimentally measured values were used and particle surface temperature were calculated from Eqs. (3.3-3.6). The overall heat transfer coefficient was then calculated from Eq (5.1).

Test materials

Water and a high temperature bath oil (100 cst at 38 °C, Fisher Scientific Ltd., Montreal), giving different viscosity levels, were used as test liquids. Nylon particles of different sizes (sphere diameter 19, 22, 25 mm) and shapes (sphere, cylinder and cube) (Hoover Precision Products, Sault Ste Marie, MI) were used as test particles. The physical properties of the liquids and particles are given in Table 4.1 in Chapter 4.

Cans of size 307 x 409 containing the test liquid and multiple particles were subjected to end-over-end processing. The thermocouple equipped particle was positioned near the geometric center of the can. The experimental variables were: spheres of three different sizes (diameter 19, 22, and 25 mm), four particle concentrations (single particle, 20, 30 and 40% volume by volume, v/v), three particle shapes (sphere, cylinder and cube), three rotational speeds (10, 15 and 20 rpm) and two kinematic viscosities (1.0×10^{-6} and $1.0\ 10^{-4}$ cm^2/s). The fixed parameters were: can headspace of 10 mm, a radius of rotation of 19 cm and a retort temperature of 120 °C. The overall heat transfer coefficient and fluid-to-particle heat transfer coefficient data were analyzed statistically. An analysis of variance (ANOVA) procedure was used to evaluate the level of significance of liquid viscosity, rotational speed, particle size, particle concentration and particle shape and their interactions.

RESULTS AND DISCUSSION

Influence of rotational speed and liquid viscosity on U and h_{fp}

Tables 5.1 and 5.2 summarize the mean values and coefficients of variation of overall heat transfer coefficients, for oil and water, obtained at various rotational speeds. U values ranged from 110 to 220 W/m^2 K for oil and 480 to 800 W/m^2 K for water. U values improved significantly with increasing rotational speeds for both water and oil. The latter could be explained by the enhanced mixing, resulting in a higher degree of turbulence. The influence of rotational speed on the resulting temperature profile of can liquids is illustrated in Figure 5.1a. This indicates that at higher rotational speeds the liquid temperature reaches the heating medium temperature relatively faster. The rapid rate of heating associated with the low viscosity liquid (water), perhaps narrowed the influence of rotation speed. The effect is most visible with the high viscosity liquid (oil). On average, the U value increased by 24% for oil and 13% for water in cans, when the rotational speed increased from 10 to 20 rpm (Tables 5.1 and 5.2). This indicates that rotational speed effects are more pronounced with a viscous liquid. Anantheswaran and

Rao (1985a) also reported that the end-over-end rotation was more effective for higher viscosity liquids. Rotational speed effects on U were also more apparent in cans with a single particle, than in cans with multiple particles. The influence of rotational speed on U was lower with larger size particles (22.25 and 25.0 mm diameter) than with a smaller size particle (19.05 mm diameter).

Table 5.1 Mean overall heat transfer coefficient (U), as influenced by ***particle size*** and ***particle concentration*** at various rotational speeds for oil and water ($n \geq 3$)

Particle size (mm)	Particle concentration (%)	Rotational speed (rpm)	Overall heat transfer coefficient	
			Oil ($W/m^2.K$)	Water ($W/m^2.K$)
19.05	0.08*	10	141 (2.9)[1]	647 (3.5)
		15	162 (2.9)	734 (3.8)
		20	186 (2.6)	781 (1.4)
	20	10	176 (1.3)	726 (3.0)
		15	198 (1.6)	760 (4.3)
		20	215 (1.4)	788 (3.8)
	30	10	151 (1.1)	658 (2.6)
		15	168 (0.7)	666 (1.0)
		20	182 (1.3)	734 (2.1)
	40	10	113 (1.0)	502 (3.2)
		15	136 (1.2)	534 (2.1)
		20	154 (3.2)	595 (2.2)
22.25	30	10	143 (0.4)	653 (0.4)
		15	157 (2.7)	656 (0.6)
		20	173 (1.6)	716 (0.2)
25.00	30	10	139 (3.0)	631 (3.8)
		15	151 (1.6)	639 (1.6)
		20	166 (0.8)	665 (2.3)

*Single particle in the can

[1]The values in parentheses are the coefficients of variation (%)

Table 5.2 Mean overall heat transfer coefficient U, as influenced by ***particle shape*** at various rotational speeds for oil and water with multiple particles (30% particle concentration) in can ($n \geq 3$)

Particle shape (Sphericity)	Rotational speed (rpm)	Overall heat transfer coefficient	
		Oil (W/m^2 K)	Water (W/m^2 K)
Sphere	10	151 (1.1)[1]	645 (3.0)
(1.000)	15	168 (0.7)	666 (1.0)
	20	182 (1.3)	734 (2.1)
Cylinder	10	138 (3.1)	598 (3.7)
(0.874)	15	163 (0.7)	654 (3.6)
	20	172 (0.4)	671 (4.1)
Cube	10	132 (2.0)	553 (5.1)
(0.806)	15	156 (1.3)	617 (4.9)
	20	171 (0.5)	629 (4.7)

[1]The values in the parentheses are coefficients of variations (%)

U values were higher for the lower viscosity liquid (water) in all processing conditions (Tables 5.1 and 5.2). As discussed earlier, this is due to a smaller thickness of boundary layer with water. The temperature of the lower viscosity liquid reached the heating medium temperature more rapidly, thus indicating a faster rate of heat transfer (Figure 5.1a). There are two factors here which influence the temperature change in the canned liquid, one opposing the other. Higher heat transfer coefficients result in a higher rise in temperature, when the heat capacities of the two liquids are same. Higher heat capacities will result in a lower rise in temperature in the liquid, when the associated heat transfer coefficients are same. If one of them is changed (for example U) by a certain margin, while managing to change the other (C_p) by the same margin, then the temperature profile remains relatively unchanged (compensating effect). Any other different change shifts the temperature profile in favor of the dominating factor. Figure 5.2 demonstrates these effects using some arbitrary values of U and C_p (using Eq. 3.7). At constant C_p, a higher U results in a higher temperature profile (see lines 2 vs 1 or 5 vs 3 in Figure 5.2). At constant U, a higher C_p results in a lower rise in temperature (see lines 1 vs 3 or 4 vs 5). The curve for U=400 W/m^2 K and C_p=4200 J/kg K (line 2) is

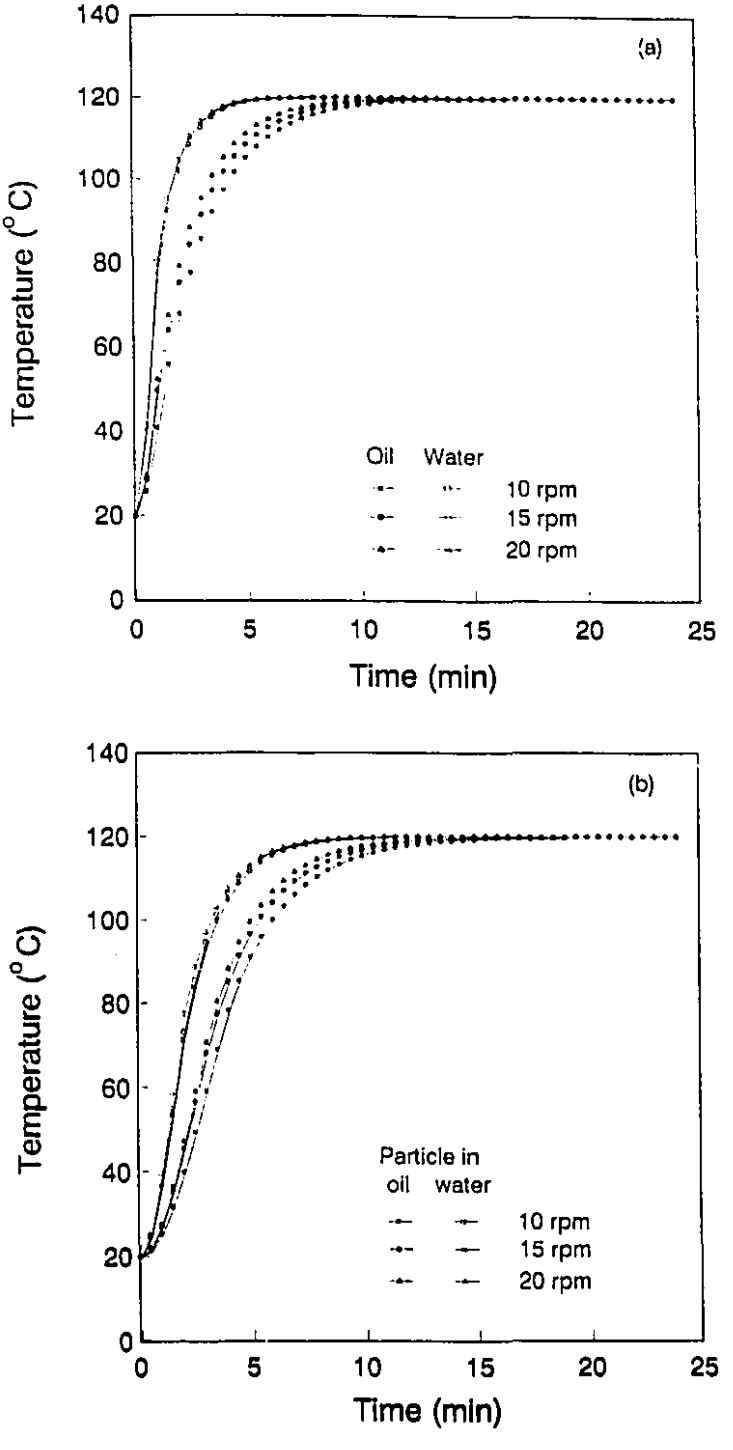

Figure 5.1 Typical time-temperature profiles of liquid and particle during end-over-end rotation, showing the influence of liquid viscosity and rotational speed

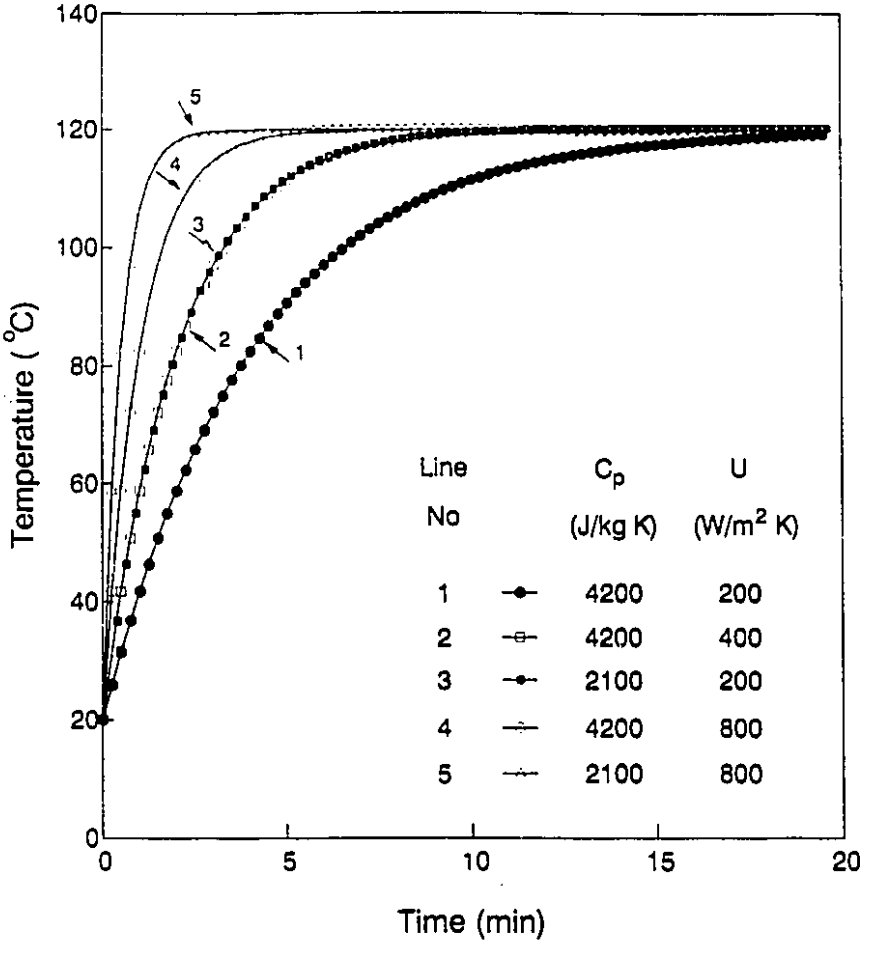

Figure 5.2 Influence of heat capacity and overall heat transfer coefficient (U) on liquid temperature profile, based on simulated data

identical to that of U=200 W/m^2 K and C_p=2100 J/kg K (line 3). The curve for U=800 W/m^2 K and C_p=2100 J/kg K (line 5) will be above all of them, and likewise the curve for U=200 W/m^2 K and C_p=4200 J/kg K (line 1) is far below all of them. In the present system, however, both C_p and U are simultaneously changed (for water and oil); hence, only the combined effects are seen. The U value associated with water is in the 400-800 W/m^2 K range, with a heat capacity of 4180 J/kg K. The U value associated with oil is about *one quarter* of that of water and the heat capacity is about *one half*. Thus, the influence of U (resulting from the lower viscosity) dominates the influence of heat capacity as shown in both figures (Figure 5.1a & 5.2).

Analysis of variance of data revealed that both liquid viscosity and rotational speed effects were highly significant ($p \leq 0.0001$), with the viscosity term explaining over 90% of the total variability. Two-way interaction effects were also significant; however, their contribution was small compared to the main effects (Tables 5.3 and 5.4).

The associated fluid to particle heat transfer coefficient values, in cans during end-over-end processing, were found to be higher with moving particles compared to those measured with restricted particle motion (Chapter 3). In the present study, depending on experimental conditions, the fluid-to-particle heat transfer coefficient, h_{fp}, ranged from 170 to 1165 W/m^2 K for oil and 175 to 1550 W/m^2 K for water. Tables 5.5 and 5.6 summarize mean values and coefficients of variation of h_{fp} values, for all the processing conditions. With spheres, analysis of variance showed that the viscosity and rotational speed effects were significant ($p \leq 0.0001$) with the same order of magnitude (Table 5.5). The increase in rotational speed improved h_{fp} values significantly and this is illustrated in Figure 5.1b. The influence of h_{fp} on particle temperature, due to higher rotational speed, was again more evident with oil than with water. On an average, increasing rotational speed from 10 to 20 rpm enhanced h_{fp} by 56% for oil and 53% for water. The h_{fp} values were lower for the high viscosity liquid (oil) presumably due to the associated thicker boundary layer and higher drag forces. This is also reflected in the temperature profile of the particle in oil and water shown, in Figure 5.1b. The particle temperature in water reached the heating medium temperature much earlier than the particle placed in oil. Higher particle temperatures with water were due to the combined effect of improved U and h_{fp}. The h_{fp}

Table 5.3 Analysis of variance showing the influence of liquid viscosity, rotational speed, ***particle size and particle concentration*** on U and h_{fp}

Source	Sum of square (%) dF	U	h_{fp}	Sum of square (%) dF	U	h_{fp}
Model	13	96.4*	91.3*	17	99.5*	96.6*
Liquid viscosity (FV)	1	95.6*	47.6*	1	96.2*	7.81*
Rotational speed (RS)	2	0.48*	30.7*	2	0.11*	11.7*
Particle size (PS)	2	0.16*	9.94*	-	-	-
Particle concentration (PC)	-	-	-	3	1.90*	73.2*
Interactions						
FV x RS	2	0.10*	0.03	2	0.29*	0.17
FV x PS	2	0.04**	2.14*	-	-	-
RS x PS	4	0.02	0.86	-	-	-
FV x PC	-	-	-	3	0.92*	1.99*
RS x PC	-	-	-	6	0.05***	1.69*
Residual (error)	54	3.60	8.70	151	0.50	3.40
	51 (h_{fp})			71 (h_{fp})		
Total	67			168		
	64 (h_{fp})			88 (h_{fp})		

* $p \leq 0.0001$
** $p \leq 0.0005$
*** $p \leq 0.005$
\- not applicable in the particular experiment set

Table 5.4 Analysis of variance showing the influence of liquid viscosity, rotational speed and ***particle shape*** with single particle (only for h_{fp}) and multiple particles (30% particle concentration) on h_{fp} and U

	h_{fp}			U	
	dF	SS Single particle	SS 30%	dF	SS 30%
Model	13	93.5*	86.7*	13	94.5*
Liquid viscosity (FV)	1	37.9*	24.5*	1	93.0*
Rotational speed (RS)	2	13.7*	54.5*	2	0.7*
Particle shape (PS)	2	26.4*	5.2*	2	0.4*
Interactions					
FV x RS	2	2.3*	2.2**	2	0.1*
FV x PS	2	13.0*	0.3	2	0.3
RS x PS	4	0.2	0.0	4	0.0
Residual (error)	61	6.5	13.3	67	5.5
	45 (with 30%)				
Total	74			80	
	58 (with 30%)				

* $p \leq 0.0001$
** $p \leq 0.005$

Table 5.5 Mean fluid to particle heat transfer coefficient, h_{fp}, as influenced by ***particle size*** and ***particle concentration*** at various rotational speeds for oil and water ($n \geq 3$)

Particle size (mm)	Particle concentration (%)	Rotational speed (rpm)	Fluid to particle heat transfer coefficient	
			Oil (W/m^2 K)	Water (W/m^2 K)
19.05	0.08*	10	173 (1.8)[1]	189 (7.9)
		15	233 (8.3)	278 (9.7)
		20	279 (8.1)	365 (8.5)
	20	10	583 (9.7)	853 (4.2)
		15	787 (2.2)	1090 (7.3)
		20	960 (5.0)	1160 (9.3)
	30	10	682 (3.8)	1020 (14)
		15	967 (1.3)	1170 (1.6)
		20	1130 (2.8)	1450 (7.4)
	40	10	640 (4.5)	878 (8.5)
		15	855 (4.6)	1090 (4.0)
		20	944 (8.1)	1430 (4.3)
22.25	30	10	625 (3.3)	934 (4.8)
		15	808 (4.5)	1170 (6.1)
		20	997 (5.8)	1320 (3.9)
25.00	30	10	501 (5.9)	910 (9.1)
		15	605 (5.4)	1120 (8.4)
		20	739 (5.0)	1280 (4.0)

*Single particle in the can

[1]The values in parentheses are the coefficients of variation (%)

Table 5.6 Mean fluid to particle heat transfer coefficient, h_{fp}, as influenced by ***particle shape*** at various rotational speeds for oil and water with single and multiple particles (30% particle concentration) in can ($n \geq 3$)

Particle concentration (%)	Particle shape (Sphericity)	Rotational speed (rpm)	Fluid to particle heat transfer coefficient	
			Oil (W/m^2 K)	Water (W/m^2 K)
0.08*	Sphere	10	173 (1.8)[1]	189 (7.0)
	(1.000)	15	233 (8.3)	278 (9.7)
		20	279 (8.1)	365 (8.5)
0.12*	Cylinder	10	238 (7.9)	435 (8.6)
	(0.874)	15	260 (5.3)	535 (8.4)
		20	324 (4.2)	460 (6.2)
0.15*	Cube	10	265 (9.4)	503 (8.1)
	(0.806)	15	273 (4.2)	601 (2.3)
		20	333 (7.1)	740 (4.4)
30	Sphere	10	682 (3.8)	1020 (14)
	(1.000)	15	967 (1.3)	1170 (4.0)
		20	1130 (2.8)	1430 (7.5)
	Cylinder	10	633 (3.7)	833 (1.5)
	(0.874)	15	903 (5.8)	1013 (6.6)
		20	1020 (5.8)	1360 (11)
	Cube	10	613 (7.5)	815 (4.3)
	(0.806)	15	830 (2.5)	967 (8.8)
		20	985 (6.3)	1340 (7.8)

*Single particle in the can

[1]The values in parentheses are the coefficients of variation (%)

values with water were nearly 20 to 110% higher than the values with oil. The influence of rotational speed on h_{fp} was also less pronounced with larger size spheres (22.25 and 25.0 mm diameter) when compared to the smaller particle. Increasing rotational speed affected h_{fp} at all particle concentrations.

Comparison with literature values

It is not possible to present an absolute comparison of U and h_{fp} values from the present study and literature values, since differences exist in experimental conditions such as the mode of can rotation (axial vs end-over-end), transient temperature gathering of experimental particle (fixed vs moving) and physical properties of liquid and particles, etc. However, U values obtained were in the range of data published by Lenz and Lund (1978), Deniston et al. (1987) and Stoforos and Merson (1992). The h_{fp} values obtained in the present study were much higher when compared to those determined by Lenz and Lund (1978) and Deniston et al. (1987). Such a discrepancy may be explained by the fact that in earlier studies the motion of the test particle was restricted by temperature measuring devices. The h_{fp} values determined in the present study were in the range reported by Stoforos and Merson (1992), who measured the particle surface temperature using liquid crystals while it moved freely in the can during axial rotation.

Influence of particle size on U and h_{fp}

At any given particle concentration, it was found that the particle size influenced ($p \leq 0.0001$) the overall heat transfer coefficient. On average, U for oil and water was found to decrease with increasing particle diameter. Figure 5.3 a&b are plots illustrating the influence of the size of Nylon spheres in oil and water at different rotational speeds. U values in oil decreased by about 9%, as the size increased from 19.05 to 25.0 mm diameter. The particle size reduced U in water by about 6%. Earlier, Lenz and Lund (1978) showed that the overall heat transfer coefficient in water and 60% aqueous sucrose solutions increased with increasing particle size. Deniston et al. (1987) did not find straightforward relationship with water and potato spheres.

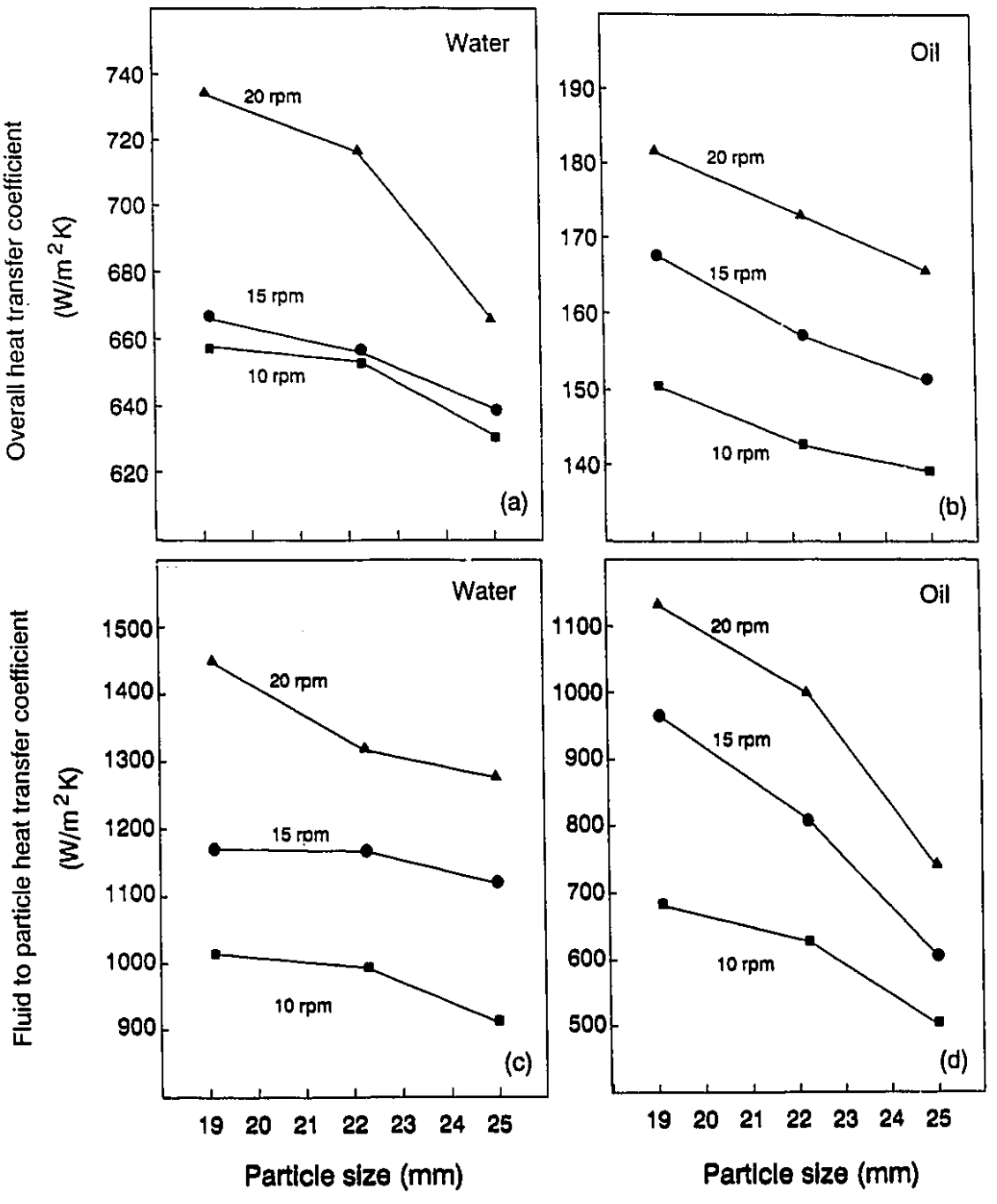

Figure 5.3 Influence of ***particle size*** on overall heat transfer coefficient (U) and fluid to particle heat transfer coefficient (h_{fp}), at different rotational speeds for oil and water

Analysis of variance showed that the particle size influence on h_{fp} was more than U (Table 5.3). Using lead particles of diameter 9.5, 20.65 and 30.15 mm immersed in water, Lenz and Lund (1978) found the h_{fp} increased with increasing particle size. With a 60% aqueous sucrose solution, the 20.6 mm diameter particle (medium size) had the lowest h_{fp}, the 9.5 mm diameter particle (smallest size) had the highest value and the 30.15 mm diameter particle (largest size) had an intermediate value. Hassan (1984) showed that h_{fp} increased with decreasing particle size, from 34.9 to 22.2 mm diameter of potato spheres. Deniston et al. (1987) also reported a small increase in h_{fp} values with decreasing particle size from 35.0 to 22.2 mm diameter. In the present study, h_{fp} values decreased as the particle size increased (Table 5.5). The decrease in h_{fp} was probably due to associated thicker velocity boundary layers with the larger diameter particles. The influence of particle size on h_{fp} is illustrated in Figure 5.3 c & d, at various rotational speeds. The fluid to particle heat transfer coefficient in oil decreased by 13%, when the particle diameter increased from 19.05 mm to 22.25 mm while a further increase in size to 25.0 mm diameter reduced h_{fp} by 24%. The influence of particle size on h_{fp} was less pronounced in water. With an increase in particle size from 19.05 to 25.0 mm diameter, h_{fp} values decreased by about 9%.

Influence of particle concentration on U and h_{fp}

As expected, the presence of particulate matter altered the flow pattern of pure liquid during end-over-end rotation and, thus, affected the heat transfer coefficients. Due to their motion the particles were expected to cause secondary agitation contributing to the mixing of can contents. However, in the presence of a high concentration of particles, the velocity gradient surrounding each particle may be affected. In this case, the viscosity of the mixture will also be considerably higher than that of the liquid; this is caused by the interference of boundary layers around the interacting solid particles, and also the increase of drag caused by the solid particles. Thus, the magnitude of heat transfer coefficients can be expected to depend upon the particle concentration.

Figure 5.4 a & b are the plots showing the influence of particle concentration on the overall heat transfer coefficient (U), for oil and water at different rotational speeds.

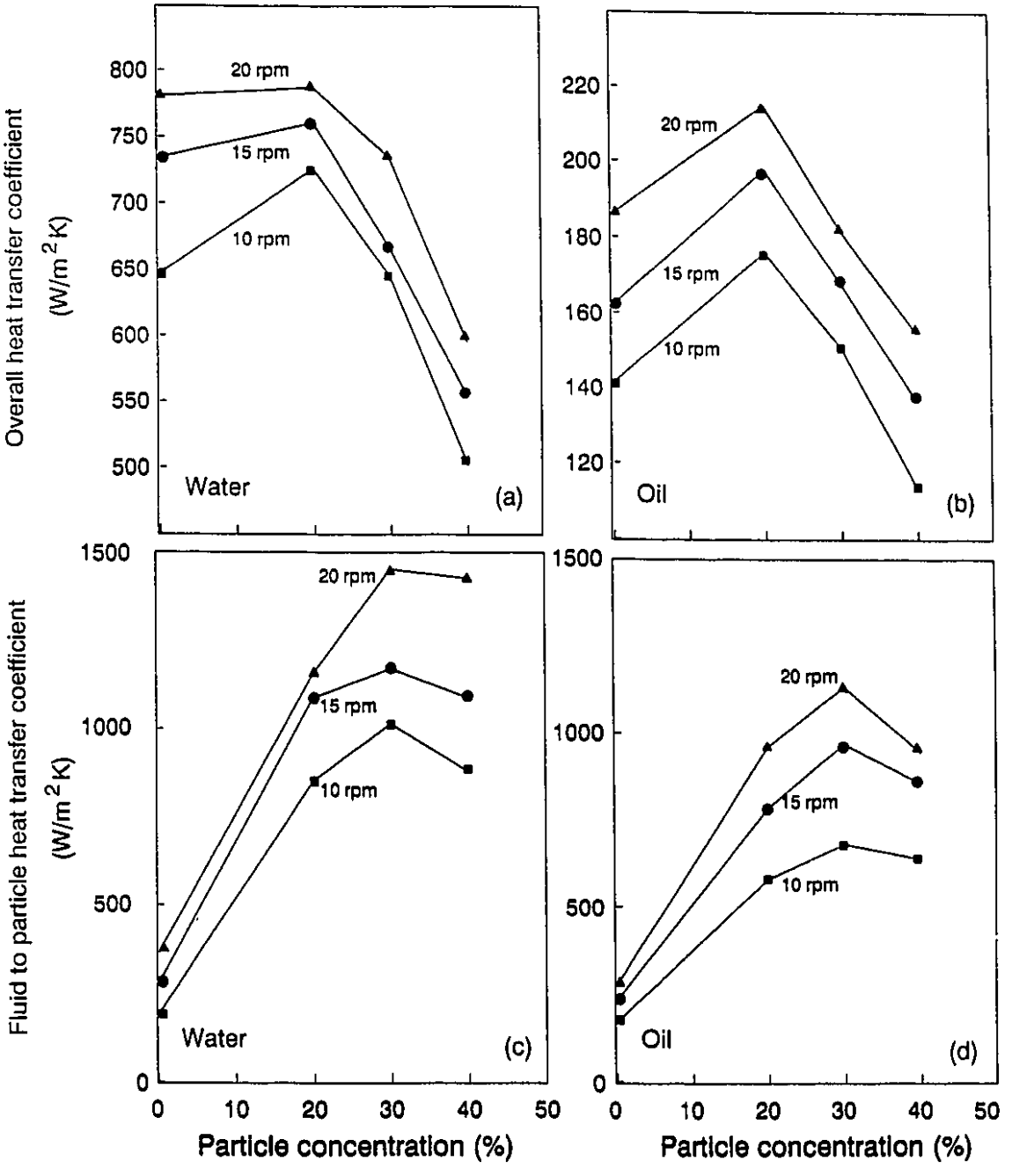

Figure 5.4 Influence of ***particle concentration*** on overall heat transfer coefficient (U) and fluid to particle heat transfer coefficient (h_{fp}) at different rotational speeds, for oil and water

U increased by 20% for oil and 5% for water, when the particle concentration increased to 20% from a single particle. However, further increase in particle concentration to 40% decreased the overall heat transfer coefficient by 31% for oil and 27% for water. The lower particle concentration (20%) made a positive contribution to the liquid mixing and thus enhanced the overall heat transfer coefficient, compared to the single particle situation. However, at higher particle concentrations (30 to 40%), the secondary agitation, effect due to the presence of particles, was probably masked by the increased drag forces exerted by the particles on the liquid. The end result was a lowering of the overall heat transfer coefficient. Lenz and Lund (1978) observed that increasing the particle volume fraction, by adding real food particles of different sizes to the liquid, also decreased the overall heat transfer coefficient. During the processing of potato spheres in water, Deniston el al. (1987) found that the overall heat transfer increased with increasing particle concentration from 10.7% to 40%, but decreased at higher particle concentrations.

The fluid-to-particle heat transfer coefficient also improved significantly ($p \leq 0.0001$) with increased particle concentration. The particle concentration effect was more pronounced on h_{fp} values than U values. Analysis of variance showed that particle concentration accounted for about 75% of total variability. The influence of particle concentration on h_{fp} is illustrated in Figure 5.4 c&d. The h_{fp} increased three fold for oil and by 3.4 for water, when the particle concentration increased to 30% from a single particle. However, a further increase in particle concentration, to 40%, resulted in tight packing in the can This restricted the free particle movement and, thus, reduced h_{fp} values by 12% and 7% for oil and water, respectively. Data from the studies of Lenz and Lund (1978) also showed that higher particle concentrations decreased h_{fp}. Hassan (1984) observed that h_{fp} improved, for 2.54 cm diameter Teflon spheres, with an increased particle concentration from 20% to 31%. Deniston et al. (1987) reported a slight increase in h_{fp} with an increase in particle concentration from 10.7% to 40%, but decreased at higher particle concentrations (45.3% and 50.6%).

Influence of particle shape on U and h_{fp}

In the presence of a single particle in the can, there was no influence of particle shape on U. Due to their motion, the presence of multiple particles tends to alter the flow pattern of pure liquids, causing secondary agitation and contributing to the mixing of can contents. Therefore, with multiple particles, the particle shape effect on U was clear and significant ($p \leq 0.0001$); although, its contribution to total variability was small in relation to other variables (Table 5.4). Two-way interaction effects on U related to particle shape were not significant ($p > 0.05$). A cylindrical shaped particle, with the same radius and length, has more volume than a sphere of the same radius; and a cube shaped particle, with the side dimension same as the radius and length of a cylinder, has more volume than the cylindrical particle. At a given particle concentration (30% in the present case) in the can, the number of cube shaped particles will be lower than the number of cylindrical particles; in turn this will be lower than the number of spherical particles. With particles of different shapes in cans results in the creation of different void spaces and resultant differences in liquid mixing. U values for oil and water were found to be highest for spherical shaped particles and lowest for cube shaped particles. This is consistent with the availability of void spaces for mixing. Figure 5.5 a & b are the plots illustrating the influence of particle shape in oil and water, at different rotational speeds. On an average, U value, for a cube in oil was 3% lower than that for a cylinder; this in turn was about 6% lower than that for a sphere. When compared to a cylindrical particle the average U value for a sphere in water was reduced by 6%. There was a further reduction of 6% for cube shaped particles.

Particle shape is generally known to have an influence on h_{fp} as a result of differences in liquid flow profile along the surfaces. For the same particulate matter and heating conditions, the cube-shaped particles will have lower heat transfer rates than cylindrical particles; in turn cylindrical particles will have lower values than spherical particles, although the volume to surface area for all three differently shaped geometries remain the same (Chandarana and Gavin, 1989).

Analysis of variance of data revealed that particle shape influenced h_{fp} more than U (Table 5.4). The particle shape effect on h_{fp} was significant ($p \leq 0.0001$) with both single

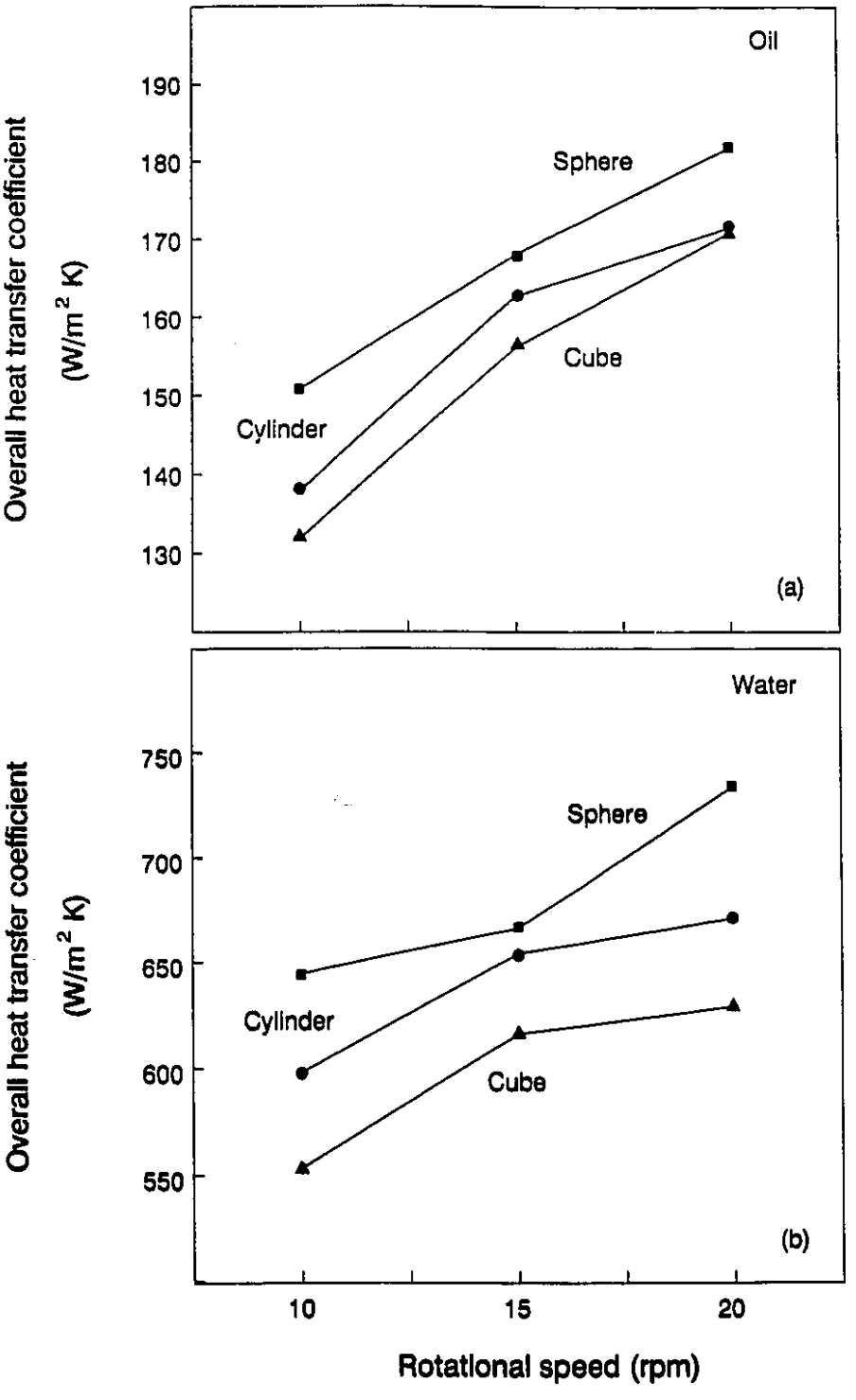

Figure 5.5 Influence of ***particle shape*** on overall heat transfer coefficient (U) at different rotational speeds, for oil and water

and multiple particles in cans. Figure 5.6 a & b and 5.7 a & b are plots showing the influence of particle shape on the fluid to particle heat transfer coefficient, for oil and water at different speeds, with single and multiple particles in the cans. With a single particle in the can, h_{fp} values were higher for a cube shaped particle compared to a cylindrical particle; and in turn h_{fp} values were higher for a cylindrical particle compared to a spherical particle. This is consistent with earlier observations. In this case, the overall mixing of can liquid was not very different for different particle shapes; however, because of the presence of a single particle, the flow field around the particle was strongly influenced by particle shape, which affected the heat transfer coefficient. The particle shape effect was probably more predominant, due to disturbance in the flow field near the surface of the cylindrical and cube shaped particles. The cube shaped particle behaved as an extreme case of a particle with a rough surface (Astrom and Bark, 1994). The h_{fp} in oil increased by 6% with the cube shaped particle, compared to that of cylindrical particle which, in turn, increased by 20% compared to spherical particle. The particle shape influence was more pronounced in water, increasing the h_{fp} by 29% with the cube shaped particle when compared to that of the cylindrical particle, and 72% with the cylindrical particle compared to that of the spherical particle.

With respect to multiple particles (30% particle concentration), the trend of h_{fp} reversed with particle shape, giving highest values for spherical particles and lowest values for cube shaped particles. This can be explained by the packability of the particles in the can, and the extent of void spaces between differently shaped particles. A can filled with spherical particles will have uniform and narrow void spaces compared to other particles of different geometry resulting in a higher liquid velocity around the particles. The cylindrical and cube shaped particles are larger in size and probably have a thicker boundary layer associated with them. At any instance during the end-over-end rotation of can, if the surface of these particles remained parallel thereby touching through their heat transfer surfaces (top or bottom side of cylinder, or any of the side of cube), this would reduce the surface area for a given volume and make the particle size much larger; thus, reducing the h_{fp} with cylindrical and cube shaped particles. The h_{fp} in oil decreased by 8% with cylindrical particles when compared to that of spherical particles; and, it reduced a

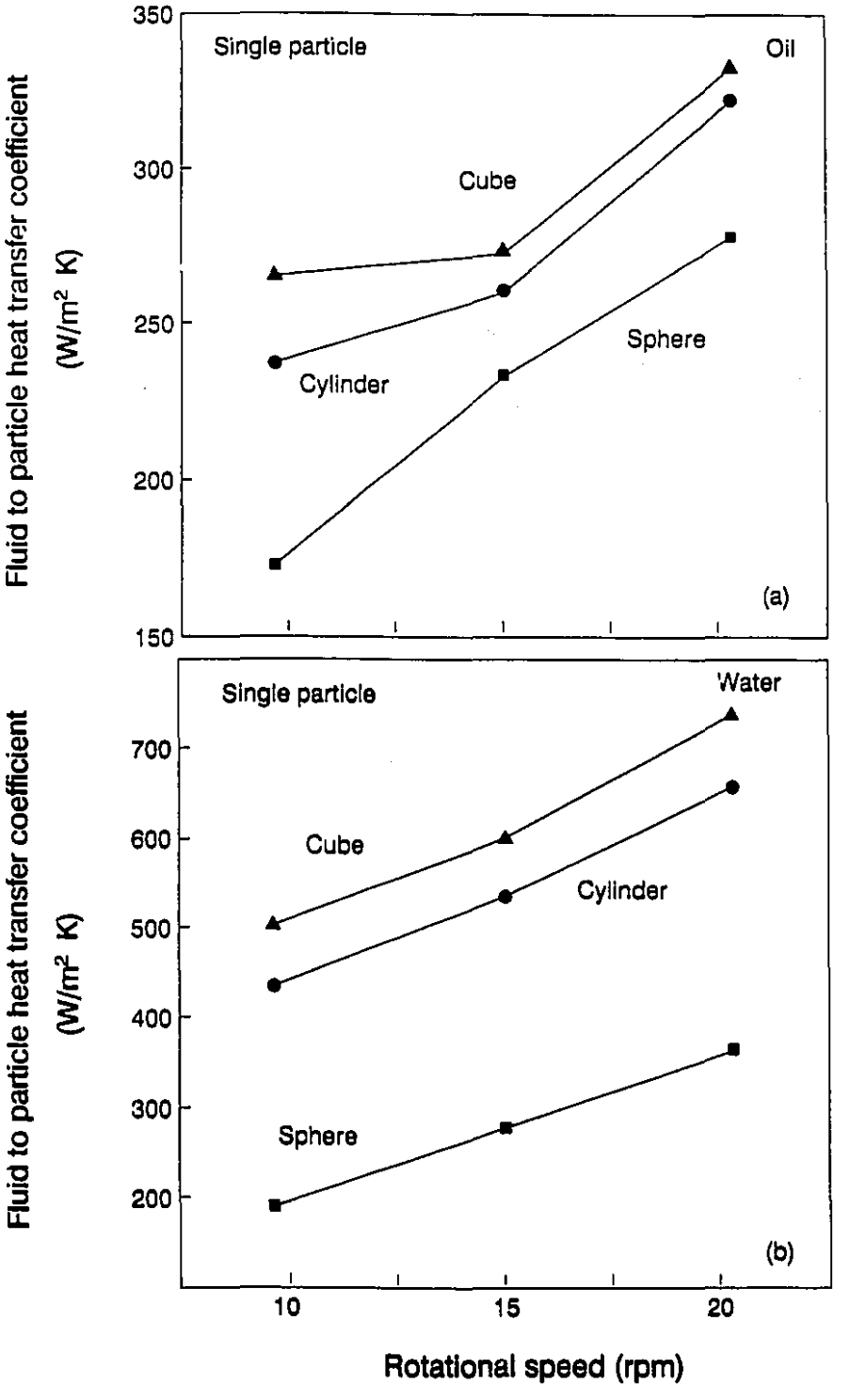

Figure 5.6 Influence of ***particle shape*** on fluid to particle heat transfer coefficient (h_{fp}) at different rotational speeds, for oil and water (with a single particle in the can)

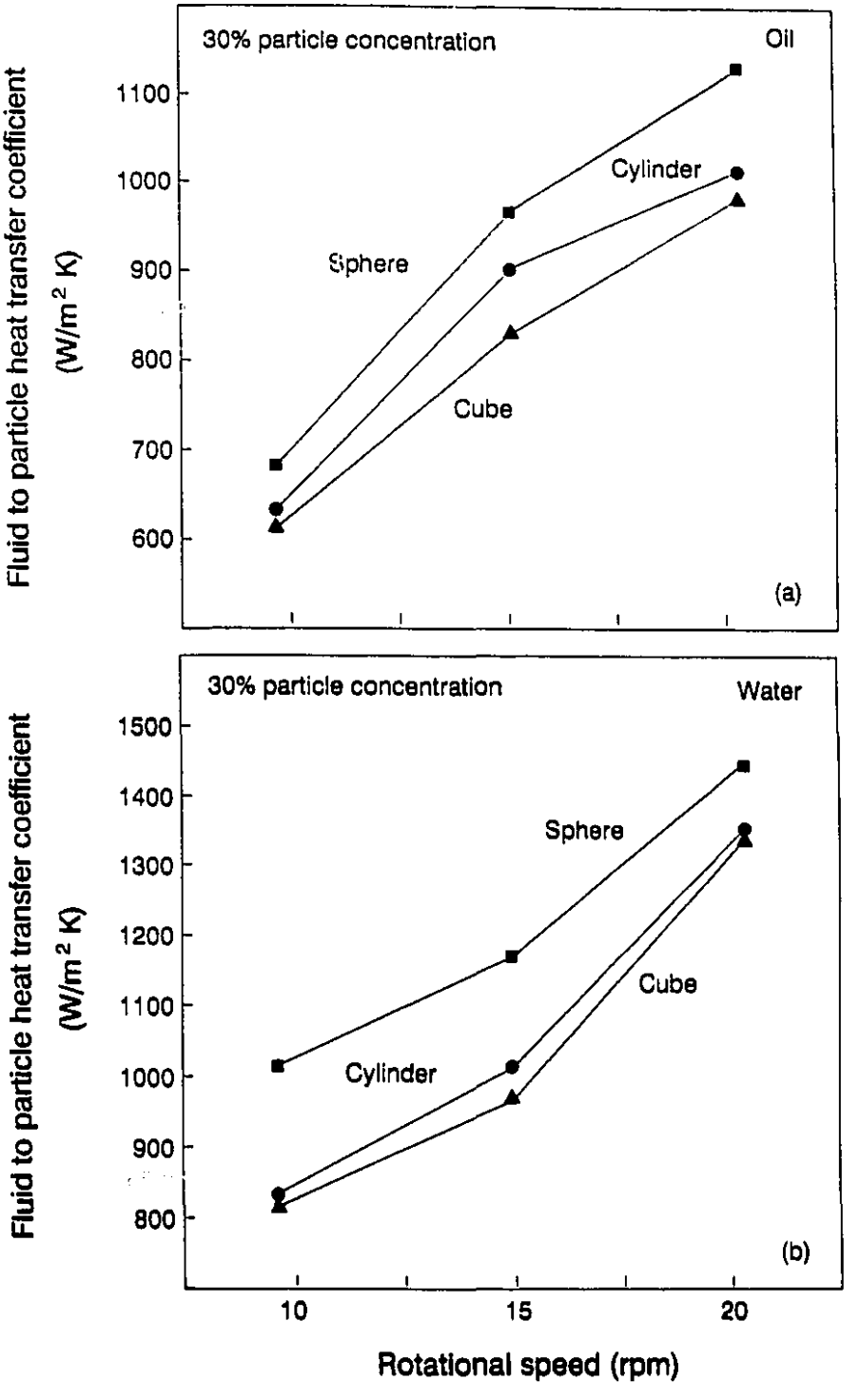

Figure 5.7 Influence of ***particle shape*** on fluid to particle heat transfer coefficient (h_{fp}) at different rotational speeds, for oil and water (with multiple particles in the can)

further 5% with cube shaped particles. In water, cylindrical particles reduced the h_{fp} by 11% when compared to spherical particles; and the cube shaped particles lowered h_{fp} by 3%, when compared to cylindrical particles.

CONCLUSIONS

The overall and fluid-to-particle heat transfer coefficient were influenced ($p \leq 0.0001$) by particle size, concentration and particle shape (with single and multiple particles), at all the rotational speeds. Using a flexible thermocouple approach for temperature measurement of the moving particle, the range of h_{fp} value obtained in the present study was comparable to some previously published values. Higher U and h_{fp} values were obtained at lower liquid viscosity and higher rotational speeds. An initial increase in particle concentration, from a single particle level, enhanced U and h_{fp}; however, particle concentrations more than 20% and 30% decreased U and h_{fp}, respectively. U and h_{fp} followed a reciprocal relationship with particle size in oil and water, at all the rotational speeds. With a single particle in the can, U was not affected by particle shape; however, under any experimental condition, h_{fp} values were lowest with the sphere and highest with the cube. In the case of multiple particles in the can, U and h_{fp} values were in decreasing order: highest with sphere, followed by cylinder and cube. The influence of particle size, particle concentration and rotational speed were more pronounced for the viscous liquid (oil). The influence of particle shape was more pronounced with a single particle in the can.

CHAPTER 6

MOTION OF SINGLE AND MULTIPLE PARTICLES IN CANS SUBJECTED TO END-OVER-END ROTATION, AS INFLUENCED BY SYSTEM AND PRODUCT PARAMETERS

ABSTRACT

The effects of system and product parameters on particle motion/mixing were investigated experimentally with single and multiple particles, in transparent plastic containers. A flexible fine-wire thermocouple extending from the container wall was attached to a particle, as in this heat transfer experiments detailed in Chapters 3-5. The containers were subjected to end-over-end rotation in a rotary retort, at room temperature, with the door held in an open position for video taping of particle motion in the container. With a single particle in the container, the effect of particle density, and with multiple particles in the container, the effects of particle concentration, particle size and particle shape were evaluated with oil and water, at different rotational speeds (10 to 20 rpm). The particle motion was affected by all the processing conditions considered in this study.

INTRODUCTION

In Chapters 4 and 5 the effect of various system and product parameters on U and h_{fp} has been quantified with single and multiple particles in cans, during end-over-end processing. In the agitation processing of cans containing liquid and solid particles, both the overall heat transfer coefficient and fluid-to-particle coefficients are influenced by particle motion. Recently, Merson and Stoforos (1990) studied the motion of spherical particles in axially rotating cans and characterized the particle-to-liquid relative velocity, under idealized conditions of particle motion in rotating containers. Their flow visualization study also revealed much more complicated particle motion than idealized in mathematical analyses. Later Stoforos and Merson (1992) used particle motion study

to explain the decrease in h_{fp} between a Teflon sphere and 350 cst silicone oil with increasing rotational speed and decreasing liquid viscosity.

The objective of this study was to characterize the particle motion/mixing at various rotational speeds, with single and multiple particles in containers, during end-over-end rotation. The effect of particle density (with a single particle), particle concentration, particle size, particle shape (with multiple particles) and liquid viscosity were studied at different rotational speeds. The flow visualization study was carried out to enable qualitative assessment of the particle motion/mixing effects on the magnitude of h_{fp}, under various experimental conditions.

MATERIALS AND METHODS

The experiments were performed in transparent containers under rotational conditions similar those employed in the heat transfer studies (Chapters 3-5). For this purpose, plastic containers of size (7.5 cm diameter and 10 cm height) were used in place of the cans and a rigid needle-type thermocouple wase installed on the side-wall with its tip reaching the geometric center of the container. Thermocouple equipped particles were placed inside the containers, as detailed with cans in Chapter 3. The effect particle density was studied with a single particle in the container. Four containers were prepared for this, each with a particle of different density (polypropylene, Nylon, Delrin and Teflon). With multiple particles in the containers, the range and values of variables were similar to those found in the heat transfer study (Chapter 5). Nylon particles were used to study the effect of particle concentration (20, 30 and 40%), particle size (19, 22 and 25 mm) and particle shape (sphere, cylinder and cube). All experiments were performed with oil and water at three rotational speeds (10, 15 and 20 rpm). Experiments were carried out in a Stock Rotomat-PR 900 at room temperature, with the processing vessel door held open for visual observation. At the beginning of experiment, with multiple particles in the container the containers were filled with two layers of particles of different colors and liquid (oil or water). The experimental particle was positioned near the geometric center of the container. The mixing of the two color particles and the motion of the thermocouple

equipped particle were observed during container rotation. All the experiments were video taped, played subsequently on a slow motion VCR/TV and photographed for characterization of the particle motion. In each run, the experiment lasted about 4-6 min.

RESULTS AND DISCUSSION

Motion of single particle

The clear plastic containers closed with a single particle (free or attached to a thermocouple wire) and test liquid, leaving a 10 mm headspace, represented a system consisting of a continuous medium of liquid (oil or water), a solid particle (polypropylene, Nylon, Delrin or Teflon) and a headspace bubble. In such a system, the magnitude of the particle to liquid relative velocity is a result of the combined effect of gravitational, drag, buoyant and centrifugal forces. The problem of theoretical characterization is complex, when it relates to particle motion and the particle-to-liquid relative velocity during end-over-end rotation of containers. In the present study, particle motion was not quantified; however, based on the particle motion in the container under different rotational conditions, a qualitative assessment was made to characterize the particle motion and relate it to the associated heat transfer coefficient.

Under any of the test conditions, the thermocouple wire inserted in the particle did not entangle with the rigid needle-type thermocouple mounted inside the container for liquid temperature measurement. The length of the thermocouple wire was also long enough for the particle to travel to any location inside the container. There was almost no rolling action when the particle was attached to the thermocouple, whereas the free particle rolled along the wall occasionally.

The motion associated with the particles under different conditions could be somewhat generalized with respect to three particle density groupings: (i) those with a density much higher than the density of the covering liquid (Delrin, Teflon), (ii) those with a moderately higher density than the liquid medium (Nylon) and (iii) the lower density polypropylene particles with a density somewhat close to that of oil, but lower than water. These are described below:

Motion of moderately dense particles

Sectional views of the container and the locations of the headspace bubble and particle, during a clock-wise end-over end rotation, is shown in the top section [(i)] of Figure 6.1. The path of the particle in the container, as it completes a full rotation at 10 to 20 rpm, is traced in the bottom section [(ii)] of Figure 6.1. It was observed that at the lower rotation speed (10 rpm), the moderately dense particle generally slid along the container wall in the direction opposite to the container rotation. At the higher rotational speeds of 15 and 20 rpm, the container surface renewed rather more quickly and the particle slowly moved away from the container wall, until it reached the wall perpendicular to it, occasionally with some sliding early on. The headspace bubble also moved along the wall, creating a wake behind, again in the direction opposite to that of the container rotation. At higher rotational speeds, the headspace bubble moved faster, resulting in a higher degree of mixing. In all cases higher settling velocities were observed in water compared to those observed in oil. In the heat transfer studies it was also found that the h_{fp} increased with increasing rotational speed and decreasing fluid viscosity. Especially at higher rotation speeds, it was observed that the Nylon particle in oil sometimes skipped the shorter surfaces (bottom and top lids), thereby occasionally jumping, for example, from the top corner to the diagonally opposite corner along a curved path.

Motion of high density particles

Delrin and Teflon particles experienced higher gravitational and centrifugal forces during the end-over-end rotation due to larger density. As shown in Figure 6.2, at the lower rotational speed (10 rpm), the Teflon particle moved in a manner similar to the moderately dense particles (Nylon). However, at higher rotational speeds, the particle neither slid along the container wall [Figure 6.2(ii)], nor went too far from the wall. Due to gravity, the particle quickly dropped to the lower surface of the container during a quarter of the turn; and, because of the large centrifugal force acting on the particle, it stayed in the corner until the container was sufficiently tilted, and then dropped again due to gravity in next quarter turn (Figure 6.2). At 20 rpm, the Teflon particle appeared to

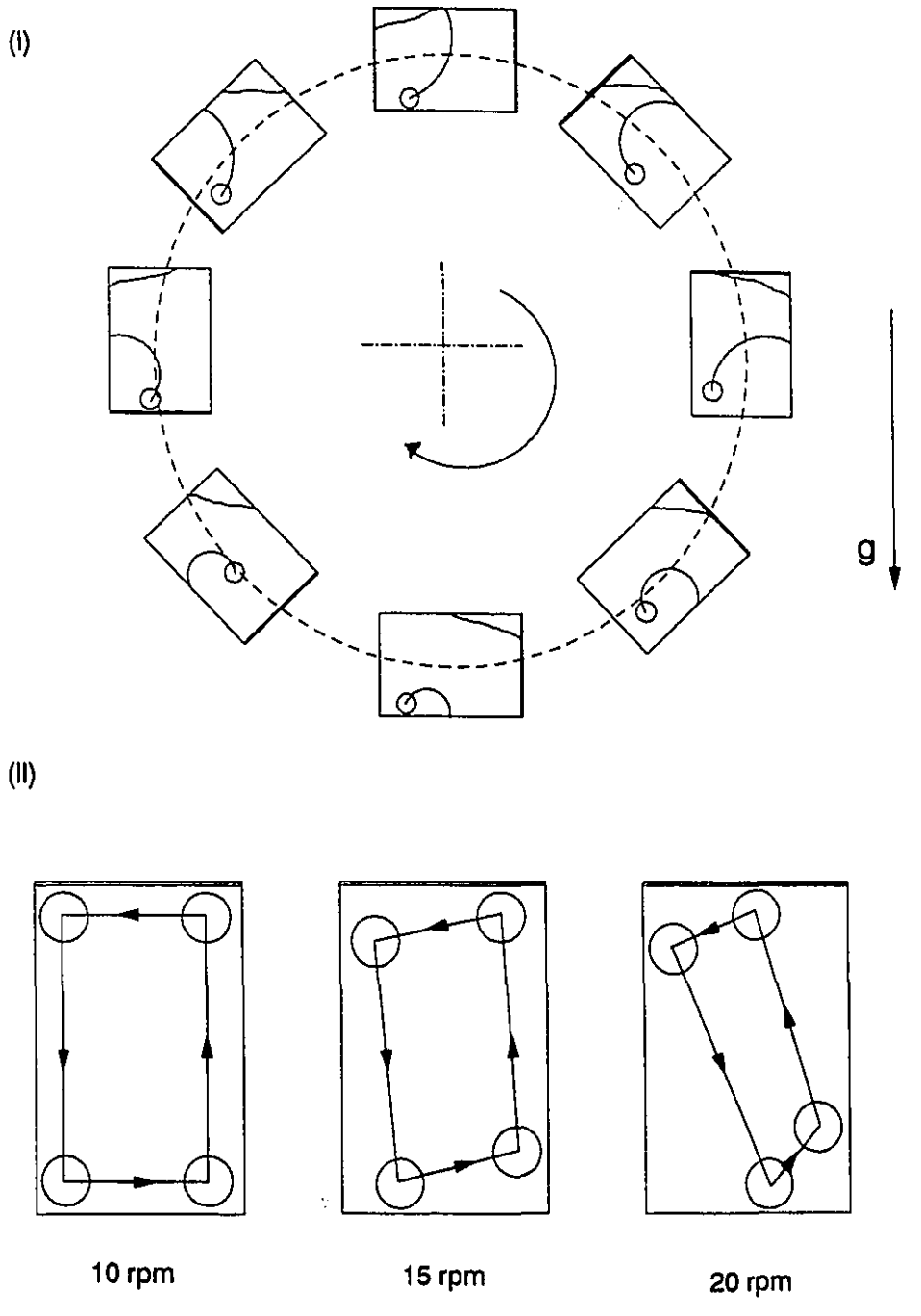

Figure 6.1 Typical sectional views of the container and the location of the headspace bubble and particle, during a clock-wise end-over-end rotation (I) and particle trajectory at 10, 15 and 20 rpm (II): ***Moderately dense particle (Nylon)***

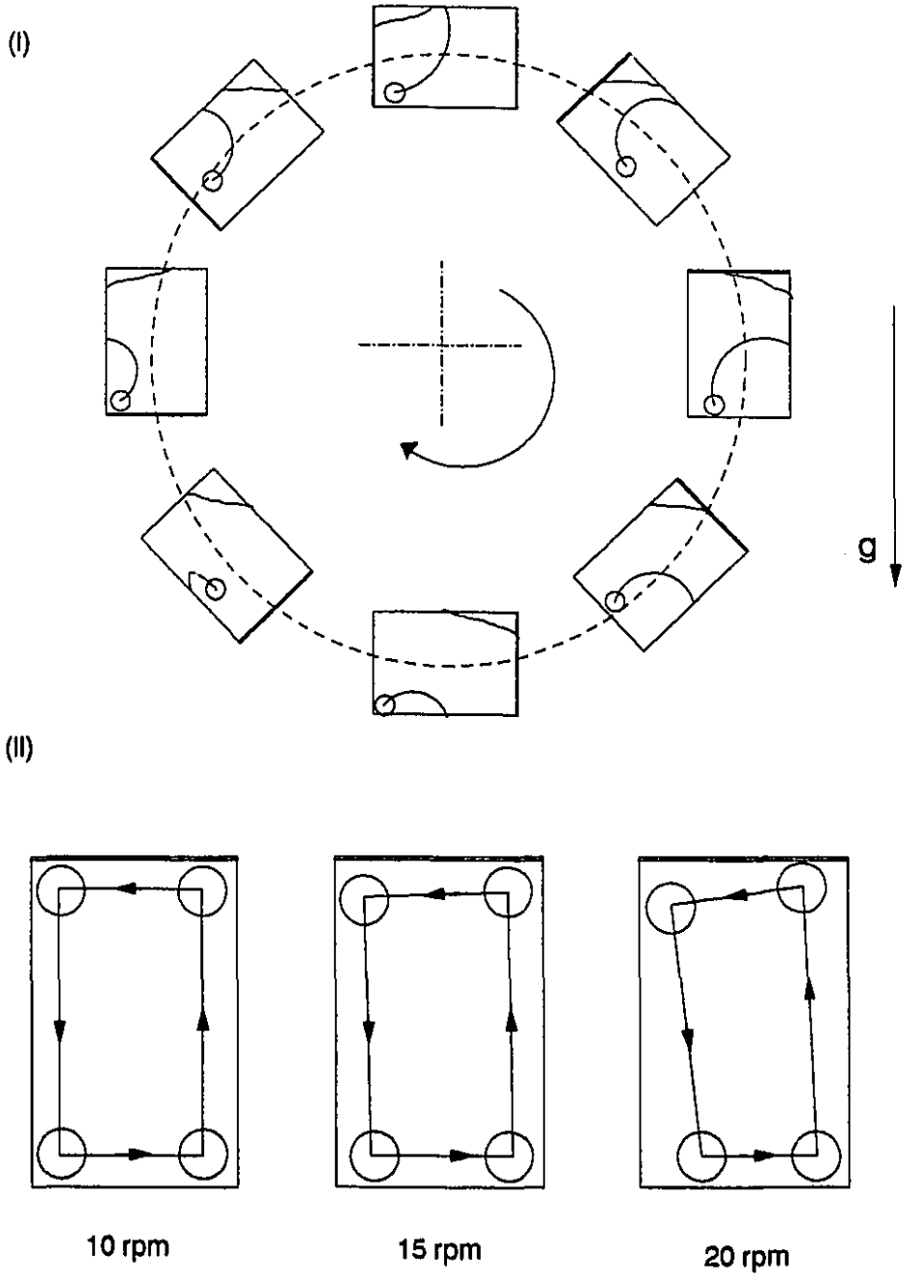

Figure 6.2 Typical sectional views of the container and the location of the headspace bubble and particle, during a clock-wise end-over-end rotation (I) and particle trajectory at 10, 15 and 20 rpm (II): ***High density particles (Teflon and Delrin)***

have more idle time at the contact points than travel time between them. This reduces the effective motion of the particle and possibly accounts for the reduced h_{fp} under similar processing conditions (Chapter 4).

Motion of lower density particles

The density of the polypropylene particle was lower than that of the water and hence, the buoyancy force acting on it was higher than the gravitational force. It was observed that the particle slid along the container wall in the opposite direction of the container rotation (Figure 6.3). The difference, between this and the other two situations discussed earlier, is that the polypropylene particle in water mostly moved with the headspace bubble rather than falling behind it. With increased rotational speeds, it slightly lagged the bubble movement. Due to lower drag forces, the particle to liquid relative velocities were higher in water than in oil.

The thermocouple equipped polypropylene particle remained lightly suspended in oil, since its density was close to that of the oil. This simulated the condition of particle and liquid of nearly equal densities. In this situation, the difference was marginal between gravitational and buoyant forces acting on the particle, and thus centrifugal and drag force (due higher viscosity of oil) became more important. The magnitude of particle to liquid to relative velocities was lower, compared to that observed in other situations; this could account for their lower associated h_{fp} values. The polypropylene particle in oil did not move along the container wall, it did with all other situations. During the rotation, centrifugal force exerted on oil was more than that exerted on the polypropylene particle; this was due to a positive density difference and therefore the particle mostly remained inwards (along the container wall closer to axis of rotation) (Figure 6.4). A slight oscillatory motion was also observed. At higher rotational speeds, particle motion remained the same with a slight decrease in amplitude of the oscillation; but, obviously, with an increased frequency due to higher rpm.

The above description of the motion of particles of different densities, at different rotational speeds in oil and water, are somewhat consistent with the observed variation in the associated h_{fp} values under similar conditions. In general, higher h_{fp} values were

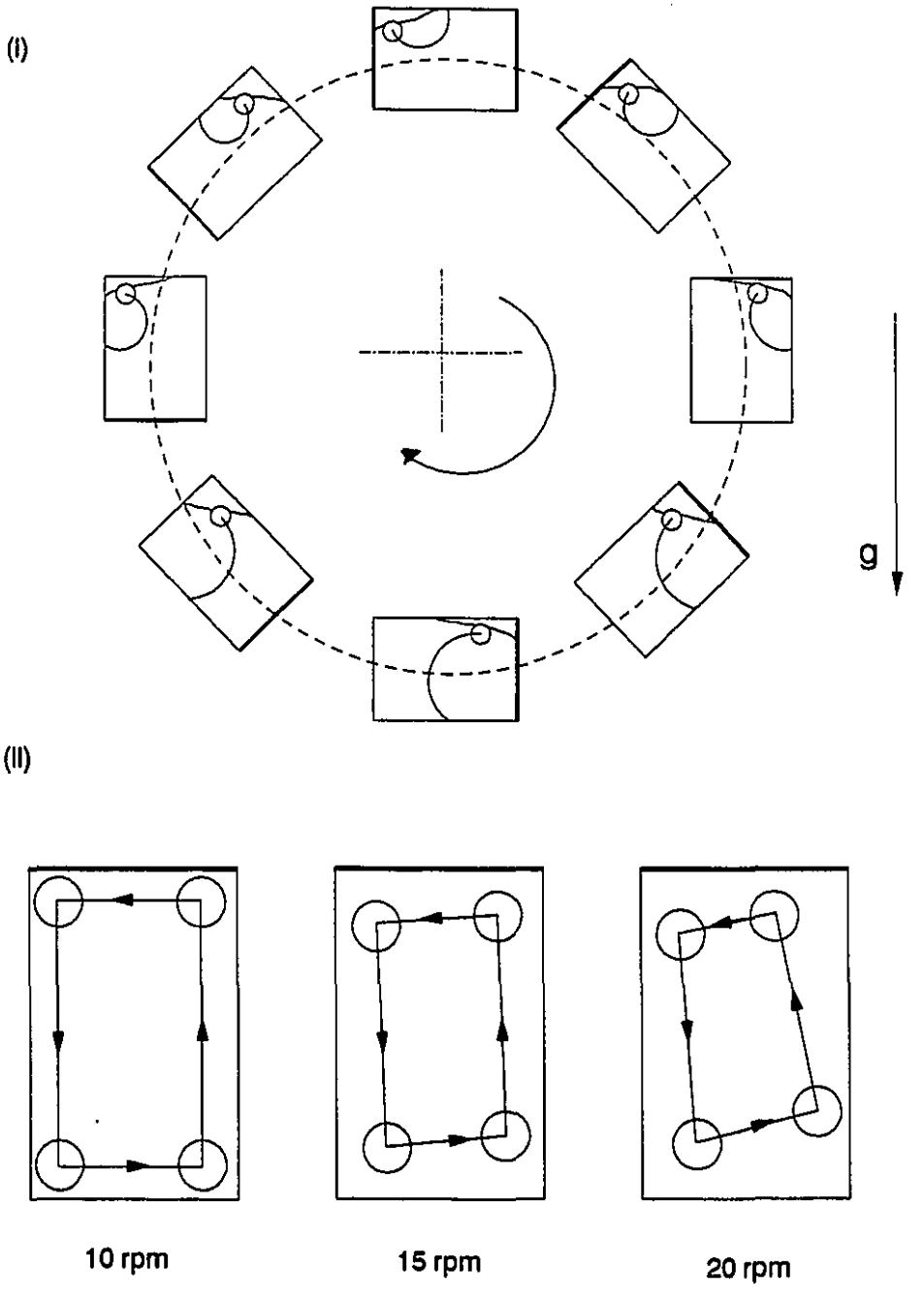

Figure 6.3 Typical sectional views of the container and the location of the headspace bubble and particle, during a clock-wise end-over-end rotation (I) and particle trajectory at 10, 15 and 20 rpm (II): ***Low density polypropylene particle in water***

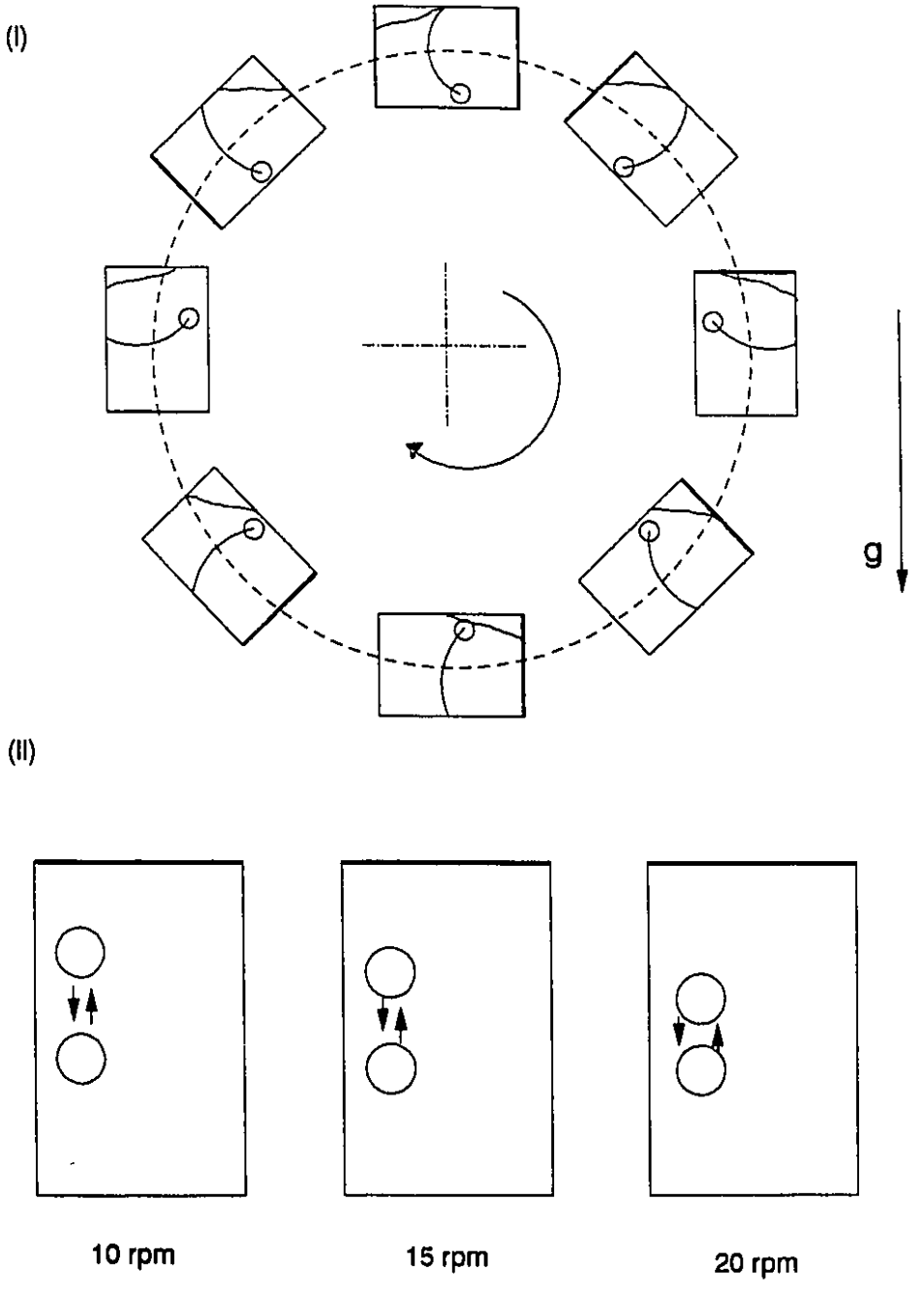

Figure 6.4 Typical sectional views of the container and the location of the headspace bubble and particle, during a clock-wise end-over-end rotation (I) and particle trajectory at 10, 15 and 20 rpm (II): ***Low density polypropylene particle in oil***

observed under conditions of faster particle movement, which in turn was interdependent on particle/liquid relative density, rotation speed and liquid viscosity.

Motion/mixing of multiple particles

Particle motion has an important effect on the associated convective heat transfer coefficient (U and h_{ip}). The presence of multiple particles are expected to cause secondary agitation, influencing the mixing of materials in the container due to their motion.

Influence of particle concentration

Sectional views of the container filled with multiple particles of two different colors at various times, are shown in Figure 6.5. The particle concentration effect was studied with spherical particles (diameter = 19 mm). At the lower concentration (20% v/v) the particles mixed very quickly and this was evident from the mixing of two color particles (shown in different shades) (Figure 6.5a). The thermocouple equipped particle mixed with all the other particles and moved freely in the container during the end-over end rotation. The particles had a good rolling action apart from random movement. At higher particle concentration (40% v/v) the container was packed tightly which restricted the free particle movement, this probably caused the measured heat transfer coefficient to be lower (Chapter 5). The particles slid mostly along the container wall, with minimal rolling action, and the particles of the two colors remained separated in layers for a longer period (Figure 6.5c). The thermocouple equipped particle stayed in the central part of the container in between other particles and for most of the time it was not visible. At the mid level of 30% particle concentration, particle mixing was somewhat in between that for the lower and higher particle concentrations (Figure 6.5b). In the early part of the experiment, particles of each color stayed separate in two large groups and then moved together. As time progressed, the larger groups were divided into smaller ones showing some degree of mixing. The thermocouple equipped particle also had sufficient movement. The particle mixing time was relatively shortened, as the rotational speed increased from 10 to 20 rpm. The particle mixing was slowed down in the higher viscosity liquid (oil), due to increased drag on particles. The particles appeared to be more

(a) 20% Particle concentration

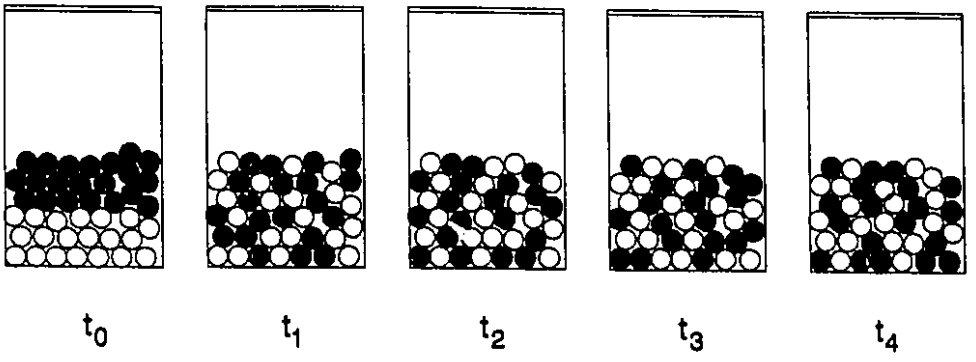

(b) 30% Particle concentration

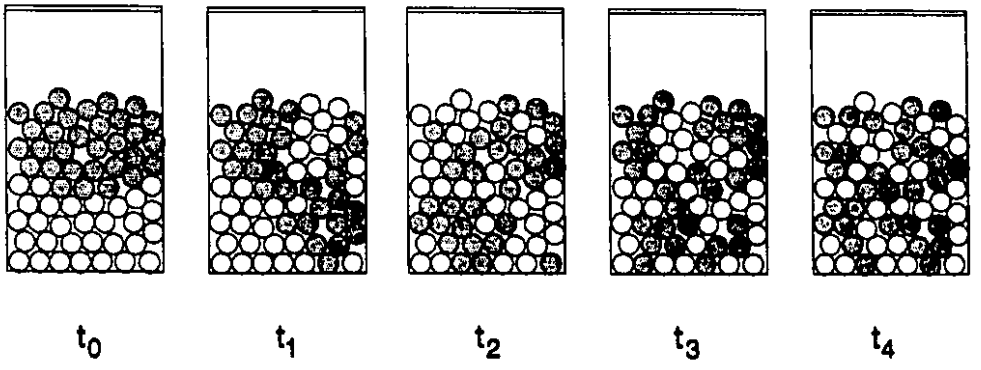

(c) 40% Particle concentration

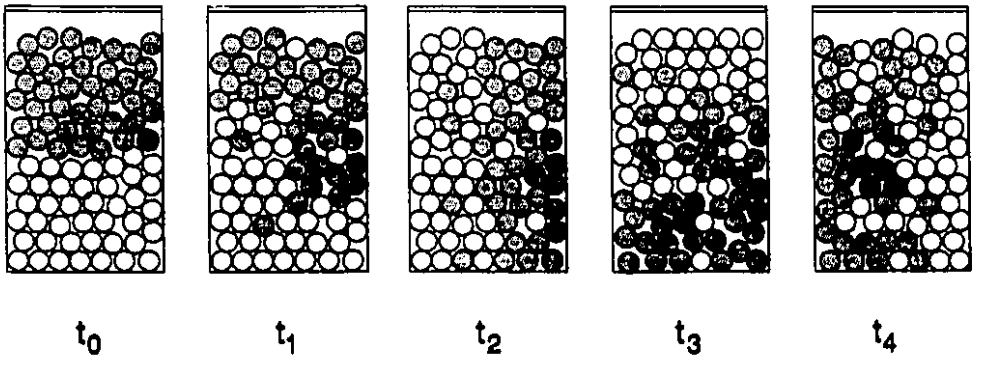

Figure 6.5 Typical sectional views of test containers, at different times during rotation of containers, with different ***particle concentrations***, showing the particle mixing behavior

suspended in oil, at a higher rotational speed. This occured because the particles had a lower settling velocity in oil, and before falling to the bottom of the container surface they turned quickly, due to higher rotational speed.

Influence of particle size

For a given particle concentration (30% v/v), with increased particle size, the container appeared more packed; thus, the particle motion/mixing was reduced slightly (Figure 6.6). In heat transfer studies it was also found that the heat transfer coefficients reduced with increasing particle size (Chapter 5). The mixing of the larger diameter (25 mm) particles at 30% particle concentration was similar to that of the smaller diameter (19 mm) particles at 40% concentration. The larger size particles mostly moved along the container wall with a reduced rolling action. The effect of liquid viscosity and rotational speed was similar to earlier observations. Increasing rotational speed and deceasing liquid viscosity reduced the particle mixing time.

Influence of particle shape

The volume of a cube shaped particle was higher than that of a cylindrical particle for the same maximum dimension; the volume of cylindrical particle was higher than that of a spherical particle. a container filled with spheres had uniform void spaces compared to the cylinder and cube shaped particles. A container filled with cylindrical and cube shaped particles appeared more packed, compared to a container with spherical particles, where the particles touched each other through their plane surfaces (top or bottom side of cylinder, or any of the side of cube). This probably reduced the heat transfer surface area for a given volume, thus reducing the heat transfer coefficient. The particle motion/mixing and rolling action were also reduced with the cylinders and cubes, when compared to spheres (Figure 6.7). The motion of the thermocouple equipped particle was lowest with the cube shaped particle. The rotational speed and liquid viscosity also affected the particle mixing time, in a manner previously observed with multiple particle concentrations.

(a) 19.05 mm diameter

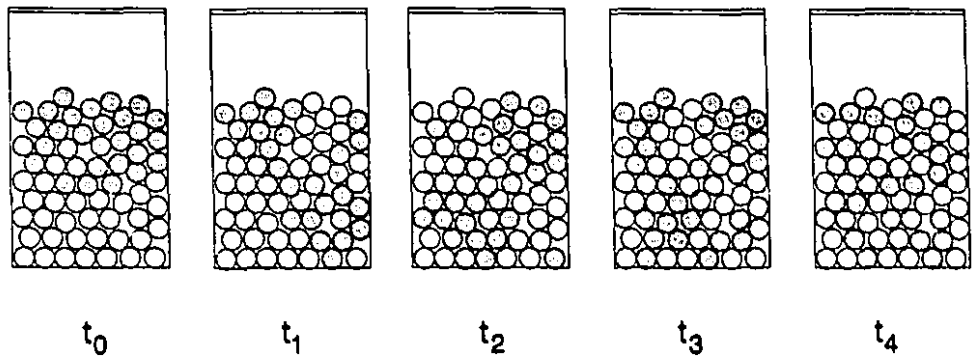

(b) 22.25 mm diameter

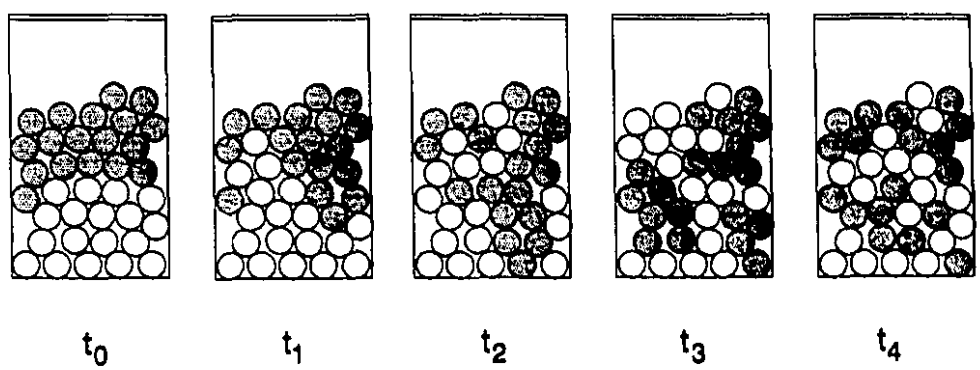

(c) 25 mm diameter

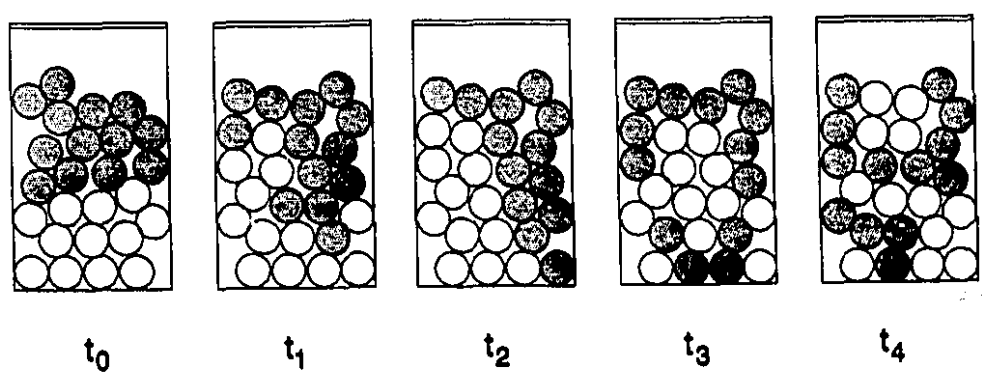

Figure 6.6 Typical sectional views of test containers, at different times during rotation of containers, with different ***particle sizes***, showing the particle mixing behavior

(a) Sphere (diameter 19.05 mm)

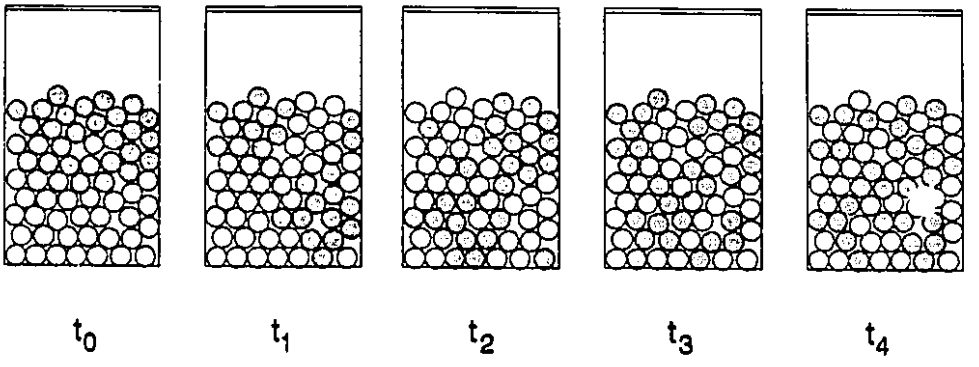

(b) Cylinder (diameter 19.05 mm and length = 19.05 mm)

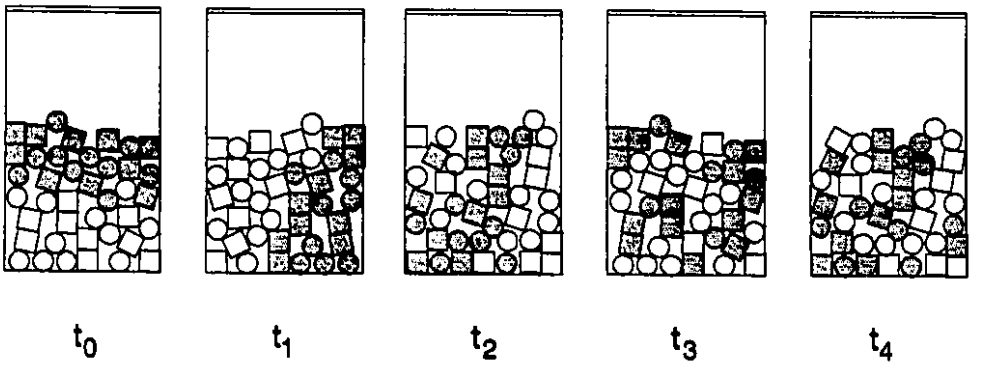

(c) Cube (length = 19.05 mm)

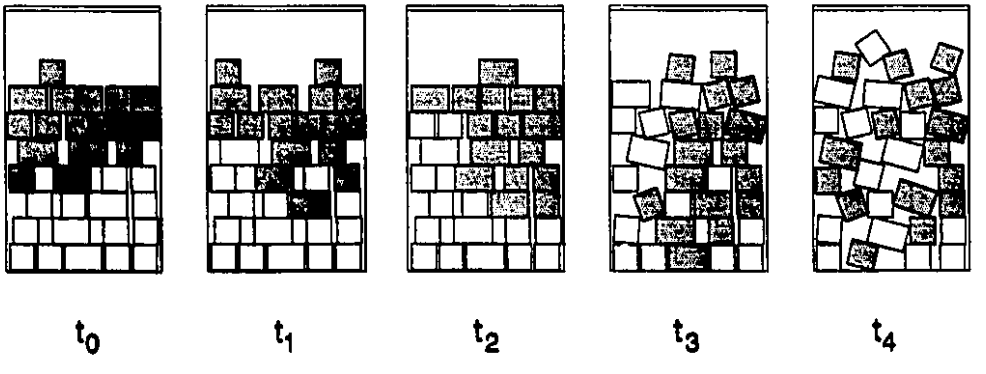

Figure 6.7 Typical sectional views of test containers, at different times during rotation of containers, with different ***particle shapes***, showing the particle mixing behavior

CONCLUSIONS

The flexible thermocouple equipped particle had sufficient movement during end-over-end rotation. The particle motion/mixing in the container, under different processing conditions, varied depending on the processing conditions. With a single particle in the container the liquid viscosity, rotational speed and particle density influenced the particle motion in the container during end-over-end rotation. Increasing particle concentration, particle size and particle shape varying from sphere to cube increased the particle mixing time. The particle mixing time was shortened at higher rotational speed and lower liquid viscosity. These results helped to explain some variations in the heat transfer coefficients detailed in preceding Chapters.

CHAPTER 7

DIMENSIONLESS CORRELATIONS FOR THE PREDICTIVE MODELING OF CONVECTIVE HEAT TRANSFER COEFFICIENTS IN CANNED LIQUID/PARTICLE MIXTURES, SUBJECTED TO END-OVER-END PROCESSING

ABSTRACT

Dimensionless correlations, for predictive modeling of forced convection heat transfer coefficients in cans with end-over-end rotation, were investigated using multiple regression of significant dimensionless groups. The data for overall heat transfer coefficient, U, and fluid to particle heat transfer coefficient, h_{fp}, were obtained for several processing conditions, and analyzed separately for single and multiple particles in the can. Heat transfer to a single particle was modeled. This was based on particle settling theory, with terminal velocity resulting from the combined forces of gravity, buoyancy, centrifugal and drag acting on it, during end-over-end rotation. In the presence of multiple particles, heat transfer to the moving liquid/particles system was modeled as in a packed bed. Attempts were made to account for the particle shape and size effects on U and h_{fp} by taking particle sphericity (Ψ = surface area of an equivalent sphere / surface area of the particle) and particle equivalent diameter (as diameter of sphere of volume equal to that of particle, d_e) into the correlation equation. For U with a single particle in the can, Nusselt number (Nu) was related to Reynolds number (Re), Prandtl number (Pr) and relative can headspace; while with multiple particles, Re, Pr, ratio of particle to liquid concentration, relative particle diameter and Ψ were found to be significant. For h_{fp} with a single particle in the can, Nu was related to Re [or Froude number (Fr)], Pr, density simplex (*a*), relative can headspace and the ratio of the sum of the diameter of rotation and diameter of the can to the can diameter, while with multiple particles, Re [or Peclet number], ratio of particle to liquid thermal conductivity, the particle to liquid concentration ratio and particle sphericity were found to be significant parameters.

INTRODUCTION

Experimental time-temperature data are commonly used to establish a thermal processing schedule for canned liquid foods containing particles. Theoretical models can also be used for the process design, optimization and validation of these systems. Successful temperature prediction, for liquid/particulate canned food, requires data on the overall heat transfer coefficient from the heating medium to the can liquid (U), and the fluid-to-particle heat transfer coefficient (h_{fp}), beside the relevant thermo-physical properties. The convective heat transfer coefficients associated with canned foods, undergoing thermal processing, are influenced by various retort operating conditions and liquid and particle properties. The effect of such parameters on U and h_{fp} in canned liquid/particle mixtures with end-over-end processing, have been quantified in Chapters 4 and 5.

Dimensional analysis is a useful technique for generalization of data as it reduces the number of variables that must be studied and permits the grouping of physical variables that affect the process of heat transfer. In the dimensional analysis of convective heat transfer, Nusselt number (Nu) (a dimensionless measure of convective heat transfer coefficient) is correlated with other dimensionless numbers like Reynolds number (Re), Prandtl number (Pr) etc. Earlier studies in this area mainly focused on the convective heat transfer in liquid foods; and therefore, the developed dimensionless correlations involved the overall heat transfer coefficient (U). An excellent review of these studies was presented by Rao and Anantheswaran (1988). However, very little information is available on using dimensional analysis for canned liquid/particle food systems. Lenz and Lund (1978) and Deniston et al. (1987) presented dimensionless correlations for U relating Nu to Re, Pr and other dimensionless quantities. They did not develop similar correlations for h_{fp}. Fernandez et al (1988) presented dimensionless correlations for h_{fp} in cans with axial rotation. They modeled the correlations based on fluidized bed and packed bed approaches, and used the modified Stanton number and Colburn j-factor in empirical correlations; however, they did not develop correlations for U. The time-temperature prediction at the particle center requires appropriate correlations for both U and h_{fp}. In the

literature, correlations are not available for U and h_{fp} in particle/liquid can with end-over-end rotation.

The objective of this study was, therefore: to develop dimensionless correlations, for overall as well as fluid to particle heat transfer coefficients and to describe the heating behavior of liquid and particles in cans with end-over-end rotation. Since U is not influenced by the presence of a single particle in the can (Chapters 4 and 5), this situation simulated the liquid only condition in the can.

THEORETICAL BACKGROUND

The heat transfer to liquid and particles, in cans with end-over-end rotation is affected by both liquid and particle physical properties and retort operating conditions. In the dimensional analysis of forced convective heat transfer, the heat transfer coefficient (U or h_{fp}) is expressed in terms of the Nusselt number (Nu), which is generally described as a function of other dimensionless numbers consisting of: liquid, particle and system properties (all symbols are detailed in nomenclature):

$$Nu = f(Re, Pr, Fr, Ar) \tag{7.1}$$

The heat transfer correlations reported in the literature for U and h_{fp} are shown in Table 7.1. Only the dimensionless correlations for processing of liquids undergoing end-over-end rotation are presented in Table 7.1, due to their direct relevance to the present study. Heat transfer correlations for h_{fp}, in the presence of multiple particles, is published only for axial rotation. Detailed information on heat transfer correlations, covering other food processing conditions (mainly aseptic processing) are detailed in Awuah et al. (1996) and Ramaswamy et al. (1996).

MATERIALS AND METHODS

Materials and experimental parameters

Water and high temperature bath oil (100 cst), giving different viscosity levels, were used as test liquids. Inert particles of different sizes, shapes and densities were used as test particles. Thermo-physical properties of the liquids and particles were measured experimentally and these are summarized in Chapter 3. The range of parameters related to liquid, particles and retort operating conditions are summarized in Table 7.2. The experimental and mathematical procedures to determine overall heat transfer coefficient and fluid to particle heat transfer coefficient, and together with the gathered data, are detailed in Chapters 4 and 5.

Table 7.1 Published dimensionless correlations for overall heat transfer coefficient (U) and fluid to particle heat transfer coefficient (h_{fp})

Heat transfer to the can liquid without particles

Duquenoy (1980) : End-over-end rotation

$$Nu = (17 \times 10^5)\, Re^{1.449}\, Pr^{1.19}\, We^{-0.551}\, (D_c/2H)^{0.932}\, (V_h/V_c)^{0.628}$$

$$Nu = U D_c / 2k_l \; ; \quad Re = 2\pi N D_c \rho_l L / (D_c+H)\mu$$

Ananthesw aran and Rao (1985) : End over-end rotation

$$Nu = 2.9\, Re^{0.436}\, Pr^{0.287}$$

$$Nu = U(D_r + H) / k_f \; ; \quad Re = (D_r + H)^2\, N\rho_f / \mu$$

Heat transfer to liquids in the presence of particle(s)

Lenz and Lund (1978) : Axial rotation

$$Nu = 115 + 15\, Re^{0.3}\, Pr^{0.08}$$ Single particle in can

$$Nu = -33 + 53\, Re^{0.28}\, Pr^{0.14}\, [d_s / S\,(1-\varepsilon)]^{0.46}$$ Multiple particles in can

$$Nu = U S / k_l \; ; \quad Re = S^2\, N\, \rho_l / \mu$$

Deniston et al. (1987) : Axial rotation

$$Nu = 1.87 \times 10^{-4}\, Re^{1.69}$$

$$[\,((\rho_p-\rho_f)/6C_D\rho_f)\,((\omega^2 D_c + 2g)/\omega^2 D_c)\,(d_s/D_c)\,]^{0.530}$$

$$(\alpha_p/\omega\, D_p^2)^{0.126}\,[\,(1-\varepsilon)\,(H_{ce}/D_{ci})\,(\omega D_c^2/\alpha_f)\,]^{-0.171}$$

$$Nu = UD_c / k_l \; ; \quad Re = \rho_l \omega D_c^2 / 2\mu$$

Heat transfer to the particles

Fernandez et al. (1988) : Axial rotation

$$Nu = 2.7 \times 10^4\, Re^{0.294}\, Pr^{0.33}\, \Psi^{6.98}$$

$$Nu = h_{fp}\, d_e / k_l \; ; \quad Re = d_e 2N\rho_l / \mu$$

Table 7.2 Range of system and product parameters used in the determination of convective heat transfer coefficients (U and h_{fp})

No.	Parameter	Symbol	Experimental Range
1.	Retort temperature	T_R	110, 120 and 130 °C
2.	Diameter of rotation	D_r	0, 0.18, 0.38 and 0.54 m
3.	Rotational Speed	N	10, 15 and 20 rpm
4.	Can headspace	h_s	0.0064 and 0.01 m
5.	Test liquids		Water and oil
6.	Test particles		Polypropylene, Nylon, Acrylic Delrin and Teflon
7.	Particle concentration	ε	Single particle, 20, 30 and 40% (v/v)
8.	Particle shape		Cube, cylinder and sphere
	sphericity	Ψ	0.806, 0.874 and 1
9.	Particle size		
	Cube	l_{cu}	0.01905 m
	Cylinder	l_{cyl} x d_{cyl}	0.01905 x 0.01905 m
	Sphere	d	0.01905, 0.02225 and 0.025 m
10.	Can dimension	D_c x H	307 x 409 (8.73 cm x 11.6 cm)

Characteristic length and regression analysis

Experimental data obtained for U and h_{fp} were used to calculate the Nusselt number from the relationship Nu = U (or h_{fp}) d_{cd} / k_l; where d_{cd} and k_l are the characteristic dimension and thermal conductivity of the liquid respectively. Other dimensionless numbers were calculated using the physical properties of liquid and particle (at the average bulk temperature), and system (operating) parameters. Prior to determining the appropriate correlation, it was important to estimate a characteristic length, for use in the dimensionless numbers. With end-over-end rotation of the can, Duquenoy (1980) used the diameter of the can (D_c) as the characteristic length in the dimensionless correlation, since the study was restricted to a zero diameter of rotation (D_r). Anatheswaran and Rao (1985a) tried different variables and found that use of D_r as characteristic length resulted in very good R^2 (= 0.92) while D_c gave a poor fit of experimental data. Lenz and Lund (1978) used the radius of the reel as the characteristic length in the dimensionless

correlation with axial rotation. Deniston et al (1987) also used D_c in correlations to describe the heating behavior of liquid in the presence of multiple particles. Fernandez et al. (1988) used the diameter of the particle in the development of a dimensionless correlation for fluid to particle heat transfer coefficient. In the present study, U and h_{fp} were both influenced by the diameter of rotation and the size of the particle. A number of combinations involving the diameter of rotation and the diameter of the can were tried as the characteristic length in the regression analysis for the overall heat transfer coefficient. In the development of the correlation for the fluid to particle heat transfer coefficient, the particle size as a characteristic length was more meaningful and hence the shortest particle dimension (d_p), and an equivalent diameter of the particle (as diameter of sphere of volume equal to that of particle, d_e) were tried as characteristic lengths.

In heat transfer correlations, for example in the tube flow situation, the fluid linear velocity is used in the dimensionless numbers (Reynolds number, Peclet number or Froude number); or in the case of the flow over bodies, particle to fluid relative velocity has been considered. The angular velocity of the can has been used in dimensionless numbers involving cans undergoing rotational processing. This has also been widely used in the studies involving mixing of liquids. In the present correlation, angular velocity ($\pi d_{ch}N/60$) was used in the dimensionless form.

Data Analysis

Heat transfer, to the can liquid in rotational processing, is primarily influenced by the forced convection induced by mechanical agitation. The influence of the system and liquid/particle related parameters on U and h_{fp} was determined, both with respect to a single particle in the can and with multiple particles in the can. Therefore, two different sets of correlations were developed for U and h_{fp}, describing heat transfer in cans with i) a single particle and ii) multiple particles.

Overall heat transfer coefficient

Analysis of variance showed that with a single particle in the can, particle properties such as shape, size, density (within the range studied) effects on U were

nonsignificant, and hence were not considered in developing the correlations. Only the influence of retort temperature, rotational speed, radius of rotation, can headspace and liquid viscosity were influential (Chapter 4), and hence included in the correlation. The dimensionless parameters accounting for these effects were Re, Fr, Pr, h_s/H and $(D_r+D_c)/D_c$. The forced convection heat transfer, in the can liquid in agitation processing has been modeled using Re and Pr (Anantheswaran and Rao, 1985a). The liquid properties were evaluated at bulk temperature, which takes account of different retort operating temperatures. The Nusselt number was modeled as function of the following dimensionless groups:

$$Nu = f\left(Re,\ Fr,\ Pr,\ \frac{h_s}{H},\ \frac{D_r + D_c}{D_c}\right) \qquad (7.2)$$

However, the influence of particle size, shape and concentration was also studied in the presence of multiple particles in the can. The effects of these parameters on U were significant and hence included in the correlation. The headspace and diameter of rotation effect were not studied with multiple particles, and hence excluded. Hassan (1984) performed a theoretical analysis on the Navier-Stokes equation, which describes the liquid velocity distribution in the can; the Archimedes number and density simplex was suggested in the dimensionless correlation for the convective heat transfer coefficient (cited by Deniston et al., 1987). A ratio of particle to liquid concentration, a ratio of equivalent particle diameter to the diameter of the can, and particle sphericity were added to the Nusselt number correlation:

$$Nu = f\left(Re,\ Fr,\ Pr,\ Ar,\ a,\ \frac{\epsilon}{100-\epsilon},\ \frac{d_e}{D_c},\ \Psi\right) \qquad (7.3)$$

Fluid to particle heat transfer coefficient

It is recognized that in tube flow systems, the shape of the particle moving in a carrier fluid has a significant influence on its flow behavior and thus on fluid to particle heat transfer coefficient. In the literature, separate heat transfer correlations have been reported for spherical and cylindrical shape particles (Ozisik, 1989). The heat transfer

coefficients, associated with pure forced convection with unbound flow, is generally evaluated from the expression:

$$Nu = A + B\,Re^{C}\,Pr^{D} \qquad (7.4)$$

In the case of forced convection tube flow, additional dimensionless terms are added to the correlation. In the present study of a single particle in a can with end-over-end rotation, the magnitude of particle to liquid relative velocity was the result of the combination of gravitational, drag, buoyant and centrifugal forces (Chapters 4 and 6). To account for this, density simplex [$a = |(\rho_p-\rho_l)/\rho_l)|$], Archimedes and Froude numbers were considered in the correlation. With a spherical particle, the effect of can headspace and radius of rotation on h_{fp} was studied and found to have a significant effect on h_{fp}. The following modified relationship was used to take this into consideration:

$$Nu = A + B\,Re^{C}\,Pr^{D}\,Fr^{E}\,Ar^{F}\,a^{G}\left(\frac{h_s}{H}\right)^{H}\left(\frac{D_r + D_c}{D_c}\right)^{I} \qquad (7.5)$$

where constants B, C, D, E, F, G, H and I are determined by multiple regression analysis on experimental data, and A is the limiting value of Nusselt number which is 2.0 for sphere and has been derived from the steady state heat conduction solution for a sphere in an infinite medium. In developing a correlation for heat transfer to a fluid flowing past a cylinder, it is assumed that the fluid density is constant and that a steady state heat conduction solution does not exist (Whitaker, 1976). Three different correlations were developed for a spherical, cylindrical and cube shaped particle.

The effect of rotational speed, liquid viscosity, particle size, shape and concentration on h_{fp} was studied (Chapter 5), with multiple particles in a can. Analysis of variance showed that these factors were highly significant ($p \leq 0.0001$). To account for these effects, Re, Fr, Ar, Pr, $\varepsilon/(100-\varepsilon)$, d_e/D_c and Ψ were considered as dimensionless parameters. Fernendez et al. (1988) modeled the heat transfer in a canned liquid/particle system as a packed bed, and developed the Nusselt number correlation as a function of Reynolds number, Prandtl number and a shape factor with an $R^2 = 0.785$. Nasr et al.

(1994) conducted an experimental study on forced convection heat transfer from a cylinder embedded in a packed bed and developed a Nusselt number correlation as function of the Peclet number (Pe = Re . Pr) and the ratio of particle to liquid thermal conductivities. Hassan (1984) also suggested a ratio of particle to liquid thermal conductivity (k_p/k_l) in the dimensionless correlation for the convective heat transfer coefficient in a canned liquid/particulate system. Therefore, Pe and k_p/k_l were also added to the dimensionless correlation. A more general correlation, that accounts for variations with associated parameters, was developed in the following form:

$$Nu = f\left(Re, Pr, \frac{k_p}{k_l}, \frac{\epsilon}{100-\epsilon}, \frac{d_e}{D_c}, \Psi\right) \qquad (7.6)$$

RESULT AND DISCUSSIONS

Overall heat transfer coefficient (U)

The diameter of rotation (D_r) and the diameter of the can (D_c) both individually and in combination, were evaluated as a characteristic length in the correlation for U. The correlation with D_r+D_c gave the higher R^2. The combination D_r+D_c also allows data, obtained with a zero diameter of rotation on a logarithmic scale, to be used in the analysis. Earlier, Anatheswaran and Rao (1985a) also found the model with the sum of the diameter of rotation and the length of the can to give the highest R^2, with end-over-end rotation.

Single particle (or liquid only situation)

A stepwise multiple regression analysis of experimental data on various factors, represented in dimensionless form, eliminated the Froude number as nonsignificant ($p>0.05$) in comparison with the other parameters. The following equation gave the best fit for the experimental data for the overall heat transfer coefficient with a single particle in can ($R^2 = 0.99$), representing the liquid alone in the can situation.

$$Nu = 0.93\ Re^{0.51}\ Pr^{0.36}\left(\frac{h_s}{H}\right)^{0.21} \qquad (7.7)$$

The validity of this equation is limited to the Reynolds number in the range, 5.2×10^2 to 5.4×10^5; Prandtl number, 2.6 to 90.7, and the relative can headspace in the range, 5.5×10^{-2} to 8.6×10^{-2}. Figure 7.1 shows the plots for the Nusselt number calculated using Eq. (7.7) vs experimental values. Although the overall heat transfer coefficient was influenced by the diameter of rotation, its specific dimensionless form $[(D_r+D_c)/D_c]$ was excluded from the final correlation, since both Nu and Re included (D_r+D_c) as a characteristic length. The exponents of Reynolds number and Prandtl number appearing in Eq. (7.7) are slightly higher than that reported by Anantheswaran and Rao (1985a); this is probably because of the significant influence of the diameter of rotation on U, and also the higher range of diameter of rotation employed in the present study. Anantheswaran and Rao (1985a) reported that over the range of diameter of rotation from 0 to 29.8 cm, an increase in diameter of rotation did not significantly improve the rate of overall heat transfer. With a single particle in the can, particle properties such as density and shape did not influence the overall heat transfer coefficient, and hence were not included in the relationship. Therefore, the above correlation equation can be used in the prediction of the overall heat transfer coefficient for thermal processing of canned liquid foods, during end-over-end rotation.

Multiple particles

The presence of multiple particles in the liquid caused secondary agitation in the can, which influenced the heat transfer to both liquids and particles. The magnitude of secondary agitation depends upon the concentration, size and shape of the particle, the liquid properties and rotational speed due to liquid-particle interactions. Again, a forward step-wise regression analysis was performed on the experimental data of U, obtained with multiple particles. Once again, the Froude number turned out to be a non-significant ($p>0.05$) factor in the correlation. The significant dimensionless numbers for Nusselt number were Re, Pr, the particle to liquid concentration ratio $[\varepsilon/(100-\varepsilon)]$, the ratio of

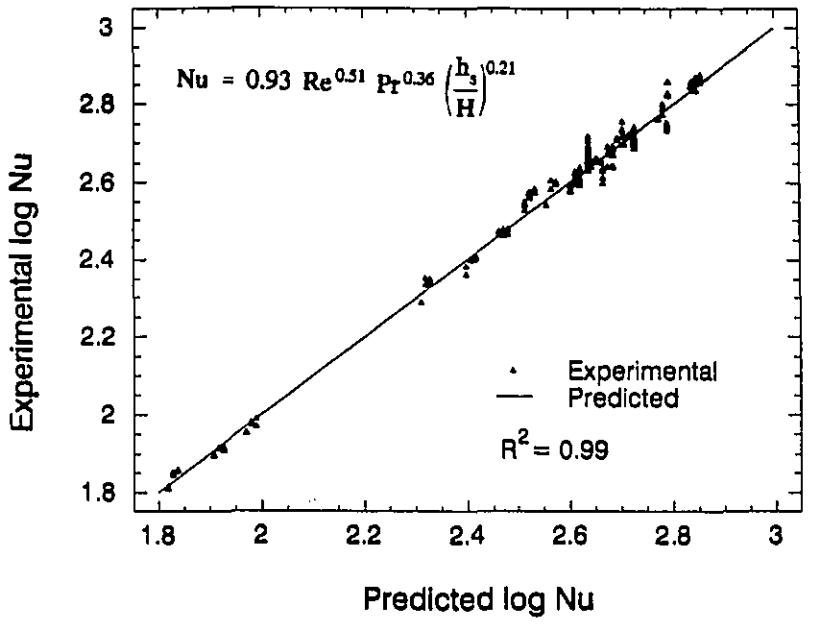

Figure 7.1 Experimental vs. regression (Eq. 7.7) predicted Nu for ***overall heat transfer coefficient (U)***, in cans with a single particle (or ***liquid only situation***)

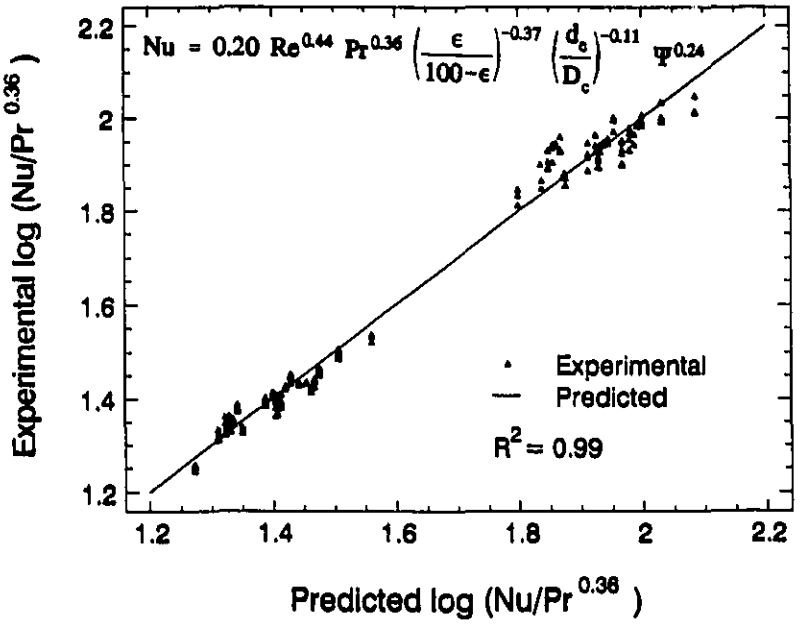

Figure 7.2 Experimental vs. regression (Eq. 7.8) predicted ($Nu/Pr^{0.33}$) for ***overall heat transfer coefficient (U)***, in cans with multiple particles

equivalent particle diameter to can diameter (d_e/D_c) and particle sphericity (Ψ), as shown in the following correlation ($R^2 = 0.99$):

$$Nu = 0.20\ Re^{0.44}\ Pr^{0.36} \left(\frac{\epsilon}{100-\epsilon}\right)^{-0.37} \left(\frac{d_e}{D_c}\right)^{-0.11} \Psi^{0.24} \qquad (7.8)$$

The characteristic length used in Eq. (7.8) was D_r+D_c. The above correlation is valid for the Reynolds number in the range, 1.7×10^4 to 5.4×10^5, Prandtl number, 2.6 to 90.7, particle concentration (ε), 20 to 40% (v/v), the ratio of particle shortest dimension to the can diameter, 0.22 to 0.29 and sphericity, 0.806 to 1. The predictive quality of Eq. (7.8) is compared in relation to the measured values in Figure 7.2. The value of the exponent of the Re and Pr were initially smaller (0.24 and 0.19 respectively) than in Eq. (7.8) giving an R^2 value of 0.86. However, in the heat transfer literature Prandtl number dependence is commonly represented with an exponent of 0.3 or 0.4, i.e. $Pr^{0.3}$ or $Pr^{0.4}$ (Whitaker, 1976). Hence, in the present heat transfer analysis, Pr was varied between 0.3 to 0.4 and regression analysis was carried out again yielding a more meaningful relationship, as finally represented in Eq. (7.8) with a better R^2 value (0.99). The exponent of Re in Eq. (7.8) was slightly lower than Eq. (7.7), probably due to increased drag and particle secondary interaction in the presence of multiple particles. The influence of particle related parameters (e.g concentration and sphericity) on Nu is in the same order of magnitude as the Reynolds number and Prandtl number (i.e. coefficients nearly in the same range). Increasing particle concentration reduces the heat transfer to liquid, which is evident from the negative exponent of particle to liquid concentration ratio. A slightly lower effect was observed with d_e/D_c. Use of a particle shortest dimension (d_p) in place of d_e resulted in a correlation ($R^2 = 0.99$) with similar exponents for all dimensionless parameters; but a slightly higher value of the exponent for sphericity.

Fluid to particle heat transfer coefficient (h_{fp})

Single particle

An equivalent particle diameter (d_e) or particle shortest dimension (d_p) were considered to be most appropriate as characteristic lengths in the correlation for h_{fp}. The

correlations with shortest particle dimension gave the slightly better R^2. Fernandez et al. (1988) also found their model, with the equivalent particle diameter as a characteristic dimension, gave a higher R^2 with axial rotation.

The flow around the particle may differ for different geometrical shapes. Experimental results also showed that particle shape effect with a single particle in a can, was more pronounced compared to that with multiple particles in a can. In the heat transfer literature, separate h_{fp} correlations have been reported for flow over spherical and cylindrical objects (Whitaker, 1976). The limiting Nusselt number value is 2.0, which represent the steady state heat conduction between fluid and sphere.

A step-wise multiple regression analysis of experimental data on h_{fp} for the spherical particle showed that the density simplex, Froude and Prandtl numbers along with the relative can headspace (h_s/H), and the dimensionless diameter of rotation [(D_r+D_c)/D_c] were significant parameters. The following was the best correlation obtained for the fluid to particle heat transfer coefficient, with the spherical particle (R^2 = 0.83):

$$Nu = 2.0 + 1971\ Fr^{0.31}\ Pr^{0.33}\ a^{0.34} \left(\frac{h_s}{H}\right)^{1.56} \left(\frac{D_r + D_c}{D_c}\right)^{0.21} \qquad (7.9)$$

The above Eq. (7.9) is valid for Froude number 5.32 x 10^{-4} to 2.13 x 10^{-3}, density simplex 3.49 x 10^{-2} to 1.51, Prandtl number 2.6 to 90.7, relative can headspace (h_s/H), 5.52 x 10^{-2} to 8.63 x 10^{-2} and diameter of rotation [(D_r+D_c)/D_c] in the range 1.0 to 7.18. The exponent of the ratio of can headspace to the can diameter was much higher compared to that in the previous Nusselt number correlation (Eq. 7.7) for U. This indicates that increasing can headspace has more effect on h_{fp}, compared to that on U. Figure 7.3 shows the comparison between [(Nu-2)/$Pr^{0.33}$] calculated using Eq. (7.9) and the [(Nu-2)/$Pr^{0.33}$] experimental.

A regression analysis with experimental data on h_{fp} for the cylindrical and cube shaped particle, resulted in following correlations:

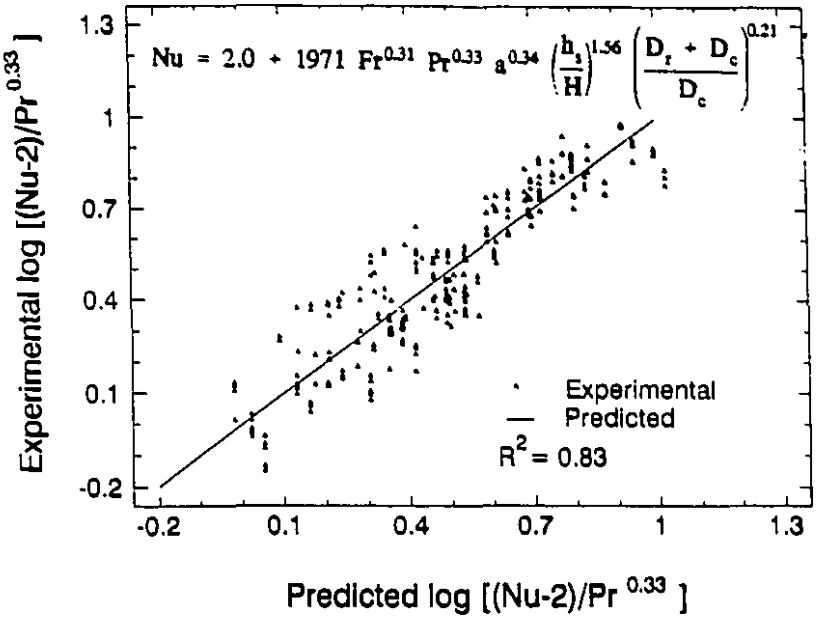

Figure 7.3 Comparision of eperimental and regression (Eq. 7.9) predicted $[(Nu-2)/Pr^{0.33}]$ for the ***fluid to particle heat transfer coefficient (h_{fp})***, in cans with a single ***spherical particle***

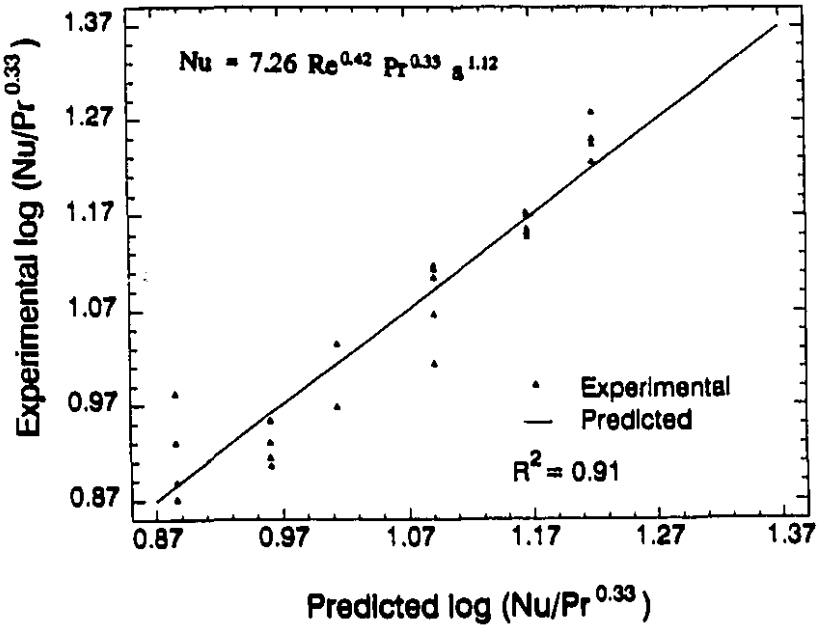

Figure 7.4 Comparision of experimental and regression (Eq. 7.10) predicted $(Nu/Pr^{0.33})$ for the ***fluid to particle heat transfer coefficient (h_{fp})***, in cans with a single ***cylindrical particle***

Cylindrical shaped particle (R^2 = 0.91):

$$Nu = 7.26\ Re^{0.42}\ Pr^{0.33}\ a^{1.12} \qquad (7.10)$$

Cube shaped particle (R^2 = 0.91):

$$Nu = 8.03\ Re^{0.52}\ Pr^{0.33}\ a^{1.63} \qquad (7.11)$$

The correlations Eqs. (7.10) and (7.11) are valid for Reynolds number, in the range, 44.0 to 1.39 x 10^3, Prandtl number, 2.6 to 78.3 and density simplex in the range 0.15 to 0.28. The dimensionless numbers were based on the equivalent particle diameter (d_e). Figures 7.4 (given on page 123) and 7.5 (given on page 125) show the relationship between calculated and experimental values of ($Nu/Pr^{0.33}$). The settling velocity of the particle in the can, during end-over-end rotation, may be the influence of particle density, liquid density and viscosity, respectively. It is important to note that in Eqs. (7.9) to (7.11), density simplex appears as a significant parameter, as in the particle settling velocity expression (Denn, 1980). Density simplex was also found significant in the dimensionless correlation for fluid to particle heat transfer coefficient by Deniston et al. (1987). The exponent of density simplex was higher in the correlations for the cylindrical and cube shaped particle (Eqs. 7.10 and 7.11) compared to the correlation for spherical particles (Eq. 7.9). This is probably due to the experimental range of the density simplex employed for the spherical particle, which describes the effect of density simplex over the larger range. In general, for spherical particles, h_{fp} improved with higher rotational speeds; however, higher density particles (Delrin and Teflon) in water showed different trends. In the flow visualization study of particle motion (Chapter 6), it was found that increased centrifugal forces, at a higher rotational speed caused the heavier particles to stay along the can wall. This could result in less effective movement of the particle, thus decreasing the associated h_{fp}. Due to these opposing trends of h_{fp} with rotational speed, the Nusselt number correlation had lower R^2 for the spherical particle, compared to that obtained with the cylindrical and cube shaped particles, where only moderately dense particles were used. Experimental data showed that the rotational speed influence on h_{fp} was more pronounced with the cube shaped particle, in comparison to the cylindrical particle; and

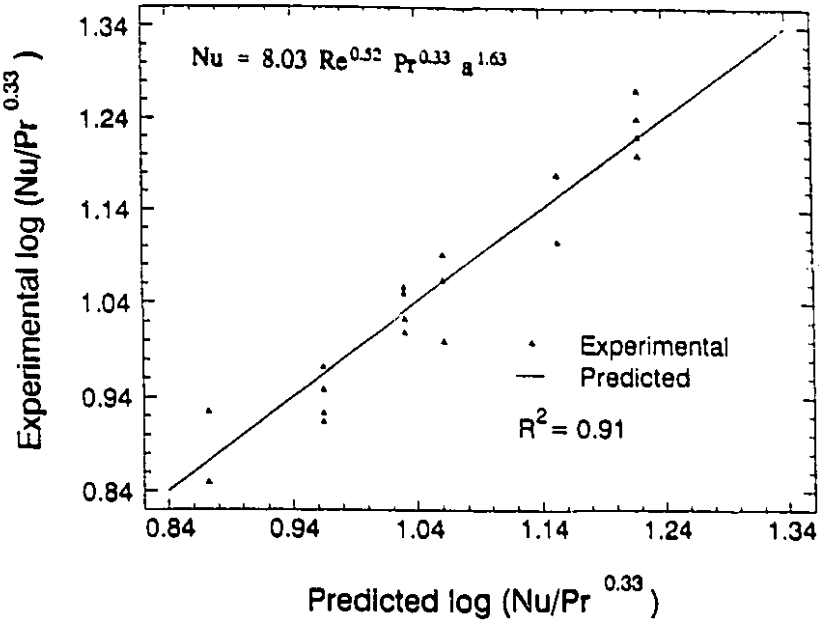

Figure 7.5 Comparision of experimental and regression (Eq. 7.11) predicted ($Nu/Pr^{0.33}$) for ***fluid to particle heat transfer coefficient*** (h_{fp}), in cans with a single ***cube particle***

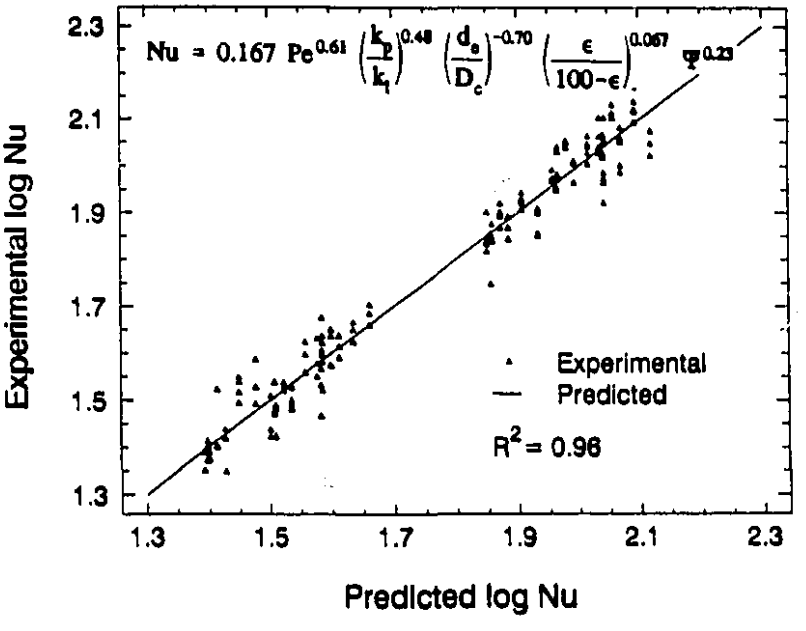

Figure 7.6 Comparision of experimental and regression (Eq. 7.12) predicted Nu for ***fluid to particle heat transfer coefficient*** (h_{fp}), in cans with ***multiple particles***

this resulted in a higher value for the constant and exponent of Reynolds number in the Nusselt number correlation (Eq. 7.11).

Multiple particles

Regression analysis of the experimental data, obtained for h_{fp} in the presence of multiple particles, gave the following Nusselt number correlations (R^2 = 0.96):

$$Nu = 0.167\ Pe^{0.61} \left(\frac{k_p}{k_l}\right)^{0.48} \left(\frac{d_e}{D_c}\right)^{-0.70} \left(\frac{\epsilon}{100-\epsilon}\right)^{0.067} \Psi^{0.23} \qquad (7.12)$$

$$Nu = 0.718\ Re^{0.61} \left(\frac{k_p}{k_l}\right)^{1.98} \left(\frac{d_e}{D_c}\right)^{-0.70} \left(\frac{\epsilon}{100-\epsilon}\right)^{0.067} \Psi^{0.23} \qquad (7.13)$$

In Eqs. (7.12) and (7.13), the dimensionless numbers were based on the equivalent particle diameter (d_e). The correlations with the particle shortest dimension were equally good, with a slight difference in the value of the constant. These correlations are valid for the Peclet number in the range, 1.18×10^3 to 7.71×10^3, Reynolds number in the range, 28 to 1.55×10^3, the ratio of particle to liquid thermal conductivity in the range, 0.56-2.24, the relative particle dimension (d_e/D_c) in the range, 0.22-0.29, particle concentration ϵ in the range 20%-40% and particle sphericity Ψ in the range 0.806 - 1.0. The significance and inclusion of particle to liquid thermal conductivity ratio in the correlations (Eqs. 7.12-7.13) suggested that h_{fp} was influenced by the particle/liquid thermal conductivity. In this case, the problem of convection heat transfer to the canned liquid/particle system may be of conjugate heat transfer. It is important to note that the density simplex and Froude number were nonsignificant ($p>0.05$) unlike the instance of single particle correlations. The Peclet number, which is the product of Reynolds and Prandtl numbers, and particle to liquid thermal conductivity ratio were found to be significant parameters. Nasr et al. (1994) also used Peclet number and particle to liquid thermal conductivity ratio to describe forced convection heat transfer in a packed bed system. An equally good fit was obtained with the Reynolds number; however, the exponent of thermal conductivity ratio was much higher (Eq. 7.13), suggesting that liquid

and particle thermal conductivities are important parameters in the present canned liquid/particles systems.

Figure 7.6 (given on page 125) shows the relationship between experimental and calculated values of Nu. There were 2 distinct groups of data points: one for oil as test liquid, and a second one for water. The particle sphericity effect on h_{fp} was similar to that observed with U, and this is evident from the exponent of Ψ in Eq. (7.8) for U and Eq. (7.13) for h_{fp}. The lower exponent of relative particle concentration suggested that its influence on Nusselt number was relatively small. Analysis of variance on h_{fp} also showed that the influence of particle concentration on h_{fp} was small when compared to other parameters.

CONCLUSIONS

Other than the particle density and shape effect on U with a single particle in the can, U and h_{fp} were influenced by all parameters considered in the present study. Correlations were developed with single and multiple particles for U and h_{fp}, with equations showing a good agreement with the experimental data. The characteristic dimension of sum of diameter of rotation and diameter of can was more appropriate for the U correlations, while particle shortest dimension or particle equivalent diameter were found to be appropriate for h_{fp} correlations. Heat transfer to liquids was modeled using the Reynolds number and Prandtl number; while different dimensionless groups were significant in the modeling of heat transfer to particle(s). For a single particle moving in an agitated can of liquid, heat transfer to the particle was modeled using Froude number, Prandtl number, Reynolds number and density simplex. Their relationship was attributed to various forces affecting the settling velocity of the single particle in the can. In the presence of multiple particles in can, the Nusselt number correlation suggested that h_{fp} was influenced by both particle and liquid thermal conductivities; hence their ratio, and Peclet number (product of Reynolds number and Prandtl number). The particle concentration effect was more pronounced with U than with h_{fp}. The particle shape effect was equally important for U and h_{fp}.

CHAPTER 8

NEURAL NETWORK MODELS FOR THE PREDICTION OF HEAT TRANSFER PARAMETERS (CONDUCTION AND CONVECTION HEATING CONDITIONS)

ABSTRACT

The application of artificial neural network (ANN) for the prediction of heat transfer parameters is presented in this chapter. In the first phase, the ANN was tested to predict heat transfer parameters associated under conduction heating conditions. A four layer neural network (1 input, 1 output and 2 hidden layers) with 3 input and 3 output neurons was trained using a back-propagation algorithm. Data needed to train the neural network were obtained using a finite difference computer simulation program. Equivalent lethality processes were obtained for a range of input variables (can size, food thermal diffusivity and kinetic parameters of quality factors) for sterilization temperatures between 110 and 134 °C (at 2 °C intervals). The computed optimal conditions and their associated quality changes were used as input variables for training and evaluation of the neural network. The trained network was found to predict optimal sterilization temperatures with an accuracy of $\pm$ 0.5 °C and other responses with less than 5% associated errors.

In the second phase of this work, the ANN was used to predict U and h_{fp} associated with canned liquid/particle mixtures, subjected to end-over-end rotation. These important parameters are needed for modeling the time-temperature profiles of liquid and particle. Experimental data obtained for U and h_{fp} in earlier studies were used for both training and evaluation. Multi-layer neural networks with 7 input and 2 output neurons (for a single particle in can), and 6 input and 2 outputs neuron (for multiple particles in can) were trained using a back-propagation algorithm. Once again, the optimal network was obtained by varying the number of hidden layers, number of neurons in each hidden layer and learning runs. The trained network was found to predict U and h_{fp} with less than 3% and 5% errors, respectively. The neural network models were more accurate than the dimensionless number models for predicting U and h_{fp}.

INTRODUCTION

Experimental time-temperature data are required to establish the thermal process schedule for canned liquid/particle food systems during agitation processing. Mathematical models can also be used to optimize the processing conditions in situations where physical experimentation is expensive and time consuming. However, development of such models for canned liquid/particle system will require the appropriate values of overall heat transfer coefficient (U) and fluid to particle heat transfer coefficient (h_{fp}). Typically, dimensionless correlations have been used for the prediction of U and h_{fp}. Using the traditional approach of multiple regression analysis, the heat transfer coefficient in the form of a Nusselt number is correlated to the other dimensionless parameters influencing its magnitude. However, selection of appropriate dimensionless groups requires prior knowledge of the phenomena under investigation. Artificial neural network (ANN) models have the capability of correlating large and complex data sets without any prior knowledge of the relationship between them (Linko et al., 1992). Neural network models have performed well even with noisy, incomplete or inconsistent data (Bochereau et al., 1992). In recent years, there has been an increasing use of such ANN models in the area of food processing/engineering.

In sensory science, neural networks have been proposed as a method of advancing the understanding of complex unstructured tasks involving human insight and judgement (Galvin and Waldrop, 1990). ANN has been used to model sensory data of such as the color quality of tomato and peaches (Thai and Shelwfelt, 1991) and for beef sensory evaluation (Park et al., 1994). Tomlins and Gay (1994) used ANN models to classify black tea samples by their phenolic composition. Horimoto et al. (1995) found that ANN predicted wheat flour loaf volumes in baking tests, which were more accurate than those predicted with principal component regression analysis.

In rheology, neural networks have been used to predict rheological properties of dough. Ruan et al. (1995) correlated the dough rheological properties measured using a farinograph and extensigraph to the torque developed during mixing. Linko et al. (1992) used neural network programming in the fuzzy control of the twin-screw extrusion cooker,

to minimize the problem associated with extrusion control systems.

In image recognition analysis, ANN has been used in some areas of food processing (Sayeed et al., 1995). For example, Liao et al. (1993) used ANN for classifying corn kernel breakage. The results indicated that shape features, based on the corn kernel morphological profile, accurately discriminated broken and whole kernel. Sayeed et al. (1995) used ANN models in snack quality evaluation, based on visual texture and morphological characteristics; and Tomlins and Gay (1994) used ANN to predict the origin of black tea based on chromatographic data.

ARTIFICIAL NEURAL NETWORK : GENERAL BACKGROUND

An artificial neural network is a collection of interconnecting computational elements which simulates neurons in a biological system. It is characterized by the network topology, neurons and learning rules. An artificial neural network has the capability of relating the input and output parameters without any prior knowledge of the relationship between them. A properly trained neural network can be used to simultaneously produce more than one output, unlike traditional models where one regression is required for each output. Recently, artificial neural networks have been used in those situations where good physical models of the process were not available and the number of output variables were more than one.

Artificial neural network models were originally developed to mimic the function of the human brain. The brain contains billions of nerve cells (neurons) highly interconnected through synapses. Each neuron processes information by receiving signals from other neurons *via* synapses and produces an output which is then transmitted to some other neurons. It is believed that the synaptic strength of junctions is altered when knowledge is stored in the brain. Consequently, a synapse can be considered as the basic memory unit of the brain.

The artificial neural network used in this study is a computer program that consists of a collection of simple elements (neurons) that work together to solve the problem. An artificial neuron is modelled (Figure 8.1) to receive (n) inputs, $X = [x_0, x_1, x_2, \ldots x_n]$ and

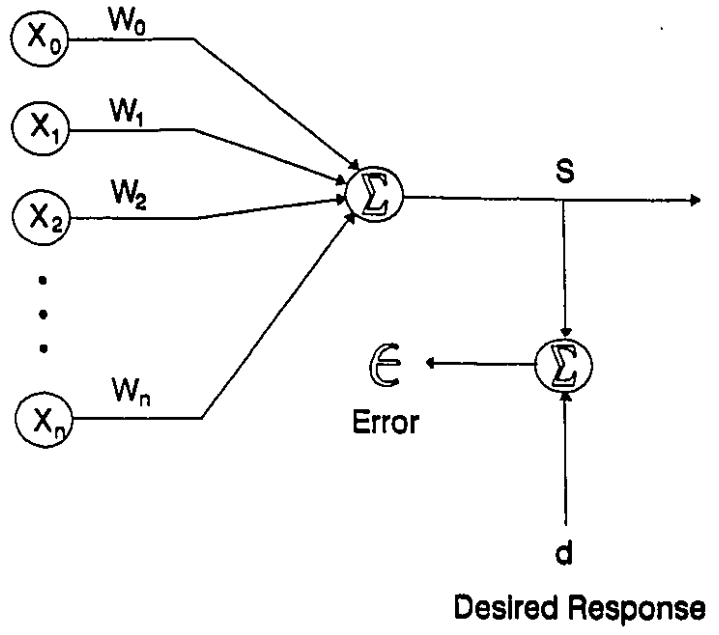

Figure 8.1 Model of an artificial neuron

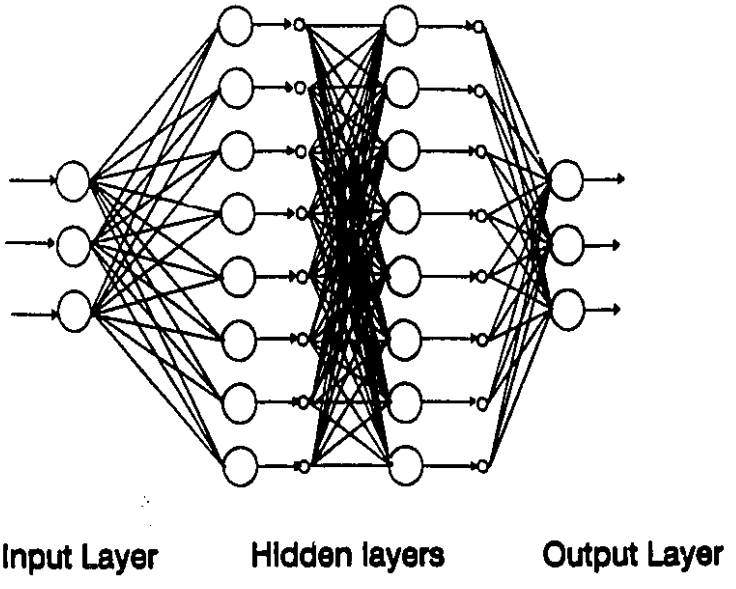

Figure 8.2 Schematic of a multi-layer neural network

yield a desired output (d), through a process of learning. The components of the input vector are weighted by a set of coefficients, W (w_0, w_1, w_2, ..., w_n). The sum of the weighted input is then computed, producing an output, $S = X^m W$ (X input vectors from mth layer). The weights are essentially continuous variables and can take negative as well as positive values. During the learning process, input vectors and desired response are presented to the network and an algorithm automatically adjusts the weights, so that output responses to input vectors will be as close as possible to their respective desired response. A popular method for adapting the weights is the simple LMS (least mean square) algorithm (Widrow and Lehr, 1993) which minimizes the sum of squares of the linear error over the learning set. The linear error (ε) is defined to be the difference between the desired response (d) and the output (S). However, when this model is applied to a multi-element neural network, the procedure for error calculation becomes more complicated (Widrow and Lehr, 1993).

The most common structure of an artificial neural network is generally a multi-layer design. A fully connected four layer network is illustrated in Figure 8.2. During learning, the response of each output neuron in the network is compared with a corresponding desired response. Error signals associated with the output elements are computed and the information transmitted from one layer to the previous layer using a back-propagation algorithm (hence the name back-propagation network). This procedure is repeated over the entire learning set for a specified number of times (learning runs), chosen by trial and error. In the layer structure, the inputs are interconnected in an input layer, and the computed outputs are interconnected in the output layer (Figure 8.2). In between these two layers, one or more hidden layers (as another variable for neural network) are interconnected depending upon the applications. The number of input neurons correspond to the number of input variables, and the number of output neurons match the number of desired output variables. The number of neurons in the hidden layer is dependent on the application of the network. In principle, if a sufficient number of these input/output combinations are used for learning/training of the neural network, such a trained network should be able to predict the output for new inputs. These learning sets can be compiled from experimental data or can be obtained from computer simulation.

The objectives of this study were to develop ANN models for the prediction of overall heat transfer coefficient and fluid to particle heat transfer coefficient, and compare the accuracy of results with traditional regression models of dimensionless correlations. Since this was the first application of an artificial neural network to thermal processing, the first part of the study, namely feasibility, was evaluated using readily available computer generated finite-difference data on time-temperature profiles of conduction heated foods, for prediction of optimal process schedules. Subsequently, the neural network modeling approach was extended to the experimental study of convective heat transfer in canned liquid/particulate systems.

METHODOLOGY

PART I - Process Optimization, Conduction Heating

In the last decade, various studies have been carried out for quality optimization of thermally processed foods. Computer simulation has made this possible since the kinetics of microorganisms and quality factors, and the physics of conduction heat transfer are very well understood and can be described with mathematical models. Optimization of the sterilization process is based on the fact that thermal inactivation of microorganisms is much more temperature dependent than quality factors (Lund, 1977) and has lead to the use of high temperature short time (HTST) processing. However, applicability of this principle to conduction heated foods is limited due to their slow heating behavior, resulting in large temperature gradients within the can during heating/cooling. Teixeira et al. (1969a,b) were probably the first to use computer simulations for quality optimization. They used a finite difference solution to the conduction heat transfer equation for cylindrical cans, coupled with kinetic data on nutrient degradation. Recently, several researchers have used such models for predicting optimal conditions for thermal processing of foods (Teixeira et al., 1969a,b; Saguy and Karel, 1979; Ohlsson, 1980; Thijssen and Kochen, 1980; Silva et al., 1992; Hendrickx et al., 1989, 1993).

Hendrickx et al. (1989) used an empirical approach to calculate optimal temperatures for maximizing quality factors. Using traditional regression analysis, they

developed empirical equations to relate optimal temperatures to various product properties (thermal diffusivity and z-value of quality factors), processing conditions (geometry and dimensions of the food, surface heat transfer coefficient, initial product temperature and retort come up time) and processing criteria (target F_0-value). Hendrickx et al. (1993) extended the correlations to more generalized conditions, accounting for cooling lethality as well as retort come-up time. The study, however, was limited to infinite shapes with one dimensional heat transfer. Silva et al. (1993) presented correlations for the optimal sterilization temperature for conduction heated foods with finite surface heat transfer coefficients. The previously mentioned studies (Hendrickx et al.,1989; Hendrickx et al., 1993 and Silva et al., 1992) were based on optimizing the surface quality. An extensive review of the modeling of optimum processing conditions for sterilization was presented by Silva et al. (1993). Recently Silva et al. (1994) presented a comparative study between surface and volumetric average quality retention in thermoprocessed foods.

Process Optimization

An optimal sterilization temperature is generally taken as the processing temperature that results in minimum volumetric heating of the food product, while meeting the constraints of commercial sterility. Such a process can be expected to preserve the bulk of thermolabile quality factors. Exceptions exist to this rule; for example, when surface discoloration due to thermal treatment is the primary consideration, the optimization should be aimed at minimizing surface cook rather than product bulk. Parameters that determine the optimal sterilization temperature are numerous: can dimension, thermal diffusivity of food, kinetic parameter of nutrient (z), lethality to be achieved, cooling water temperature, initial temperature of food, retort come-up time, convective heat transfer coefficient at the can outer surface, etc. A mathematical model for conduction heat transfer in a cylindrical container was coupled with volume average thermal destruction kinetics of quality factor and center point destruction of a target micro-organism (or F_0 value), in order to obtain optimal sterilization temperatures in this study. Modeling of such a process involves the mathematical description of (i) numerical solution of the two-dimensional heat conduction equation for a finite cylinder and (ii)

first order kinetics, describing the thermal destruction of micro-organisms and quality change.

Heat transfer Model

The heat flow in the cylindrical geometry of a finite shape was represented by the following partial differential equation (Ozisik, 1989);

$$\frac{\partial^2 T}{\partial r^2} + \frac{1}{r}\frac{\partial T}{\partial r} + \frac{\partial^2 T}{\partial z^2} = \frac{1}{\alpha}\frac{\partial T}{\partial t} \qquad (8.1)$$

where α is the thermal diffusivity and r and z are the radial and axial coordinates, respectively.

The initial and boundary conditions were;

$$T = T_i \quad \text{at} \quad t = 0 \qquad (8.2)$$

$$\frac{\partial T}{\partial r} = 0 \quad \text{at} \quad r = 0 \quad \text{and} \quad t > 0 \qquad (8.3)$$

$$\frac{\partial T}{\partial z} = 0 \quad \text{at} \quad z = \frac{h}{2} \quad \text{and} \quad t > 0 \qquad (8.4)$$

$$T = T_\infty \quad \text{at} \quad r = a, \quad z = 0, \quad z = h \quad \text{and} \quad t > 0 \qquad (8.5)$$

All thermophysical properties were assumed to be temperature independent, and the external heat transfer resistance at the can surface was considered to be negligible, as in the case of processing cans in steam. A finite difference computer program was employed using Crank-Nicholson scheme for spatial derivatives and a fully implicit scheme for time derivative (Ozisik, 1989). The numerical procedure involved with the finite difference method is detailed in the appendix. Due to symmetry around both axes of a cylindrical can, only one quarter of the cylinder was modelled using a 20 x 20 grid. Since an unconditionally stable implicit scheme was used, a time step size between 2 to 20 seconds, was used depending on the can size. The computer program was written in

FORTRAN 77, to compute the transient temperature distribution in a cylindrical geometry.

Kinetics of thermal destruction

A primary objective of thermal processing is to achieve a pre-set level of commercial sterility. The intended process lethality (or thermal times), measured in terms of an F_o value, is used for this purpose:

$$F_o = \int_0^t 10^{\frac{(T - T_{ref})}{z_m}} dt \qquad (8.6)$$

where F_o is the integrated lethality (min), t is the time of processing (heating, holding and cooling), T is the temperature at the geometric center of the can, T_{ref} is the reference temperature (121.1 °C) and z_m is the temperature sensitivity indicator of the thermal destruction of the micro-organism under consideration (typically, z_m=10 C° for spores of *Clostridium botulinum*). The integrated lethality was continuously computed and the process simulation continued until the heating lethality reached the target value of 10 min. Based on the contribution of lethality during cooling, the computation process was then adjusted by trial and error to give a combined lethality (heating and cooling) of 10 min. The integrated heating time (F_{oq}) with respect to a quality attribute of food product was calculated at the reference temperature by:

$$F_{oq} = \int_0^t \left[\left(\frac{1}{V}\right) \int_0^V 10^{\frac{(T - T_{ref})}{z_q}} dv \right] dt \qquad (8.7)$$

The above equation is similar to the F_o value except that the F_{oq} is based on volumetric/mass average destruction, which is of greater interest for quality retention (e.g. nutrient retention). z_q indicates the temperature sensitivity indicator quality factor in question (used as a variable in this study). Using the calculated F_{oq}, the quality retention following a process can be obtained using the relationship:

$$\log N = \log N_0 - \frac{F_{oq}}{D_{ref}} \qquad (8.8)$$

where D_{refq} is the decimal reduction time for quality factor, N_0 initial quality, and N is the quality remaining after processing, F_{oq} determines the extent of retention of quality factors based on their respective D and z values and was used as a criterion for optimization in this study.

Variable Selection

The three factors used in this study were: can size, thermal diffusivity, and z value of quality factor (Table 8.1). Other parameters (initial product temperature = 80 °C, retort come up time = 0 min, process lethality = 10 min and z value of micro-organisms = 10 C°) were kept constant. Since can has two-dimensions: radius (a) and height (h), in order to reduce the number of input variables for neural network analysis, a characteristic dimension was calculated using the following equation (Ramaswamy et al., 1982):

$$\text{Characteristic dimension} = \frac{2.303}{\left[\frac{2.467}{(h/2)^2} + \frac{5.783}{a^2}\right]} \qquad (8.9)$$

Thirteen operating temperatures were employed in the range 110 to 134 °C (at 2 °C intervals).

Calculation of input/output data needed

Data on optimal process temperature, corresponding process time and associated quality factor were needed in order to construct and train the neural network. These were obtained first of all by identifying the process times required at each of the thirteen operating temperatures, in order to achieve the preselected F_0 value of 10 min. Simulation processes were run for these calculated times and the extent of quality factor destruction was computed for each z value. From a plot of quality destruction vs operating temperature, the optimal temperature for minimum quality destruction was obtained, again for each z value (representing arbitrary quality factor). The simulation was then rerun at

this optimal process temperature to get the exact process time and quality factor retention.

Table 8.1 Levels and range of input variables used in thermal processing optimization

Variables	No. of test levels	Range
Can size	30	200 x 211 to 401 x 411[1]
Thermal diffusivity x 10^7 m^2/s	3	1.2 1.4 1.6
z value of quality factors, °C	4	15 25 35 45
Temperature, °C	13	110 to 134 °C (2 °C interval)

[1]30 can sizes (Lopez, 1987); 201 x 211 means a can of 2 1/16" diameter and 2 11/16" height (standard notations in canning industry)

Neural Network

The software program employed was NEURALWORKS Professional Plus (NeuralWare Inc., Pittsburgh, PA). A four layer neural network (i.e. 1 input, 1 output and 2 hidden layers) was used in this study. The input layer consisted of 3 neurons which corresponded to 3 input variables (characteristics can dimension, thermal diffusivity of food product and z value of quality factor). The output layer also had 3 neurons, one each for optimal sterilization temperature, process time and F_{oq}. A standard back-propagation algorithm was used for learning/training of the network. A range of 2 to 16 neurons in each hidden layer and 1,000 to 100,000 learning runs were tested, in order to find the optimum configuration of neural network for the present problem. The optimal configuration with respect to number of neurons and learning runs was found using 360 cases for training and same 360 cases for testing. The optimal configuration was based on minimizing the difference between the neural network and the desired outputs. Several statistical parameters (mean absolute error, standard deviation of error, mean relative error, standard deviation of relative error) were used for the determination of the optimal number of neurons in the hidden layer, and also the number of learning runs. The following criteria were used with respect to the statistical/error parameters:

Error (ε) = Finite difference output - Neural network response

Relative Error % (ε_r) = (ε/ finite difference output) x 100

Mean Absolute Error (MAE) = Mean of ε values

Standard Deviation of Error (SDE) = Standard deviation in ε values

Mean Relative Error % (MRE) = Mean of relative error % (ε_r)

Standard Deviation of Relative Error % (SRE) = Standard deviation of relative error % (ε_r)

The above parameters were used to give a broader range of selection criteria. The error magnitudes in user units (MAE, SDE in °C or min) are more meaningful with respect to process temperature and process times, while the relative error (MRE, SRE in %) better described the network performance with respect to quality factor retention.

PART II - Heat Transfer Parameters, Convection Heating

The experimental data of U and h_{fp} were divided into two groups : (i) single particle in the can and (ii) multiple particles in the can, and separate neural network models were developed. The performance of developed models were compared with the traditional regression models, developed earlier using dimensional analysis.

Neural Network

For test data with a single particle in the can, the input layer consisted of 7 neurons which corresponded to 7 input variables (particle sphericity, particle density, rotational speed, diameter of rotation, can headspace, liquid thermal diffusivity and kinematic viscosity). The output layer had 2 neurons, one each for U and h_{fp}. With multiple particles in the can, the input layer consisted of 6 neurons corresponding to 6 input variables (particle sphericity, particle size, particle concentration, rotational speed, liquid thermal diffusivity, kinematic viscosity). The number of output neurons remained 2, one each for U and h_{fp}. The standard back-propagation algorithm was used for learning/training of the network.

Optimal configuration

For each data-set, the optimal value of neural network variables such as number of hidden layers, number of neurons in each hidden layers and learning runs needed to be determined, again. In order to find the optimum configuration 1 to 3 hidden layers, with a range of 5 to 40 neurons in each hidden layer and 25,000 to 100,000 learning runs were tested. The neural network was trained and its prediction capability was tested with the full set of data (single particle, 315 cases; multiple particles, 180 cases). The optimum value was based on minimizing the difference between the neural network output and the desired output. Once the optimal configuration with respect to number of neurons and learning runs was found, the performance of the neural network was tested on different sizes of data-sets. The data-set of 315 cases, for a single particle in the can, was randomly divided into three groups. The first group consisted of all 315 cases for learning and a randomly chosen 85 cases for the test. In the second group, 85 cases were selected for learning and 85 cases for the test, all chosen randomly from the set of 315 cases. In the third group, 85 cases were taken for learning and all 315 cases for the test. In a similar fashion, the data-set of multiple particles was divided into three groups by combining 180/50 , 50/50 and 50/180 learning/test data-sets. Error parameters described earlier were used to determine adequacy of the neural network output response for a given input data set.

RESULTS AND DISCUSSION

PART I : Process Optimization, Conduction Heating

Computer simulation

A total number of 4680 (13 temperatures ranging from 110 to 134 °C with an interval of 2 °C for 360 test conditions) time-temperature simulations and associated quality changes were obtained, to generate optimal processing parameters for 360 test conditions. The optimal sterilization temperature was clearly dependent on the can size, thermal diffusivity and z value of the quality factor. Lower values of characteristic

dimension of the can and higher values of thermal diffusivity resulted in a higher optimal process temperature, probably due to the resulting lower thermal gradients. This was also shown by Silva et al. (1992) while minimizing surface cook value. At higher z values (30 and 45 C°), the optimal sterilization temperatures were at the higher end of the range, while the opposite was true when the associated z values for quality factor were lower (15 and 25 C°). This was expected, since a higher value of z_q represents a more thermal resistant quality factor. Process time and F_{oq} were also significantly influenced ($p<0.05$) by all three parameters. Process times were larger for the bigger can size and/or lower thermal diffusivity, while quality retention was found to be higher (since lower F_{oq}) for a smaller can size and/or higher thermal diffusivity. Process times were shorter with increasing z values, since the associated optimal process temperatures were higher. Average quality retention values have been reported to vary with z_q and a lumped parameter, f_h, which depends on can size and thermal diffusivity (Silva et al., 1994). In this study, it was found that for smaller cans and lower thermal diffusivity, the optimal process temperatures were higher and nutrient retention values were lower at higher z_q values. However, at higher thermal diffusivity, the nutrient retention data showed a curvi-linear trend, initially decreasing and then increasing with increasing z_q. With larger cans, on the otherhand, irrespective of the thermal diffusivity value in the range studied, optimal process temperatures increased and the quality retention values decreased with z_q.

Learning/Training of Neural Network

Theoretically, once the neural network is learned/trained using the learning/training data, its performance can be evaluated by using the same data chosen in a random fashion (Huang and Mujumdar, 1993). However, before the learning process, the optimal configuration of the neural network should be determined since it has two variables: number of neurons in each hidden layer and number of learning runs. Several error parameters were used to determine adequacy of the neural network output response for a given input data set.

First, by keeping the number of learning runs constant (arbitrarily chosen as 50,000), the number of neurons in each hidden layer was varied from 2 to 16. The errors

associated with optimal sterilization temperature, as a function of the number of neurons, are shown in Figure 8.3. The calculated errors converged to a minimum value at 8 neurons in each hidden layer. Increasing the neurons beyond this level only resulted in increased computation time, with no additional benefits. The trend was similar with the other two output responses, process time and F_{oq}, as well as other selected levels of learning runs, demonstrating a minimum at 8 neurons. The magnitude of the deviations were, however, slightly higher for process time and F_{oq}.

In the next step, with the number of neurons in each hidden layer fixed at 8, the learning runs were varied from 1,000 to 100,000. The variations in different errors are compared in Figure 8.4 as a function of learning runs, for process time, shown as an example output. The convergence was observed at about 50,000 learning runs, beyond which the changes were small. The trend with respect to errors was again similar for the other two output responses, optimal sterilization temperature and F_{oq}, with just some differences in their magnitudes.

The prediction performance of the neural network is shown in Figure 8.5 as plots of neural network predicted values vs computer output values (actual values), for all three variables. The predicted values were more evenly and tightly distributed around the regression line, with a slight scattering of deviation at the higher end. The associated errors with the neural network outputs are compared in Table 8.2. The observed high R^2 values (>0.98) indicated excellent correlations of neural network predicted values with the finite difference output. Relatively, slightly lower correlations were observed while predicting the changes in quality factors (F_{oq}). The deviation in optimal process temperature prediction (MAE) was 0.35 ± 0.32 °C. The mean relative error in process times was about 5%, with the standard deviation of relative error of ~5%. The relatively large standard deviations associated with process time predictions by neural network were due to deviations observed under conditions of low (<30 min) and high (>100 min) process times. The mean relative error with F_{oq} was ~2%. The neural network prediction showed deviation from the desired output mostly at the higher end of F_{oq} values.

Overall, the relative errors associated with the process time prediction were the highest and those associated with the process temperature were the lowest, somewhat in

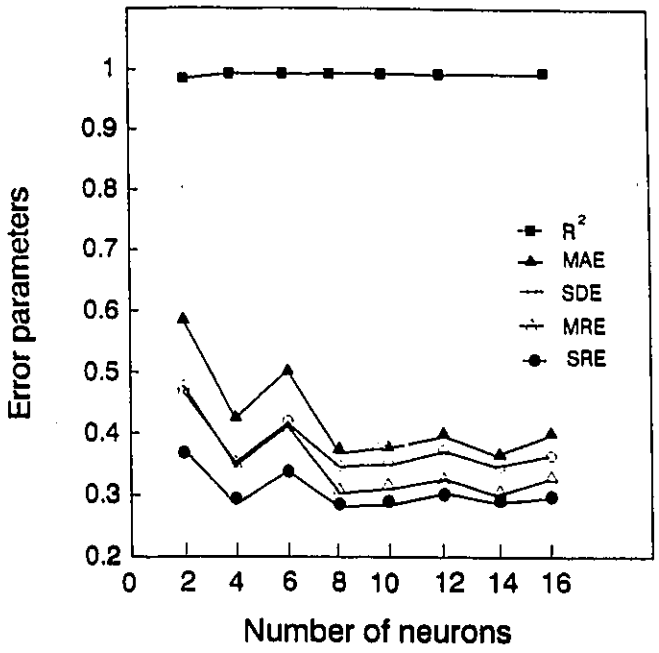

Figure 8.3 Error parameters as a function of number of neurons for optimal sterilization temperature

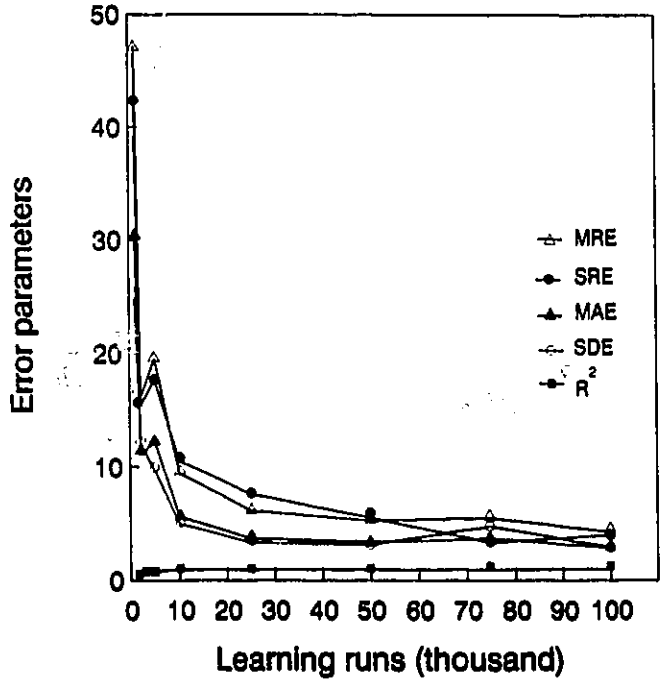

Figure 8.4 Error parameters as a function of learning runs for process time

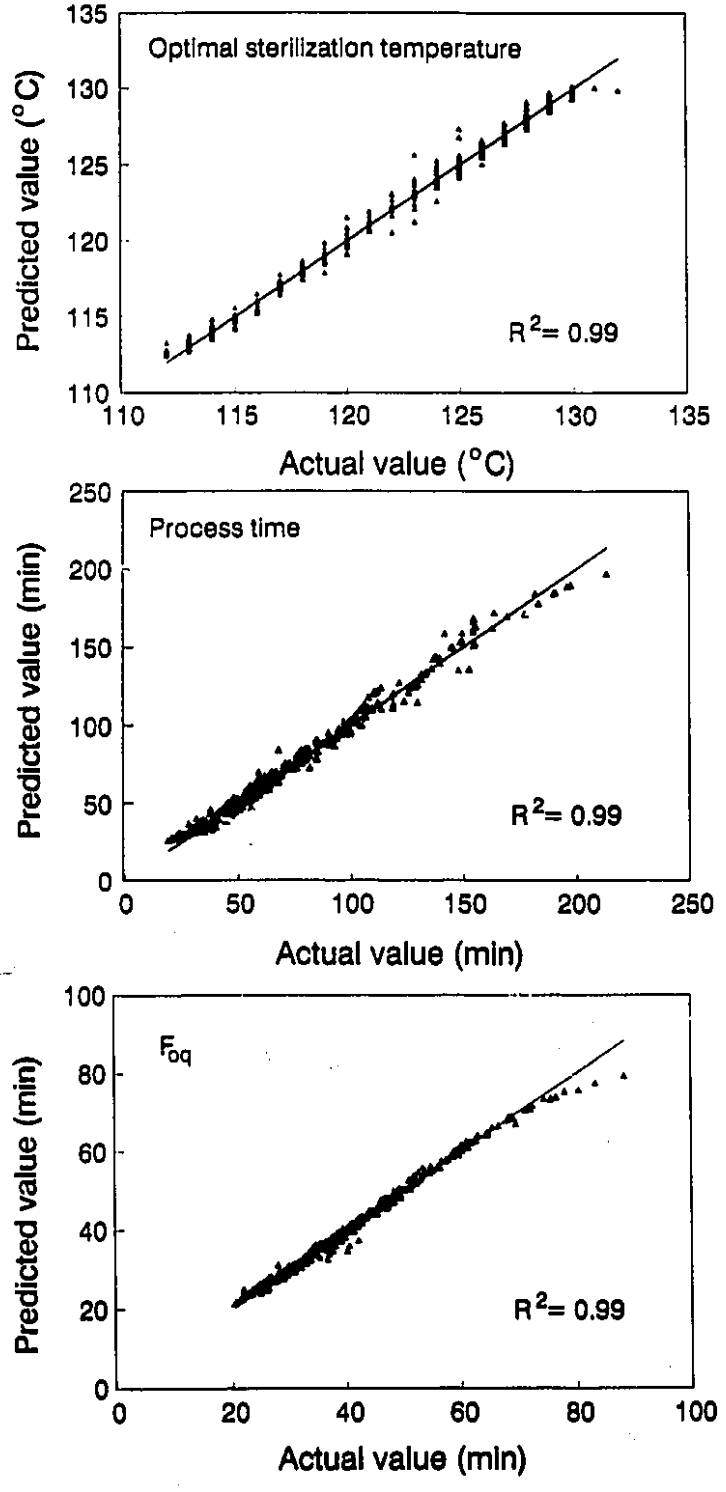

Figure 8.5 Correlation of neural network predicted values vs. actual values (finite difference output) for optimal sterilization temperature, process time and F_{oq}

proportion to the range of values (optimal process temperature from 112 to 132 °C, process time from 20 to 165, min and F_{oq} from 20 to 90 min) employed for these variables. On a percentage basis, compared to the midpoint values, the range associated with process times was ±80%, while the same with process temperature was only ±9%. With F_{oq}, the range was ±60%. These differences are also due to the logarithmic nature of both the process time and the quality factor retention in relation to optimal process temperature. In the neural network, the weights were adjusted to result in a minimum error in the simultaneous prediction of all three parameters, which are quite different in their nature. The relative errors found were on an average within 5% of the above ranges. In general, these errors will have an even smaller influence on quality factor retention in real processing conditions. For example, the neural network prediction error of ±5% at lower end of F_{oq} values would mean ±1.2% error in thiamine retention [F_{oq} = 23.6 min, D_{ref} = 163 min (Lund, 1975), z = 25 C°, can size = 202 x 204, thermal diffusivity = 2.0 x 10^{-7}] at 123 °C and at higher end of F_{oq} values ±1.9% error [F_{oq} = 69.6 min, D_{ref} = 163 min, z = 25 C°, can size = 401 x 411, thermal diffusivity = 1.2 x 10^{-7}] at 115 °C.

Table 8.2 Error parameters for optimal sterilization temperature, process time and F_{oq}

Error Parameters	T_{opt} (°C)	PT (min)	F_{oq} (min)
MAE	0.37	3.12	0.81
SDE	0.35	2.86	0.95
MRE (%)	0.30	4.83	2.11
SRE (%)	0.28	4.84	2.21
R^2	0.99	0.99	0.99

PART II - Heat Transfer Parameters, Convection Heating

Learning/Training of ANN

Initially, all five error parameters (R^2, MAE, SDE, MRE and SRE) were determined by keeping learning runs fixed at 50,000; whereas the number of hidden layers (1, 2 and 3) and the number of neurons in each hidden layer (5,10, 15, 20, 30 and 40) were varied. The error parameter results indicated that the prediction accuracy of neural network slightly increased (up to 1% in MRE and SRE, results not shown) when the number of hidden layer was increased to 2; however, a further increase in the number of hidden layers to 3 did not improve the prediction accuracy. Earlier studies (Ruan et al., 1995 and Tomlins and Gay, 1994) also found that the neural network prediction accuracy improved with two hidden layers compared to that one hidden layer. Hence a four layer network was constructed with 1 input, 1 output and 2 hidden layers. Later, the number of neurons in each hidden layer varied from 2 to 12 and learning runs from 25,000 to 100,000. The optimal number of neurons in each hidden layer and learning runs were obtained from error parameters for U and h_{fp}. The mean relative errors associated with U and h_{fp} as a function of the number of neurons and learning runs, are shown in Figures 8.6 and 8.7. The computed errors converged to a minimum value at 8 or 10 neurons in each hidden layer and 50,000 learning runs. Increasing the neurons and/or learning runs beyond these levels resulted only in increased computation time with no additional benefits. The trend of four remaining error parameters with the number of neurons and learning runs was similar to the one observed with mean relative error. The actual value of the relative errors remained relatively constant (and in some cases showed a fluctuating trend with an occasional increase in errors) after the number of neurons exceeded 10.

Performance of ANN

A neural network configuration with 10 neurons in each hidden layer and 50,000 learning runs was evaluated for performance testing on the three sets of data with both single and multiple particle data-sets. The prediction performance of the neural network for all the sets is shown in Figures 8.8-8.11 for the single particle and in Figures 8.12-

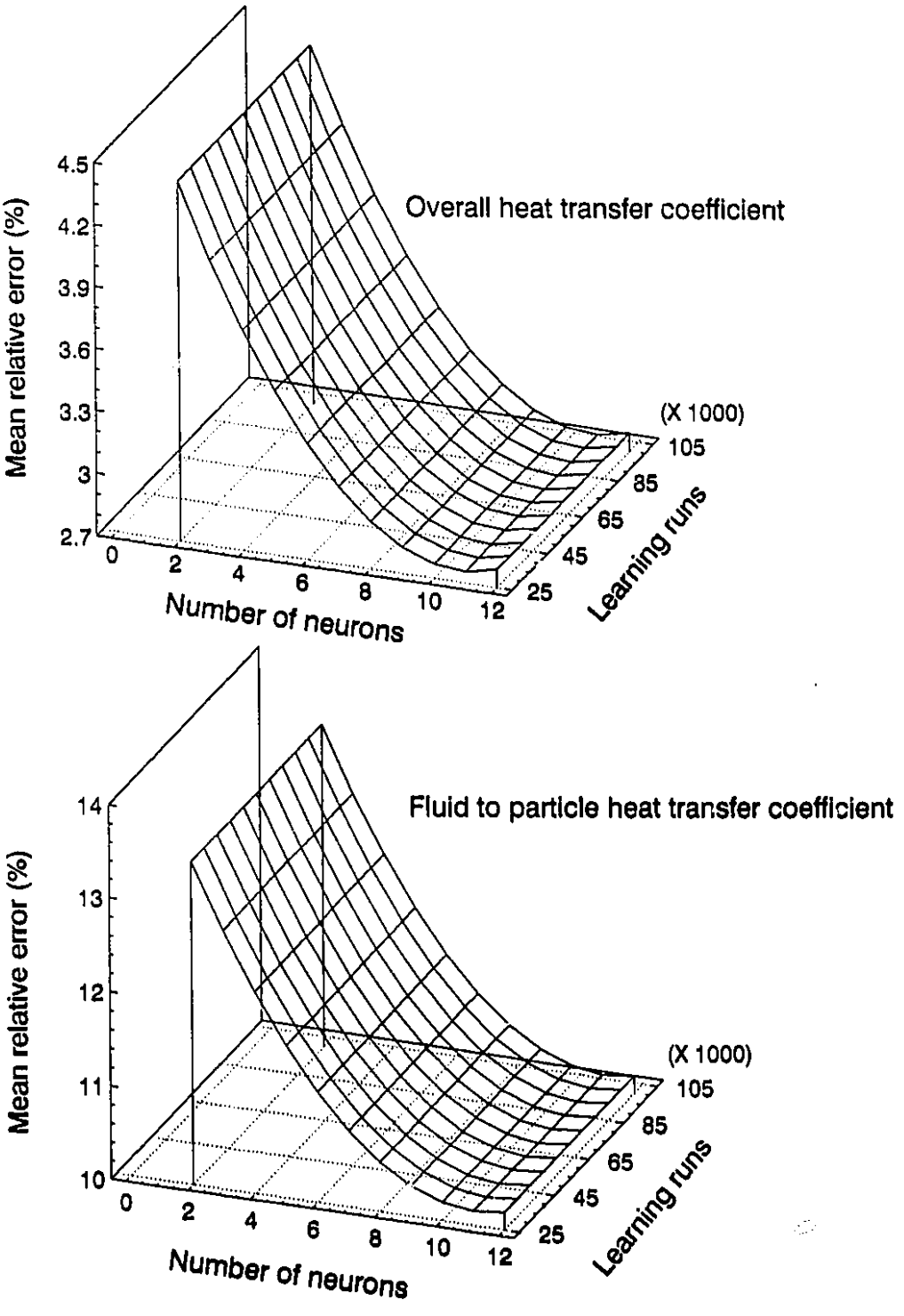

Figure 8.6 Response surface plots for mean relative error as function of number of neurons and learning runs for U and h_{fp}, with a ***single particle*** in the can (315 cases for learning and 315 cases for testing)

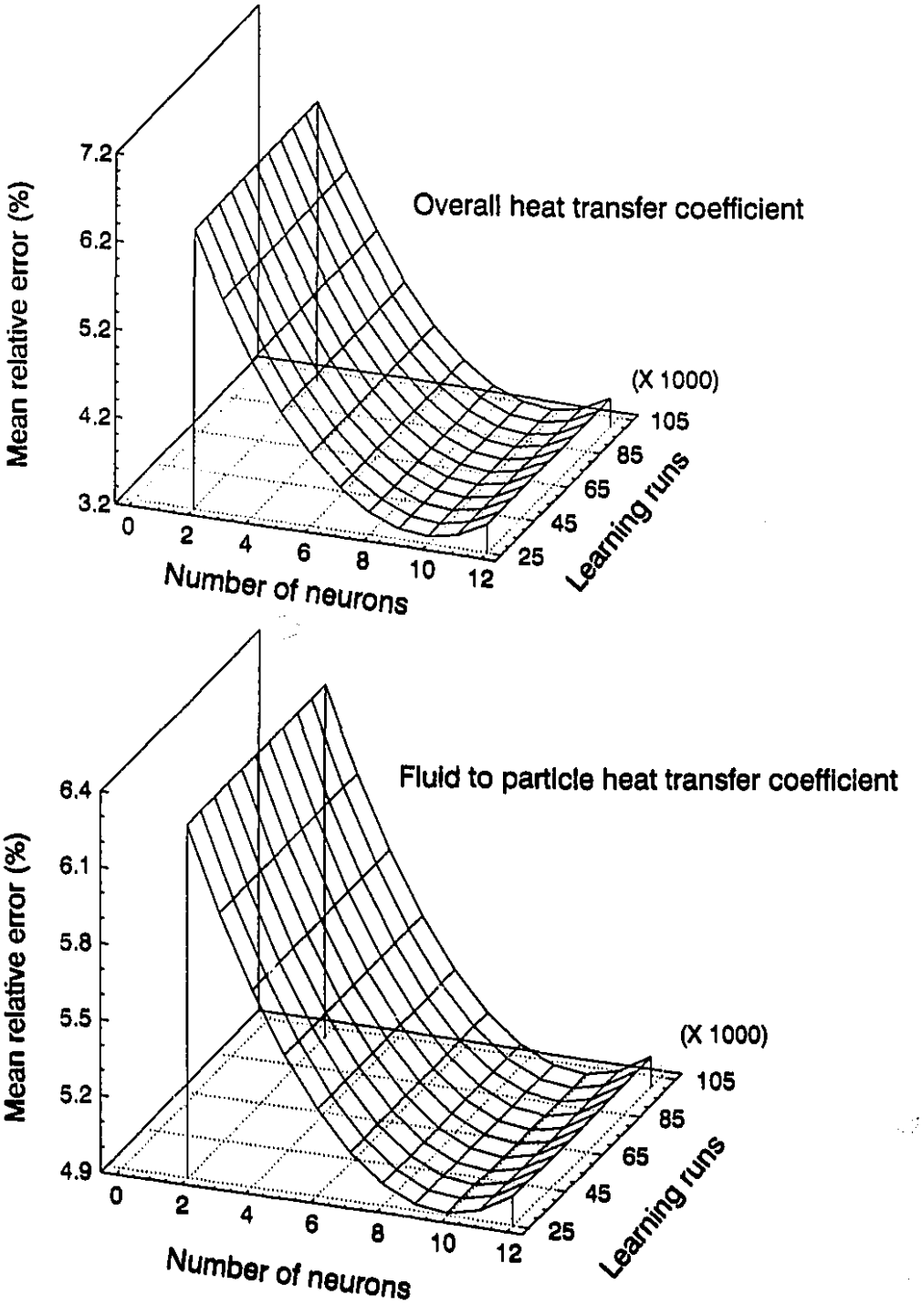

Figure 8.7 Response surface plots for mean relative error as function of number of neurons and learning runs for U and h_{fp}, with ***multiple particles*** in the can (180 cases for learning and 180 cases for testing)

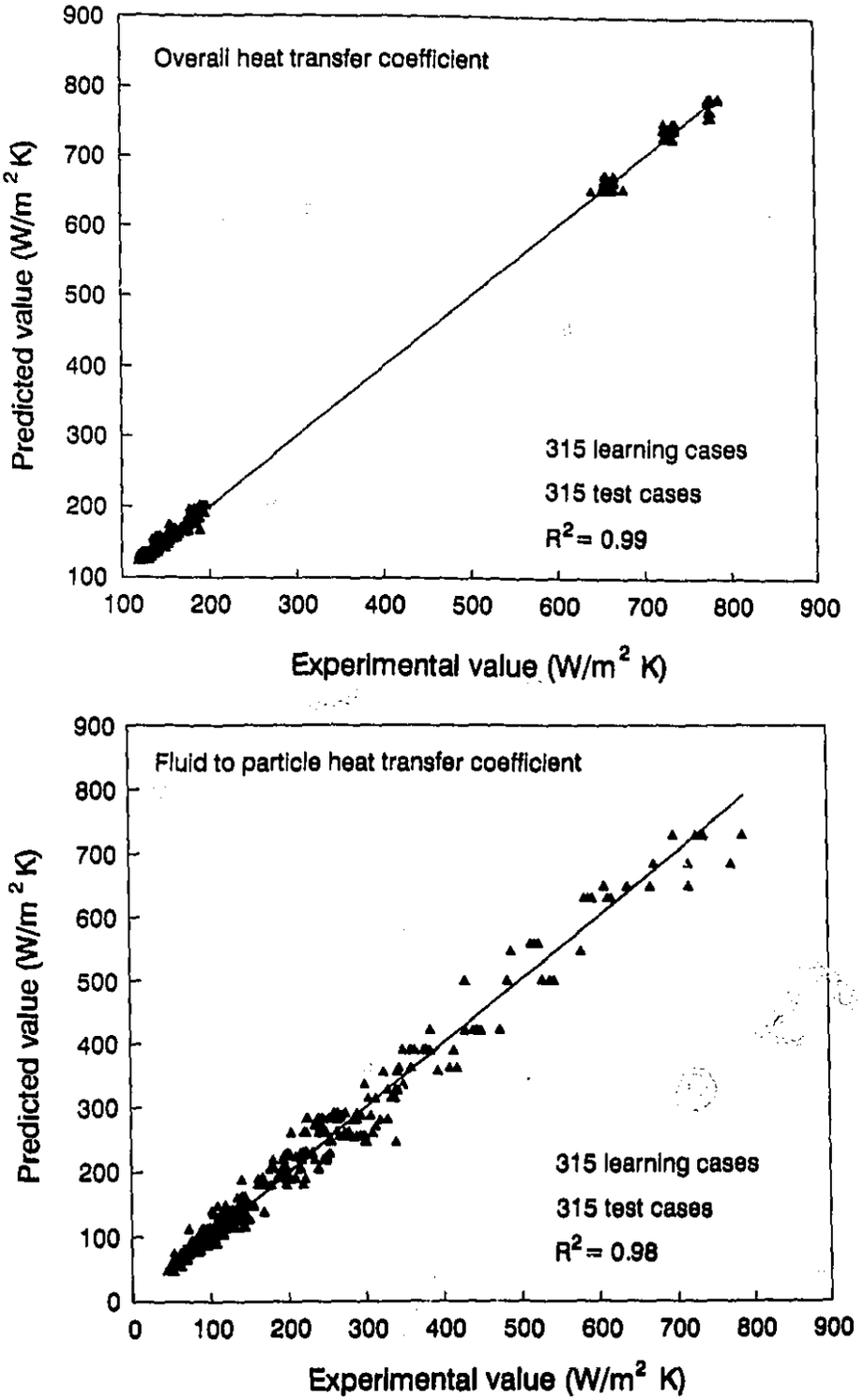

Figure 8.8 Correlation of neural network predicted values vs. experimental values for U and h_{fp}, with a ***single particle*** in the can for ***315 learning cases and 315 test cases***

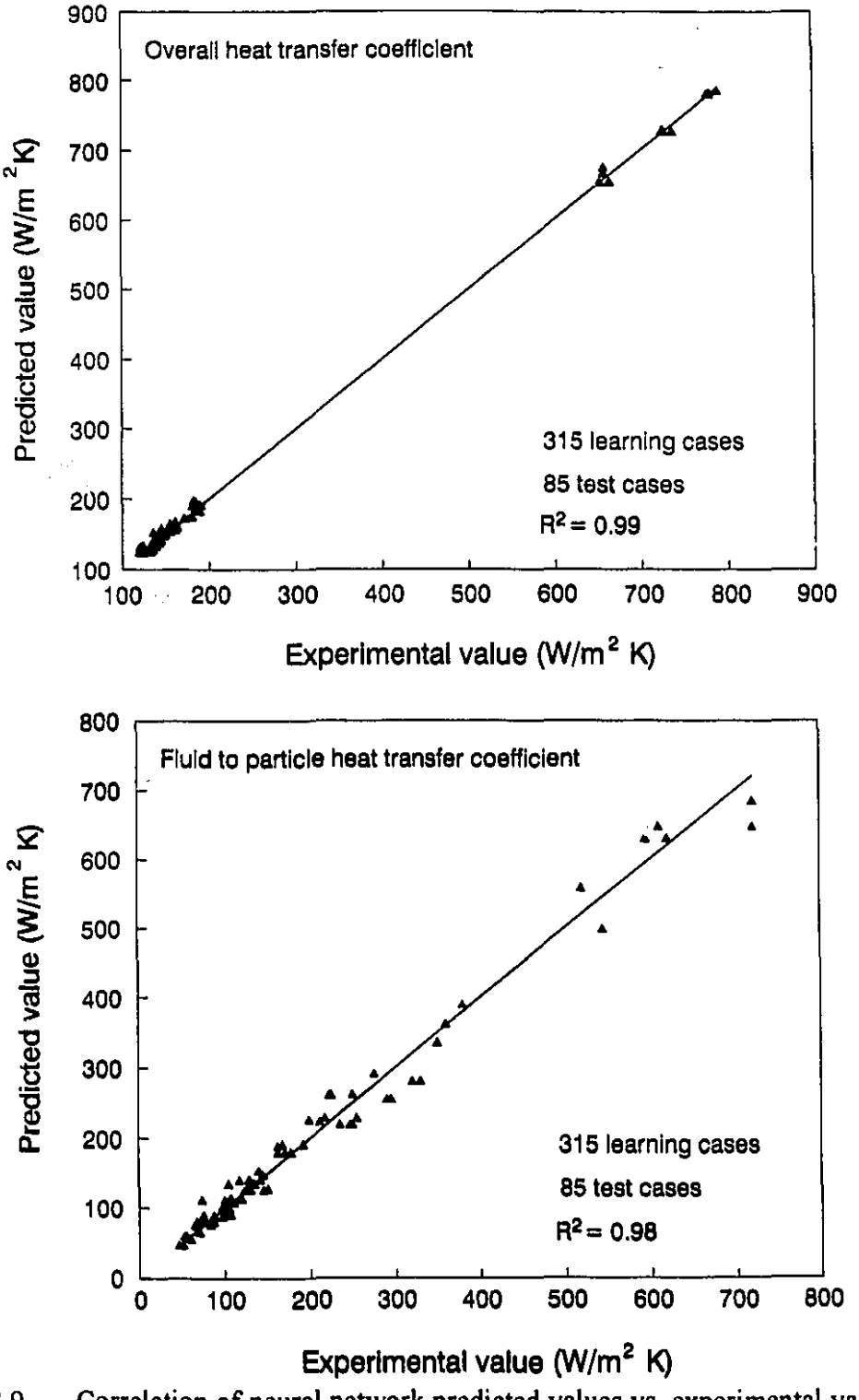

Figure 8.9 Correlation of neural network predicted values vs. experimental values for U and h_{fp}, with a ***single particle*** in the can for ***315 learning cases and 85 test cases***

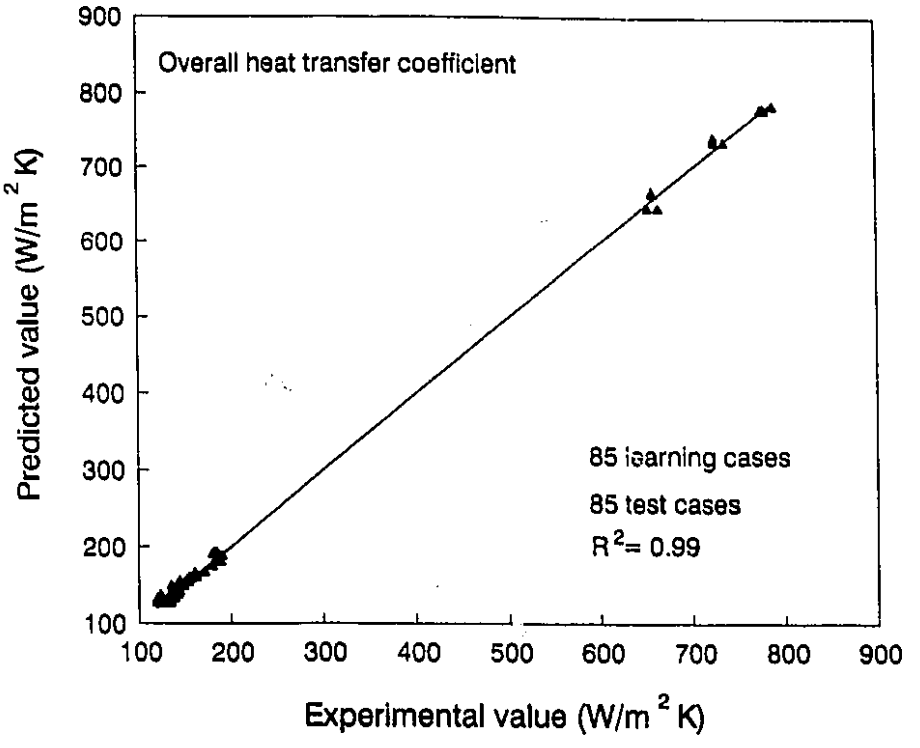

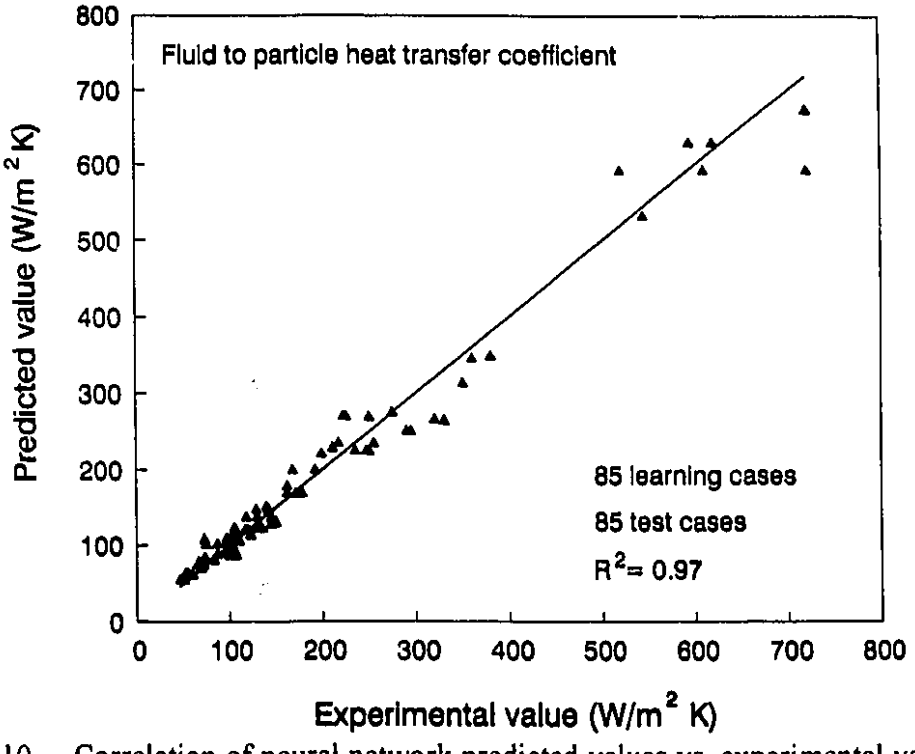

Figure 8.10 Correlation of neural network predicted values vs. experimental values for U and h_{fp}, with a ***single particle*** in the can for ***85 learning cases and 85 test cases***

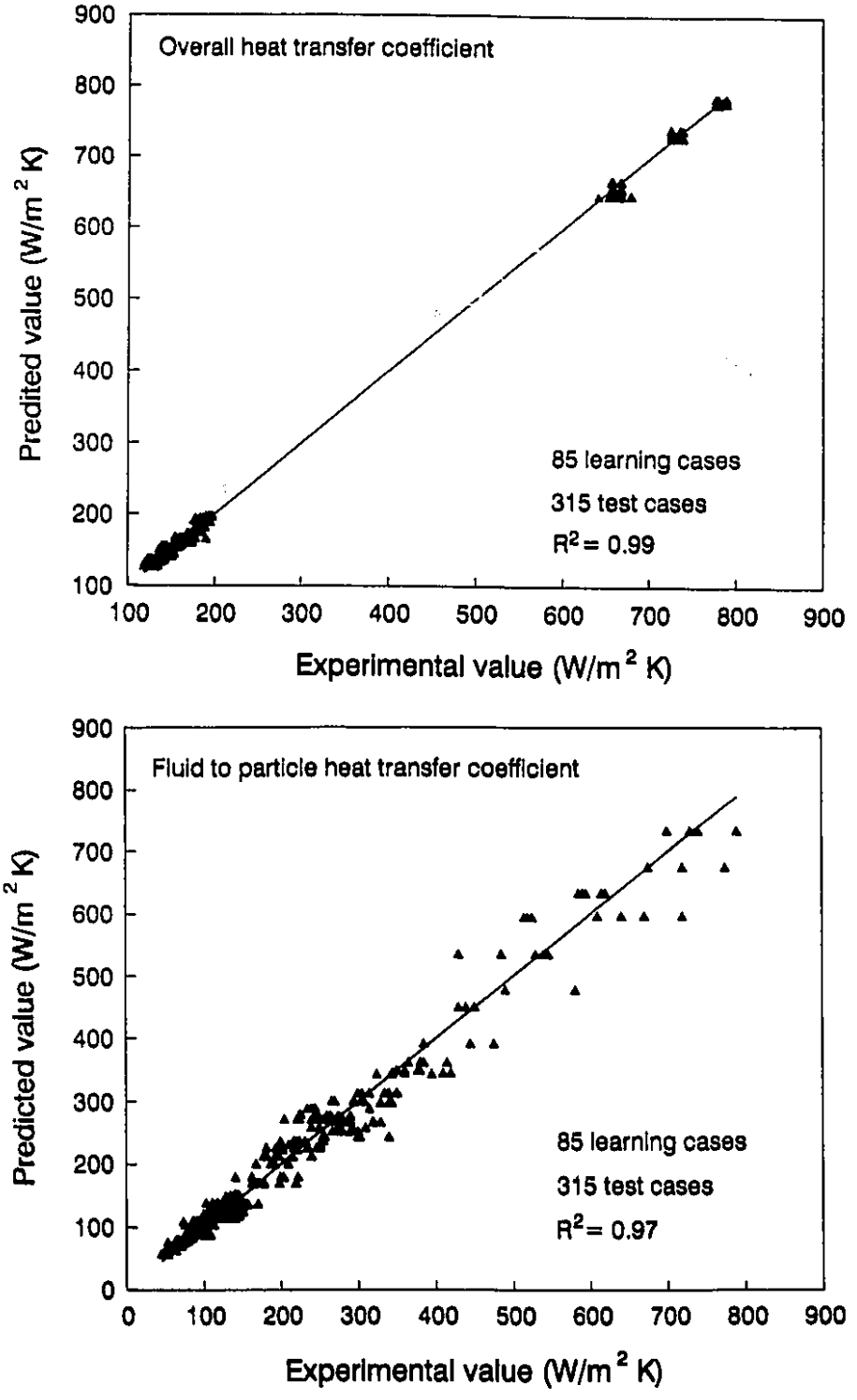

Figure 8.11 Correlation of neural network predicted values vs. experimental values for U and h_{ip}, with a ***single particle*** in the can for ***85 learning cases and 315 test cases***

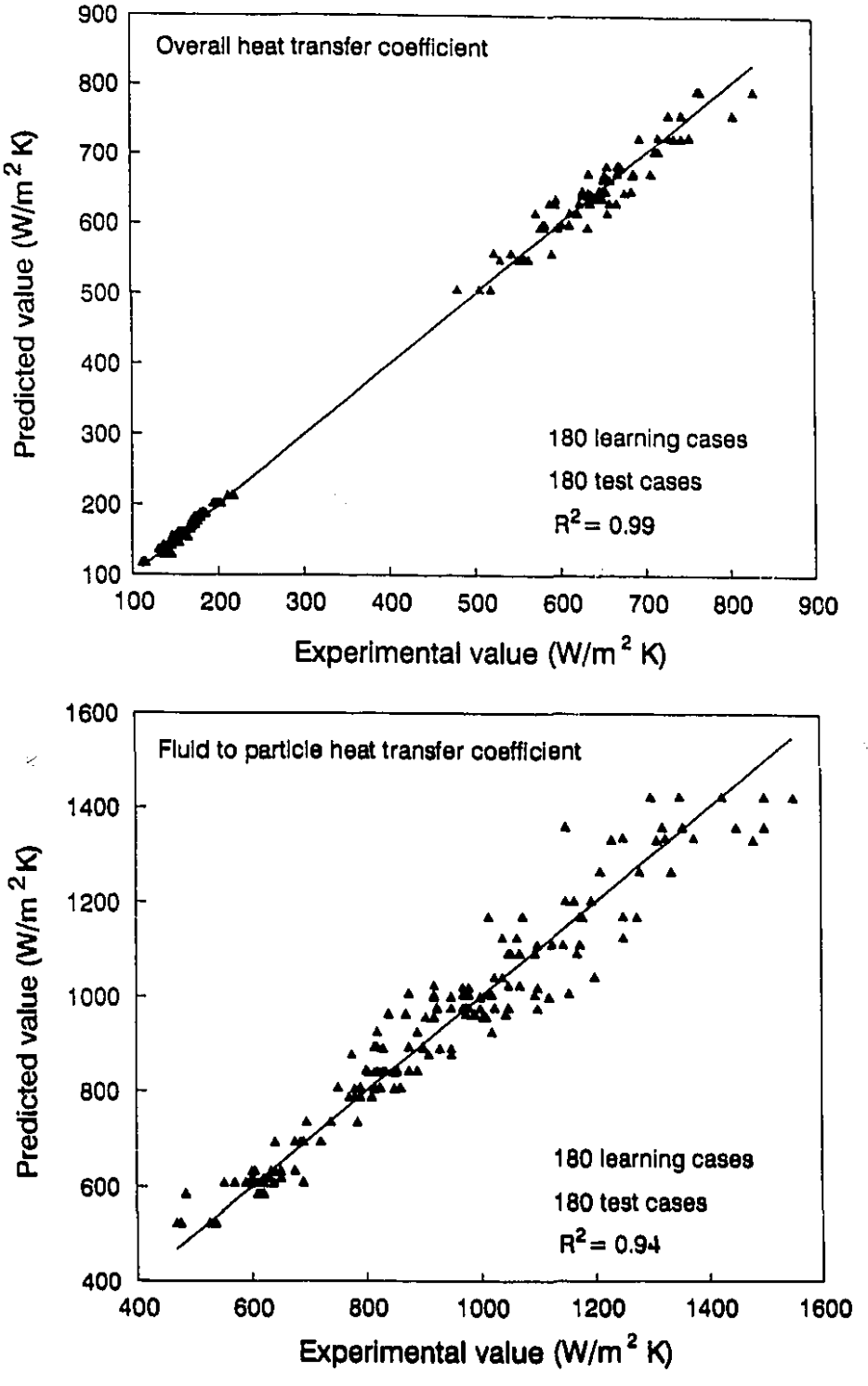

Figure 8.12 Correlation of neural network predicted values vs. experimental values for U and h_{fp}, with ***multiple particles*** in the can for ***180 learning cases and 180 test cases***

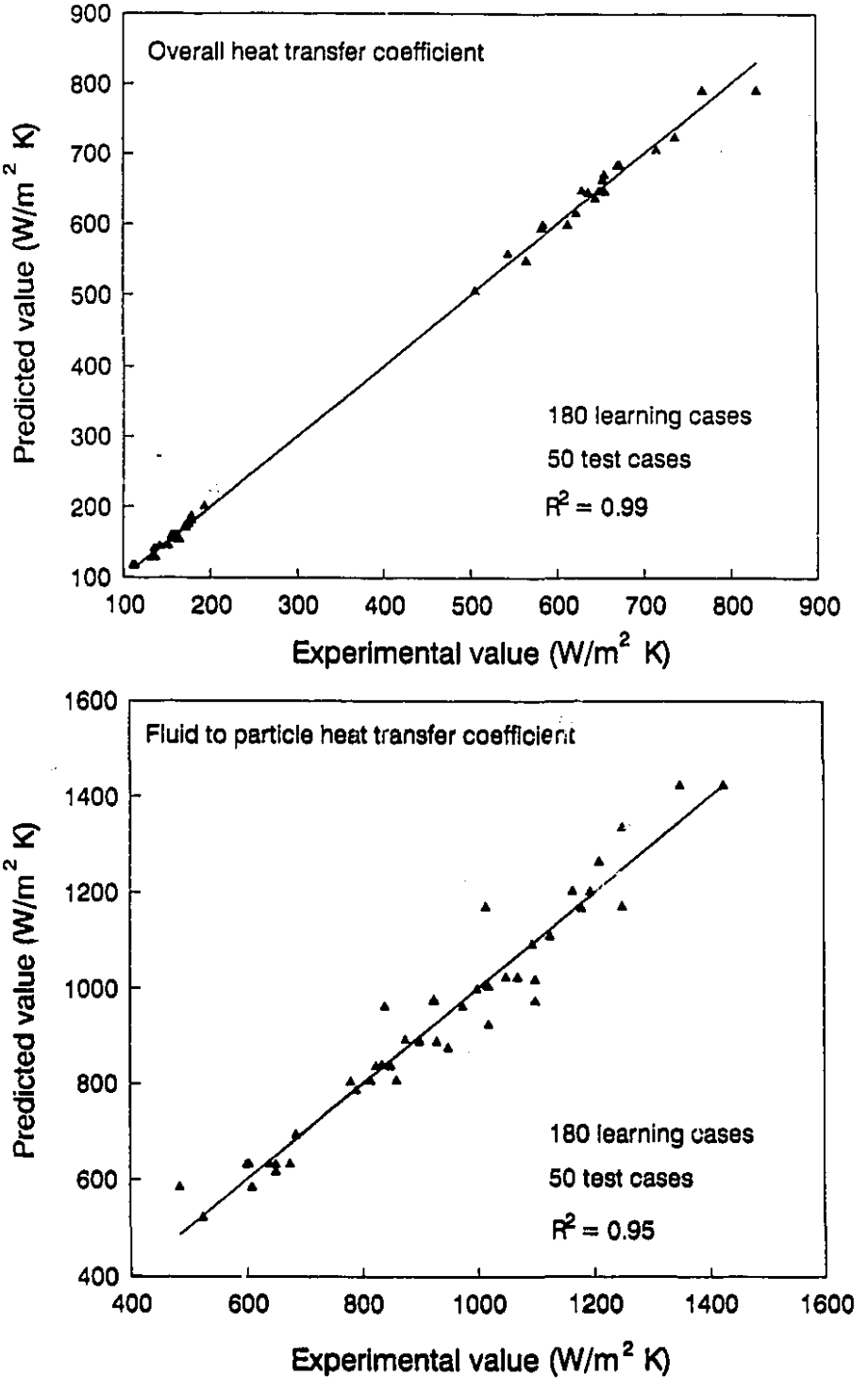

Figure 8.13 Correlation of neural network predicted values vs. experimental values for U and h_{fp}, with ***multiple particles*** in the can for ***180 learning cases and 50 test cases***

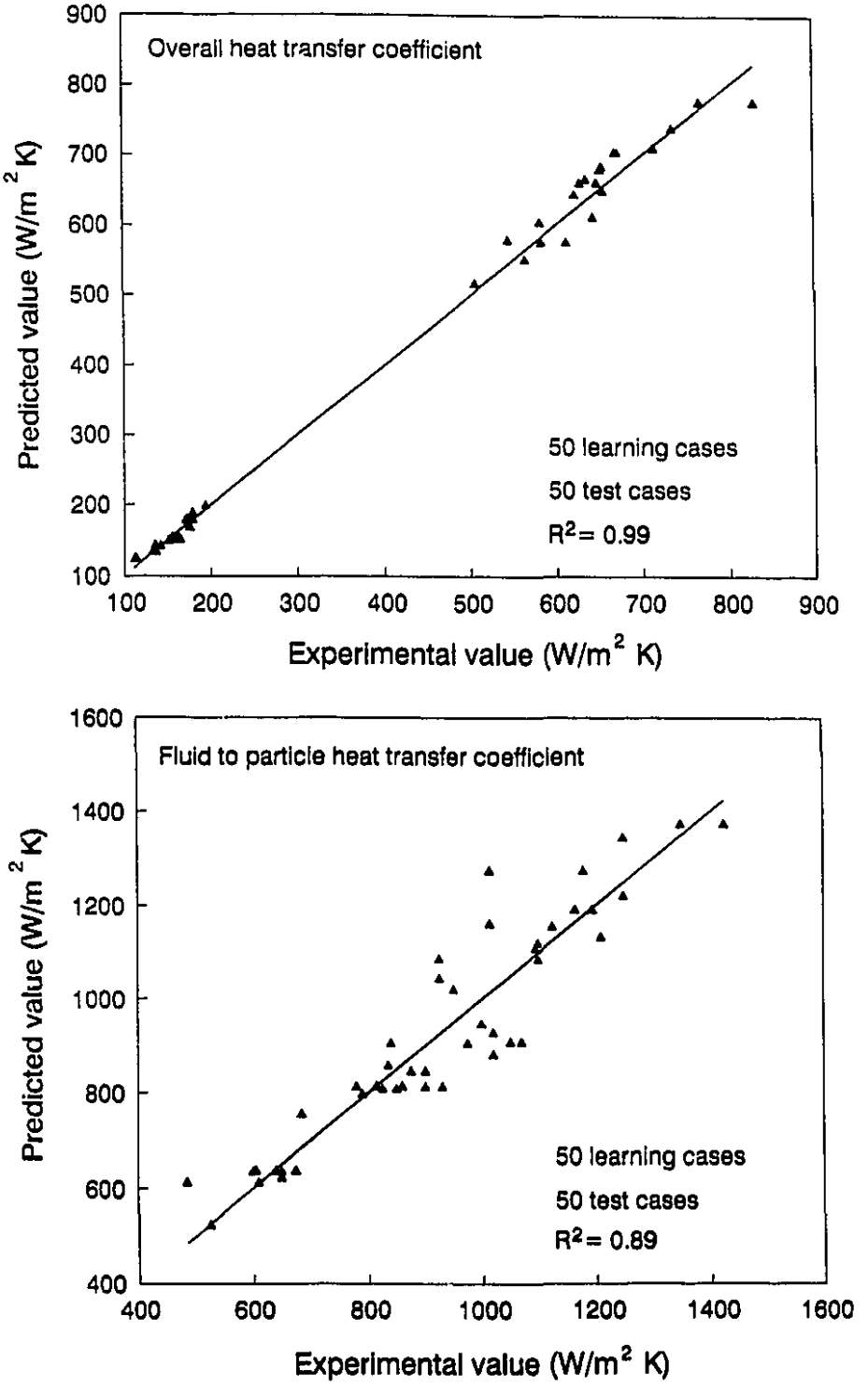

Figure 8.14 Correlation of neural network predicted values vs. experimental values for U and h_{fp}, with ***multiple particles*** in the can for ***50 learning cases and 50 test cases***

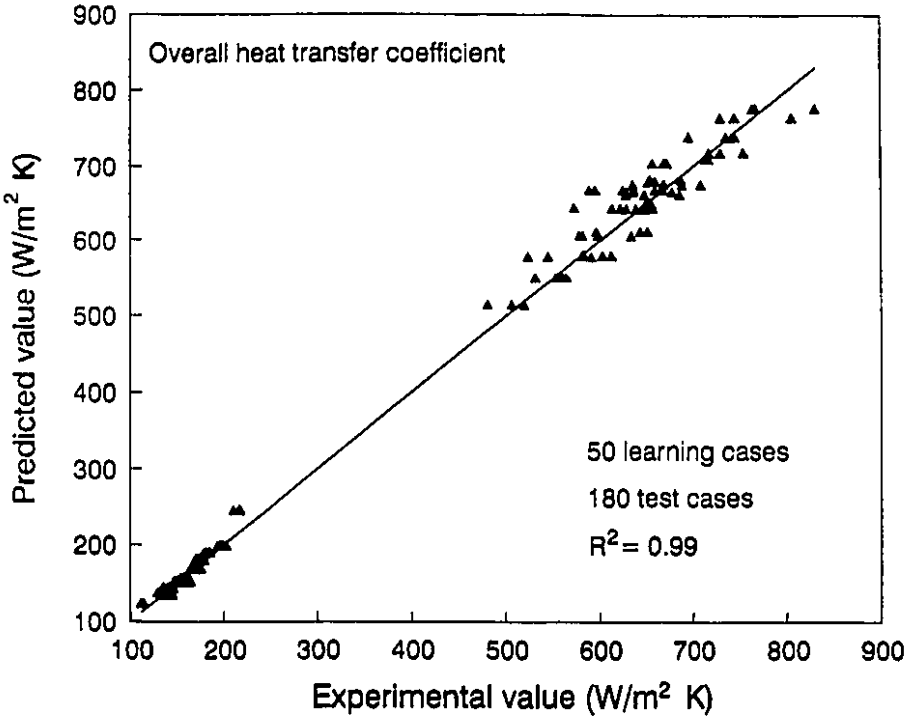

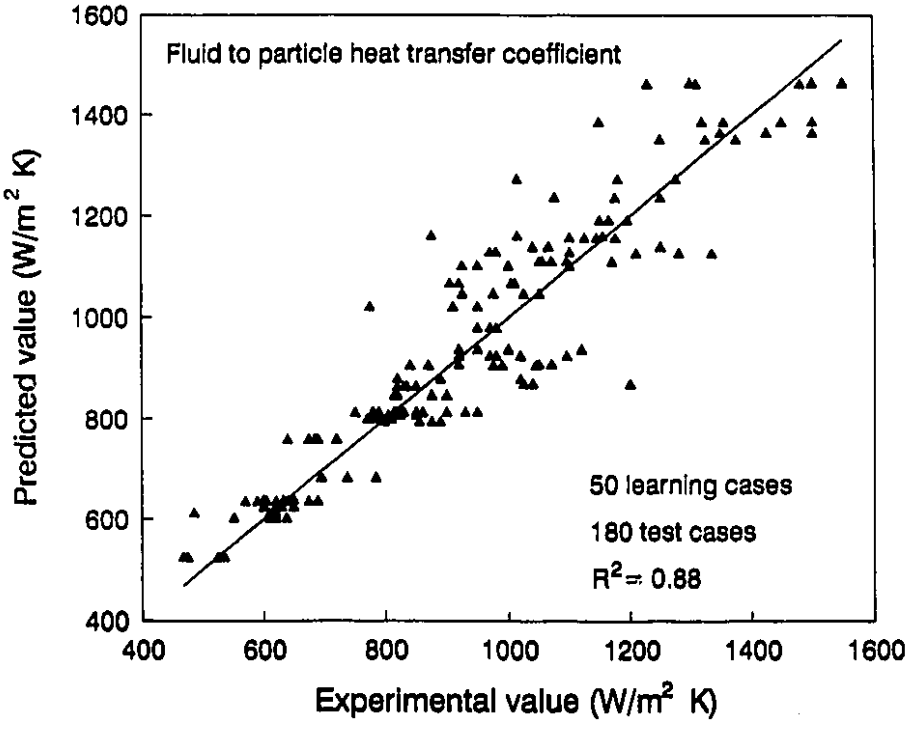

Figure 8.15 Correlation of neural network predicted values vs. experimental values for U and h_{fp}, with ***multiple particles*** in the can for ***50 learning cases and 180 test cases***

8.15 for multiple particles, as plots of neural network predicted values vs experimental output values for both U and h_{fp}. The predicted values were more evenly and tightly distributed around the regression line for the first set involving the full set of learning cases (315 or 180). With lower number of learning cases (85 or 50) also, the predicted values were in fairly close agreement with experimental values, with a slight deviation at higher ends. This implies that when representative data are available, even a smaller set of data used for training can reasonably predict the output performance over the entire range. However, care should be taken to avoid extrapolation of the results, because in reality a neural network cannot accurately give the output response, like any other polynomial regression technique, outside the range of input parameter used for training.

Single particle in the can situations

The associated errors with the neural network outputs are compared in Table 8.3 for the single particle in the can situations. The high R^2 (>0.99) values for U indicate excellent correlations of neural network predicted values with experimental values. Relatively, lower correlations were observed while predicting h_{fp}. This is probably due to the slightly higher experimental variation associated with h_{fp} evaluations. On average, the magnitude of errors for all groups was nearly the same as those for the reference group for U, while it increased for h_{fp} (MRE increased from 6 to 10%). These errors were within the range of experimental variability (coefficient of variations in h_{fp} was about 10%) for the measured value of h_{fp}. On average, the mean relative error in U prediction was essentially of 2.5 $\pm$ 2.4 % (W/m^2 K) for all the groups. The mean relative error in h_{fp} prediction was about 5.8 % with the reference group and about 9% with the remaining groups; however, the standard deviation of relative error was ~7% with all groups. The relatively larger standard deviations associated with h_{fp} predictions by neural network, were mostly due to deviations observed under conditions of high fluid to particle heat transfer coefficient value (h_{fp}>400 W/m^2K). Neural network prediction showed a deviation from the desired output mostly at the higher end of h_{fp} values when all 315 cases were used for learning purpose. However, when only 85 cases were used for learning, the predicted values deviated at both ends (Figures 8.10 and 8.11).

Table 8.3 Comparisons of error parameters for different sizes of learning and test cases for a single particle in the can

Error Parameters	R.G[1]		F.G[2]		S.G[3]		T.G[4]	
	U (W/m^2 K)	h_{fp} (W/m^2 K)	U (W/m^2 K)	h_{fp} (W/m^2 K)	U (W/m^2 K)	h_{fp} (W/m^2 K)	U (W/m^2 K)	h_{fp} (W/m^2 K)
MAE	5.11	17.2	4.24	15.0	4.43	17.4	4.80	19.6
SDE	4.76	16.0	3.76	14.3	3.90	19.2	4.51	20.2
MRE (%)	2.46	5.82	2.47	8.65	2.46	9.70	2.40	9.91
SRE (%)	2.51	7.00	2.43	7.13	2.37	7.63	2.46	7.44
R^2	0.99	0.98	0.99	0.98	0.99	0.97	0.99	0.97

[1]Reference group : learning = 315 cases and testing = 315 cases; [2]First group : learning = 315 cases and testing = 85 cases; [3]Second group : learning = 85 cases and testing = 85 cases; [4]Third group : learning = 85 cases and testing = 315 cases

Multiple particles in the can situations

Table 8.4 summarizes the associated errors in U and h_{fp}, with the neural network output for multiple particles in the can. The error parameters were of similar magnitude compared to that observed with the single particle cases. Again, excellent correlations were observed (R^2>0.99) for U values predicted by neural network vs the experimental outputs; and relatively, lower correlations were observed while predicting h_{fp}. The standard deviations in experimental h_{fp} values were slightly higher compared to that of the experimental U values. The prediction performance of a neural network trained with smaller size of data-sets was slightly lower when compared to a trained full data-set. This was probably due to some degree of associated extrapolation. However, the increased errors were within the limits of experimental variability in measured values of U and h_{fp}. On average, the magnitude of error for the first group was nearly the same as those of the reference group for U and h_{fp}. However, with the second and third groups, the errors were relatively higher compared to the errors of the reference or first group, for both U and h_{fp}, especially with reference to relative error (MRE) and standard deviation (SRE). The mean relative error for the reference and first group in the U prediction was of 2.5 $\pm$ 1.75%, and

with second and third group it was 3.5 ± 2.75%. The mean relative error in h_{fp} was about 4.25 % with the reference and first group, and about 6.5% with the second and third group; however, the standard deviation of relative error was ~4% and ~6%, respectively.

Overall, the relative errors associated with h_{fp} prediction were the higher, and those associated with the U were the somewhat lower in proportion to their standard deviations in experimental data. In a neural network, the weights are adjusted to reflect minimum error in the prediction of both parameters U and h_{fp} simultaneously; however, the independent variables may be affected differently. Figure 8.16 shows a typical continuous response plot of neural network predicted values, and experimental values of U and h_{fp} at various rotational speeds; this demonstrates some nonlinearity. Such a plot will be useful in assessing the continuity of the predictions under extrapolation situations.

Table 8.4 Comparisons of error parameters for different sizes of learning and test cases, for multiple particles in the can

Error Parameters	R.G[1]		F.G[2]		S.G[3]		T.G[4]	
	U (W/m^2 K)	h_{fp} (W/m^2 K)	U (W/m^2 K)	h_{fp} (W/m^2 K)	U (W/m^2 K)	h_{fp} (W/m^2 K)	U (W/m^2 K)	h_{fp} (W/m^2 K)
MAE	9.85	48.1	8.24	36.7	13.2	58.1	12.4	63.2
SDE	11.0	40.5	6.75	37.1	12.1	53.8	14.6	63.8
MRE (%)	2.57	4.52	2.47	4.03	3.75	6.38	3.23	6.70
SRE (%)	1.96	3.90	1.55	4.20	2.48	5.96	2.99	6.34
R^2	0.99	0.94	0.99	0.95	0.99	0.89	0.99	0.88

[1]Reference group : learning = 180 cases and testing = 180 cases; [2]First group : learning = 180 cases and testing = 50 cases; [3]Second group : learning = 50 cases and testing = 50 cases; [4]Third group : learning = 50 cases and testing = 180 cases

Comparison of the neural network models with the regression models

The performance of neural network models were compared with regression models previously obtained with dimensional analyses (Chapter 7). Table 8.5 summarizes the error parameters for dimensionless correlations and neural network models. Although R^2 values obtained for both modeling approaches were comparable for all cases (except for

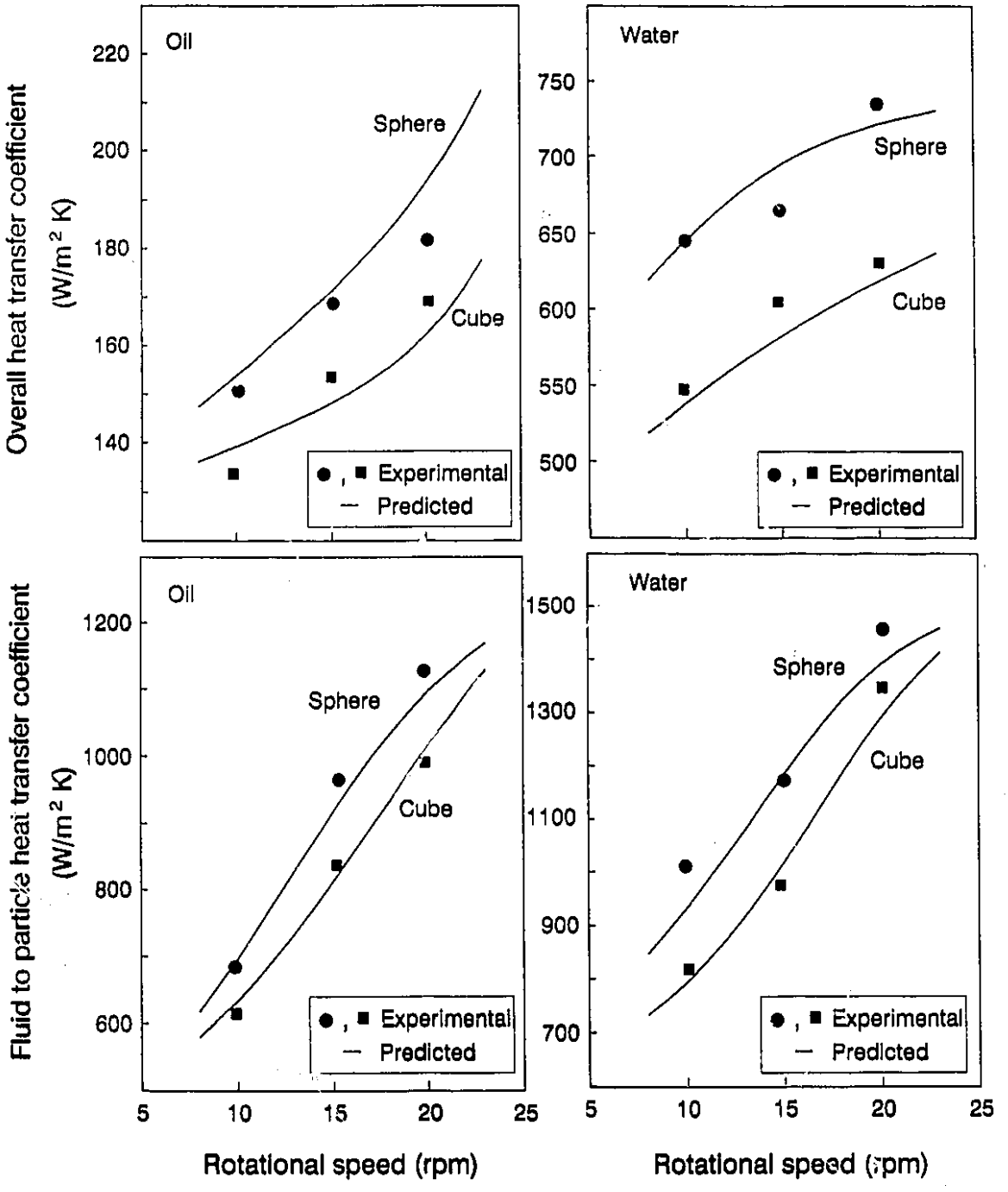

Figure 8.16 A response plot of neural network predicted values and experimental values of U and h_{fp}, at various rotational speeds for oil and water

h_{fp} with a single particle in the can), the absolute and relative errors in heat transfer coefficients were higher with dimensionless correlations compared to that obtained by the neural network. The mean relative error and standard deviation in heat transfer coefficients with the neural network were nearly half of the those obtained with dimensionless correlations. The errors in h_{fp} prediction with a single particle in a can were quite high in the dimensionless correlation; this was due to the nonlinear behavior of h_{fp} with rotational speed for high density particles. These trends were difficult to incorporate in dimensional analysis, which is based on the understanding of the physical nature of the phenomena. In such situations, neural network modeling has a clear advantage over traditional multiple regression analysis. However, as opposed to the neural network which is generally described as the 'black box' regression model, the dimensional analysis approach may give a better insight into the physical phenomena which otherwise cannot be obtained with neural network models.

Table 8.5 Comparison of error parameters for neural network model vs dimensionless correlation

Error Parameters	Single particle				Multiple particles			
	U		h_{fp}		U		h_{fp}	
	DC (W/m^2 K)	NN (W/m^2 K)	DC (W/m^2 K)	NN (W/m^2 K)	DC (W/m^2 K)	NN (W/m^2 K)	DC (W/m^2 K)	NN (W/m^2 K)
MAE	17.1	5.11	31.3	17.2	25.1	9.85	75.4	48.1
SDE	25.4	4.76	43.3	16.0	32.9	11.0	63.4	40.7
MRE (%)	5.00	2.46	16.9	5.82	5.70	2.57	8.26	4.52
SRE (%)	3.76	2.51	11.9	7.00	4.65	1.96	7.12	3.90
R^2	0.99	0.99	0.83	0.98	0.98	0.99	0.96	0.94

DC - Dimensionless correlations; NN - Neural network

CONCLUSION

In neural network modeling applications, the number of hidden layers, the number of neurons in the hidden layers and the number of learning runs need to be optimized before using the neural network. For conduction heating conditions, a neural network with 8 neurons in hidden layers and 50,000 learning runs was found as the optimum for its performance. The trained network was found to predict response with less than 5% associated errors, with respect to optimal sterilization temperature, process times and quality factor retention.

A neural network with 10 neurons in the hidden layers and 50,000 learning runs was found optimal for its performance with convection heating systems. The trained network was found to predict responses with less than 3% and 5% associated errors with respect to the overall heat transfer coefficient and the fluid to particle heat transfer coefficient, respectively. Even when a smaller group of data-sets was used for training, the prediction accuracy of the network was found to be within the experimental variability of measured U and h_{fp} values. The prediction accuracies of neural network models were higher compared to the multiple regression models of dimensionless correlation.

CHAPTER 9

GENERAL CONCLUSIONS, CONTRIBUTION TO KNOWLEDGE AND RECOMMENDATIONS

A. GENERAL CONCLUSIONS

1. A methodology was developed for the measurement of convective heat transfer coefficients, associated with canned liquid/particle mixtures subjected to end-over-end processing. The assumption of uniform temperatures of liquid in cans, subjected to agitation processing, was verified using heat penetration parameters and standard deviation of temperature at different locations and at various rotational speeds. Of the two different objective functions, one based on minimizing the sum of the square of the differences between experimental and predicted temperatures (LSLD) and other based on minimizing the difference between the measured and predicted lethality (LALD), the later was found to be more appropriate for the estimation of h_{fp}. The measured h_{fp} values were higher with moving particles compared to those for a fixed particle. The method differentiated U and h_{fp} values at different rotational speeds.

2. Using the methodology developed, the influence of system and product parameters on U and h_{fp} were evaluated. With a single particle in the can situation, the rotational speed effect on U and headspace effect on h_{fp} were predominant among the four system variables studied. The particle density had no significant influence ($p > 0.05$) on U; however, U was influenced by liquid viscosity at all the rotational speeds (0 to 20 rpm). Both liquid viscosity and particle density had a significant effect on h_{fp}. In general, decreasing liquid viscosity, increasing particle density (except with Teflon and Delrin) and increasing rotational speed improved h_{fp}. The particle density effect on h_{fp} was higher than those of rotational speed and liquid viscosity.

Errors in thermocouple placement, within the particle, during temperature data gathering caused relatively lower errors in the evaluated h_{fp} than those associated with errors due to measured thermal diffusivity and thermal conductivity. The errors in evaluated h_{fp} were lower with higher thermal diffusivity particles and, hence, particles with higher thermal diffusivity were preferred to others.

3. With multiple particles in cans, the influence of liquid viscosity, rotational speed, particle size, particle concentration as well as particle shape on U and h_{fp} were investigated, with end-over-end processing conditions. All the above parameters had a significant influence on U and h_{fp}. The range of h_{fp} values obtained in the present study was comparable to some previously published values under moving particle situations. The increasing rotational speed and decreasing liquid viscosity improved U and h_{fp}. Initial increase in particle concentration from a single particle (to 20% for U and to 30% for h_{fp}) enhanced the heat transfer coefficients; however, a further increase in concentration to 40% (v/v) decreased the heat transfer coefficients. Higher U and h_{fp} were obtained with decreasing particle size in oil and water, at all the rotational speeds. With a single particle in the can, decreasing particle sphericity (sphere to cube) improved h_{fp} in all conditions, because of increasing roughness; however, U was not affected by the particle shape. With multiple particles in the can, U and h_{fp} values were highest with the sphere, followed by the cylinder and then the cube; this was explained by the packability of the particles in the can. The influence of particle size, particle concentration and rotational speed were more pronounced with the viscous liquid (oil). The influence of particle shape was more pronounced with a single particle in the can.

4. A flow visualization study under end-over-end rotational conditions assisted in making a qualitative assessment of the particle motion/mixing effect on the magnitude of U and h_{fp} under various experimental conditions. In the single particle in a can situation, the motion of the particle under different conditions was

described with three particle density groupings: low, moderate and heavy density particles compared to that of the liquid density. The particle motion was influenced in all experimental conditions. With multiple particles in the can, the particle concentration, particle size and particle shape influenced the particle mixing. The particle mixing time was reduced with increasing rotational speed and decreasing liquid viscosity.

5. Dimensionless correlations describing Nusselt number as a function of Reynolds number and Prandtl number were developed for convective heat transfer to liquids in cans with (i) a single particle (or liquid only situation) and (ii) multiple particles, subjected to end-over-end processing. The characteristic length, used in the dimensionless numbers, was the sum of the diameter of rotation and the diameter of can for U correlations. In the modeling of heat transfer to a single particle, forces affecting the particle settling velocity in the agitating can liquid were significant; hence, dimensionless numbers such as Froude number, Prandtl number, Reynolds number and density simplex, accounting for these forces, were significant. Additional dimensionless groups were significant in the modeling of heat transfer to multiple particles; particle to liquid thermal conductivity ratio and Peclet number (product of Reynolds and Prandtl numbers). The particle shortest dimension and particle equivalent diameter were equally good as the characteristic length in dimensionless numbers for h_{fp} correlations. The particle concentration effect was more pronounced on U compared to that on h_{fp}. The particle shape effect was equally important with U and h_{fp}.

6. Multi-layer neural network models were developed to predict the heat transfer parameters with conduction and convection heated canned foods. The neural network models can predict several outputs simultaneously, unlike conventional regression models where one equation is needed for each output. With conduction heated food, the trained neural network with 8 neurons in each hidden layer (2 hidden layers) and 50,000 learning runs predicted the response with less than 5%

associated errors, with respect to optimal sterilization temperature, process times and quality factor retention. The overall heat transfer coefficient and fluid to particle heat transfer coefficient, the two important parameters needed for theoretical prediction of time temperature profiles of convection heated canned liquid/particle mixtures, were predicted simultaneously using the artificial neural network. A 4 layer neural network provided optimal performance, with 10 neurons in each hidden layer and 50,000 learning runs. The trained network predicted responses with less than 3% associated errors for overall heat transfer coefficient and less than 5% associated errors for fluid to particle heat transfer coefficient. The prediction accuracy of the neural network model remained within the experimental variability of measured U and h_{fp} values, even when a smaller group of data-sets were used for training. The prediction accuracies of neural network models were higher than the multiple regression models of dimensionless correlation.

B. CONTRIBUTION TO KNOWLEDGE

1. A methodology was developed to measure the overall and fluid to particle heat transfer coefficients, associated with canned liquid/particle mixtures subjected to end-over-end processing. The method allowed the particle movement inside the cans while measuring the transient temperature of particle in cans during agitation processing.

2. A comprehensive study to establish the influence of both system and product parameters on associated convective heat transfer coefficients in canned liquid/particle mixtures with end-over-end processing. The following were examined and discussed: effects of retort temperature, radius of rotation, can headspace, rotational speed, particle density, liquid viscosity and particle size, particle concentration and particle shape on overall heat transfer coefficient and fluid to particle heat transfer coefficient.

3. A qualitative discussion was included for particle motion/mixing, which incorporated the influence of particle to liquid density, liquid viscosity and rotational speed on the motion of single particle in a can, and particle concentration, particle size, particle shape, liquid viscosity and rotational speed on the mixing behavior of multiple particles and their resulting effects on the magnitude of the overall heat transfer coefficient and the fluid to particle heat transfer coefficient.

4. Dimensionless correlations for the prediction of convective heat transfer to liquid and particles in cans, subjected to end-over-end rotation, were developed in terms of physically meaningful groups. With a single particle in the can, forces affecting the particle settling velocity were significant in the correlations (for h_{fp}), while heat transfer to the particles in canned liquids was described using a packed bed system.

5. Neural network modeling was evaluated as a new approach for the prediction of convective heat transfer coefficients associated with canned liquid/particle mixtures. The neural network model predicted U and h_{fp} with less than 3 and 5% errors respectively.

C. RECOMMENDATIONS FOR FUTURE RESEARCH

Scope of the current research could be broadened by :

1. Quantifying the influence of can size, can shape, can materials and different retort heating media on U and h_{fp}, in canned liquid/particle mixtures with rotational processing.

2. Evaluating heat transfer to canned liquid/particle mixtures subjected to oscillatory agitation.

3. Quantifying the particle motion/mixing in containers under various experimental conditions of agitation processing and relating it to variations in heat transfer coefficients.

4. Biological validation of thermal processes using predicted convective heat transfer coefficients.

5. Extension of the present work of heat transfer and flow visualization to non-Newtonian liquids and food particles.

REFERENCES

Anantheswaran, R. C. and Rao, M. A. 1985a. Heat transfer to model Newtonian liquid foods in cans during end-over-end rotation. J. Food Eng. 4, 1-19.

Anantheswaran, R. C. and Rao, M. A. 1985b. Heat transfer to model non-Newtonian liquid foods in cans during end-over-end rotation. J. Food Eng. 4, 21-35.

Astrom, A. and Bark, G. 1994. Heat transfer between fluid and particles in aseptic processing. J. Food Eng. 21, 97-125.

Awuah, G. B. and Ramaswamy, H. S. 1996. Dimensionless correlations for mixed and forced convection heat transfer to spherical and finite cylindrical particles in an aseptic processing holding tube simulator. J. Food Proc. Eng. *(In press)*

Awuah, G. B., Ramaswamy, H. S. and Simpson, B. K. 1995. Comparison of two methods for evaluating fluid-to-surface heat transfer coefficients. Food Res. Int., 28, 261-271.

Ball, C. O. 1923. Thermal process times for canned foods. Bull. 37. National Research Council, Washington, D. C.

Ball, C. O. and Olson, F. C. W. 1957. Sterilization in Food Technology, McGraw Hill Book. Co., New York, NY.

Bigelow, W. C. Bohart, G. S., Richardson, A. C. and Ball, C. O. 1920. Heat penetration in processing canned foods, National Canners Association, Bull 16L.

Berry, M. R. Jr. and Dickerson, R. W. Jr. 1981. Heating characteristics of whole kernel corn processed in a Steritort. J. Food Sci. 46, 889-895.

Berry, M. R. Jr., Savage, R. A. and Pflug, I. J. 1979. Heating characteristics of cream-style corn processed in a Steritort: Effect of headspace, reel speed and consistency. J. Food Sci. 44, 831-835.

Berry, M. R. Jr. and Bradshaw, J. G. 1980. Heating characteristics of condensed cream of celery soup in a Steritort: Heating penetration and spore count reduction. J. Food Sci. 45, 869-874, 879.

Berry, M. R. Jr. and Bradshaw, J. G. 1982. Heat penetration for sliced mushrooms in brine processed in still and agitating retorts with comparisons to spore count reduction. J. Food Sci. 47, 1698-1704.

Bochereau, L., Bourgine and Palagos, B. 1992. A method fro prediction by combining data analysis and neural networks: Application to prediction of apple quality Near Infra-Red spectra. J. Agric. Eng. Res. 51, 201-216.

Chandarana, D. I., Gavin, A. and Wheaton, F. W. 1990. Particle/fluid interface heat transfer under UHT conditions at low particle/fluid relative velocities. J. Food Proc. Eng. 13, 191-206.

Chandarana, D. I. and Gavin, A. III. 1989. Establishing thermal processes for heterogeneous foods to be processed aseptically: a theoretical comparison of process development methods. J. Food Sci. 54, 198-204.

Clark, P. J. 1978. Mathematical modelling in sterilization processes. Food Technol. 32 (3), 73-75.

Clifcorn, L. E., Peterson, G. T., Boyd, J. M. and O'Neil, J. H. 1950. A new principle for agitating in processing of canned foods. Food Technol. 4, 450-457.

Datta, A. K. 1992. Thermal sterilization of liquid food. In *Encyclopedia of Food Science and Technology*. Y. H. Hui (ed.) John-Wiley & Sons, Inc. New York. NY. 2566-2578.

Deniston, M. F. Hassan, B. H. and Merson, R. L. 1987. Heat transfer coefficients to liquids with food particles in axially rotating cans. J. Food Sci. 52, 962-966, 979.

Denn, M. M. 1980. Process Fluid Mechanics. Prentice-Hall, Inc. New Jersey.

Duquenoy, A. 1980. Heat transfer to canned liquids. In *Food Process Engineering*, Vol 1: Food Processing Systems. P. Linko et al., (eds.) Applied Science Publishers Ltd, London. 483-489.

Eisner, M. 1988. Introduction into the Technique and Technology of Rotary Sterilization. Second edition, Private Authour's Edition, Milwaukee, WI.

Fernandez, C. L., Rao, M. A., Rajavasireddi, S. P. and Sastry, S. K. 1988. Particulate heat transfer to canned snap beans in Steritort. J. Food Proc. Eng. 10, 183-198.

Galvin, J. R. and Waldrop, H. L, Jr. 1990. The future of sensory evaluation in the food industry. Food Technol. 44, (1), 95-96, 100.

Ghazala, S. Ramaswamy, H. S., Smith ,J. P. and Simpson, B. K. 1991. Thermal process time calculations for thin profile packages: Comparison of Formula methods. J. Food Process Eng. 13, 269-282

Hassan, B. H. 1984. Heat Transfer Coefficients for Particles in Liquid in Axially Rotating Cans, PhD thesis, Dept of Agricultural Engineering, Univ. of California, Davis, CA.

Hayakawa, K. I. 1978. A critical review of mathematical procedures for determining proper heat sterilization processes. Food Technol. 32 (3), 59-65

Hayakawa, K. I. 1970. Experimental formulas for accurate estimation of transient temperature of food and their application to thermal process evaluation. Food Technol. 24 (12) 89.

Hendrickx, M., Silva, C. L. M., Oliveira. F. and Tobback, P. 1993. Generalizes (semi) - empirical formulae for optimal sterilization temperatures of conduction-heated foods with infinite surface heat transfer coefficients. J. Food Eng. 19, 141-158.

Hendrickx, M., Van Genechten, K. and Tobback, P. 1989. Optimizing quality attributes of conduction heated foods, a simulation approach. Paper presented at International Conference on Engineering and Food, 5, Cologne, Germany, 25 May - 3 June.

Heppel, N. J. 1985. Measurement of the liquid-solid heat transfer coefficient during continuous sterilization of foodstuffs containing particles. Presented at the 4th Congress on Engineering and Foods, Edmonton, AB, Canada. July 7-10.

Hiddink, J. 1975. Natural convection heating of liquids with reference to sterilization of canned food. Agric. Res. Rep. #839. Center for Agric. Publ. Documentation, Wageningen, Netherlands.

Horimoto, Y., Durance, T., Nakai, S. and Lukow, O. M. 1995. Neural networks vs principal component regression for prediction of wheat flour loaf volume in baking tests. J. Food Sci. 60, 3, 429-433.

Huang B. and Mujumdar, A. S. 1993. Use of neural network to predict industrial dryer performance. Drying Technol., 11(3), 525-541.

Hunter, G. M. 1972. Continuous sterilization of liquid media containing suspended particles. Food Technol. Aust. 24, 158-165.

Jaluria, Y. and Torrance, K. E. 1986. Computational Heat Transfer. Hemisphere Publishing Corporation New York, NY.

Kreith, F. 1965. Principles of Heat Transfer . International Textbook Co. Scranton, PA.

Lekwauwa, A. N. and Hayakawa, K. I. 1986. Computerized model for the prediction of thermal responses of packaged solid-liquid food mixture undergoing thermal processes. J. Food Sci. 51, 1042-1049,1056.

Lenz, M. K. and Lund, D. B. 1978. The lethality-Fourier number method. Heating rate variations and lethality confidence intervals for forced-convection heated foods in containers. J. Food Proc. Eng. 2, 227-271.

Liao , K., Paulsen, M. R. and Reid, J. F. 1993. Corn kernel breakage classification by machine vision using a neural network classifier. Tran ASAE 36, 1949-1953.

Linko, P., Uemura, K., and Eerikainen, T. 1992. Neural network in fuzzy extrusion control. In *Food Engineering in a Computer Climate*, Institution of Chemical Engineers, Rugby, UK, Hemisphere Publishing Corporation, 401-410.

Lopez, A. 1987. A complete Course in Canning, Book I. The Canning Trade, Baltimore, MD.

Lund, D. B. 1977. Design of thermal processes for maximizing nutrient retention. Food Technol., 31(2), 71-78.

Lund, D. B. 1975. Heat processing. In *Principle of Food Science Part II. Physical Principles of Food Preservation*, Ed. by O. R. Fenema, Mercel Dekker, Inc. New York, 32-92.

Macagno, E. O. 1969. Flow Visualization in Liquids. IIHR Report #114, Iowa Institute of Hydraulic Reseach, The University of Iowa, Iowa City, IO.

Maesmans, G., Hendrickx, M., DeCordt, S., and Fransis, A. 1992. Fluid-to-particle heat transfer coefficient determination of heterogeneous foods: A review. J. Food Proc. Preserv. 16, 29-69.

Maesmans, G., Hendrickx, M., DeCordt, S., and Tobback, P. 1994. Feasibility of the use of a time temperature integrator and a mathematical model to determine fluid-to-particle heat transfer coefficients. Food Res. Int. 27, 39-51.

Manson, J. E., Zahradnik, J. W. and Stumbo, C. R. 1970. Evaluation of lethality and Nutrient retention of conduction-heating food in rectangular containers. Food Technol. 24 (11), 109.

Mckenna, A. B. and Holdsworth, S. D. 1990. Sterilization and cooking of ffod particulates, a review. Tech. Bull. No. 75, Campden Food and Drink Assoc., Chipping Campden, U. K.

Merson, R. L. and Stoforos, N. G. 1990. Motion of spherical particles in axially rotating cans. Effect of liquid-particle heat transfer. In Engineering and Food, Vol. 2, W. E. L. Spiess and H. Schubert (ed.) Elsevier Science Publishing Co., Inc., New York, NY, 60-69.

Merzkirch, W. 1987. Flow Visualization. Second edition, Academic Press, Inc., Orlando, FL.

Nasr, K., Ramadhyani, S. and Viskanta, R. 1994. An experimental investigation on forced convection heat transfer from a cylinder embedded in a packed bed. ASME J. Heat Transfer, 99, 300-305.

Naveh, D. and Kopelman, I. J. 1980. Effect of some processing parameters on the heat transfer coefficients in a rotating autoclave. J. Food Proc. Preserv. 4, 67-77.

Ohlsson, T. 1980. Optimal sterilization temperatures for flat containers. J. Food Sci., 45, 848-59.

Ozisik, M. N. 1989. Heat Transfer: A Basic Approach. International Edition, McGraw-Hill Book Co. Singapore.

Parchomchuk, P. 1977. A simplified method for agitation processing of canned foods. J. Food Sci. 42, 265-268.

Park, B., Chen, Y. R., Whittaker, A. D., Miller, R. K. and Hale, D. S. 1994. Neural network modelling for beef sensory evaluation. Transaction of the ASAE, 37, 1547-1553.

Pflug, I. J., Blaisdell, J. L. and Kopelman, I. J. 1965. Developing temperature-time curves for objects that can be approximated by a sphere, infinite plate or infinite cylinder. ASHRAE Trans. 71, 238.

Quast, D. G. and Siozawa, Y. Y. 1974. Heat transfer rates during axially rotated cans. Proc. Int. Congr. Food Sci. Technol., 4, 458-468

Ramaswamy, H. S. and Abbatemarco, C. 1996. Thermal Processing of Fruits. In *Processing of Fruits - Science and Technology. Vol. 1, Biology, Principles, and Applications.* L. P. Somogyi, H. S. Ramaswamy and Y, H, Hui (eds.). Technomic Publishing Company, Inc. Lancaster, PA.

Ramaswamy, H. S., Awuah, G. B. and Simpson, B. K. 1996. Heat transfer and lethality consideration in aseptic processing of liquid/particulate mixtures. Critical Review Food Sci. Nutri., CRC Press, Inc. Baton Roca, FL.

Ramaswamy, H. S., Abbatemarco, C., and Sablani, S. S. 1993. Heat transfer rates in a canned food model as influenced by processing in an end-over-end rotary steam/air retort. J. Food Proc. Preserv. 17, 269-286.

Ramaswamy, H. S., Abdelrahim, K. and Smith, J. 1992. Thermal processing and computer modelling. In *Encyclopedia of Food Science and Technology*. Y. H. Hui (ed.) John-Wiley & Sons, Inc. New York. NY 2538-2552.

Ramaswamy, H. H. and Gazala, S. 1990. Centerpoint nutrient degrdation in heat processed conduction heating food model. J. Food Proc. Eng. 12, 159-169.

Ramaswamy, H. S., van de Voort, F. R. and Ghazala. 1989. An analysis of TDT and Arrhenius methods for handling process and kinetic data. J. Food Sci. 54, 1322-1326

Ramaswamy, H. S. and Tung, M. A. 1986. Modeling heat transfer in steam/air processing of thin profile packages. Can. Inst. Food Sci. Technol. J. 19 (5), 215-222.

Ramaswamy, H. S., Tung, M. A. and Stark, R. 1983. A method to measure surface heat transfer from steam/air mixtures in batch retorts. J. Food Sci., 48, 900-904.

Ramaswamy, H. S., Lo, K. V., and Tung, M. A. 1982. Simplified equations for transient temperatures in conductive foods with convective heat transfer at the surface. J. Food Sci., 47, 2042-2047.

Ramaswamy, H. S. and Tung, M. A. 1981. Thermo-physical properties of apples in relation to freezing. J. Food Sci. 46, 724-729.

Rao, M. A. and Anantheswaran, R. C. 1988. Convective heat transfer to fluid foods in cans. Adv. Food Res. 32, 39-84.

Rao, M. A., Cooly, H. J., Anantheswaran, R. C. and Ennis, R. E. 1985. Convective heat transfer to canned liquid foods in a Steritort. J. Food Sci. 50, 150-154.

Ruan, R., Almaer, S. and Zhang, J. 1995. Prediction of dough rheological properties using neural networks. Cereal Chemistry, 72, 3, 308-311.

Saguy, I. and Karel, M. 1979. Optimal retort temperature profile in optimizing thiamin retention in conduction-type heating of canned foods. J. Food Sci., 44, 1485-90.

Sastry, S. K. 1984. Convective heat transfer coefficients for canned mushrooms processed in still retorts. ASAE paper 84-6517.

Sayeed, M. S., Whittaker, A. D. and Kehtarnavaz, N. D. 1995. Snack quality evaluation method based on image features and neural network prediction. Transactions of the ASAE, 33, 6: 2037-2044

Schiesser, W. E. 1983. DSS/2, An introduction to the use of mathematical software for ordinary and partial differential equations. Guidelines for the programming of a numerical method of lines code. Lehigh University, Bethlehem, PA.

Silva, C. L. M., Hendrickx, M., Oliveira. F. and Tobback, P. 1992. Critical evaluation of commonly used objective functions to optimize overall quality and nutrient retention of heat-preserved foods. J. Food Eng., 17, 241-58.

Silva, C. L. M., Oliveria. F. A. R. and Hendrickx, M. 1993. Modeling optimum processing conditions for the sterilization of prepackaged foods. Food Control, 4 (2), 67.

Silva, C. L. M., Oloveira, F. A. R., Pereira, P. A. M. and Hendrickx, M. 1994. Optimum sterilization: a comparative study between average and surface quality. J. Food Proc. Eng. 17, 155-176.

Singh, R. P. 1982. Thermal diffusivity in food processing. Food Technol. 36(2), 87-91.

Soule, C. L. and Merson, R. L. 1985. Heat transfer coefficients to Newtonian liquids in axially rotated cans. J. Food Proc. Eng. 8, 33-46.

Stoforos, N. G. and Merson, R. L. 1995. A solution to the equations governing heat transfer in agitating liquid/particulate canned food. J. Food Proc. Eng. 18, 165-185.

Stoforos, N. G. and Merson, R. L. 1992. Physical property and rotational speed effect on heat transfer in axially rotating liquid/particulate canned foods. J. Food Sci., 57, 749 - 754.

Stoforos, N. G. and Merson, R. L. 1991. Measurement of heat transfer coefficients in rotating liquid/particle systems. Biotechnol. Prog., 7, 267-271.

Stoforos, N. G. and Merson R. L. 1990. Estimating heat transfer coefficients in liquid/particulate canned foods using only liquid temperature data. J. Food Sci. 55, 478-483.

Stoforos, N. G. 1988. Heat transfer in axially rotating canned liquid/particulate food systems. Ph.D. thesis, Dept. of Agricultural Engineering, Univ. of California, Davis, CA.

Stumbo, C. R. 1973. Thermobacteriology in Food Processing. Second Edition, Academic Press, New York, NY.

Teixeira, A. A. and Shoemaker, F. C. 1989. Computerized Food Processing Operations, AVI Publishing Co., Inc., Westport, CT.

Teixeira, A. A. 1978. Conduction heating considerations in thermal processing of canned foods. ASME San Francisco Paper # 78-WA/HT-55.

Teixeira, A. A., Zinsmeister, G. E. and Zahradnik, J. W. 1975. Computer simulation of variable retort control and container geometry as possible means of improving thiamine retention in thermally processed foods. J. Food Sci., 40, 656.

Teixeira, A. A., Dixon, J. R. Zahradnik, J. W. and Zinsmeister, G. E. 1969a. Computer determination of spore survival distribution in thermally-processed conduction heated foods. Food Technol. 23, 352-354.

Teixeira, A. A., Dixon, J. R., Zahradnik, J. W. and Zinsmeister, G. E. 1969b. Computer optimization of nutrient retention in the thermal processing of conduction-heated foods. Food Technol., 23, 845-850.

Thai, C. N. and Shewfelt. R. L. 1991. Modelling sensory color quality of tomato and peach: Neural networks and statistical regression. Trans. ASAE 34, 950-955.

Thijssen, H. A. C. and Kochen, L. H. P. 1980. Calculation of optimum sterilization conditions for packed conduction-type foods. J. of Food Sci., 45, 1267-72.

Tomlins, K. I. and Gay, C. 1994. Prediction of quality and origin of black tea and pine resin samples from chromatographic and sensory information : evaluation of neural networks. Food Chemistry 50, 157-161

Weng, Zhijun, Hendrickx, M., Maesmans, G., and Tobback, P. 1992. The use of a time-temperature-integrator in conjunction with mathematical modelling for determining liquid/particle heat transfer coefficients. J. Food Eng. 16, 197-214

Whitaker, S. 1976. Elementary Heat Transfer Analysis. Pergamon Press Inc. New York.

Widrow, B. and Lehr, M. A. 1993. Adaptive neural networks and their applications. Int. J. Intelligent Systems, Vol. 8, 453-507.

APPENDIX

FINITE DIFFERENCE FORMULATION AND NUMERICAL PROCEDURES

The governing partial differential equations in different shaped geometry with appropriate initial and boundary conditions are (Ozisik, 1989):

(i) Spherical geometry

$$\frac{\partial T}{\partial t} = \alpha_p \left(\frac{\partial^2 T}{\partial r^2} + \frac{2}{r} \frac{\partial T}{\partial r} \right) \qquad \text{(A.1)}$$

The initial and boundary conditions are :

$$T(r, 0) = T_i \qquad \text{at} \quad t = 0 \qquad \text{(A.2)}$$

$$\frac{\partial T(0, t)}{\partial r} = 0 \qquad \text{at} \quad t > 0 \qquad \text{(A.3)}$$

$$k_p \cdot \frac{\partial T}{\partial r} = h_{fp} \cdot (T_l - T_{l,s}) \qquad \text{at} \quad r = a \quad \text{and} \quad t > 0 \qquad \text{(A.4)}$$

(ii) Cylindrical geometry

$$\frac{\partial T}{\partial t} = \alpha_p \left(\frac{\partial^2 T}{\partial r^2} + \frac{1}{r} \frac{\partial T}{\partial r} + \frac{\partial^2 T}{\partial z^2} \right) \qquad \text{(A.5)}$$

The initial and boundary conditions are:

$$T(r, z, 0) = T_i \qquad \text{at} \quad t = 0 \qquad (A.6)$$

$$\frac{\partial T(0, z, t)}{\partial r} = 0 \qquad \text{at} \quad t > 0 \ \text{and} \ 0 < z < L \qquad (A.7)$$

$$\frac{\partial T(r, 0, t)}{\partial r} = 0 \qquad \text{at} \quad t > 0 \ \text{and} \ 0 < r < a \qquad (A.8)$$

$$k_p \cdot \frac{\partial T}{\partial r} = h_{fp} \cdot (T_l - T_{ps}) \qquad \text{at} \quad r = a \ ; \ 0 < z < L \ \text{and} \ t > 0 \qquad (A.9)$$

$$k_p \cdot \frac{\partial T}{\partial z} = h_{fp} \cdot (T_l - T_{ps}) \qquad \text{at} \ z = L \ ; \ 0 < r < a \ \text{and} \ t > 0 \qquad (A.10)$$

(iii) Rectangular geometry

$$\frac{\partial T}{\partial t} = \alpha_p \left(\frac{\partial^2 T}{\partial x^2} + \frac{\partial^2 T}{\partial y^2} + \frac{\partial^2 T}{\partial z^2} \right) \qquad (A.11)$$

The initial and boundary conditions are:

$$T(x, y, z, 0) = T_i \qquad \text{at} \quad t = 0 \qquad (A.12)$$

$$\frac{\partial T(x, 0, z, t)}{\partial y} = 0 \qquad \text{at} \ t > 0 \ ; \ 0 < x < a \ \text{and} \ 0 < z < a \qquad (A.13)$$

$$\frac{\partial T(0, y, z, t)}{\partial x} = 0 \qquad \text{at} \ t > 0 \ ; \ 0 < y < a \ \text{and} \ 0 < z < a \qquad (A.14)$$

$$\frac{\partial T(x, y, 0, t)}{\partial z} = 0 \text{ at } \quad t > 0 \; ; \; 0 < x < a \text{ and } 0 < y < a \qquad \text{(A.15)}$$

$$k_p.\frac{\partial T}{\partial x} = h_{fp}.(T_l - T_{ps}); \text{ at } x=a; \; 0 < y < a; \; 0 < z < a \; ; \; t>0 \qquad \text{(A.16)}$$

$$k_p.\frac{\partial T}{\partial y} = h_{fp}.(T_l - T_{ps}); \text{ at } y=a; \; 0 < x < a; \; 0 < z < a \; ; \; t>0 \qquad \text{(A.17)}$$

$$k_p.\frac{\partial T}{\partial z} = h_{fp}.(T_l - T_{ps}); \text{ at } z=a; \; 0 < x < a; \; 0 < y < a \; ; \; t>0 \qquad \text{(A.18)}$$

Numerical procedure

The solution of the second order parabolic equations (spherical, cylindrical and rectangular coordinate system) with their associated initial and boundary conditions was carried out using finite difference methods. The Crank-Nicholson scheme was used for first and second order spatial derivatives appeared in the heat flow equations and backward difference scheme for first order derivative in convective boundary equations. An implicit method was used for time derivatives. Since transformed equations contain temperature values of next time steps, it was necessary to employ iterative technique in the solution procedure.

Finite difference approximation

(i) Spherical geometry

The computational grid details are shown in Fig. A.1. Due to the nature of boundary condition over the spherical surface the heat flow in the sphere can be considered as one-dimensional. In the radial direction, region ($0 \leq r \leq a$) was divided into N equal divisions. Space index i = 1 represents the center of the sphere where symmetry (adiabatic) boundary condition was applied and i = N+1 represent the sphere surface where convective boundary condition was applied. The subscript i specify the nodal points and superscript n is used for time indexing, with n = 0 means time = 0 and the step size

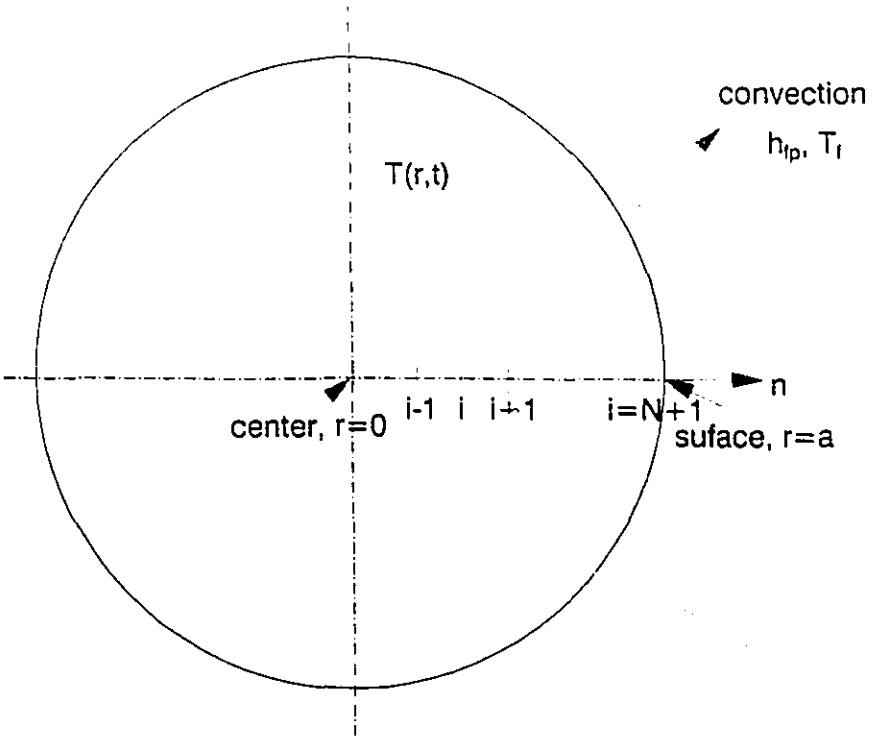

Figure A.1 Finite difference grid system for one-dimensional heat transfer in a sphere with the convection boundary conditions at the surface

being:

$$\Delta r = \frac{a}{N} \tag{A.19}$$

$$r_i = (i-1) \Delta r \tag{A.20}$$

$$t^n = n \Delta t \tag{A.21}$$

Finite difference approximations of the various derivatives, appearing in the energy equations and boundary conditions, used in this numerical scheme are given in Table A.1. The heat flow equation for the spherical geometry can be written as:

$$\left(\frac{\partial^2 T}{\partial r^2}\right)_i + \left(\frac{2}{r}\right)_i \left(\frac{\partial T}{\partial r}\right)_i = \frac{1}{\alpha_p} \left(\frac{\partial T}{\partial t}\right)_i \tag{A.22}$$

This reduces to following form for all internal nodes, in the finite difference formulation, given by:

$$A_i\, T_{i-1}^{n+1} + B\, T_i^{n+1} + C_i\, T_{i+1}^{n+1} = (-A_i)\, T_{i-1}^{n} + D\, T_i^{n} + (-C_i)\, T_{i+1}^{n} \tag{A.23}$$

where

$$A_i = \frac{1}{2\Delta r^2} - \frac{1}{2(i-1)\Delta r^2};\ B = \frac{-1}{\Delta r^2} - \frac{1}{\Delta t};\ C_i = \frac{1}{2\Delta r^2} + \frac{1}{2(i-1)\Delta r^2};\ D = \frac{1}{\Delta r^2}$$

The nodal equations for node i=1 and i=N+1 can be given by:

$$B \,.\, T_1^{n+1} + \frac{1}{\Delta r^2} \,.\, T_2^{n+1} = D \,.\, T_1^{n} + \frac{-1}{\Delta r^2} \,.\, T_2^{n} \tag{A.24}$$

$$\frac{-1}{\Delta r} T_{N-1} + \left(\frac{1}{\Delta r} + \frac{h_{fp}\, \Delta r}{k}\right) T_N = \frac{h_{fp}\, \Delta r}{k}\, T_f \tag{A.25}$$

Table A.1 Finite difference approximations of derivatives

Derivatives	Difference approximation
First order in space	
$\left(\frac{\partial T}{\partial r}\right)_i^{n+1}$	$\left[\frac{T_{i+1}^{n+1} - T_{i-1}^{n+1} + T_{i+1}^{n} - T_{i-1}^{n}}{4 \cdot \Delta r}\right]$
Second order in space	
$\left(\frac{\partial^2 T}{\partial r^2}\right)_i^{n+1}$	$\left[\frac{T_{i+1}^{n+1} - 2\,T_i^{n+1} + T_{i-1}^{n+1} + T_{i+1}^{n} - 2\,T_i^{n+1} + T_{i-1}^{n}}{2 \cdot \Delta r^2}\right]$
First order in time	
$\left(\frac{\partial T}{\partial t}\right)_i^{n+1}$	$\left[\frac{T_i^{n+1} - T_i^{n}}{\Delta t}\right]$
First order in space (used in convective boundary condition)	
$\left(\frac{\partial T}{\partial r}\right)_i^{n+1}$	$\left[\frac{T_i^{n+1} - T_{i-1}^{n+1}}{\Delta r}\right]$

(ii) Cylindrical geometry

The numerical procedure described above for one-dimensional heat flow in spherical geometry can be extended for two-dimensional heat flow in finite cylindrical geometry. Since the nature of boundary condition over the cylindrical surface creates two-dimensional symmetry, only one quarter of the cylinder was considered for analysis. The computational grid details are shown in Fig A.2. In the radial direction region ($0 \leq r \leq a$) is subdivided into N equal divisions. Space index i = 1 represents the central axis of cylinder (r = 0) where symmetry (adiabatic) boundary condition was applied and i = N+1 represents the curved surface of the cylinder where convective boundary condition was applied. The other space coordinate ($0 \leq z \leq +L$), which is divided into M equal divisions, is indexed by the subscript j. The plane of symmetry passes through the location j = 1 and flat (top) surface of the cylinder is represented by j = M+1 where convective boundary condition was applied. The superscript n indexes the time step with n=0 representing zero time (t=0). The following relations hold good for the grid system;

$$\Delta r = \frac{1}{N} \tag{A.26}$$

$$\Delta z = \frac{1}{M} \tag{A.27}$$

$$r_i = (i-1)\,\Delta r \tag{A.28}$$

$$t^n = n\,\Delta t \tag{A.29}$$

Finite difference approximation of the various derivatives, appearing in two-dimensional heat flow equation in cylindrical coordinate system, used in this numerical scheme are given in Table A.1. The following is the finite difference form of the heat flow equation;

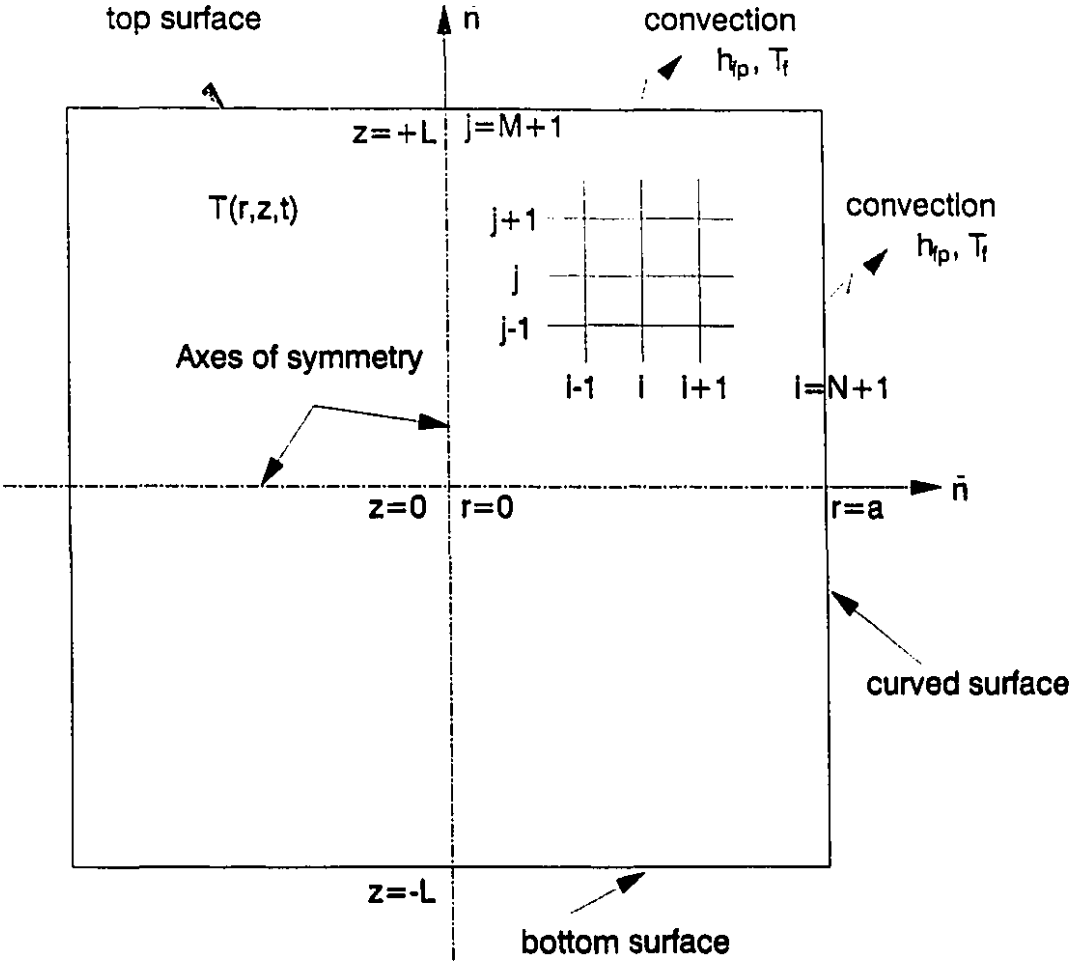

Figure A.2 Finite difference grid system for two-dimensional heat transfer in a cylinder with the convection boundary conditions at the surface

$$\left(\frac{\partial^2 T}{\partial r^2}\right)_i + \left(\frac{1}{r}\right)_i \left(\frac{\partial T}{\partial r}\right)_i + \left(\frac{\partial^2 T}{\partial z^2}\right)_i = \frac{1}{\alpha_p}\left(\frac{\partial T}{\partial t}\right)_i \qquad \textbf{(A.30)}$$

The nodal equations for internal nodes, $0 < r < a$ and $0 < z < +L$

$$A_i\, T_{i-1,j}^{n+1} + B\, T_{i,j}^{n+1} + C_i\, T_{i+1,j}^{n+1} + D\, T_{i,j-1}^{n+1} + D\, T_{i,j+1}^{n+1}$$

$$= (-A_i)\, T_{i-1,j}^{n} + E\, T_{i,j}^{n} + (-C_i)\, .\, T_{i+1,j}^{n} + (-D)\, T_{i,j-1}^{n} + (-D)\, T_{i,j+1}^{n} \qquad \textbf{(A.31)}$$

Nodal equations for symmetry axis, $0 < r < a$ and $z=0$

$$A_i\, T_{i-1,j}^{n+1} + B\, T_{i,j}^{n+1} + C_i\, T_{i+1,j}^{n+1} + 2D\, T_{i,j+1}^{n+1}$$

$$= (-A_i)\, T_{i-1,j}^{n} + E\, T_{i,j}^{n} + (-C_i)\, .\, T_{i+1,j}^{n} + (-2D)\, T_{i,j+1}^{n} \qquad \textbf{(A.32)}$$

Nodal equations for symmetry axis, $r=0$ and $0 < z < +L$

$$B\, T_{i,j}^{n+1} + (A_i + C_i)\, T_{i+1,j}^{n+1} + D\, T_{i,j-1}^{n+1} + D\, T_{i,j+1}^{n+1}$$

$$= E\, T_{i,j}^{n} + (-A_i - C_i)\, .\, T_{i+1,j}^{n} + (-D)\, T_{i,j-1}^{n} + (-D)\, T_{i,j+1}^{n} \qquad \textbf{(A.33)}$$

Nodal equation for the center point, $r=0$ and $z=0$

$$B\, T_{i,j}^{n+1} + (A_i + C_i)\, T_{i+1,j}^{n+1} + 2D\, T_{i,j+1}^{n+1}$$

$$= E\, T_{i,j}^{n} + (-A_i - C_i)\, .\, T_{i+1,j}^{n} + (-2D)\, T_{i,j+1}^{n} \qquad \textbf{(A.34)}$$

coefficient in above Eqs. (A.32) to (A.34) are:

$$A_i = \frac{1}{2\,\Delta r^2} - \frac{1}{4\,(i-1)\,\Delta r^2}\,; \qquad B = -\frac{1}{\Delta r^2} - \frac{1}{\Delta z^2} - \frac{1}{\alpha_p\,\Delta t}$$

$$C_i = \frac{1}{2\,\Delta r^2} + \frac{1}{4\,(i-1)\,\Delta r^2}\,; \qquad D = \frac{1}{2\,\Delta z^2}\,; \qquad E = \frac{1}{\Delta r^2} + \frac{1}{\Delta z^2} - \frac{1}{\alpha_p\,\Delta t}$$

Nodal equations for curved surface, $r= +a$ and $0 < z < +L$

$$A\ T_{N-1,j}^{n+1} + (-A-2B-C-D)\ T_{N,j}^{n+1} + B\ T_{N,j-1}^{n+1} + B\ T_{N,j+1}^{n+1}$$

$$= -C\ T_{N,j}^{n} - D\ T_{f}^{n+1} \qquad \textbf{(A.35)}$$

Nodal equation for node at the intersection of curved surface and symmetry axis, r= +a and z=0

$$A\ T_{N-1,1}^{n+1} + (-A-2B-C-D)\ T_{N,1}^{n+1} + 2\ B\ T_{N,2}^{n+1}$$

$$= -C\ T_{N,1}^{n} - D\ T_{f}^{n+1} \qquad \textbf{(A.36)}$$

coefficient in above Eqs. (A.35) and (A.36) are:

$$A = \frac{1}{\Delta r^2}\ ; \qquad B = \frac{1}{2\ \Delta z^2}\ ; \qquad C = \frac{1}{2\ \alpha_p\ \Delta t}\ ; \qquad D = \frac{h_{fp}}{k\ \Delta r}$$

Nodal equations for top surface, 0 < r < +a and z= +L

$$A\ T_{i,M-1}^{n+1} + (-A-B-C-D-E)\ T_{i,M}^{n+1} + B\ T_{i-1,M}^{n+1} + C\ T_{i+1,M}^{n+1}$$

$$= -D\ T_{i,M}^{n} + -E\ T_{f}^{n+1} \qquad \textbf{(A.37)}$$

Nodal equation for the node at the intersection of top surface and symmetry axis, r=0 and z =+L

$$A\ T_{N,M-1}^{n+1} + (-A-B-C-D-E)\ T_{N,M}^{n+1} + (B+C)\ T_{N-1,M}^{n+1}$$

$$= -D\ T_{N,M}^{n} + -E\ T_{f}^{n+1} \qquad \textbf{(A.38)}$$

coefficient in above Eqs. (A.37) and (A.38) are:

$$A=\frac{1}{\Delta z^2}\ ;\ B=\left[1-\frac{1}{2(i-1)}\right]\frac{1}{2\Delta r^2}\ ;\ C=\left[1+\frac{1}{2(i-1)}\right]\frac{1}{2\Delta r^2}\ ;\ D=\frac{1}{2\ \alpha_p\ \Delta t}\ ;\ E=\frac{h_{fp}}{k\ \Delta z}$$

Nodal equation for top right corner node, r= +a and z= +L

$$A\ T^{n+1}_{N-1,M}\ +\ (-A-B-C-D-E)\ T^{n+1}_{N,M}\ +\ B\ T^{n+1}_{N,M-1}$$

$$=\ (-C-D)\ T^{n+1}_{f}\ -\ E\ T^{n}_{N,M} \qquad \textbf{(A.39)}$$

coefficients in above Eq. (A.39) are:

$$A=\frac{1}{\Delta r^2};\quad B=\frac{1}{\Delta z^2};\quad C=\frac{h_{fp}}{k_p\ \Delta z};\quad D=\frac{h_{fp}}{k_p\ \Delta r};\quad E=\frac{1}{2\ \alpha\ \Delta t}$$

The finite difference formulation of energy equation along with boundary conditions lead to a system of algebraic equations that form a banded matrix. Various numerical methods have been developed to solve simultaneous algebraic equations by a digital computer. Iterative methods are particularly preferred over direct methods due lower roundoff errors associated with these methods. In the present analysis successive overrelaxation (SOR), an improved version of Gauss-Seidel iterative procedure was used to solve simultaneous algebraic equations (Jaluria and Torrance, 1986).

(iii) Rectangular geometry

The heat flow equation for the rectangular geometry immersed in a fluid medium becomes three dimensional. The application of finite difference method to three dimensional systems require no additional concepts. However the number of nodal equations are significantly high. In the present study a software package based on numerical methods was used to solve three dimensional energy equation. This package utilizes a new technique, called the numerical method of lines (NMOL) to solve initial-boundary value problems.

The problem-domain is discretized, as in the finite difference method, so that the governing partial differential equation is equally valid at all the nodal points. The spatial derivatives in the differential equation are approximated by algebraic expressions based on the Taylor series. However, the time derivative is left alone. This results in a set of ordinary differential equations, one foe each nodal point, which can be solved by any method available for solving ordinary differential equations. The guidelines for solving and programming initial-boundary value problems using NMOL are detailed in Schiesser (1983).